UTS UNIVERSITY OF TECHNOLOGY SYDNEY

Modeling the Impacts of Compound Dry and Hot Extremes on Australia's Wheat

by Siyi Li

Thesis submitted in fulfilment of the requirements for the degree of

Doctor of Philosophy

under the supervision of Prof Alfredo Huete, Prof Qiang Yu, Dr De Li Liu, and Dr Bin Wang

University of Technology Sydney
Faculty of Science

March 2024

Certificate of Original Authorship

I, Siyi Li declare that this thesis is submitted in fulfillment of the requirements for the award of Doctor of Philosophy, in the School of Life Sciences/Faculty of Sciences at the University of Technology Sydney.

This thesis is wholly my own work unless otherwise referenced or acknowledged. In addition, I certify that all information sources and literature used are indicated in the thesis.

This document has not been submitted for qualifications at any other academic institution.

This research is supported by the Australian Government Research Training Program.

Signature of student: Production Note:
Signature removed prior to publication.

Date: 20 February 2024

Acknowledgement

Reflecting on my doctoral journey, from the initial excitement and anticipation at the start, through moments of helplessness and regret, to the pride and sense of achievement in overcoming challenges, and finally to the current feelings of relief and gratitude, all these memories and emotions gradually become clear. The journey of PhD is indeed a challenging and irreplaceably unique experience, immensely valuable to both my personal life and academic journey. Here, I am honored to express my deepest gratitude to those who have supported and guided me through this process.

Above all, I must extend my deepest appreciation to my principal supervisor, Professor Alfredo Huete. He was the one who took me on when I had to switch supervisors halfway through my PhD, allowing me to continue my doctoral study. He offered constructive suggestions and comments for my work, and generously encouraged me, boosting my confidence throughout my studies. His patient guidance and support were the strong backbone that enabled me to successfully complete my thesis.

I also owe a special thanks to my co-supervisor, Professor Qiang Yu. Without his selfless help and encouragement, I would not have had the opportunity to apply for and pursue a doctoral degree at the University of Technology Sydney (UTS). He provides invaluable academic guidance and meanwhile respects and supports my research ideas. It is also him, supporting me in collaborating with the principal research scientist Dr. De Li Liu and his team at the Wagga Wagga Agricultural Institute, NSW Department of Primary Industries (NSW DPI). His scientific achievements and noble character have had a profound impact on me that will last a lifetime.

I would like to express my profound gratitude to my external supervisor, the principal research scientist Dr. De Li Liu. It was he who recommended me to Professor Qiang Yu, giving me the opportunity to pursue a PhD. At the same time, I am grateful to Dr. De Li Liu for fostering a pure, welcoming, and open-minded academic environment that allowed me to immerse myself fully. Throughout my entire PhD, he encouraged me, offering selfless advice and assistance to overcome all difficulties. He contributed insightful feedback and constructive suggestions on my work at various stages of my doctoral research and taught me numerous academic skills essential for my thesis. Without his supervision, I could not have completed this work. Dr. De Li Liu's passion for research, deep expertise, and meticulous scholarly approach have profoundly impacted me and will undoubtedly influence my future career.

I extend my deep gratitude to Dr. Wang Bin at NSW DPI, who has not only been an external supervisor but also a supportive friend. Throughout my doctoral studies, he paid close attention to every detail of my research, from careful consideration of my thesis topic to strict review of my research content and detailed expression in my writing. Whenever I encountered problems, he always made time to provide help and

feedback. His profound criticism and continuous encouragement helped me make rapid progress, and his broad academic vision and industrious work habits always inspired me to move forward. In life, Dr. Bin Wang also always provided timely help and support. His guidance was crucial for the successful completion of this thesis.

I want to thank three colleagues who were in NSW DPI when I first arrived in Australia in 2019. Professor Puyu Feng at China Agricultural University. When I first arrived in Australia, he selflessly helped me with both life and study, allowing me to quickly settle in and dive into research. Without his generous sharing of data and hands-on teaching of programming skills, I might not have been able to complete my research work on time. Dr. Lijie Shi at Yangzhou University, took care of me like a sister in life, helping me quickly adapt to the environment in NSW DPI and providing companionship and encouragement. Her generous help and support were also indispensable for me to successfully complete my studies. Dr. Mingxia Huang's optimistic attitude affected me, and she offered advice when I was confused about work, helping me quickly regain my focus and direction. Her companionship is a precious experience in my difficult doctoral studies. Additionally, I also want to thank a peer Professor Xiaofang Wang at the Northeast Agriculture University, whose intelligence and diligence I admire. Because of our similar life and studying experiences, we had the most in common, not only exchanging academic suggestions but also mutually encouraging and motivating each other to make progress. Additionally, I thank a peer Mengjie Wu at the Northwest A&F University, who not only taught me how to use ArcGIS but also provided me with positive energy and emotional support during my challenging doctoral journey.

I extend my thanks to fellows from UTS, including Qinggaozi Zhu, Rong Gan, Shijin Yao, Huanghuang Wang, Keyu Xiang, as well as to the fellows and visiting scholars at NSW DPI, including Zikui Wang, Liping Guo, Lihong Wu, Hao Quan, and Fangzheng Chen. Thank you for your kindness, motivation, and backing, and for experiencing both the memorable joyful and challenging moments with meI appreciate the substantial contributions from my co-authors, Dr. Chao Chen and Dr. Cathy Waters, in enriching the early drafts of our manuscripts for publication. Furthermore, I am grateful for the administrative support from the staff at UTS and the NSW DPI, which significantly contributed to a supportive and efficient environment throughout my PhD study.

I would like to give special thanks to my family, my mother Yanling Xu, my father Youxing Li, my brother Hainan Li, and my sister-in-law Yueping Wang, who supported my pursuit of a doctoral degree and encouraged me throughout the process. Especially during the two years of the COVID-19 pandemic when I was studying from home, they not only provided me with a good study environment but also solved all my life and financial problems and tried their best to help and encourage me when I was overwhelmed by stress. In my heart, they are the best family in the world. I also want to thank my two little nephews, Yinhao

Li and Yinjia Li, whose videos and photos always cheered me up when I was sad or missing home. They made me maintain an optimistic attitude even when living alone abroad. I am also thankful to my friends in China, who contacted me and cared for me, making my days in a foreign land less lonely. Your encouragement and energy, like my family, are always my strongest support.

I acknowledge the China Scholarship Council and UTS for providing financial support and the NSW DPI for the facilities and support offered for this work.

Publications arising from this thesis

Journal papers directly included in this thesis

Siyi Li, Bin Wang, Puyu Feng, et al, 2022. Assessing climate vulnerability of historical wheat yield in south-eastern Australia's wheat belt. Agricultural Systems, 196: 103340. (IF=6.6) DOI: https://doi.org/10.1016/j.agsy.2021.103340. (Chapter 2)

Siyi Li, Bin Wang, De Li Liu, et al, 2024. Can agronomic options alleviate the risk of compound drought-heat events during the wheat flowering period in southeastern Australia? European Journal of Agronomy, 153: 127030. (IF=5.2) DOI: https://doi.org/10.1016/j.eja.2023.127030. (Chapter 3)

Siyi Li, Bin Wang, De Li Liu, et al. Compound drought and extreme temperature events intensify wheat yield loss in Australia. Earth's Future. (IF=8.2) Under Review. (Chapter 4)

Siyi Li, Bin Wang, De Li Liu, et al. The role of climate driver on compound drought and extreme temperature events varied temporally and spatially across Australia's wheat belt. Prepare to submit to the journal of Weather and Climate Extremes in March 2024. (Chapter 5)

Peer-reviewed International Conference proceedings

Siyi Li, Bin Wang, De Li Liu, et al. Compound drought and extreme temperature events intensify wheat yield loss in Australia. Australia' The 25th International Congress on Modelling and Simulation (MODSIM), Darwin, Australia, July 2023. (Extended Abstract, Accepted).

Contents

List of Figures

List of Tables

Abstract

Compound dry and hot events, which refer to the simultaneous occurrence of drought and heat events in both time and space, have garnered increasing attention over recent decades due to their amplified detrimental effects on agricultural production compared to the impacts of either drought or heat alone. Such compound events may continue to escalate under future climate change, presenting a severe challenge for rain-fed cropping systems. For instance, rain-fed wheat production in Australia is particularly vulnerable, experiencing significant yield fluctuations or losses due to recurrent extreme weather conditions. While the effects of individual events like drought or heat on wheat yields have been extensively quantified, the compound dry and hot remains less understood. Addressing this knowledge gap, further research focusing on the relationship between compound events and wheat yield in Australia is essential to enhance our comprehension of climate change's impacts on the agricultural sector. In this project, a novel daily-scale agricultural compound dry-heat index was developed based on the APSIM crop model, which is capable of precisely quantifying compound dry and hot events during critical growth periods of wheat. To address the complex relationship between Australian wheat yields and compound dry-hot events, four interrelated studies were conducted.

(1) An indicator-based method using exposure, sensitivity, and adaptive capacity was used to assess the vulnerability of wheat yield to climate change in southeastern Australia's wheat belt. The mean climate vulnerability across the wheat belt decreased by 33% from 1924 to 1998. This is mainly due to increased adaptive capacity with the improvement of agronomic management practices, and technological and socio-economic progress. The areas with the highest vulnerability were in the northwestern regions of the wheat belt while the least vulnerable areas were located in the southeast.

(2) Based on the simulated wheat phenology and plant available water using the APSIM model, a daily scale compound dry and hot (DH) index was developed. Meanwhile, by utilizing the APSIM model, we quantified the potential of adjusting sowing time and changing cultivars to reduce the risk of DH. The frequency, duration, and intensity of DH events were projected to increase by 49%, 44%, and 5% in 2100, respectively. Such increases in DH events were mainly due to enhanced heat events. Early sowing and planting of wheat cultivars with early flowering had great potential to lower the risk of future DH events.

(3) A biophysical-statistical hybrid modeling approach was used to quantify the impacts of drought, heat, frost, and compound drought and extreme temperature (DET) events on wheat yield variations in Australia. During the past three decades, individual drought, heat, and frost events contributed to 45% of yield variation, while the percentage increased to 55% after including DET events. In

extreme low-yield years, the relative importance of DET events surpassed the sum importance of individual drought, heat, and frost events.

(4) Based on the analytical methods of composite difference and joint probability distribution, assessed the connections between large-scale climate drivers of El Niño Southern Oscillation (ENSO)/ Indian Ocean Dipole (IOD) and compound drought and extreme temperature events across Australia's wheat belt. The impacts of ENSO and IOD varied across different phases and distinct temporal periods. The eastern part of Australia's wheat belt was more responsive to ENSO and IOD than the western parts. Specifically, El Niño and positive IOD phases were associated with greater intensity of compound drought and extreme temperature (DETI) and greater probability of occurring high-intensity DET events, whereas La Niña and negative IOD phases tend to result in lower DETI and lower probability of occurring high-intensity DET events, compared to the neutral conditions.

This study highlights the need to factor compound dry and hot events into climate risk management to inform agricultural production under the changing climate.

Chapter 1. Introduction

1.1 Research background

Compound dry and hot extremes describe simultaneous occurrences of drought and heat events in both time and space. In recent decades, such compound extremes have gained increased attention due to their significantly more destructive impacts on society and the environment compared to the effects of individual extremes. For the agricultural sector, compound dry and hot extremes have been linked to severe yield losses and crop failure. Moreover, in the context of global warming, compound dry and hot extremes are expected to increase and escalate, which will pose significant challenges to crop production. Thus, it is crucial to quantify the characteristics and influences of compound dry and hot extremes, as well as to identify future changes and potential agronomic adaptations, in order to achieve sustainability in crop production under climate change. We will include a comprehensive literature review covering climate change, weather and climate extremes, compound extremes and their impacts, and methods used to explore the connection between climate and crop yields. With the aim of demonstrating the background information essential for this Ph.D. project.

1.1.1 Climate change

There is clear evidence from long term and large scale observations that the climate is changing globally. This is supported by definitive conclusions drawn from the Intergovernmental Panel on Climate Change (IPCC) in the Fifth and Sixth Assessment Reports (AR5&AR6) (Lee et al., 2023; Pachauri et al., 2014).

1). Over the past two centuries, the global surface temperature has risen by more than 1°C, with the rate of warming accelerating in recent decades.

2). Changes in precipitation patterns have been observed to vary across different regions globally. Specifically, global precipitation over land in mid-latitude regions has seen an increase since 1950, with a more rapid rate of increase occurring since the 1980s.

3). The climate and weather extreme events, including hot extremes, agricultural drought, and heavy rain, have increased in both frequency and intensity since the 1950s.

4). The rising emissions of greenhouse gases are the primary driver of climate change. Without effective control and mitigation measures, all components of the climate system will continue changing.

In line with global warming trends, Australia's average continental temperature has risen by 0.8°C since 1910, with the majority of this increase occurring post-1950 (Hughes, 2003). Additionally, the rate of increase in minimum temperatures has outpaced that of maximum temperatures. Although there has been a

slight rise in annual total rainfall across Australia since 1900, the pattern of these changes is more complex on both regional and seasonal levels. The northern, eastern, and southern parts of the continent have seen increases in rainfall, whereas the western areas have experienced decreases. Seasonally, there is a decrease in autumn and winter rainfall, contrasted with increases during spring and summer. Future climate projections for Australia indicate a continuing trend of rising temperatures, characterized by more extremely hot days and fewer extremely cool days. Additionally, there is an expectation of increased extreme rainfall events across much of the country (Csiro and BOM, 2015).

1.1.2 Climate and weather extreme events

The climate system is undergoing a substantial change characterized by global warming (IPCC, 2014). This warming trend does more than just raise surface temperatures; it also intensifies the hydrological cycle, resulting in shifts in rainfall patterns (Liu and Allan, 2013) and heightened variability in both rainfall and temperature (Gourdji et al., 2013). Consequently, these changes are expected to amplify the frequency and severity of weather and climate extreme events (Planton et al., 2008; Zheng et al., 2012). Climate and weather extremes are defined as occurrences that significantly deviate from the typical climate and weather patterns observed in a specific region or time frame, relative to historical averages. Including heatwave, low temperature, drought, and frost, etc (IPCC, 2012).

These extremes pose notable challenges to human society and the natural environment, such as agriculture, economics, public health (Easterling et al., 2000). Among them, the adverse impacts of extreme events on agricultural production not only threaten food security but also result in significant economic losses (Lesk et al., 2016). Extreme weather events typically emerge and evolve rapidly, making them difficult to forecast. They can affect the physiological and biochemical processes of crops, and even directly cause physical damage (Poudel et al., 2020; Prasad et al., 2008), eventually leading to crop yield reduction or crop failure (Vogel et al., 2019). Comprehending the impacts of various extreme conditions on the growth and development of crop is essential for helping crops withstand these negative impacts.

1.1.2.1 Heat

Heat events is a major problem that plagues agricultural production. It was pointed out to be responsible for the 3.0% reduction in global total grain production from 2000 to 2007 (Lesk et al., 2016). The instances included the remarkably hot summer of 2010 in western Russia, with daily maximum temperatures exceeding climatological norms by 5 to 15 °C (Schumacher et al., 2019b). Wheat in this region experienced the hottest July since 1880, resulting in a loss of over half the grain harvest compared to the previous year (Christian et al., 2020; Wegren, 2011). The severe reduction in wheat production prompted Russia to impose an export ban, leading to a significant surge in global wheat prices that year (Welton, 2011). A similar recent

event occurred in the USA, where the heat wave from May to July 2012 significantly impacted the corn belt, leading to a reduction in maize production by 13% compared to the production in 2011. (Chung et al., 2014).

Heat stress affects crops in several ways, impacting their growth, development, and productivity. Specifically, heat can impair the photosynthetic process by breakdown of photosynthetic enzymes, increase transpiration rates, accelerate crop development and shorten the growth cycle, inhibit protein synthesis and alter nutrient allocation, reduce enzymatic activity etc. (Eyshi Rezaei et al., 2015; Hassan et al., 2021; Lipiec et al., 2013). Nevertheless, the effects of heat on crops vary depending on the specific growth stages of the crops. The heat events occurring in the reproductive stage is more harmful than that occurring during the vegetative stage, directly reducing the number and weight of grains. For instance, heat stress at wheat flowering stage reduces the grain number, and heat stress at wheat grain-filling stage decreases the grain size (Liu et al., 2016). Based on the nine years of satellite data tracking wheat growth in India, Lobell et al. (2012) proved that heat stress (greater than 34°C) significantly accelerate the senescence rate of wheat. Accelerated senescence shortens the flowering period and the pollination window. Meanwhile, heat stress can create non-reversible morphological abnormalities in floral organs (stigmas, styles, pollen and ovaries), and reduce fertilization efficiency and pollen viability. Then reduce the number of fertile grains (Prasad and Djanaguiraman, 2014; Talukder et al., 2014). Concurrently, the accelerated senescence abbreviates the duration available for grain filling (Stone et al., 1995). Moreover, this accelerated aging reduces the green leaf area, restricting photosynthesis and thereby decreasing the availability of photoassimilates supply for grain filling (Talukder et al., 2014). It also reduces the activity of key enzymes responsible for starch accumulation in wheat grains, thereby slowing starch accumulation and reducing grain growth (Zhao et al., 2008).

1.1.2.2 Drought

Drought is the main challenge of the rain-fed cropping system, it caused 3.2% loss of global total grain production (Lesk et al., 2016). Typically, over half of the land cultivated with wheat experiences periodic drought (Rajaram, 2001). A notable instance occurred in January 2018 when a flash drought led to a 53% decrease in winter crop production in eastern Australia, relative to the average of the previous two decades (Feng et al., 2020). From 1933 to 1939, ongoing droughts led to significant wheat yield losses each year across the Great Plains in USA, with the losses peaking at 32% in 1933 (Warrick, 1984).

Wheat is commonly subjected to drought conditions across its growth cycle, the negative effects are significantly more pronounced when drought strikes during the reproductive stages, such as the anthesis and grain-filling stages (Reynolds et al., 2005). Such drought occurrences are classified as terminal drought. Predominantly in Mediterranean climates, terminal drought presents a recurring impediment to wheat

production, frequently culminating in significant yield losses (Reynolds et al., 2005; Turner, 2004). Drought resulted in the lack of water supply for wheat, the impacted magnitude depends on the severity and duration of this water defict. During the wheat reproductive phase, insuffcient water supply not only accelerates leaf senescence to reduce the photosynthesis and photosynthetic production (Farooq et al., 2014; Farooq et al., 2009), but also reduce carbon fixation and assimilate translocation rates (Asada, 2006). These processes restrict grain development and eventually result in reduction in grain weight. Meanwhile, drought in reproductive phase may induce pollen sterility, which influence grain set then reduce the number of fertile grains (Cattivelli et al., 2008).

1.1.2.3 Frost

Frost also represents a significant threat to crop growth. From a regional perspective, yield losses attributed to frost typically average around 10%, but in areas particularly vulnerable to frost, such as parts of the USA and Australia, losses can exceed 80% (Boer et al., 1993; Paulsen and Heyne, 1983).

Frost adversely affects the growth of crops at any growth stage, it can cause irreversible damage to different parts of crops at different growth stages (Al-Issawi et al., 2013; Fuller et al., 2007). At early stages, wheat is susceptible to frost, which can cause leaf damage and scorching, with severe frost potentially resulting in seedling death (Fuller et al., 2007). During the booting stage, frost can harm the wheat stem; damage to the upper part may may lead to head loss (Frederiks et al., 2008), while damage to the lower part can increase the risk of lodging (Barlow et al., 2015). If frost occurs when the spike has formed but before anthesis, it may lead to damage to the spike through the production of sterile florals, thereby decreasing the number of grains (Frederiks et al., 2008). During the early flowering stage, exposure to frost can result in the mortality of embryos and anthers, leading to sterility in florets and spikelets (Cromey et al., 1998). Additionally, frost can harm the partially filled grains and may even cause grain death during grain-filling stage, ultimately decreasing both the weight and number of grains (Cromey et al., 1998).

1.1.3 Compound dry and hot events

What's worse, climate and weather extreme events do not just appear independently, they often appear together and interact with each other (Lesk et al., 2021; Prasad et al., 2008). Just like 2003, 2010, and 2018, Europe experienced mega-heatwaves coinciding with severe soil water deficits (Buras et al., 2020; Ciais et al., 2005). In 2010, the extreme dry heat weather happened in Russia (Schumacher et al., 2019a). What's more, in the summer of 2013-2014, outstanding concurrent drought and heatwave conditions occurred in Brazil (Geirinhas et al., 2021). During the period of 1980-2017, the intensity and duration of heatwaves in China were aggravated by the drought that concurrent (Shi et al., 2021). There is also the long-term drought accompanied repeated heatwaves, aroused concerns due to the summer mega-bushfire in Australia in 2019

(Nolan et al., 2020). The negative effects caused by such compound climate and weather extreme events are often more serious than the extreme events that occurred alone (Heino et al., 2023; Li et al., 2022). For example, compared with single heat or drought, compound extreme events caused a more serious crop yield reduction, 65% compared to 33 and 48%, respectively (Li et al., 2022). Compared with alone drought, compound extreme events led to more yield loss, increasing from 9% to 11%. What's more, this effect was more obvious in comparation with heat independently, increasing from 19% to 29% (Ribeiro et al., 2020). Besides, under the general trend of global warming, there will be an increase in the frequency, intensity, and duration of compound extreme events (Mukherjee and Mishra, 2021). They may gradually become the main factors restricting agricultural production (Li et al., 2022).

The influence of compound events cannot be represented by the mere aggregation of the impacts stemming from their individual components. This is primarily due to, firstly, the interactions among the component events, which often exacerbate their collective effects (Lesk et al., 2022). Specifically, for compound dry and hot events, the interaction between drought and heat events is significantly influenced by the soil moisture-temperature feedback (Bastos et al., 2021; Benson and Dirmeyer, 2021; Berg et al., 2016; Zscheischler and Seneviratne). This interaction can be delineated through two key processes: 1. Dry soil and plants restrict evapotranspiration (and latent heat flux), which not only potentially increases surface air temperature and sensible heat flux but also diminishes precipitation. This occurs because the amount of moisture released into the atmosphere decreases, leading to less cloud formation and, consequently, reduced precipitation. 2. The elevated evapotranspiration, driven by high vapor pressure deficit (VPD) and radiation during heat events, tends to exhaust soil moisture, culminating in soil water deficits or drought conditions (Hao et al., 2022).

Secondly, simultaneously occurring extreme events exhibit synergistic impacts on crops, driven by complex physiological interactions within the plant that ultimately affect yield (Lesk et al., 2022). For example, compared to individual drought or heat events, compound dry-hot events further shorten the crop growth period, reducing the time available for overall assimilate accumulation (Awasthi et al., 2014; Cohen et al., 2021). This adversely affects biomass accumulation and the number and weight of grains. Drought and heat can individually decrease stomatal conductance, but compound dry-hot exacerbates this reduction (Rizhsky et al., 2004; Mittler, 2006) and significantly decreases chlorophyll content (Qaseem et al., 2019), severely limiting photosynthesis. Furthermore, compound events escalate cellular respiration demands for carbohydrates, leading to a scenario of low output and high consumption that disrupts the carbon balance (Zhao et al., 2013). During the reproductive phase, drought can induce pollen sterility (Yu et al., 2019), and when combined with heat, it further reduces pollen viability and damages floral organs (Fábián et al., 2019; Jiang et al., 2019). This increases the probability and severity of floral and fruit abortion, ultimately

resulting in a significant decrease in grain yield. Moreover, compared to individual extreme events, compound events more profoundly decrease the activity of key enzymes in the starch biosynthesis pathway, thereby severely reducing the grain-filling rate (Cohen et al., 2021).

1.1.4 Adaptative strategies

To mitigate the negative impacts of weather and climate extreme events on agriculture and food security, many researchers were committed to finding suitable adaptation strategies to adjust agricultural production (Vogel et al., 2019). They mainly included land use and land cover change (Hong et al., 2022), improving cultivation practices (Korres et al., 2017), and developing crop varieties (Gouache et al., 2012). Among them, land cover and land use change affect the physical and biochemical processes of the land surface by changing the land surface characteristics, therefore affecting the regional and global climate (Mahmood et al., 2014). Selecting suitable land use scenarios can predict extreme temperature and extreme precipitation events by 14% and 118.4%, respectively (Hong et al., 2022). Improving cultivation and management practices is an effective means to alleviate the adverse impacts of extreme weathers, and they are also common and easy-to-implement strategies for farmers (Bahinipati and Venkatachalam, 2015). Specific practices include variety selection, sowing date adjustment, irrigation, and crop residue incorporation, etc. Selecting varieties and adjusting sowing dates can make the key growth stages of crops escape from extreme weather events (Collins and Chenu, 2021; Shavrukov et al., 2017), and measures such as irrigation and residue incorporation can alleviate the damage of extreme events to crops, thus reducing yield loss (Behzadnejad et al., 2020; Troy et al., 2015). The breeding of extreme tolerance crop varieties is a long-term adaptation, which is considered to be the most promising measure. Even under the climate change conditions in the far future, it is still expected to effectively reduce the negative impacts of extreme weather events on crops (Collins and Chenu, 2021; Gouache et al., 2012). At present, most of the adaptive studies were aimed at a single extreme event, and it is not clear whether these adaptations are effective for compound events or not.

1.1.5 Process-based crop model

Process-based crop models are computational tools designed to describe the responses of crop growth and yield to management, soil, crop species characteristics, and climate (Thorp et al., 2014). During the recent decades, several process-based crop models were developed, such as Crop Environment Resource Synthesis (CERES), WOrld FOod Studies (WOFOST), and Agricultural Production Systems sIMulator (APSIM) (Hadiya et al., 2018). These models integrate knowledge from disciplines such as crop physiology, climatology, and soil science, providing guidance for crop management and research (Jones et al., 2017; Thorp et al., 2014).

For example, utilizing the CERES-Maize model, Kapetanaki and Rosenzweig (1997) determined that maize yields are expected to decline under future climate scenarios using current management practices. However, strategies such as earlier sowing dates and the introduction of new maize varieties with extended grain-filling periods could counteract this reduction. Similarly, Khordadi et al. (2019) applied the WOFOST and AquaCrop models to assess yield fluctuations for maize and wheat in northeast Iran due to climate change. Their findings indicated potential yield decreases of 8%-34% by 2040, noting that adjusting sowing times and selecting appropriate cultivars could help mitigate these anticipated losses. Furthermore, Kouadio et al. (2015) employed the APSIM-wheat model to forecast wheat yields in Canada under future climate conditions, projecting losses of 24%-94% with existing management techniques. Adopting an earlier sowing strategy was identified as a viable approach to mitigate the impact of climate change on Canada's spring wheat.

Nevertheless, most of process-based crop models face challenges in accurately capturing the responses of crops to climate and weather extreme events (Palosuo et al., 2011), particularly concerning the impact of heat events on the growth and development of crops (Wheeler et al., 2000). Additionally, using crop models for climate impact assessment introduces significant uncertainty, particularly regarding model structure. Different crop models diverge in their foundational assumptions, algorithms, and parameter configurations. As a result, even when given identical inputs, they can produce disparate results (Asseng et al., 2001). Palosuo et al. (2011) evaluated the capabilities of eight widely used crop models to simulate wheat yields under different climatic conditions across Europe, and found that despite rigorous calibration, the simulation outcomes from these models varied considerably.

1.2. Research problems and objectives

At Present, numerous studies are focused on individual drought (Collins and Chenu, 2021; Feng et al., 2019a) or heat (Deryng et al., 2014; Teixeira et al., 2013), revealing their historical and future characteristics and changes, and quantifying their impacts on crop yields, to put forward and evaluate the corresponding adaptation strategies. This probably underestimates the climate risk in agricultural production, and because of they ignored the interaction of drought and heat (Zscheischler et al., 2018). In recent years, indeed, more and more researchers have begun to pay attention to the impact of DH on agricultural production (Lesk et al., 2021; Sedlmeier et al., 2018). However, most of them are based on control experiments (Elferjani and Soolanayakanahally, 2018; Ostmeyer et al., 2020), and it is hard to apply this method to different regions to assess the characteristics and impacts of DH due to the huge spatial variability in soil and climate factors. A few studies have also discussed the related impacts of DH in a large area, but most of them are based on years, seasons, or months scales (Geirinhas et al., 2021; Ribeiro et al., 2020; Shi et al., 2021), or based on the empirical crop growing season (Li et al., 2022). They have not focused on the critical growth stage of

crops, so the obtained results may not be accurate enough. Moreover, due to the influence of climate change, the future growth periods of crops may be advanced (Xiao et al., 2020), it is unreasonable to choose fixed or empirical month intervals, because it may stagger the key growth stages of crops. Furthermore, research on the impacts of compound extreme events on crops has predominantly centered on maize, given its summer growth season (Feng et al., 2019b; Guo et al., 2022). This focus leaves a notable knowledge gap regarding the effects on wheat.

Wheat ranks as the foremost extensively cultivated food crop globally (FAO, 2021) and serves as the primary food source for nearly 40% of the world's population (Giraldo et al., 2019). Australia, as one of the top five global wheat exporters, plays an important role in global food security, consistently contributing about 11% of global wheat exports since 1961 (FAO, 2021). Nevertheless, Australian wheat generally relies on rainfed, making it highly susceptible to climate variability (Feng et al., 2022). During the past decades, recurring drought in Australia has resulting large wheat yield losses (Chenu et al., 2013; Feng et al., 2020). Moreover, the increased incidence of heat and frost has been identified as a substantial challenge to Australian wheat production (Barlow et al., 2013; Zheng et al., 2012). The untimely frost in spring (Marcellos and Single, 1975) and the rising frequency of heat events during the wheat flowering and grain-filling stages (Ababaei and Chenu, 2020) both can simultaneously co-occur with drought events. However, to our knowledge, no study has quantified the impacts of compound dry and hot events on wheat in Australia.

This study was designed to systematically investigate the spatio-temporal characteristics of compound dry and hot events, as well as their effects on wheat yield across Australia's wheat belt, spanning from the previous century up to 2100. Meanwhile, this study also tries to identify the drivers of compound dry and hot events and examine potential agronomic strategies for mitigation. This study aims to address the following critical questions:

- How vulnerable is wheat to the adverse impacts of climate change?
- What is the historical evolution and future projection of compound dry-hot events?
- How did wheat yields respond to compound drought and extreme temperature events?
- What role do large-scale climatic drivers play in compound drought and extreme temperature events?

This study aims to:

- Quantify spatial and temporal changes in the vulnerability of wheat yields to historical climate change and identify the vulnerable hotspots.
- Quantify the changes in compound dry and hot events under historical and future climate conditions

using the APSIM model.

- Identify feasible agronomic adaptation to reduce the risk of future DH events.
- Evaluate the impacts of compound dry and hot events on Australia's wheat yields through a hybrid biophysical-statistical modeling approach.
- Assess the influence of large-scale climate drivers on compound dry and hot events occurring during the critical growth season of Australia's wheat.

1.3 Statement of Significance

Compound dry and hot events are more destructive than any single extreme event of drought or heat. The increasing heat events around wheat flowering and grain-filling stages can simultaneously co-occur with prolong drought in Australia. These compound dry and hot events exacerbate the adverse effects on wheat through complex heat–moisture and crop–atmosphere interactions. A thorough understanding of their evolution, impact, and driving factors can offer new insights into the comprehension of climate change impacts. Simultaneously, the findings of this study will improve stakeholders' capability to alleviate the adverse impacts of climate change.

1.4 Reference

Ababaei, B., Chenu, K., 2020. Heat shocks increasingly impede grain filling but have little effect on grain setting across the Australian wheatbelt. Agricultural and Forest Meteorology 284, 107889.

Al-Issawi, M., Rihan, H.Z., El-Sarkassy, N., Fuller, M.P., 2013. Frost Hardiness Expression and Characterisation in Wheat at Ear Emergence. Journal of Agronomy and Crop Science 199, 66-74.

Asada, K., 2006. Production and Scavenging of Reactive Oxygen Species in Chloroplasts and Their Functions. Plant Physiology 141, 391-396.

Asseng, S., Turner, N., Keating, B.A.J.P., 2001. Analysis of water-and nitrogen-use efficiency of wheat in a Mediterranean climate. Plant and Soil 233, 127-143.

Awasthi, R., Kaushal, N., Vadez, V., Turner, N.C., Berger, J., Siddique, K.H.M., Nayyar, H., 2014. Individual and combined effects of transient drought and heat stress on carbon assimilation and seed filling in chickpea. Functional Plant Biology 41, 1148-1167.

Bahinipati, C.S., Venkatachalam, L., 2015. What drives farmers to adopt farm-level adaptation practices to climate extremes: Empirical evidence from Odisha, India. International Journal of Disaster Risk Reduction 14, 347-356.

Barlow, K., Christy, B., O'Leary, G., Riffkin, P., Nuttall, J., 2013. Simulating the impact of extreme heat and frost events on wheat production: the first steps, 20th International Congress on Modelling and Simulation. Modelling and Simulation Society of Australia and New Zealand, Adelaide, Australia.

Barlow, K.M., Christy, B.P., O'Leary, G.J., Riffkin, P.A., Nuttall, J.G., 2015. Simulating the impact of extreme heat and frost events on wheat crop production: A review. Field Crops Research 171, 109-119.

Bastos, A., Orth, R., Reichstein, M., Ciais, P., Viovy, N., Zaehle, S., Anthoni, P., Arneth, A., Gentine, P., Joetzjer, E., 2021. Vulnerability of European ecosystems to two compound dry and hot summers in 2018 and 2019. Earth system dynamics 12, 1015-1035.

Behzadnejad, J., Tahmasebi-Sarvestani, Z., Aein, A., Mokhtassi-Bidgoli, A., 2020. Wheat Straw Mulching Helps Improve Yield in Sesame (Sesamum indicum L.) Under Drought Stress. International Journal of Plant Production 14, 389-400.

Benson, D.O., Dirmeyer, P.A., 2021. Characterizing the relationship between temperature and soil moisture extremes and their role in the exacerbation of heat waves over the contiguous United States. Journal of Climate 34, 2175-2187.

Berg, A., Findell, K., Lintner, B., Giannini, A., Seneviratne, S.I., van den Hurk, B., Lorenz, R., Pitman, A., Hagemann, S., Meier, A., Cheruy, F., Ducharne, A., Malyshev, S., Milly, P.C.D., 2016. Land–atmosphere feedbacks amplify aridity increase over land under global warming. Nature Climate Change 6, 869-874.

Boer, R., Campbell, L.C., Fletcher, D.J., 1993. Characteristics of frost in a major wheat-growing region of Australia. Australian Journal of Agricultural Research 44, 1731-1743.

Buras, A., Rammig, A., Zang, C.S., 2020. Quantifying impacts of the 2018 drought on European ecosystems in comparison to 2003. Biogeosciences 17, 1655-1672.

Cattivelli, L., Rizza, F., Badeck, F.-W., Mazzucotelli, E., Mastrangelo, A.M., Francia, E., Marè, C., Tondelli, A., Stanca, A.M., 2008. Drought tolerance improvement in crop plants: An integrated view from breeding to genomics. Field Crops Research 105, 1-14.

Chenu, K., Deihimfard, R., Chapman, S.C., 2013. Large-scale characterization of drought pattern: a continent-wide modelling approach applied to the Australian wheatbelt – spatial and temporal trends. New Phytologist 198, 801-820.

Christian, J.I., Basara, J.B., Hunt, E.D., Otkin, J.A., Xiao, X., 2020. Flash drought development and cascading impacts associated with the 2010 Russian heatwave. Environmental Research Letters 15, 094078.

Chung, U., Gbegbelegbe, S., Shiferaw, B., Robertson, R., Yun, J.I., Tesfaye, K., Hoogenboom, G., Sonder, K., 2014. Modeling the effect of a heat wave on maize production in the USA and its implications on food security in the developing world. Weather and Climate Extremes 5-6, 67-77.

Ciais, P., Reichstein, M., Viovy, N., Granier, A., Ogée, J., Allard, V., Aubinet, M., Buchmann, N., Bernhofer, C., Carrara, A., Chevallier, F., De Noblet, N., Friend, A.D., Friedlingstein, P., Grünwald, T., Heinesch, B., Keronen, P., Knohl, A., Krinner, G., Loustau, D., Manca, G., Matteucci, G., Miglietta, F., Ourcival, J.M., Papale, D., Pilegaard, K., Rambal, S., Seufert, G., Soussana, J.F., Sanz, M.J., Schulze, E.D., Vesala, T., Valentini, R., 2005. Europe-wide reduction in primary productivity caused by the heat and drought in 2003. Nature 437, 529-533.

Cohen, I., Zandalinas, S.I., Huck, C., Fritschi, F.B., Mittler, R., 2021. Meta-analysis of drought and heat stress combination impact on crop yield and yield components. Physiologia Plantarum 171, 66-76.

Collins, B., Chenu, K., 2021. Improving productivity of Australian wheat by adapting sowing date and genotype phenology to future climate. Climate Risk Management 32, 100300.

Cromey, M.G., Wright, D.S.C., Boddington, H.J., 1998. Effects of frost during grain filling on wheat yield and grain structure. New Zealand Journal of Crop and Horticultural Science 26, 279-290.

Csiro, BOM, 2015. Climate change in Australia information for Australia's natural resource management regions: technical report. CSIRO and Bureau of Meteorology Australia.

Deryng, D., Conway, D., Ramankutty, N., Price, J., Warren, R., 2014. Global crop yield response to extreme heat stress under multiple climate change futures. Environmental Research Letters 9, 034011.

Easterling, D.R., Meehl, G.A., Parmesan, C., Changnon, S.A., Karl, T.R., Mearns, L.O., 2000. Climate Extremes: Observations, Modeling, and Impacts. Science 289, 2068-2074.

Elferjani, R., Soolanayakanahally, R., 2018. Canola Responses to Drought, Heat, and Combined Stress: Shared and Specific Effects on Carbon Assimilation, Seed Yield, and Oil Composition. Frontiers in Plant Science 9.

Eyshi Rezaei, E., Webber, H., Gaiser, T., Naab, J., Ewert, F., 2015. Heat stress in cereals: Mechanisms and modelling. European Journal of Agronomy 64, 98-113.

Fábián, A., Sáfrán, E., Szabó-Eitel, G., Barnabás, B., Jäger, K., 2019. Stigma functionality and fertility are reduced by heat and drought co-stress in wheat. Frontiers in Plant Science 10, 244.

FAO, 2021. The Food and Agriculture Organization of the United Nations. Statistic data base. https://www.fao.org/faostat/en/#data/QCL. The last accessed date: 25 May 2021.

Farooq, M., Hussain, M., Siddique, K.H.M., 2014. Drought Stress in Wheat during Flowering and Grain-filling Periods. Critical Reviews in Plant Sciences 33, 331-349.

Farooq, M., Wahid, A., Kobayashi, N., Fujita, D., Basra, S.M.A., 2009. Plant drought stress: effects, mechanisms and management. Sustainable agriculture, 153-188.

Feng, P., Liu, D.L., Wang, B., Waters, C., Zhang, M., Yu, Q., 2019a. Projected changes in drought across the wheat belt of southeastern Australia using a downscaled climate ensemble. International Journal of Climatology 39, 1041-1053.
Feng, P., Wang, B., Luo, J.-J., Liu, D.L., Waters, C., Ji, F., Ruan, H., Xiao, D., Shi, L., Yu, Q., 2020. Using large-scale climate drivers to forecast meteorological drought condition in growing season across the Australian wheatbelt. Science of The Total Environment 724, 138162.
Feng, P., Wang, B., Macadam, I., Taschetto, A.S., Abram, N.J., Luo, J.-J., King, A.D., Chen, Y., Li, Y., Liu, D.L., Yu, Q., Hu, K., 2022. Increasing dominance of Indian Ocean variability impacts Australian wheat yields. Nature Food 3, 862-870.
Feng, S., Hao, Z., Zhang, X., Hao, F., 2019b. Probabilistic evaluation of the impact of compound dry-hot events on global maize yields. Science of The Total Environment 689, 1228-1234.
Frederiks, T.M., Christopher, J.T., Borrell, A.K., 2008. Low temperature adaption of wheat post head-emergence in northern Australia.
Fuller, M.P., Fuller, A.M., Kaniouras, S., Christophers, J., Fredericks, T., 2007. The freezing characteristics of wheat at ear emergence. European Journal of Agronomy 26, 435-441.
Geirinhas, J.L., Russo, A., Libonati, R., Sousa, P.M., Miralles, D.G., Trigo, R.M., 2021. Recent increasing frequency of compound summer drought and heatwaves in Southeast Brazil. Environmental Research Letters 16, 034036.
Giraldo, P., Benavente, E., Manzano-Agugliaro, F., Gimenez, E., 2019. Worldwide Research Trends on Wheat and Barley: A Bibliometric Comparative Analysis. Agronomy 9, 352.
Gouache, D., Le Bris, X., Bogard, M., Deudon, O., Pagé, C., Gate, P., 2012. Evaluating agronomic adaptation options to increasing heat stress under climate change during wheat grain filling in France. European Journal of Agronomy 39, 62-70.
Gourdji, S.M., Sibley, A.M., Lobell, D.B., 2013. Global crop exposure to critical high temperatures in the reproductive period: historical trends and future projections. Environmental Research Letters 8, 024041.
Guo, Y., Lu, X., Zhang, J., Li, K., Wang, R., Rong, G., Liu, X., Tong, Z., 2022. Joint analysis of drought and heat events during maize (Zea mays L.) growth periods using copula and cloud models: A case study of Songliao Plain. Agricultural Water Management 259, 107238.
Hadiya, N.J., Kumar, N., Mote, B.M., 2018. Use of WOFOST model in agriculture-A review. Agricultural Reviews 39, 234-240.
Hao, Z., Hao, F., Xia, Y., Feng, S., Sun, C., Zhang, X., Fu, Y., Hao, Y., Zhang, Y., Meng, Y., 2022. Compound droughts and hot extremes: Characteristics, drivers, changes, and impacts. Earth-Science Reviews, 104241.
Hassan, M.U., Chattha, M.U., Khan, I., Chattha, M.B., Barbanti, L., Aamer, M., Iqbal, M.M., Nawaz, M., Mahmood, A., Ali, A., 2021. Heat stress in cultivated plants: Nature, impact, mechanisms, and mitigation strategies—A review. Plant Biosystems-An International Journal Dealing with all Aspects of Plant Biology 155, 211-234.
Heino, M., Kinnunen, P., Anderson, W., Ray, D.K., Puma, M.J., Varis, O., Siebert, S., Kummu, M., 2023. Increased probability of hot and dry weather extremes during the growing season threatens global crop yields. Scientific Reports 13, 3583.
Hong, T., Wu, J., Kang, X., Yuan, M., Duan, L., 2022. Impacts of Different Land Use Scenarios on Future Global and Regional Climate Extremes. Atmosphere 13, 995.
Hughes, L., 2003. Climate change and Australia: Trends, projections and impacts. Austral Ecology 28, 423-443.
IPCC, 2014. Climate Change 2014: Synthesis Report. Contribution of Working Groups I, II and III to the Fifth Assessment Report of the Intergovernmental Panel on Climate Change [Core Writing Team, R.K. Pachauri and L.A. Meyer (eds.)]. IPCC, Geneva, Switzerland, 151 pp.
IPCC, 2012. Managing the risks of extreme events and disasters to advance climate change adaptation. Special report of the Intergovernmental Panel on Climate Change. Journal of Clinical Endocrinology & Metabolism, 18(6): 586-599.
Jiang, Y., Davis, A.R., Vujanovic, V., Bueckert, R.A., 2019. Reproductive development response to high daytime temperature in field pea. Journal of Agronomy and Crop Science 205, 324-333.
Jones, J.W., Antle, J.M., Basso, B., Boote, K.J., Conant, R.T., Foster, I., Godfray, H.C.J., Herrero, M., Howitt, R.E., Janssen, S., Keating, B.A., Munoz-Carpena, R., Porter, C.H., Rosenzweig, C., Wheeler, T.R., 2017.

Toward a new generation of agricultural system data, models, and knowledge products: State of agricultural systems science. Agricultural Systems 155, 269-288.
Kapetanaki, G., Rosenzweig, C., 1997. Impact of Climate Change on Maize Yield in Central and Northern Greece: A Simulation Study with Ceres-Maize. Mitigation and Adaptation Strategies for Global Change 1, 251-271.
Khordadi, M.J., Olesen, J.E., Alizadeh, A., Nassiri Mahallati, M., Ansari, H., Sanaeinejad, H., 2019. CLIMATE CHANGE IMPACTS AND ADAPTATION FOR CROP MANAGEMENT OF WINTER WHEAT AND MAIZE IN THE SEMI-ARID REGION OF IRAN. Irrigation and Drainage 68, 841-856.
Korres, N.E., Norsworthy, J.K., Burgos, N.R., Oosterhuis, D.M., 2017. Temperature and drought impacts on rice production: An agronomic perspective regarding short-and long-term adaptation measures. Water resources and rural development 9, 12-27.
Kouadio, L., Newlands, N., Potgieter, A., McLean, G., Hill, H., 2015. Exploring the potential impacts of climate variability on spring wheat yield with the APSIM decision support tool. Agricultural Sciences 6, 686-698.
Lee, H., Calvin, K., Dasgupta, D., Krinner, G., Mukherji, A., Thorne, P., Trisos, C., Romero, J., Aldunce, P., Barrett, K., 2023. Climate change 2023: synthesis report. Contribution of working groups I, II and III to the sixth assessment report of the intergovernmental panel on climate change.
Lesk, C., Anderson, W., Rigden, A., Coast, O., Jägermeyr, J., McDermid, S., Davis, K., Konar, M., 2022. Compound heat and moisture extreme impacts on global crop yields under climate change. Nature Reviews Earth & Environment 3, 872–889.
Lesk, C., Coffel, E., Winter, J., Ray, D., Zscheischler, J., Seneviratne, S.I., Horton, R., 2021. Stronger temperature–moisture couplings exacerbate the impact of climate warming on global crop yields. Nature Food 2, 683-691.
Lesk, C., Rowhani, P., Ramankutty, N., 2016. Influence of extreme weather disasters on global crop production. Nature 529, 84-87.
Li, E., Zhao, J., Pullens, J.W.M., Yang, X., 2022. The compound effects of drought and high temperature stresses will be the main constraints on maize yield in Northeast China. Science of The Total Environment 812, 152461.
Lipiec, J., Doussan, C., Nosalewicz, A., Kondracka, K., 2013. Effect of drought and heat stresses on plant growth and yield: a review. International Agrophysics 27.
Liu, B., Asseng, S., Liu, L., Tang, L., Cao, W., Zhu, Y., 2016. Testing the responses of four wheat crop models to heat stress at anthesis and grain filling. Global Change Biology 22, 1890-1903.
Liu, C., Allan, R.P., 2013. Observed and simulated precipitation responses in wet and dry regions 1850–2100. Environmental Research Letters 8, 034002.
Lobell, D.B., Sibley, A., Ivan Ortiz-Monasterio, J., 2012. Extreme heat effects on wheat senescence in India. Nature Climate Change 2, 186-189.
Mahmood, R., Pielke Sr, R.A., Hubbard, K.G., Niyogi, D., Dirmeyer, P.A., McAlpine, C., Carleton, A.M., Hale, R., Gameda, S., Beltrán-Przekurat, A., Baker, B., McNider, R., Legates, D.R., Shepherd, M., Du, J., Blanken, P.D., Frauenfeld, O.W., Nair, U.S., Fall, S., 2014. Land cover changes and their biogeophysical effects on climate. International Journal of Climatology 34, 929-953.
Marcellos, H., Single, W., 1975. Temperatures in wheat during radiation frost. Australian Journal of Experimental Agriculture 15, 818-822.
Mittler, R., 2006. Abiotic stress, the field environment and stress combination. Trends in Plant Science 11, 15-19.
Mukherjee, S., Mishra, A.K., 2021. Increase in Compound Drought and Heatwaves in a Warming World. Geophysical Research Letters 48, e2020GL090617.
Nolan, R.H., Boer, M.M., Collins, L., Resco de Dios, V., Clarke, H.G., Jenkins, M., Kenny, B., Bradstock, R.A.J.G.c.b., 2020. Causes and consequences of eastern Australia's 2019-20 season of mega-fires.
Ostmeyer, T., Parker, N., Jaenisch, B., Alkotami, L., Bustamante, C., Jagadish, S.V.K., 2020. Impacts of heat, drought, and their interaction with nutrients on physiology, grain yield, and quality in field crops. Plant Physiology Reports 25, 549-568.

Pachauri, R.K., Allen, M.R., Barros, V.R., Broome, J., Cramer, W., Christ, R., Church, J.A., Clarke, L., Dahe, Q., Dasgupta, P., 2014. Climate change 2014: synthesis report. Contribution of Working Groups I, II and III to the fifth assessment report of the Intergovernmental Panel on Climate Change. Ipcc.

Palosuo, T., Kersebaum, K.C., Angulo, C., Hlavinka, P., Moriondo, M., Olesen, J.E., Patil, R.H., Ruget, F., Rumbaur, C., Takáč, J., Trnka, M., Bindi, M., Çaldağ, B., Ewert, F., Ferrise, R., Mirschel, W., Şaylan, L., Šiška, B., Rötter, R., 2011. Simulation of winter wheat yield and its variability in different climates of Europe: A comparison of eight crop growth models. European Journal of Agronomy 35, 103-114.

Paulsen, G.M., Heyne, E.G., 1983. Grain Production of Winter Wheat after Spring Freeze Injury1. Agronomy Journal 75, 705-707.

Planton, S., Déqué, M., Chauvin, F., Terray, L., 2008. Expected impacts of climate change on extreme climate events. Comptes Rendus Geoscience 340, 564-574.

Poudel, P.B., Poudel, M.R.J.J.o.B., World, T.s., 2020. Heat stress effects and tolerance in wheat: A review. Journal of Biology and Today's World 9, 1-6.

Prasad, P.V.V., Djanaguiraman, M., 2014. Response of floret fertility and individual grain weight of wheat to high temperature stress: sensitive stages and thresholds for temperature and duration. Functional Plant Biology 41, 1261-1269.

Prasad, P.V.V., Staggenborg, S.A., Ristic, Z., 2008. Impacts of Drought and/or Heat Stress on Physiological, Developmental, Growth, and Yield Processes of Crop Plants, Response of Crops to Limited Water, pp. 301-355.

Qaseem, M.F., Qureshi, R., Shaheen, H., 2019. Effects of Pre-Anthesis Drought, Heat and Their Combination on the Growth, Yield and Physiology of diverse Wheat (Triticum aestivum L.) Genotypes Varying in Sensitivity to Heat and drought stress. Scientific Reports 9, 6955.

Rajaram, S., 2001. Prospects and promise of wheat breeding in the 21st century. Euphytica 119, 3-15.

Reynolds, M.P., Mujeeb-Kazi, A., Sawkins, M., 2005. Prospects for utilising plant-adaptive mechanisms to improve wheat and other crops in drought- and salinity-prone environments. Annals of Applied Biology 146, 239-259.

Ribeiro, A.F.S., Russo, A., Gouveia, C.M., Páscoa, P., Zscheischler, J.J.B., 2020. Risk of crop failure due to compound dry and hot extremes estimated with nested copulas. Biogeosciences 17, 4815-4830.

Rizhsky, L., Liang, H., Shuman, J., Shulaev, V., Davletova, S., Mittler, R., 2004. When Defense Pathways Collide. The Response of Arabidopsis to a Combination of Drought and Heat Stress Plant Physiology 134, 1683-1696.

Schumacher, D.L., Keune, J., Van Heerwaarden, C.C., Vilà-Guerau de Arellano, J., Teuling, A.J., Miralles, D.G., 2019a. Amplification of mega-heatwaves through heat torrents fuelled by upwind drought. Nature Geoscience 12, 712-717.

Schumacher, D.L., Keune, J., Van Heerwaarden, C.C., Vilà-Guerau de Arellano, J., Teuling, A.J., Miralles, D.G.J.N.G., 2019b. Amplification of mega-heatwaves through heat torrents fuelled by upwind drought. 12, 712-717.

Sedlmeier, K., Feldmann, H., Schädler, G.J.T., climatology, a., 2018. Compound summer temperature and precipitation extremes over central Europe. Theoretical and Applied Climatology 131, 1493-1501.

Shavrukov, Y., Kurishbayev, A., Jatayev, S., Shvidchenko, V., Zotova, L., Koekemoer, F., De Groot, S., Soole, K., Langridge, P., 2017. Early flowering as a drought escape mechanism in plants: how can it aid wheat production? Frontiers in plant science 8, 1950.

Shi, Z., Jia, G., Zhou, Y., Xu, X., Jiang, Y., 2021. Amplified intensity and duration of heatwaves by concurrent droughts in China. Atmospheric Research 261, 105743.

Stone, P.J., Savin, R., Wardlaw, I.F., Nicolas, M.E., 1995. The Influence of Recovery Temperature on the Effects of a Brief Heat Shock on Wheat. I. Grain Growth. Functional Plant Biology 22, 945-954.

Talukder, A.S.M.H.M., McDonald, G.K., Gill, G.S., 2014. Effect of short-term heat stress prior to flowering and early grain set on the grain yield of wheat. Field Crops Research 160, 54-63.

Teixeira, E.I., Fischer, G., van Velthuizen, H., Walter, C., Ewert, F., 2013. Global hot-spots of heat stress on agricultural crops due to climate change. Agricultural and Forest Meteorology 170, 206-215.

Thorp, K.R., Ale, S., Bange, M.P., Barnes, E.M., Hoogenboom, G., Lascano, R.J., McCarthy, A.C., Nair, S., Paz, J.O., Rajan, N., 2014. Development and application of process-based simulation models for cotton production: A review of past, present, and future directions. Journal of Cotton Science 18, 10-47.

Troy, T.J., Kipgen, C., Pal, I., 2015. The impact of climate extremes and irrigation on US crop yields. Environmental Research Letters 10, 054013.
Turner, N.C., 2004. Sustainable production of crops and pastures under drought in a Mediterranean environment. Annals of Applied Biology 144, 139-147.
Vogel, E., Donat, M.G., Alexander, L.V., Meinshausen, M., Ray, D.K., Karoly, D., Meinshausen, N., Frieler, K., 2019. The effects of climate extremes on global agricultural yields. Environmental Research Letters 14, 054010.
Warrick, R.A., 1984. The possible impacts on wheat production of a recurrence of the 1930s drought in the U.S. Great Plains. Climatic Change 6, 5-26.
Wegren, S.K., 2011. Food security and Russia's 2010 drought. Eurasian Geography and Economics 52, 140-156.
Welton, G., 2011. The impact of Russia's 2010 grain export ban. Oxfam Policy and Practice: Agriculture, Food and Land 11, 76-107.
Wheeler, T.R., Craufurd, P.Q., Ellis, R.H., Porter, J.R., Vara Prasad, P.V., 2000. Temperature variability and the yield of annual crops. Agriculture, Ecosystems & Environment 82, 159-167.
Xiao, D., Liu, D.L., Wang, B., Feng, P., Bai, H., Tang, J., 2020. Climate change impact on yields and water use of wheat and maize in the North China Plain under future climate change scenarios. Agricultural Water Management 238, 106238.
Yu, J., Jiang, M., Guo, C., 2019. Crop pollen development under drought: from the phenotype to the mechanism. International journal of molecular sciences 20, 1550.
Zhao, H., Dai, T., Jiang, D., Cao, W., 2008. Effects of High Temperature on Key Enzymes Involved in Starch and Protein Formation in Grains of Two Wheat Cultivars. Journal of Agronomy and Crop Science 194, 47-54.
Zhao, J., Hartmann, H., Trumbore, S., Ziegler, W., Zhang, Y., 2013. High temperature causes negative whole-plant carbon balance under mild drought. New Phytologist 200, 330-339.
Zheng, B., Chenu, K., Fernanda Dreccer, M., Chapman, S.C., 2012. Breeding for the future: what are the potential impacts of future frost and heat events on sowing and flowering time requirements for Australian bread wheat (Triticum aestivium) varieties? Global Change Biology 18, 2899-2914.
Zscheischler, J., Seneviratne, S.I., Dependence of drivers affects risks associated with compound events. Science Advances 3, e1700263.
Zscheischler, J., Westra, S., van den Hurk, B.J.J.M., Seneviratne, S.I., Ward, P.J., Pitman, A., AghaKouchak, A., Bresch, D.N., Leonard, M., Wahl, T., Zhang, X., 2018. Future climate risk from compound events. Nature Climate Change 8, 469-477.

Chapter 2. Assessing climate vulnerability of historical wheat yield in south-eastern Australia's wheat belt

This chapter is based on the following publication (journal paper):

Li, S., Wang, B., Feng, P., Liu, D.L., Li, L., Shi, L., Yu, Q., 2022. Assessing climate vulnerability of historical wheat yield in south-eastern Australia's wheat belt. Agricultural Systems 196, 103340.

Abstract

Agricultural vulnerability assessment is a comprehensive and powerful analytical tool to locate hotspots with states of susceptibility to harm and powerlessness of agricultural system. It plays an important role in guiding policy makers to plan and implement adaptation practices to mitigate potential climate risks to crop. However, due to the diversity in the methodology of vulnerability assessment, there are still knowledge gaps in assessing and comparing crop vulnerability to climate in different regions of the world, including Australia. Our main objectives were to: (1) present a vulnerability analytical method for wheat yield, which can be applied to different areas where long-term crop yield and climate data are available. (2) quantify temporal changes of the vulnerability of wheat yield to historical climate. (3) identify the most vulnerable region in study area to provide guidance for climate mitigation. Our study developed an indicator-based method using exposure, sensitivity, and adaptive capacity to assess the vulnerability of crop yield. We used the long-term recorded wheat yield data, combining with comprehensive exposure index to assess climate vulnerability of historical yield with a case study area of southeastern Australia's wheat belt. The results showed that from the 1930s to the 1990s, both climate exposure and sensitivity had large inter-annual variations with no significant trends detected. However, adaptive capacity increased by 34% from 1930s to 1950s, 54% from 1950s to 1970s, and 54% from 1970s to 1990s. By contrast, climate vulnerability across the wheat belt decreased by 13% from 1930s to 1950s, 15% from 1950s to 1970s, and 33% from 1970s to 1990s. This is mainly due to increased adaptive capacity with the improvement of agronomic management practices, technological and socio-economic progress. We identified the areas with the highest vulnerability were in the northwestern parts of wheat belt while the least vulnerable areas located in the southeast. We expect that these identified vulnerable hotspots can be used by different landholders to allocate natural resources and policymakers to plan the priority mitigation to adapt to climate change in the local scale. Moreover, the method of vulnerability assessment used in this study can be applied to other regions around the world where long-term crop yield and climate data are available.

Keywords: Climate vulnerability; Wheat yield; Exposure index; Adaptive capacity; Wheat belt; South-eastern Australia

2.1 Introduction

Climate change has great impacts on agro-ecological environments, leading to significant changes in crop productivity (Yang et al., 2015; Kurukulasuriya and Mendelsohn, 2008). For example, from 1980 to 2008, global wheat yield has decreased by 1.4%-2.0% per decade due to the warming climate (Lobell et al., 2011). The cycles of droughts and flooding associated with the El Niño phenomenon have explained between 15% and 35% of global yield variability (Howden et al., 2007). The unstable crop yield may increase difficulty of maintaining global food security with the growing world population (Ray et al., 2013).

Numerous studies have used vulnerability assessment to assess the impacts of climate change on agricultural crop yield (Lal et al., 1998; Li et al., 2014; Sonkar et al., 2019). Climate vulnerability of crop yield can be defined as the "degree that crop is susceptible to, or unable to cope with, adverse effects of climate change, including climate variability and extremes" (McCarthy et al., 2001; IPCC, 2007; IPCC, 2012). It is a function of the sensitivity, exposure, and adaptive capacity of crop yield to climate change. Vulnerability assessment for crop yield can not only assess the impact of climate change and socio-economic development on crop productivity, but also analyze the effectiveness and adaptability of different agronomic adaptations (Kamali et al., 2018b; Wang et al., 2020). It is a powerful analytical tool to locate hotspots with states of susceptibility to harm and powerlessness (Adger, 2006), which can guide policy makers to plan and implement adaptation practices to slow down or eliminate potential harm to cropping systems. It plays an important role in promoting crop productivity to actively adapt to climate change, keeping stable and continuous growth of crop yield, and ensuring food security (Senapati et al., 2021; Kamali et al., 2018a).

In recent years, different methods, mainly including the process-based crop growth model (Yue et al., 2015; Wang et al., 2020; Li et al., 2015) and the indicator-based method (Sendhil et al., 2018; Neset et al., 2019; Gbetibouo et al., 2010), were developed to evaluate the vulnerability of crop yield to historical and future climate change around the world. The crop growth model is driven by different climate data and can simulate the response of yield to climate change, which is used to assess the vulnerability under some specific events, such as water stress (Li et al., 2015; Kamali et al., 2018a) and heat stress (Semenov and Shewry, 2011). However, this method is not comprehensive enough, because it usually separately assesses crop vulnerability caused by single limiting factor, rainfall (Li et al., 2015; Yue et al., 2015) or temperature (Semenov and Shewry, 2011). In general, these limiting factors of climate on crop yield can occur at the same time (Sun et al., 2019), and often interact on each other (Zaitchik et al., 2006; Bandyopadhyay et al., 2016). In addition, the crop growth model has a less accurate performance in simulating the impacts of extreme weather events, and the model cannot consider the impacts of pests and diseases, socio-economic, and technological progress (Semenov and Shewry, 2011; Wang et al., 2020). On the contrary, the indicator-

based method can evaluate the vulnerability of a system from multiple dimensions (Pandey et al., 2017; Ahmadalipour and Moradkhani, 2018). Indicators related to the system are selected from multiple sectors (climate, social economy, land use, resources, and infrastructure, etc.) to obtain relatively comprehensive vulnerability results. Additionally, the indicator-based method has strong customization, as it can select relevant indicators according to different research objects and objectives. Therefore, this method is a better choice for a relatively comprehensive assessment of crop yield vulnerability. Nonetheless, this method also has shortcomings. It is limited in producing a unified set of indicators due to the different backgrounds of social economy and management measures in different regions. Some researchers have reported that this method is unfavourable for vulnerability assessment and comparison on a large scale (Hinkel, 2011). We intended to create the possibility of assessing and comparing the vulnerability on a large scale. Therefore, we used a modified indicator-based method to assess the climate vulnerability of agricultural crop yields based on the data of climate and yields.

Australia is a major food producer and exporter, and its wheat, barley, and canola have made up 10%-40% of the world's export trade (AEGIC, 2021). Australia's grain production is crucial to the national economy, and makes an important contribution to the global food security and the stability of agricultural product prices. However, the crop yield in Australia varied greatly from year to year, and even showed a stagnant trend in the past 30 years (Hochman et al., 2017). For example, during 1989 to 2020, the wheat yield ranged from 0.92 to 2.61 t/ha (ABARES, 2021). This disturbing trend of yield was largely explained by climate variability. Climate variability resulted in 43% of the total wheat yield variation in Australia from 1979 to 2008 (Ray et al., 2015). Therefore, it is necessary to assess the climate vulnerability in agricultural crop yield to identify those vulnerable hotspots in Australia. This knowledge would allow the development of more targeted policy and management implementation to mitigate current climatic challenges and reduce future risk (Ericksen et al., 2011; Abson et al., 2012).

Few studies have assessed the climate vulnerability of crop yield in Australia (Bryan et al., 2015; Huai, 2016; Wang et al., 2020). Most of these studies used crop simulation models to assess vulnerability under climate change. For example, Wang et al. (2020) assessed the biophysical vulnerability of wheat to future climate change using the yield simulated from APSIM-Wheat model under different scenarios. However, they did not consider the impact of socio-economic factors and advances in agronomic managements on adaptive capacity. Similarly, other researchers assessed the vulnerability based on crop yield, and also analyzed the correlation between vulnerability and different capital indicators (e.g. social, human, physical, natural, and financial capital) (Bryan et al., 2015; Huai, 2016). However, these studies used a single climate index (relative standardized precipitation and evapotranspiration index or maximum annual temperature) to characterize exposure. They did not fully take into account the impacts of extreme climate events

associated with both temperature and rainfall. Thus, there are still knowledge gaps on how vulnerable Australia's wheat production is in response to climate change.

Here, our study developed a modified indicator-based method based on exposure, sensitivity, and adaptive capacity to assess the vulnerability of historical wheat yield to climate change in south-eastern Australia. Our main objectives were to: (1) present a vulnerability analytical method for wheat yield, which can be applied to different areas where long-term crop yield and climate data are available. (2) quantify temporal changes of the vulnerability of wheat yield to historical climate. (3) identify the most vulnerable region in the study area to provide guidance for climate change mitigation.

2.2 Materials and methods

2.2.1 Study area and data sources

Our study area is located in the state of New South Wales (NSW) wheat belt in the southeast of Australia and covered by 66 shires (Table 2-1), which is a major wheat producing area in Australia. The wheat production in this area accounts for 27% of total national wheat production and 26% of total national wheat planted area (ABARES, 2021). Over the past three decades (1989-2020), annual wheat production in NSW wheat belt ranged between 3423 kt and 13110 kt, and the harvested area in NSW varied from 2123 to 3800 kha (ABARES, 2021). Overall, yield per hectare varied greatly from 1.61 to 3.45 t/ha. The large inter-annual fluctuation in wheat yield can be largely attributed to climate variability and change (Wang et al., 2015).

There are large variations in the climate and topography across the wheat belt. During the wheat growing season (April to November), average rainfall ranges from 159 mm in the southwest to 677 mm in the northeast of the NSW wheat belt (Wang et al., 2017). Wheat growing season temperature gradually decreases from 14 °C in the north to 12 °C in the south (Feng et al., 2018). The terrain of eastern parts of study area is hills with an altitude of over 500 m. The topography of the western and central region of the wheat belt is mainly occupied by plains. According to climate and topography, the wheat belt was divided into three sub-regions: (I) northern plains (12 shires), (II) southern plains (33 shires), and (III) eastern slopes (21 shires) (Figure 2-1).

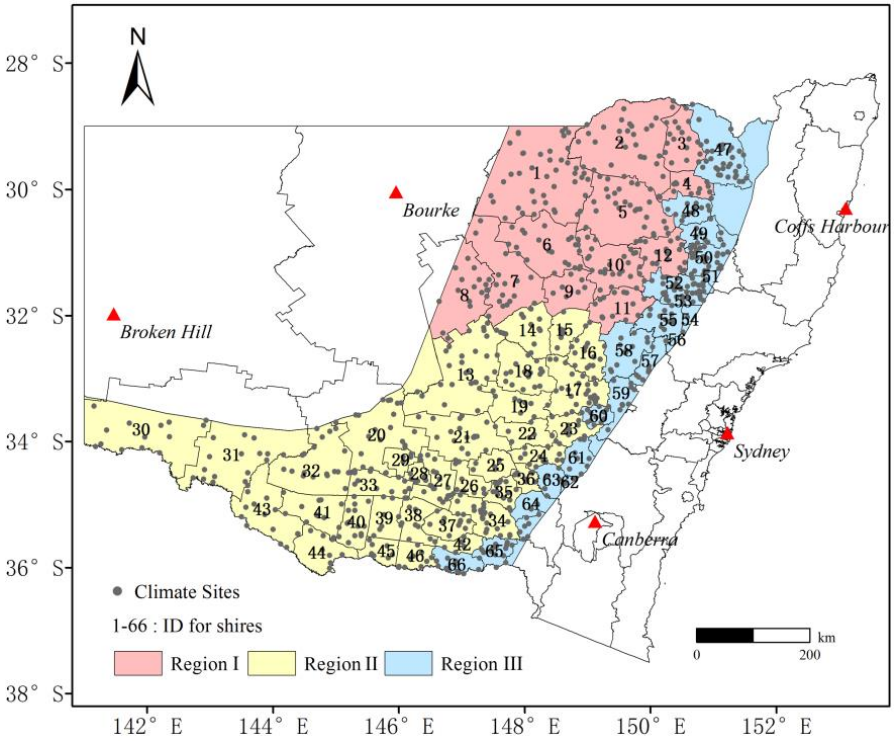

Figure 2-1. The distribution of 66 shires and 940 climate stations in three sub-regions in the NSW wheat belt. 1-66 represents the ID of the 66 selected shires in Table 2-1.

Wheat yields of 66 shires in the NSW wheat belt were collected from Fitzsimmons (2001). Historical daily climate data (rainfall, solar radiation, evapotranspiration, maximum, and minimum temperature) for 940 weather stations in the study area were obtained from Scientific Information for Land Owners (SILO) patched point dataset (Jeffrey et al., 2001).

Table 2-1. Time period of wheat yield data in 66 selected shires in the NSW wheat belt

Region	ID	Shire	Period	Region	ID	Shire	Period
I	1	Walgett	1966-2000		34	Wagga wagga	1922-2000
	2	Moree Plains	1922-2000		35	Junee	1922-2000
	3	Yallaroi	1922-2000		36	Cootamundra	1922-2000
	4	Bingara	1922-1996		37	Lockhart	1922-2000
	5	Narrabri	1922-2000		38	Urana	1922-2000
	6	Coonamble	1922-2000		39	Jerilderie	1922-2000
	7	Warren	1958-2000	II	40	Conargo	1922-2000
	8	Bogan	1958-2000		41	Windouran	1922-1996
	9	Gilgandra	1922-2000		42	Culcairn	1922-2000
	10	Coonabarabbran	1922-2000		43	Wakool	1922-2000
	11	Coolah	1922-2000		44	Murray	1922-2000
	12	Gunnedah	1922-2000		45	Berrigan	1922-2000
II	13	Lachlan	1922-2000		46	Corowa	1922-2000
	14	Narromine	1922-2000	III	47	Inverell	1922-2000
	15	Dubbo	1922-2000		48	Barraba	1922-1996
	16	Wellington	1922-2000		49	Manilla	1922-1996
	17	Cabonne	1922-2000		50	Parry	1922-2000
	18	Parkes	1922-2000		51	Nundle	1922-1996
	19	Forbes	1922-2000		52	Quirindi	1922-2000
	20	Carrathool	1922-2000		53	Murrurundi	1922-2000
	21	Bland	1922-2000		54	Scone	1922-1996
	22	Weddin	1922-2000		55	Merriwa	1922-2000
	23	Cowra	1922-2000		56	Muswellbrook	1922-1996
	24	Young	1922-2000		57	Rylstone	1922-1996
	25	Temora	1922-2000		58	Mudgee	1922-1996
	26	Coolamon	1922-2000		59	Evans	1922-1996
	27	Narrandera	1922-2000		60	Blayney	1922-1996
	28	Leeton	1927-2000		61	Boorowa	1922-2000
	29	Griffith	1927-2000		62	Yass	1922-1996
	30	Wentworth	1922-2000		63	Harden	1922-2000
	31	Balranald	1960-2000		64	Gundagai	1922-1996
	32	Hay	1961-2000		65	Holbrook	1922-1996
	33	Murrumbidgee	1922-2000		66	Hume	1922-2000

Region I: 12 shires, northern NSW wheat belt; Region II: 33 shires, southern NSW wheat belt; Region III: 21 shires, eastern NSW wheat belt. ID number is the shire number in Figure 2-1.

2.2.2 Vulnerability assessment framework

We selected the wheat yield and different climate indices in the NSW wheat belt to conduct a case study. We systematically assessed the spatio-temporal change of exposure (*EI*), sensitivity (*SI*), adaptive capacity (*AC*), and vulnerability (*VI*) of 66 shires in 1924-1998. Sensitivity is the response of the crop production system to climate change, including both beneficial and harmful effects. Exposure indicates the extent of change mainly in climate (IPCC, 2012). Adaptive capacity is the ability or potential of the crop production system to respond successfully to climate and includes adjustments in behaviors, resources, and

technologies (Watson et al., 1996; Watson et al., 1997). Historical observed crop yield usually reflects the influence of climate-related and non-climate-related factors on cropping system (Eq. 2-1). Climatic factors are the main reasons for wheat yield fluctuation. Non-climatic factors are the main driving forces of yield increase, including management practices (breeding, fertilization, and pesticide application), socio-economic, and technology progress, etc.

$$Y = Y_c + Y_t + e \tag{2-1}$$

where Y is the statistical crop yield (kg/ ha); Y_c (kg/ ha) is the climatic yield, which is mainly affected by climate variability; Y_t (kg/ ha) is the non-climatic yield, which mainly represents the role of agricultural managements; and e is the yield composition influenced by other random factors, which can be ignored (Dong et al., 2018).

We used a commonly-used detrending approach, namely 5-year center moving average model (CMA, Eqs. 2-3) (Lu et al., 2017), to separate wheat yield into climatic yield (Y_{cCMA}) to express the sensitivity (climatic yield is negatively related to the sensitivity, thus we use Eq. 2-5 to express), and non-climatic yield (Y_{tCMA}) to represent the adaptive capacity of wheat yield to historical climate (Eq. 2-6) (Dong et al., 2015). Exposure was calculated by the sum of six weighted climatic indices in Table 2-2 (Eq. 2-8). Finally, the historical vulnerability was calculated by adding EI and SI then subtracting AC (Eq. 2-9) (Wang et al., 2020).

The CMA method regarded the crop yield series for 5 consecutive years as a changing linear function, which reflected the historical trend of the yield series as a whole. The average value simulated by sliding linear regression at each year point was the value of the trend at that year. They were calculated as:

$$mY_i = \sum_{j=-2}^{2} \frac{1}{5} Y_{i+j} \tag{2-2}$$

$$Y_{tCMA_i} = mY_i \tag{2-3}$$

$$Y_{cCMA_i} = Y_i - mY_i \tag{2-4}$$

where Y_i is the original crop yield for the ith year; and mY_i is the 5-year moving averaged crop yield for the ith year; i = 1,2,…,n; Y_{tCMAi} and Y_{cCMAi} are the trend yield and climate yield for the ith year, respectively.

$$SI = -Y_{cCMA} \tag{2-5}$$

$$AC = Y_{tCMA} \tag{2-6}$$

To identify whether different detrending approaches affect the results of vulnerability assessment, we also used another two detrending methods, HP Filter (HP) (Eq. 2-S1-2-S2) and first difference (FD) (Eq. 2-S3-2-S5), to evaluate the vulnerability of wheat yield in the NSW wheat belt. We only showed the results using the CMA detrending method in the main text. The calculation details of the other two detrending methods were provided in our supplementary material.

Since *EI*, *SI*, and *AC* had different orders of magnitude, we used Eq. 2-7 to standardize *EI*, *SI*, and *AC*, respectively (Wang and Zhang, 2009). Meanwhile, this equation was applicable to all data standardization in this study.

$$M_i^{'} = \frac{M_i - M_{\min}}{M_{\max} - M_{\min}} \tag{2-7}$$

where $M_i^{'}$ is the i element of time series $\{M_1, M_2,..., M_n\}$ after standardization; M_i is the i element of time series $\{M_1, M_2,..., M_n\}$ before standardization; M_{min}= min $\{M_1, M_2,..., M_n\}$, M_{max}= max $\{M_1, M_2,..., M_n\}$.

$$EI = \sum_{i=1}^{n} W_i S_i \tag{2-8}$$

where Wi is the weighting value of the ith indicators (the weighting method of six climate indices was shown in 2.3); and S_i is the value of the ith indicators. We first normalized S_i using Eq. 2-7 (see above) to make it dimensionless and then used derived weight to calculate *EI* (Eq. 2-8).

After *EI*, *SI,* and *AC* were obtained, *VI* was calculated according to:

$$VI = SI + EI - AC \tag{2-9}$$

2.2.3 Calculation for climate exposure

We first calculated CDD, CWD, rSPEI, TX90P, FD, and Tmean for each climate sites. The 940 sites were assigned into each shire based on the boundary of the shire. The number of climate sites in each shire was shown in Table 2-S2. Then, the CDD, CWD, rSPEI, TX90P, FD, and Tmean for climate sites within each shire were averaged respectively. Here, we followed a previous study of Feng et al. (2018) to predict Y_c based on these six climate indices with random forest (RF) model (Table 2-2).

RF is a non-parametric technology based on classification and regression trees proposed by Breiman (2001). It uses bootstrap resampling technology to repeatedly extract k samples from the original training sample set N to generate a new training sample set, then generates k classification trees to form a random forest according to the self-service sample set. Finally, the prediction result is obtained by the voting score of the classification tree (Breiman, 2001). In addition, random forest has a great advantage when classifying data: it can give the importance score of each variable in the classification process, according to the score, and it

can screen out the relatively important variables. At the same time, the higher importance score of a variable, the more capable it is to classify outcome variables. RF has been widely applied to agricultural and meteorological research due to the high precision, tolerance of abnormal value, and ability to model complex interactions between variables (Feng et al., 2018; Jeong et al., 2016). The default parameters of RF (ntree = 500 and mtry = 3) were used in our analysis. The "%IncMSE" metric was used to calculate relative importance of each index. When the variables were randomly replaced, the %IncMSE represented the average increase of the mean square error of the nodes using a variable in the RF model.

Our RF model had a good performance in predicting Y_c with R^2 of 0.89 and nRMSE of 7%. Then, we used the standardized importance values of CDD, CWD, rSPEI, TX90P, FD, and Tmean derived by RF model (Table 2-S1) as the weight of each index for calculating the exposure of each shire (Eq. 2-8).

Table 2-2. Climate variables for calculating exposure index

	Indicator Name	Definition	Unit
CDD	Maximum length of dry spell	Maximum number of consecutive days with rainfall < 1mm	Days
CWD	Maximum length of wet spell	Maximum number of consecutive days with rainfall ≥ 1mm	Days
rSPEI	Relative standardized precipitation evapotranspiration index of Apr.-Nov.	It characterizes drought by standardizing the difference between precipitation and potential evapotranspiration.	
TX90P	Percentage of days when *TX* (daily maximum temperature) > 90th percentile	Let TX_{ij} be the daily maximum temperature on day *i* in period *j* and let $TX_{in}90$ be the calendar day 90th percentile centred on a 5-day window for the base period 1961-1990. The percentage of time for the base period is determined where: $TX_{ij} > TX_{in}90$	%
FD	Number of frost days	Annual count of days when daily minimum temperature < 0℃.	Days
Tmean	The change in daily temperature	Average value of daily Tmean	℃

2.2.4 Statistical tests

Statistical analysis of *EI*, *SI*, *AC,* and *VI* in time series is helpful to understand their long-term change process under climate change conditions, and to identify their regular characteristics and change trends. We used Mann-Kendall (MK) trend test and continuous wavelet transform (CWT) to identify temporal characteristics of *EI*, *SI*, *AC,* and *VI* in three sub-regions and the whole NSW wheat belt from 1924 to 1998. The M-K test was used to analyze data collected over time for consistently increasing or decreasing trends (monotonic) in *Y* values. CWT can identify the periodic signal of data in time series (Torrence and Compo, 1998; Zeri et al., 2019), and it was used as a supplementary test method for data without significant change trend by numerous researchers (Beecham and Chowdhury, 2010; Li et al., 2019). In addition, *EI*, *SI*, *AC*, and *VI* were derived from climatic factors and wheat yield, which may have obvious inter-annual fluctuation in time series. Therefore, it is necessary to investigate the fluctuation status of these indicators to test whether they have periods with the CWT analysis.

2.2.4.1 Mann-Kendall trend test

MK test is a non-parametric trend test method (Mann 1945; Kendall 1975), which is often used to evaluate the statistical significance of time series trends. Its advantage is its ability to test linear or nonlinear trends. In addition, MK test is less sensitive to the distribution type of data, and also can deal with missing and

abnormal values of data. In MK test, the statistic S and the standardized test statistic Z_{MK} were calculated as follows (Sang et al., 2014; Sayemuzzaman and Jha, 2014):

$$S = \sum_{i=1}^{n-1} \sum_{j=i+1}^{n} \operatorname{sgn}\left(X_j - X_i\right) \tag{2-10}$$

$$\operatorname{sgn}\left(X_j - X_i\right) = \begin{cases} +1 \ if \ \left(X_j - X_i\right) > 0 \\ 0 \quad if \ \left(X_j - X_i\right) = 0 \\ -1 \ if \ \left(X_j - X_i\right) < 0 \end{cases} \tag{2-11}$$

$$Var\left(S\right) = \frac{1}{18}\left[n\left(n-1\right)\ \left(2n+5\right) - \sum_{p=1}^{q} t_p \left(t_p - 1\right)\ \left(2t_p + 5\right) \right] \tag{2-12}$$

$$Z_{MK} = \begin{cases} \dfrac{S-1}{\sqrt{Var\left(S\right)}} & if\ S > 0 \\ 0 & if\ S = 0 \\ \dfrac{S+1}{\sqrt{Var\left(S\right)}} & if\ S < 0 \end{cases} \tag{2-13}$$

where X_i and X_j are the corresponding data values of i and j in the time series ($j > i$); n is the length of the data set; t_p is the number of data in the tied group. A Positive value of Z_{MK} indicates an increasing trend in time series, while a negative Z_{MK} value shows a decreasing trend. When $|Z_{MK}| > Z_{(1-\alpha/2)}$, there is a significant trend in time series. The $Z_{(1-\alpha/2)}$ value can be found in the standard normal distribution table. At the 5% and 1% significance level (95% or 99% confidence intervals), time series trends are significant if $|Z_{MK}| > 1.96$ and $|Z_{MK}| > 2.58$ (Han et al., 2018).

2.2.4.2 Wavelet analysis

CWT is widely used to identify the statistical characteristics of climate-related indicators in time series. Morlet wavelet is used in this study (Rossi et al., 2011; Roushangar et al., 2018):

$$\psi_0\left(\eta\right) = \pi^{-1/4} e^{i\omega_0 \eta} e^{-\eta^2/2} \tag{2-14}$$

where ω_0 is dimensionless frequency with a value of 6 here; η ($\eta = s*t$) is dimensionless time, s is the time scale.

Continuous wavelet transform of time series (x_n, n = 1, …, N) with uniform time step (δ_t) can be defined as the convolution of x_n and wavelet normalization (Grinsted et al., 2004). It is defined as:

$$W_n^X(s) = \sqrt{\frac{\delta t}{s}} \sum_{n'=1}^{N} x_{n'} \psi_0 \left[(n' - n) \frac{\delta t}{s} \right] \quad (2\text{-}15)$$

where n is the localized time index; n' is the time variable.

2.2.5 Kernel density plot

Kernel density plot is used to display the distribution of data in x-axis continuous data segments. This plot is a variant of the histogram, using a smooth curve to draw horizontal values. The advantage of kernel density plot over histogram is that it is not affected by the number of grouped data and can better show the distribution shape.

We divided the NSW wheat belt into three sub regions (Figure 2-1 and Table 2-1), and then calculated the average values for *EI*, *SI*, *AC*, and *VI* in the 1930s, 1950s, 1970s, and 1990s in each subregion. The "ggplot2" package in R software was used to make kernel density plot.

2.2.6 Classification for *EI*, *SI*, *AC,* and *VI*

We divided these indices into five evaluation grades (Table 2-3) to clearly describe the changes of *EI*, *SI*, *AC*, and *VI* of 66 shires in NSW wheat belt in different historical periods.

Table 2-3. The value interval of different *EI*, *SI*, *AC,* and *VI* assessment levels

Indicators	Very Low	Low	Moderate	High	Very High
Exposure (*EI*)	*EI*<0.10	0.10≤*EI*<0.30	0.30≤*EI*<0.50	0.50≤*EI*<0.70	*EI*≥0.70
Sensitivity (*SI*)	*SI*<0.47	0.47≤*SI*<0.57	0.57≤*SI*<0.67	0.67≤*SI*<0.77	*SI*≥0.77
Adaptive Capacity (*AC*)	*AC*<0.10	0.10≤*AC*<0.30	0.30≤*AC*<0.50	0.50≤*AC*<0.70	*AC*≥0.70
Vulnerability (*VI*)	*VI*<0.20	0.20≤*VI*<0.40	0.40≤*VI*<0.60	0.60≤*VI*<0.80	*VI*≥0.80

2.3 Results

2.3.1 Descriptive statistics of wheat yield and climate variables

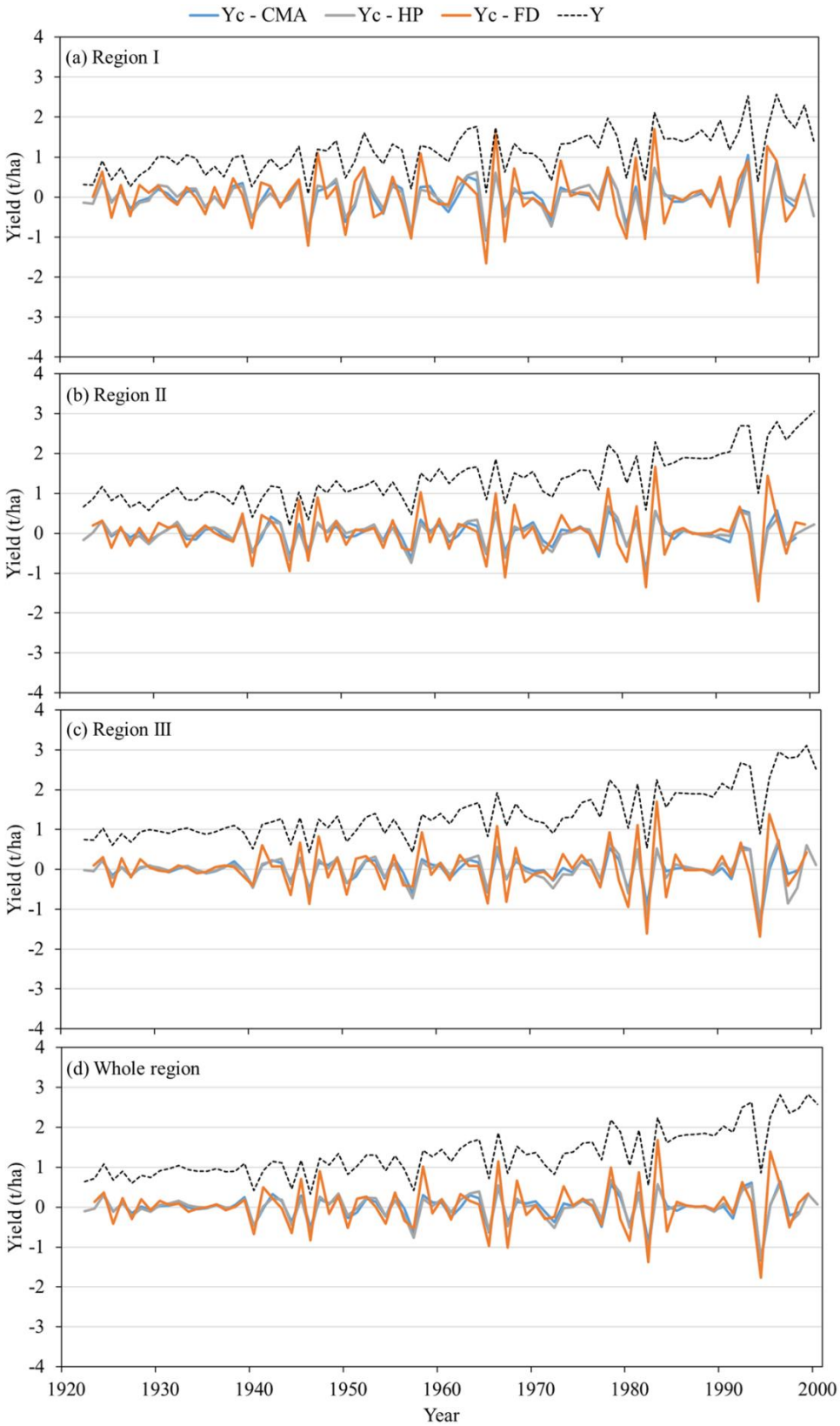

Figure 2-2. Averaged observed (Y) and detrending (Y_c) wheat yields obtained by CMA, HP, and FD methods in three sub regions and the whole NSW wheat belt.

The long-term wheat yield of the three sub-regions and the whole region showed an obvious increase trend (Figure 2-2). Y_c had a great inter-annual fluctuation in all sub regions, and the fluctuation range of region I was the largest from about -2.1 to 1.7 t/ha. From 1924 to 1998, the fluctuation range of Y_c gradually increased indicating that the impact of historical climate on wheat yield was gradually intensified. There were small differences in Y_c obtained by three detrending methods. Note that for FD method, the Y_c fluctuated more than that of another two methods in all sub regions. For the six climate indices, they all had large inter-annual fluctuations (Figure 2-3), but there was no significant trend of increasing or decreasing except CWD and rSPEI showing an upward trend.

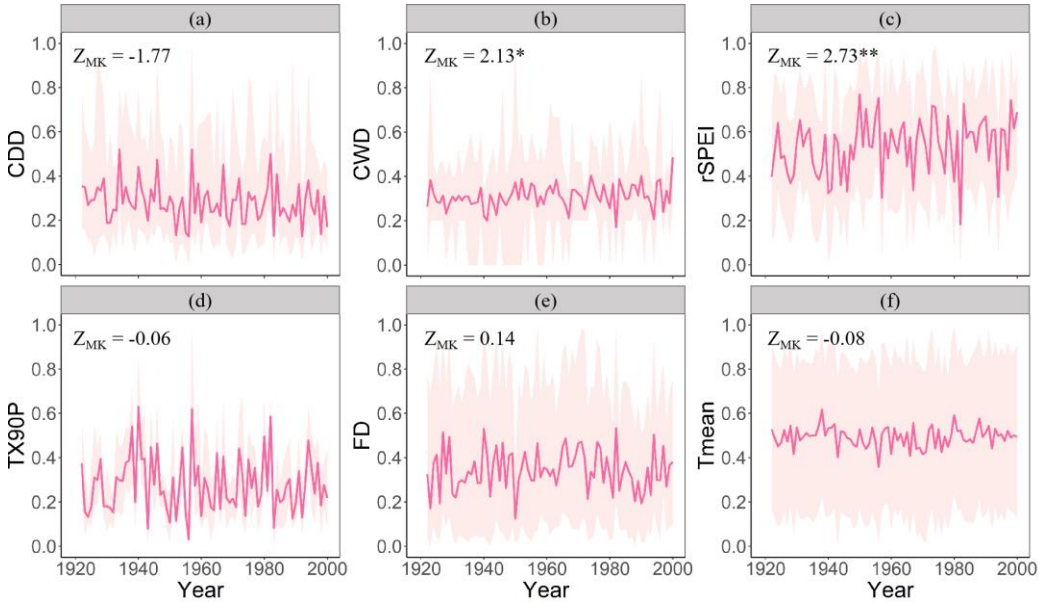

Figure 2-3. Averaged value of standardized CDD, CWD, rSPEI, TX90P, FD, and Tmean in 66 shires of the NSW wheat belt.

2.3.2 Exposure

Spatially, the exposure level of NSW wheat belt gradually decreased from northwest to southeast (Figure 2-4 a-d). The number of shires with low and very low exposure increased from 34 to 40 and 1 to 13, respectively. Conversely, the number of shires with moderate, high, and very high exposure decreased gradually from 1930s to 1990s, that is, from 20 to 8, 6 to 4, and from 4 to 1, respectively. According to the kernel density plots of exposure (Figure 2-5 a-d), for three sub-regions and the whole region, the density distribution curve and the average value line of exposure showed an overall slight leftward translation trend. The exposure was decreasing from 1930s to 1990s. In addition, the peak value of exposure density was the lowest in region I, which meant that the differences of exposure level among different shires in region I were quite large. The peak in region II, region III, and the whole region were obviously higher than that in region I. For the three sub-regions, from 1924 to 1998, the variation of exposure showed large inter-annual

fluctuations. (Figure. 2-6 a-d). The exposure of region I was the highest and had the largest fluctuation during the whole study period. It fluctuated from 0.2-0.8. However, there was a decreasing trend from 1924-1998. The temporal changes of exposure in region II and region III were similar, about 0.1-0.6.

2.3.3 Sensitivity

Figure 2-4 e-h showed that the spatial distribution of sensitivity level in different study periods was varied. In 1930s, the sensitivity of wheat belt gradually increased from northwest to southeast. In 1950s, the sensitivity was the lowest as a whole. There were no shires with high and very high sensitivity, and the sensitivity in the western areas was higher than that in the east. In 1970s, the sensitivity of the whole wheat belt was relatively higher. There were 26 shires with high sensitivity. In 1990s, the number of shires with high sensitivity increased sharply from 1 in 1930s to 13 in 1970s, and they were mainly distributed in the southern NSW wheat belt. There were also obvious differences in kernel density plots of the sensitivity in different sub-regions (Figure 2-5 e-h). However, for all sub-regions, the sensitivity in 1950s had the highest peak value and the lowest average value. This showed that in 1950s, the sensitivity level was the lowest in all regions, and the sensitivity differences among different shires were also small. For region I, the average sensitivity from 1930s to 1990s was about 0.6, and the sensitivity differences among different shires were small. For region II and region III, the average sensitivity values in 1930s, 1970s, and 1990s were all about 0.6, and the peak of density decreased gradually with time. That is to say, the sensitivity levels of different shires were gradually polarized. In 3 sub-regions, the sensitivity changed similarly with time (Figure 2-6 e-h), fluctuating between 0.25 and 0.75. Its inter-annual variation was quite large.

We found that the spatial distribution of sensitivity obtained by different detrending methods was quite different (Figure 2-4, Figure 2-S1, and Figure 2-S2). For CMA method, the high climate sensitivity of the whole NSW wheat belt appeared in 1970s and 1990s, while that of FD method appeared in 1950s and 1990s, and HP method only generated high sensitivity in 1950s. For each study period, there were also differences in the spatial distribution of sensitivity among the three methods. Take 1950s as an example, the sensitivity based on CMA method was higher in the northwest of the NSW wheat belt, that obtained by HP method was higher in the middle area, and the sensitivity based on FD method was the highest in the southern wheat belt. According to density plots (Figure 2-5, Figure 2-S3, and Figure 2-S4), the sensitivity value in different detrending methods also had large difference in all regions. The order of peak values of sensitivity density of the three methods from high to low was $SI_{FD}>SI_{CMA}>SI_{HP}$. In addition, the sensitivity value of three methods showed no significant trend from 1924-1998 in line plots. They all had great inter-annual fluctuations during the whole study period, and the magnitudes of fluctuation increased with time. However, the magnitudes of the fluctuation (*MF*) of three methods were obviously varied and ordered as $MF_{FD}>MF_{CMA}>MF_{HP}$ (Figure 2-6, Figure 2-S5, and Figure 2-S6).

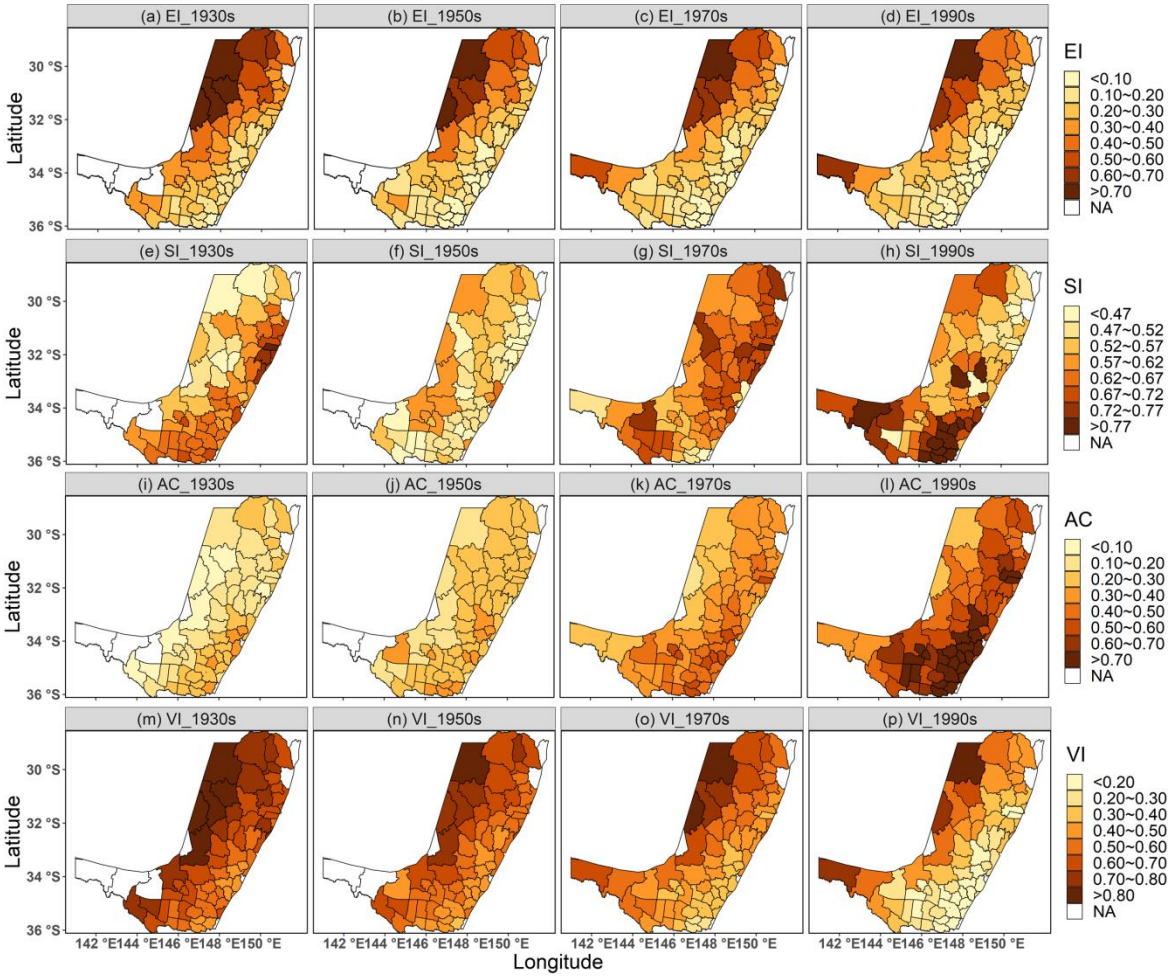

Figure 2-4. Spatial distribution of *EI*, *SI*, *AC*, and *VI* in NSW wheat belt for 1930s, 1950s, 1970s, and 1990s based on CMA method.

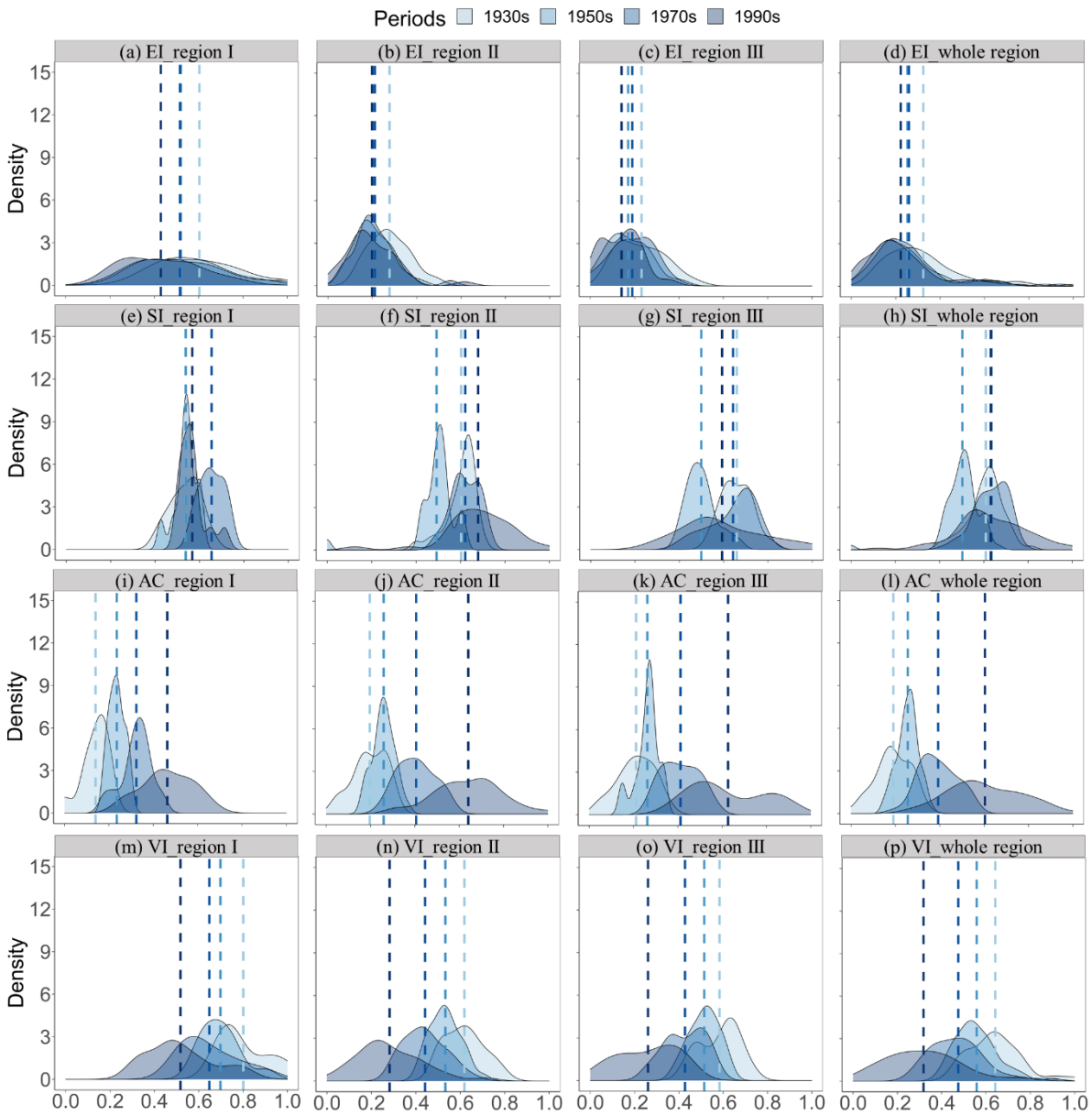

Figure 2-5. Kernel density of *EI*, *SI*, *AC*, and *VI* based on CMA method in three sub-regions and the whole NSW wheat belt. The vertical blue dotted line from shallow to deep represent the average value of the indicator in 1930s, 1950s, 1970s, and 1990s, respectively.

Figure 2-6. The annual averaged value of *EI*, *SI*, *AC*, and *VI* based on CMA method in three sub-regions and the whole NSW wheat belt in 1924-1998. The top and bottom boundaries of shaded areas represent the maximum and minimum value, respectively. Z_{MK} is the increasing (decreasing) rate of *EI*, *SI*, *AC*, and *VI* during the period from 1924 to 1998 in three sub-regions and the whole NSW wheat belt (*** $p < 0.001$, ** $p < 0.01$, * $p < 0.05$).

2.3.4 Adaptive Capacity

The adaptive capacity increased gradually from 1930s-1990s in NSW wheat belt (Figure 2-4 i-l). The number of shires with low and very low adaptive capacity declined from 57 to 2, while the number of shires with high and very high adaptive capacity rose from 0 to 47. The spatial distribution of adaptive capacity for the wheat belt was consistent, which increased gradually from west to east. From 1930s to 1990s, the kernel density curve and mean value line of adaptive capacity for all regions shifted from left to right overall (Figure 2-5 i-l), indicating an increasing trend in all regions of the study area. However, the adaptive

capacity of region I was lower than that of region II and region III in each year period. Moreover, since the 1950s, the growth rate of adaptive capacity became lower than that of the other two sub-regions. For all regions, the peak value in 1950s was the highest, and the peaks of adaptive capacity in 1930s, 1970s, and 1990s gradually decreased with time. This indicated that the gap in adaptive capacity between different shires decreased rapidly from 1930s to 1950s, and had gradually increased since 1950s. The adaptive capacity of the three sub-regions in NSW wheat belt had an obvious increasing trend in time series (Figure 2-6 i-l). The adaptive capacity level of region I increased from 0.1 to 0.5, and that of region II and region III increased more, both from about 0.2 to 0.75. At the same time, the extreme values of the adaptive capacity level of region II and region III were slightly larger than that of region I in the whole time series.

We found that the adaptive capacity obtained by three methods all showed a similar spatial distribution, and gradually increased from northwest to southeast (Figure 2-4, Figure 2-S1, and Figure 2-S2). According to the kernel density plots, the distribution characteristics of adaptive capacity obtained by the three methods were also similar, and the adaptive capacity increased gradually from 1930s to 1990s (Figure 2-5, Figure 2-S3, and Figure 2-S4). Meanwhile, the adaptive capacity based on three detrending methods significantly increased from 1924-1998 in all regions. However, the magnitude of their inter-annual fluctuation showed differences in three detrending methods, ordered in $MF_{FD}>MF_{CMA}>MF_{HP}$ (Figure 2-6, Figure 2-S5, and Figure 2-S6).

2.3.5 Vulnerability

According to the spatial distribution of vulnerability in NSW wheat belt (Figure 2-4 m-p), the vulnerability was decreasing from northwest to southeast. Meanwhile, from 1930s to 1990s, the vulnerability of the whole region also decreased. The number of high and very high vulnerable shires reduced from 39 to 4, and these shires were mainly located in the western and northern part of the wheat belt. The number of shires with moderate vulnerability increased by 20 from 1930s to 1950s, but gradually decreased by 29 after 1950s. Moderately vulnerable shires were mainly located in the centre of the study area. The number of low and very low vulnerable shires increased from 0 in 1930s to 47 in 1990s.

According to the kernel density plots of vulnerability (Figure 2-5 m-p), from 1930s to 1990s, the density curve and mean value line in three sub-regions and the whole region showed a trend of overall translation to the left. We conclude that the vulnerability of the NSW wheat belt was decreasing. At the same time, we can know that the density curve and mean line of vulnerability in region I were basically between 0.2-1.0 and 0.5-0.8, respectively, and this was obviously higher than those between 0-0.8 and 0.2-0.6 in regions II and III, respectively. This revealed that the vulnerability of region I was higher than that of region II and region III during the whole historical period. In addition, the peak value of vulnerability kernel density in different regions had little difference, which increased slightly from 1930s to 1950s, and gradually

decreased after 1950s. We infer that, apart from 1950s, the vulnerability difference among different shires in all regions increased gradually from 1930s to 1990s.

For the three sub-regions, vulnerability all decreased from 1924 to 1998, although its inter-annual differences were relatively large (Figure 2-6 m-p). The vulnerability of region I was the highest and had the largest fluctuation during the study period. The average vulnerability of region I decreased from 0.9 to 0.4, which was greater than that of region II and region III, decreasing from 0.8 to 0.3. In all sub-regions, the maximum inter-annual variation of vulnerability occurred after 1980. Meanwhile, during 1960 to 1998, the extreme value of the vulnerability level increased obviously, which indicated that the difference of the vulnerability level of different shires increased. However, for region III, the vulnerability difference among different shires was small, only the minimum vulnerability range in the last 20 years has widened. We think that the vulnerability of different shires in region III was similar from 1924 to 1980, while that of low vulnerability shires were lower from 1980 to 1998.

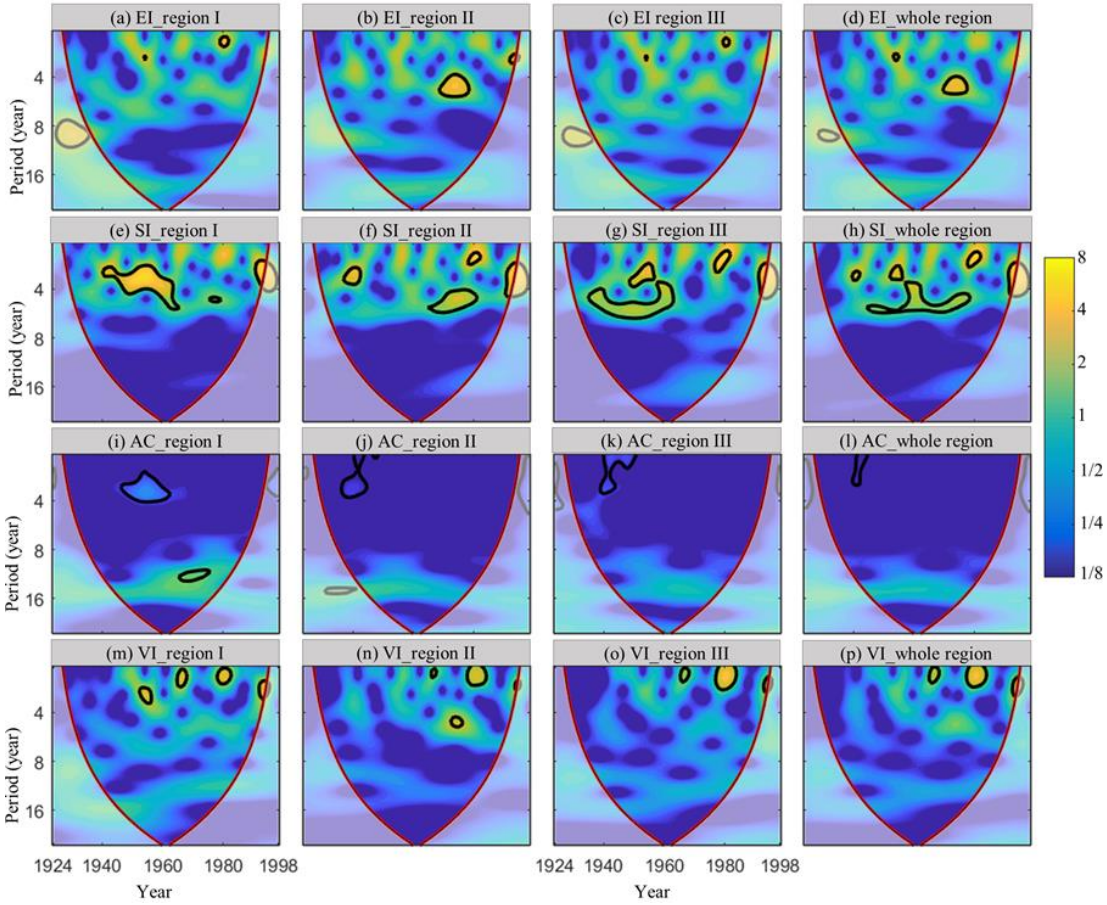

Figure 2-7. The wavelet-spectra of annual *EI*, *SI*, *AC*, and *VI* based on CMA method in three sub-regions and the whole NSW wheat belt in 1924-1998. The red line denotes the cones of influence, and the thick solid line shows the 95% confidence level. Yellow and blue area in the figure represent the peak and valley of wavelet energy density, respectively.

We found that the spatial distributions of vulnerability obtained by the three detrending methods were similar, gradually decreasing from northwest to southeast throughout the NSW wheat belt (Figure 2-4, Figure 2-S1, and Figure 2-S2). The kernel density of vulnerability based on three methods in different sub regions also showed a similar trend, which gradually decreased from 1930s to 1990s (Figure 2-5, Figure 2-S3, and Figure 2-S4). In addition, the vulnerability derived from the three detrending methods significantly decreased from 1924-1998, and showed inter-annual fluctuation in different amplitudes (Figure 2-6, Figure 2-S5, and Figure 2-S6).

We used MK test to analyze the trends of exposure, sensitivity, adaptive capacity, and vulnerability (Figure 2-6 a-p). Meanwhile, the time and period characteristics of these four indicators were combined by continuous wavelet transform (Figure 2-7). The exposure showed a slight decreasing trend in three sub-regions and the whole region, but only the exposure of region I had passed the significance test (Figure 2-6 a-d). At the same time, the results of wavelet analysis showed that the high frequency part (HFP) of exposure was mainly distributed in 0-10a in three sub-regions, and the wavelet power spectrum energy changed discontinuously in HFP. Among them, region I and region III had an 8-10a period passed the significance test in 1930s, while the period of significance for region II was 4-6a in 1972 (Figure 2-7 a-d). Sensitivity level had no significant change trend in all regions (Figure 2-6 e-h). However, its periodicity was obvious, and had a main oscillation period of 4.5-7.7a in all regions. The HFP mainly concentrated in 0-7.7a, but the change was discontinuous. In addition, in region I and region III, there were 2-6a periods in 1941-1960 and 1996, had passed the significance test. The periods of significance for region III were shorter, mainly concentrated in 1978 and 1996 (Figure 2-7 e-h). Adaptive capacity in different regions all had significantly increased (Figure 2-.6 i-l), while the periodicity was not significant, and the HFP existed only in 11.2-16.5a of region I (Figure 2-7 i-l). The vulnerability of the three sub-regions and the whole region decreased significantly with time (Figure 2-6 m-p). The results of wavelet analysis showed that the HFP of vulnerability in different regions was mainly between 0-3.6a. In 1966, 1978 and 1996, there were short periods of 0-1.8a, which passed the significance test. Also, region I had a significant short period of 2-3.6a in 1954 (Figure 2-7 m-p).

To sum up, the trend and periodicity of data can supplement each other. Taking adaptive capacity as an example, it had an obvious increasing trend with a weak periodic signal in the time series across the three subregions and the whole NSW wheat belt. Meanwhile, the data with large inter-annual fluctuations, such as exposure, had discontinuous periods in the time series.

2.4 Discussion

Our study used a comprehensive index method to assess the vulnerability of wheat yield to climate change. We used the trend of historical yield as proxy of adaptive capacity, which considered the contribution of management, socio-economic, and technological progress to crop yield (Franke et al., 2019; Bogunovic et al., 2018; Adimassu and Kessler, 2016; Olesen et al., 2011). Sensitivity was represented by detrending yield, which characterized the final result of wheat affected by climate variability and extreme weather events. Furthermore, we developed a RF model to predict detrending yield based on six representative climate indices. The variable importance derived from RF was used to give the weight of six climate indices. Then the weighted sum of the six climate indices represented exposure. The exposure index we developed here considered the average changes and extreme events of rainfall and temperature.

Sensitivity and exposure are both related to climate factors. The differences between them are: when assessing the vulnerability of agricultural system to climate change, exposure is essentially the magnitude of extrinsic change in climate itself. Conversely, sensitivity is the amount of corresponding change to these given amount of exposure (Kling et al., 2020). Note that the regions with high sensitivity are not always the ones with high exposure. For example, in 1930s, 1950s, and 1990s, the value of sensitivity for those shires in the eastern and southern parts of wheat belt was higher than that in northwestern areas, where exposure was the highest during the whole study period (Figure 2-4).

Most previous studies regarding the impact of historical climate on crops often use different detrending methods to remove non-climatic yield (Y_t). Then only climatic yield (Y_c) and different climate variables were used to establish the relationship between crops and climate change. They identified dominant climatic drivers that determine yield variations (e.g., Wang et al. 2015). In this study, we not only separated Y_c and Y_t, but also used both Y_c and Y_t to conduct vulnerability analysis. Our vulnerability index can not only reflect the impact of climate on crop production system, but also consider the resilience of the system itself. This comprehensive assessment is very helpful for locating those areas that are unable to cope with adverse climate impacts, which often have high sensitivity and exposure, and low adaptive capacity. This method is more helpful to the planning of adaptation measures and the rational allocation of agricultural resources, compared with studies only considering the effects of climate factors.

We demonstrated that the vulnerability gradually decreased from 1924 to 1998. Exposure and sensitivity did not increase or decrease significantly throughout the study periods, although they fluctuated greatly from year to year. However, the adaptive capacity significantly increased with time. We found that the adaptive capacity was increased mainly because of the improvement of agronomic management practices, technological, and socio-economic progress. This aligns with a previous study that emphasized

improvements in wheat yields in Australia resulting from changed management and from better genetics, as well as advances in mechanization (Richards et al., 2014). For example, adjusting the sowing date of crops can make crops grow in a more favourable climate condition, avoid frequent risk periods such as heat, frost, and drought, then reduce the adverse effects of climate and weather on crop production (Gomez-Macpherson and Richards., 1995). Furthermore, the emergence of new crop varieties, the application of herbicides and chemical fertilizers improve the productivity of crops (Anderson et al., 2005). In addition, the improvement of agricultural machinery as well as the progress of communication and computer technology have improved the efficiency of agricultural production and the speed and range of farmers receiving information (Kingwell and Pannell, 2005). Finally, the increase of farmers' livelihood capital is also the reason for enhancing adaptive capacity (Huai, 2016). As for sensitivity and exposure, they are highly correlated with climate conditions. The climate indices had large inter-annual fluctuations (Figure 2-3) with no significant trend of increasing or decreasing except CWD and rSPEI.

Spatially, we found that the vulnerability of region I, located in the northwest of the wheat belt, was about 0.45-0.80, higher than the 0.24-0.60 of the other two sub-regions. At the same time, from 1930s to 1990s, the vulnerability of region II was slightly higher than that of region III, but the difference was small. The main reason was that, under the condition of small difference in sensitivity among the three sub-regions, the exposure of region I was the highest (Figure 2-5), while its adaptive capacity was the lowest (Figure 2-5). Climate conditions in region I were less favourable for wheat growth than other two regions (Figure 2-5 a). For example, compared with the southeast, the northwest of wheat belt has less precipitation and higher temperature (Feng et al., 2019b). This dry and hot climate tends to aggravate the adverse effects on wheat production (Wang et al., 2020). Moreover, the rainfall pattern in the northwest is mainly summer dominant, which means that the main rainfall does not fall in the wheat growth period, resulting in less available water for wheat in the northwest. On the contrary, rainfall in southwest is generally uniform or winter dominant (Wang et al., 2018), therefore, wheat in this area can use more effective precipitation. In region I, we mainly attributed the lowest adaptive capacity to the poorest accessible to natural, financial, and physical resources in the northwestern NSW compared with other regions (Schirmer and Hanigan, 2015).

We highlight the need to assess vulnerability on the shire scale. From shire scale, we found that Warren (ID: 7), Coonamble (ID: 6), Bogan (ID: 8), and Walgett (ID: 1) were the most vulnerable areas based on CMA detrending method, and they were all located in region I. Also, the exposure level of these shires was the highest among 66 shires, while their adaptive capacity was almost the lowest. We suspect that this combination of factors may explain why they had the highest vulnerability. Policy makers and farmers should give priority to the application of effective agricultural adaptation and capital investment in these shires. Farmers can try to plant drought-resistant and heat-resistant wheat, adjust the sowing date of wheat,

or use residue mulching to alleviate or eliminate the adverse effects of climate (drought, high temperature, frost, etc.) in these shires. These techniques may improve the adaptive capacity under high exposure (Zhao et al., 2015). Based on the APSIM simulations of the impacts of climate change on wheat production for Walgett, Crimp et al. (2019) suggested choosing new varieties with heat and drought resistance, and altering planting decisions to adapt climate changes. Furthermore, policy makers and farmers should consider whether these shires need to transform and stop growing wheat. This proposal was consistent with the change of farming methods in the crop belt of northern NSW after the 1990s. Taking Walgett as an example, from 1995 to 2001, the planting area of wheat decreased from 85% to 70%, while that of chickpea increased from 2% to 23% (GRDC, 2004).

Conversely, Holbrook (ID: 65), Hume (ID: 66), Harden (ID: 63), and Boorowa (ID: 61) were shires with the lowest vulnerability in the wheat belt based on CMA detrending method. They were all in region III and located in the southeast of the study area. In these shires, the planting area of wheat should be appropriately increased, so as to make full use of the advantages of low vulnerability, thus increasing the wheat production. Moreover, the agricultural managements practised in these shires can be passed on to other areas with high vulnerability, helping them to reduce the vulnerability of wheat production, so as to achieve stable and sustained growth of wheat yield.

We found that there was no difference among the three detrending methods in locating shires with the highest vulnerability in the NSW wheat belt. The four most vulnerable shires in NSW wheat belt were consistent in the three methods. However, when locating shires with lowest vulnerability, the results obtained by the three detrending methods were different (Holbrook (ID: 65), Hume (ID: 66), Blayney (ID: 60), and Cootamundra (ID: 36) for HP method; Holbrook (ID: 65), Hume (ID: 66), Blayney (ID: 60), and Culcairn (ID: 61) for FD method).

More work are still needed to explore the issues raised in our research. Although we investigated the spatiotemporal changes of exposure, sensitivity, adaptive capacity, and vulnerability in the NSW wheat belt, we did not assess the vulnerability from 2001 to 2021 due to lack of yield data for each shire after 2000. In addition, by comparing the vulnerability results of three detrending methods, we found that different detrending methods can lead to different results in vulnerability assessment spatially. This has been reported by a previous study of Lu et al. (2017), showing detrending methods significantly affect Y_c and Y_t. In addition, Ye et al. (2015) used multiple detrending methods to assess crop yield risk and found that the estimated yield loss rate varied with different detrending methods. Thus, pre-selecting suitable detrending methods according to specific research objectives and contents is necessary to reduce the possibility of significant differences. Understanding the vulnerability of crop yield to historical climate is an indispensable step for assessing the vulnerability of crop productivity to future climate change (Uddin et

al., 2019; Wang et al., 2020; Ahmadalipour and Moradkhani, 2018). The drought intensity of NSW wheat belt was predicted to increase in the next few decades, and the drought affected area will expand from west to east (Feng et al., 2019a). Meanwhile, warm days (TX90P) also show an increasing trend, especially in the northeast of wheat belt (Wang et al., 2016). Hence, the exposure in NSW is likely to increase in the future, and the area with high exposure will gradually expand from northwest towards eastern and southern districts. In this case, how will the vulnerability of the east and south of wheat belt change in the future? Can future adaptive capacity offset this increasing exposure? Also, do these regions need to increase additional agricultural adaptation practices and investment, so as to enhance their adaptive capacity? These questions can be answered by assessing vulnerability under future climate change. We expect that our vulnerability assessment method can be combined with process-based crop model driven by global climate models to predict the vulnerability of wheat yield in the future. Therefore, we can determine whether those less vulnerable areas (the eastern and southern parts of the wheat belt) in historical periods can still keep low vulnerability under the future climate change.

2.5 Conclusion

We used the data of crop yield and climatic indices in 1924-1998, combining with the methods of yield de-trending and comprehensive exposure index to assess wheat yield vulnerability to climate as a case study in south-eastern Australia. We found that, from the 1930s to the 1990s, both exposure and sensitivity had large inter-annual variations without significant increasing or decreasing trend. However, adaptive capacity increased by 34% from 1930s to 1950s, 54% from 1950s to 1970s, and 54% from 1970s to 1990s. The vulnerability in the wheat belt decreased by 13% from 1930s to 1950s, 15% from 1950s to 1970s, and 33% from 1970s to 1990s. This is mainly due to increased adaptive capacity with the improvement of agronomic management practices, technological and socio-economic progress. Our results highlight that the hotspots of wheat yield vulnerability were located in the north-western parts of NSW wheat belt. Our study provides useful information for policymakers to plan and implement the priority adaptations and investments to mitigate the vulnerability in these areas. Meanwhile, policymakers should also find ways to make full use of the favourable conditions in the southeastern NSW wheat belt, so as to improve the state wide potential of wheat productivity.

Our study emphasizes that vulnerability assessment based on crop yield and climate change indices is a useful approach. Additionally by using this method, researchers can assess the vulnerability of crop yield to future climate change in combination with process-based model simulated results. So, we can know whether the exposure and sensitivity will increase significantly under future climate change, and whether the improvement of adaptive capacity can offset their increase. The vulnerability prediction will provide effective guidance for agricultural resource allocation and investment planning, so as to achieve the

maximum benefit of agricultural productivity. We highlight the need to apply a simple and universal method for vulnerability assessment. It facilitates the comparison of vulnerability in different regions and the prediction of future vulnerability. This is of great significance to policymakers' precise agricultural management and planning. This information will help industry leaders facilitate change in production systems of several industries, including wheat, to better prepare farmers for climate change and hence, to maintain productivity and profitability into the future.

2.6 Supporting information

2.6.1 Methods

2.6.1.1 HP (Hodrick-Prescott) Filter

Let Y_i denote the natural logarithm of a wheat yield series over the sample from $i = 1$ to T. HP Filter analysis divides Y_i into trend yield Y_{tHP} and fluctuating yield Y_{cHP}, in which Y_{tHP} is a stable high-frequency trend signal and Y_{cHP} is an unstable low-frequency disturbance signal. The principle is to eliminate the low-frequency signal Y_{cHP} by filtering, so as to detect the high-frequency signal Y_{tHP} from the yield sequence (Harvey and Trimbur, 2008). HP Filtering decomposes Y_i into:

$$Y_i = Y_{tHP_i} + Y_{cHP_i} \tag{2-S1}$$

where Y_i is the original crop yield for the ith year; $i = 1,2,\ldots,n$; Y_{tHP_i} and Y_{cHP_i} are the trend yield and climate yield for the ith year, respectively, obtained by HP Filter.

The HP-filter involves the estimation of the trend component from the solution to the following minimization problem for fixed λ:

$$\min_{\{Y_{tHPi}\}_{i=1}^{T}} \left\{ \sum_{i=1}^{T} \left(Y_i - Y_{tHP_i} \right)^2 + \lambda \sum_{i=2}^{T-1} \left[\left(Y_{tHP_{i+1}} - Y_{tHP_i} \right) - \left(Y_{tHP_i} - Y_{tHP_{i-1}} \right) \right]^2 \right\} \tag{2-S2}$$

where λ is HP Filter parameter, in this study, $\lambda = 100$.

2.6.1.2 First difference

The first difference (FD) is defined as the difference of crop yields between 2 successive years:

$$\Delta Y_i = Y_i - Y_{i-1} \tag{2-S3}$$

$$Y_{cFD_i} = \Delta Y_i \tag{2-S4}$$

$$Y_{tFD_i} = Y_i - \Delta Y_i \tag{2-S5}$$

where Y_i is the original crop yield for the ith year; Y_{i-1} is the original crop yield for the (i-1)th year; ΔY_i is the first difference of yield for the ith year; i = 1,2,…,n; Y_{tFD_i} and Y_{cFDi} are the trend yield and climate yield for the ith year, respectively, obtained by first difference method.

2.6.1.3 Calculating equations for rSPEI and TX90P

A SPEI value generally indicates the deviation of P-PET (precipitation - evapotranspiration) from "normal conditions" at a given station within a given period. Due to the difference of "normal conditions" between dry stations and wet stations, SPEI values are usually not comparable when used to evaluate the relative drought situation of different stations in a same region. Feng et al. (2019) proposed the rSPEI which corrects the shortcomings of the original SPEI and can be used for spatial comparison. The calculation details are as follows:

Integrate monthly P-PET total values of all 940 sites as a reference P-PET series,

$$\overline{D_j} = \overline{P_j} - \overline{\mathrm{PET}_j} \tag{2-S6}$$

where $\overline{P_j}$, $\overline{\mathrm{PET}_j}$, and $\overline{D_j}$ are the averaged total precipitation, the accumulated PET, and the deficit of jth month at the 940 climate sites. Then, the averaged accumulated P-PET at k-month scale is calculated by:

$$\begin{cases} \overline{X}_{i,j}^{k} = \sum_{l=13-k+j}^{12} \overline{D}_{i-1,l} + \sum_{l=1}^{j} \overline{D}_{i,l} & \text{if } j < k \\ \overline{X}_{i,j}^{k} = \sum_{l=j-k+1}^{j} \overline{D}_{i,l} & \text{if } j < k \end{cases} \tag{2-S7}$$

where $\overline{X}_{i,j}^{k}$ is the accumulated P-PET at k-month scale in jth month of ith year; $\overline{D}_{i,l}$ is the monthly P-PET in lth month of ith year. The parameters of the log-logistic distribution were obtained from this reference series. Then, the rSPEI relative to the reference distribution function were acquired for each station. In this study, the rSPEI was calculated for wheat growing season (Apr-Nov).Calculating equations for TX90P is shown as below:

$$TX90P = \frac{D_{TX_{ij} > TX_{in}90}}{D_P} \tag{2-S8}$$

where $D_{TXij>TXin90}$ is the number of days when TX_{ij} is higher than $TX_{in}90$ during the period j (j is the growing season of wheat in NSW wheat-belt); D_P is the number of days during the period j; TX_{ij} is the daily maximum temperature on day i in period j; $TX_{in}90$ is the calendar day 90th percentile centred on a 5-day window for the base period 1961-1990.

2.6.2 Supplementary Tables

Table 2-S1. The weighting value of each climate indicator for 66 shires in the NSW wheat belt

Region	ID	Shire	CDD	CWD	rSPEI	TX90P	FD	Tmean
I	1	Walgett	0.01	0.02	0.78	0.11	0.01	0.07
	2	Moree	0.22	0.05	0.4	0.25	0.01	0.07
	3	Yallaroi	0.01	0.05	0.65	0.22	0.02	0.05
	4	Bingara	0.08	0.09	0.71	0.01	0.08	0.03
	5	Narrabri	0.16	0.01	0.41	0.24	0.08	0.1
	6	Coonamble	0.01	0.01	0.69	0.21	0.02	0.06
	7	Warren	0.15	0.01	0.57	0.14	0.05	0.08
	8	Bogan	0.06	0.01	0.49	0.2	0.01	0.23
	9	Gilgandra	0.11	0.08	0.49	0.26	0.05	0.01
	10	Coonabarabbran	0.18	0.01	0.43	0.26	0.11	0.01
	11	Coolah	0.12	0.01	0.36	0.33	0.11	0.07
	12	Gunnedah	0.14	0.01	0.59	0.22	0.03	0.01
II	13	Lachlan	0.08	0.01	0.44	0.35	0.01	0.11
	14	Narromine	0.16	0.05	0.35	0.3	0.01	0.13
	15	Dubbo	0.12	0.03	0.43	0.28	0.01	0.13
	16	Wellington	0.17	0.04	0.43	0.26	0.09	0.01
	17	Cabonne	0.01	0.01	0.62	0.16	0.07	0.13
	18	Parkes	0.13	0.08	0.37	0.29	0.01	0.12
	19	Forbes	0.14	0.02	0.45	0.34	0.04	0.01
	20	Carrathool	0.13	0.08	0.31	0.38	0.01	0.09
	21	Bland	0.08	0.16	0.5	0.24	0.01	0.01
	22	Weddin	0.15	0.01	0.59	0.22	0.02	0.01
	23	Cowra	0.14	0.02	0.52	0.28	0.01	0.03
	24	Young	0.18	0.01	0.44	0.22	0.05	0.1
	25	Temora	0.03	0.01	0.42	0.23	0.22	0.09
	26	Coolamon	0.04	0.01	0.43	0.34	0.11	0.07
	27	Narrandera	0.15	0.02	0.37	0.41	0.01	0.04
	28	Leeton	0.08	0.27	0.43	0.17	0.04	0.01
	29	Griffith	0.12	0.02	0.21	0.36	0.01	0.28
	30	Wentworth	0.22	0.08	0.47	0.07	0.01	0.15
	31	Balranald	0.22	0.05	0.37	0.33	0.02	0.01
	32	Hay	0.07	0.43	0.22	0.01	0.17	0.1
	33	Murrumbidgee	0.11	0.05	0.38	0.32	0.01	0.13
	34	Wagga	0.1	0.01	0.38	0.38	0.02	0.11
	35	Junee	0.03	0.11	0.42	0.25	0.18	0.01
	36	Cootamundra	0.09	0.01	0.33	0.24	0.22	0.11
	37	Lockhart	0.13	0.11	0.32	0.24	0.01	0.19
	38	Urana	0.01	0.12	0.29	0.45	0.01	0.12
	39	Jerilderie	0.1	0.03	0.35	0.39	0.12	0.01
	40	Conargo	0.17	0.17	0.39	0.22	0.04	0.01
	41	Windouran	0.17	0.17	0.43	0.14	0.01	0.08
	42	Culcairn	0.17	0.23	0.32	0.12	0.01	0.15
	43	Wakool	0.16	0.14	0.44	0.23	0.01	0.02
	44	Murray	0.07	0.21	0.4	0.28	0.03	0.01
	45	Berrigan	0.01	0.2	0.47	0.25	0.01	0.06
	46	Corowa	0.07	0.34	0.28	0.19	0.01	0.11

Region	ID	Shire	CDD	CWD	rSPEI	TX90P	FD	Tmean
III	47	Inverell	0.01	0.07	0.72	0.13	0.02	0.05
	48	Barraba	0.01	0.07	0.68	0.16	0.07	0.01
	49	Manilla	0.09	0.05	0.57	0.26	0.01	0.02
	50	Parry	0.08	0.13	0.35	0.28	0.01	0.15
	51	Nundle	0.01	0.06	0.36	0.33	0.19	0.05
	52	Quirindi	0.1	0.01	0.46	0.28	0.06	0.09
	53	Murrurundi	0.08	0.02	0.43	0.36	0.01	0.1
	54	Scone	0.03	0.06	0.36	0.5	0.01	0.04
	55	Merriwa	0.2	0.01	0.28	0.27	0.13	0.11
	56	Muswellbrook	0.01	0.06	0.44	0.31	0.15	0.03
	57	Rylstone	0.07	0.01	0.42	0.43	0.06	0.01
	58	Mudgee	0.18	0.05	0.34	0.35	0.01	0.07
	59	Evans	0.21	0.3	0.11	0.01	0.22	0.15
	60	Blayney	0.01	0.15	0.38	0.15	0.14	0.17
	61	Boorowa	0.05	0.13	0.58	0.19	0.01	0.04
	62	Yass	0.01	0.11	0.43	0.24	0.09	0.12
	63	Harden	0.1	0.01	0.4	0.18	0.14	0.17
	64	Gundagai	0.01	0.09	0.41	0.1	0.15	0.24
	65	Holbrook	0.01	0.19	0.43	0.18	0.02	0.17
	66	Hume	0.19	0.09	0.28	0.18	0.01	0.25

Table 2-S2. Number of climate sites in each shire in the NSW wheat belt

Region	ID	Shire	Number of climate sites	Region	ID	Shire	Number of climate sites
I	1	Walgett	44		34	Wagga	23
	2	Moree	30		35	Junee	13
	3	Yallaroi	16		36	Cootamundra	10
	4	Bingara	14		37	Lockhart	9
	5	Narrabri	29		38	Urana	10
	6	Coonamble	19		39	Jerilderie	9
	7	Warren	16	II	40	Conargo	14
	8	Bogan	18		41	Windouran	11
	9	Gilgandra	9		42	Culcairn	5
	10	Coonabarabbran	25		43	Wakool	15
	11	Coolah	13		44	Murray	7
	12	Gunnedah	20		45	Berrigan	7
II	13	Lachlan	29		46	Corowa	11
	14	Narromine	14	III	47	Inverell	36
	15	Dubbo	7		48	Barraba	12
	16	Wellington	16		49	Manilla	7
	17	Cabonne	26		50	Parry	32
	18	Parkes	17		51	Nundle	3
	19	Forbes	8		52	Quirindi	23
	20	Carrathool	22		53	Murrurundi	16
	21	Bland	18		54	Scone	1
	22	Weddin	8		55	Merriwa	14
	23	Cowra	12		56	Muswellbrook	1
	24	Young	12		57	Rylstone	9
	25	Temora	5		58	Mudgee	12
	26	Coolamon	9		59	Evans	8
	27	Narrandera	19		60	Blayney	14
	28	Leeton	7		61	Boorowa	8
	29	Griffith	5		62	Yass	2
	30	Wentworth	14		63	Harden	5
	31	Balranald	19		64	Gundagai	7
	32	Hay	17		65	Holbrook	16
	33	Murrumbidgee	21		66	Hume	12

2.6.3 Supplementary Figures

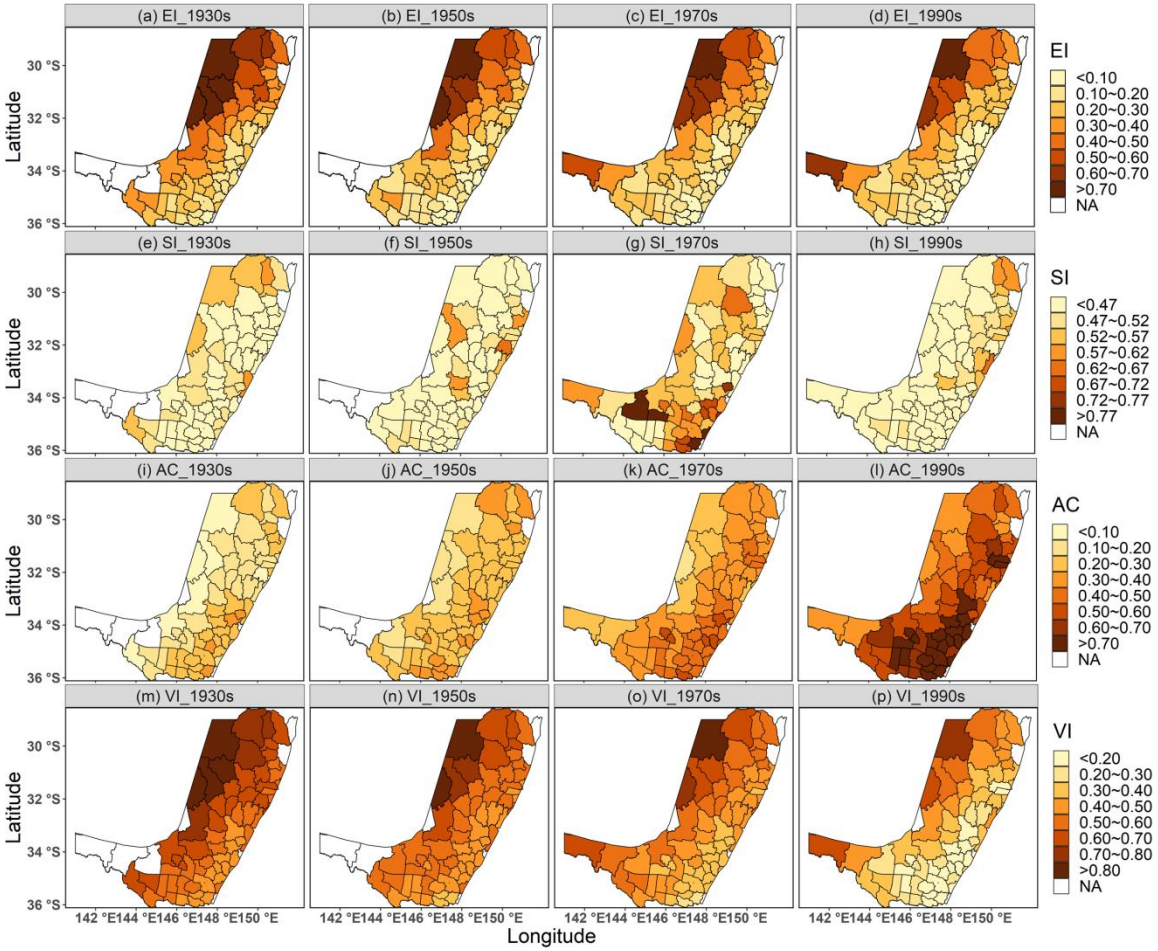

Figure 2-S1. Spatial distribution of *EI*, *SI*, *AC*, and *VI* in NSW wheat belt for 1930s, 1950s, 1970s, and 1990s based on HP method.

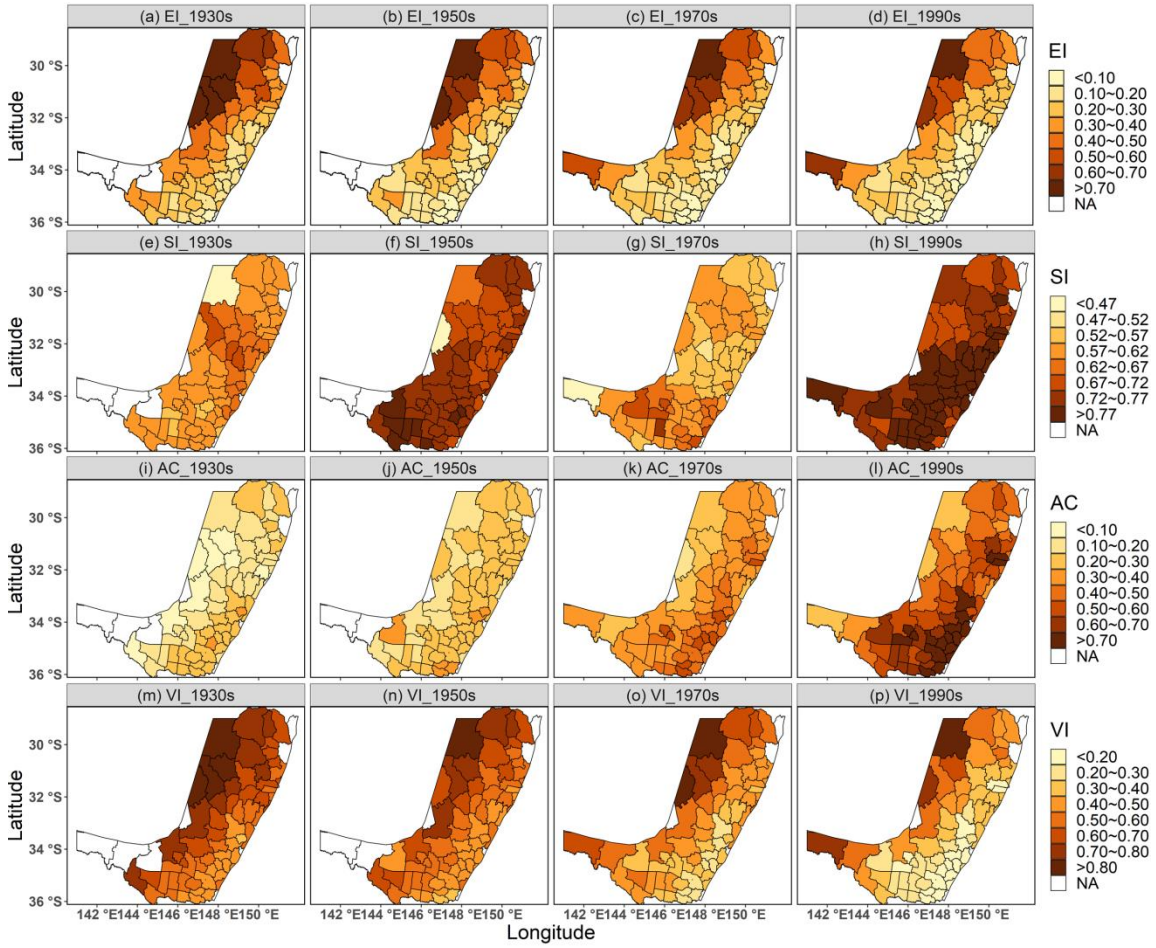

Figure 2-S2. Spatial distribution of *EI*, *SI*, *AC*, and *VI* in NSW wheat belt for 1930s, 1950s, 1970s, and 1990s based on FD method.

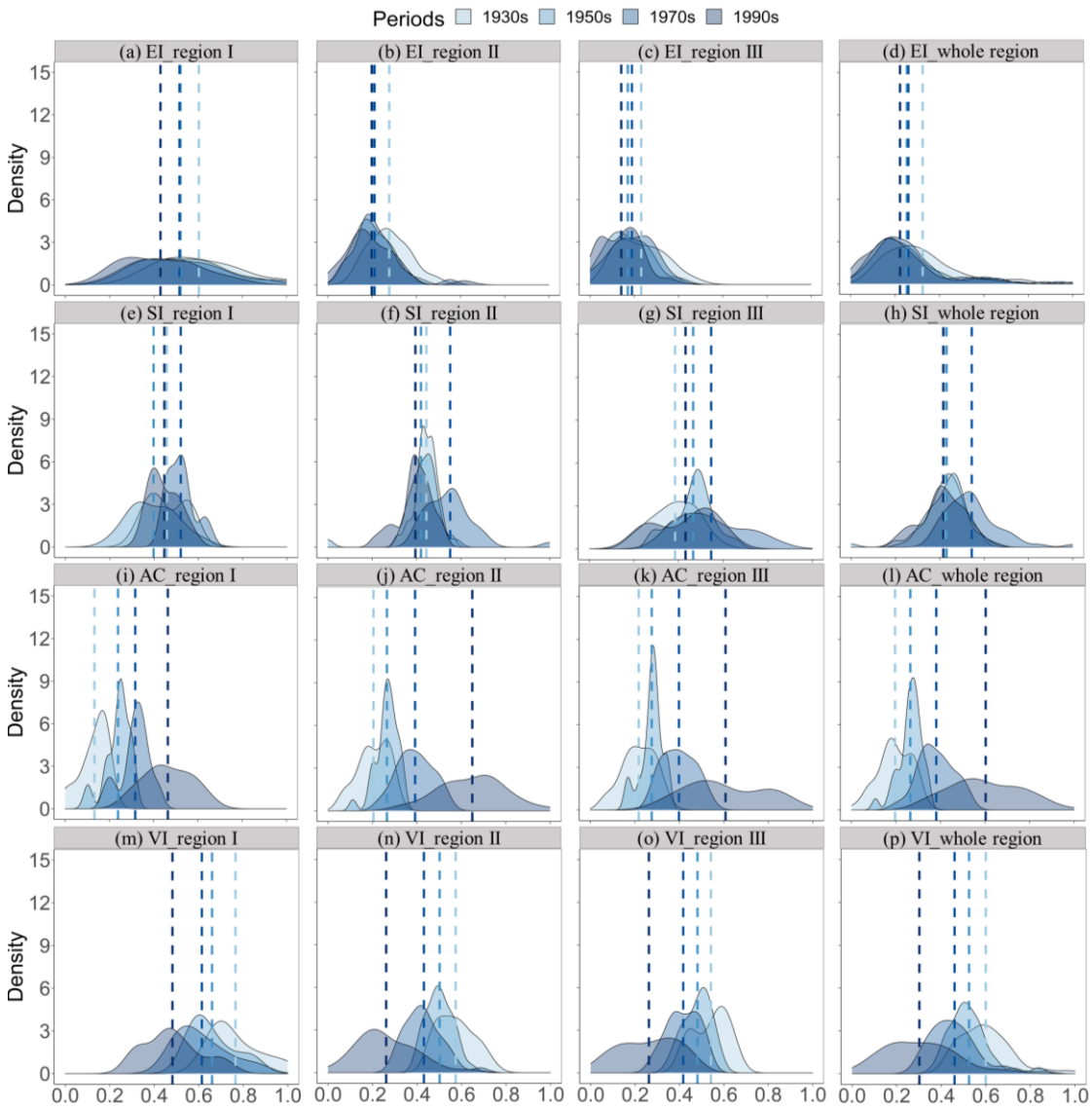

Figure 2-S3. Kernel density of *EI*, *SI*, *AC*, and *VI* based on HP method in three sub-regions and the whole NSW wheat belt. The vertical blue dotted line from shallow to deep represent the average value of the indicator in 1930s, 1950s, 1970s, and 1990s, respectively.

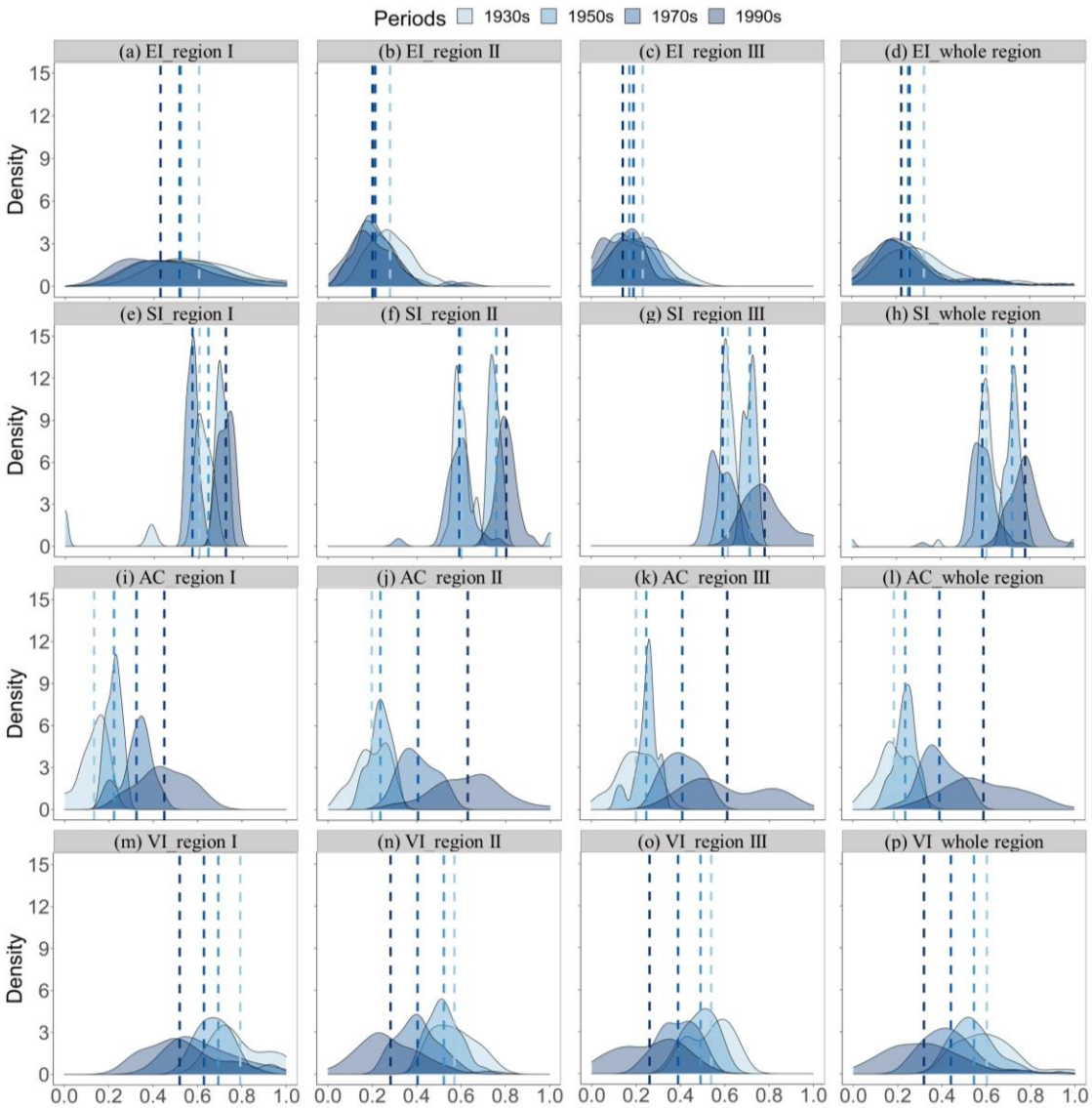

Figure 2-S4. Kernel density of *EI*, *SI*, *AC*, and *VI* based on FD method in three sub-regions and the whole NSW wheat belt. The vertical blue dotted line from shallow to deep represent the average value of the indicator in 1930s, 1950s, 1970s, and 1990s, respectively.

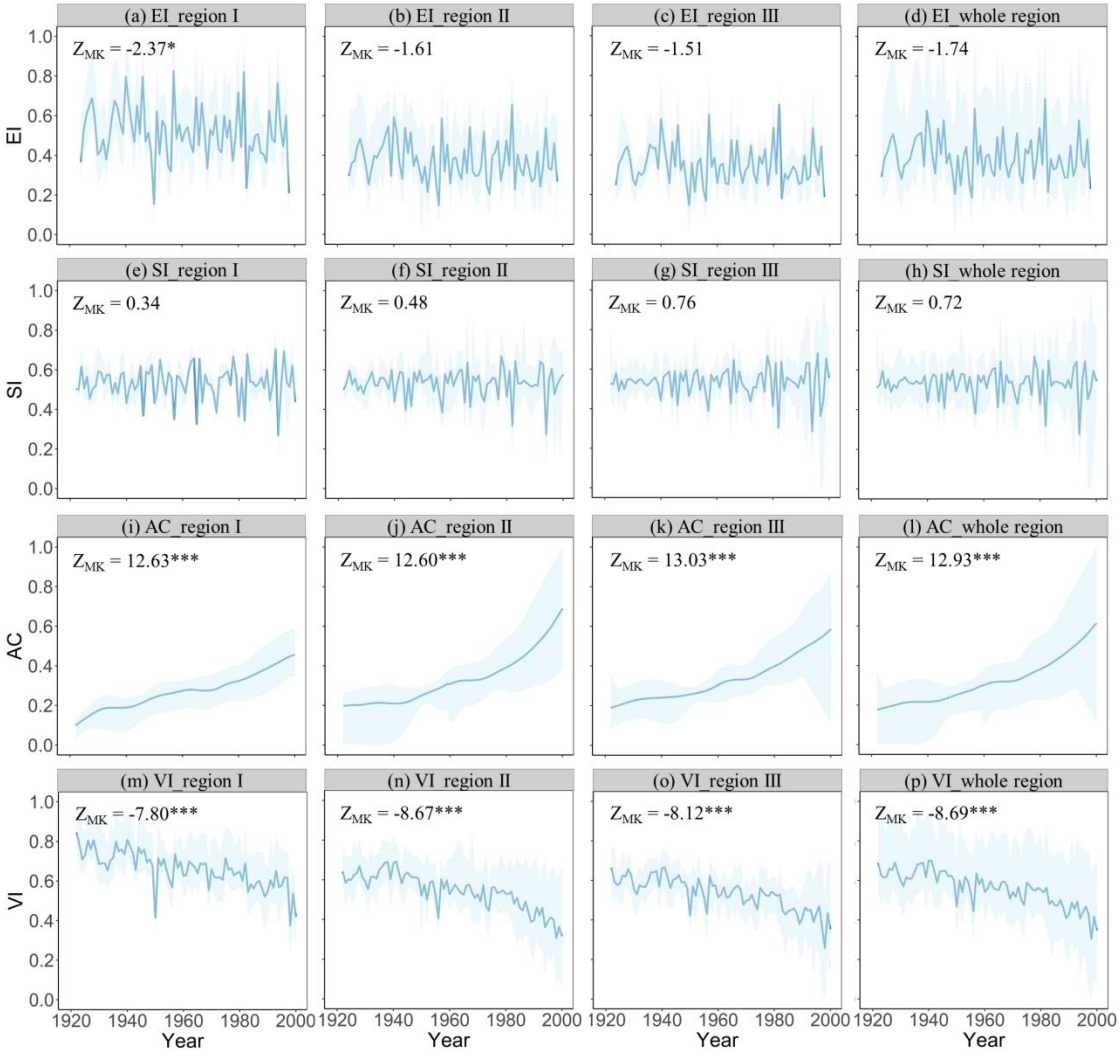

Figure 2-S5. The annual averaged value of *EI*, *SI*, *AC*, and *VI* based on HP method in three sub-regions and the whole NSW wheat belt in 1924-1998. The top and bottom boundaries of shaded areas represent the maximum and minimum value, respectively. Z_{MK} is the increasing (decreasing) rate of *EI*, *SI*, *AC*, and *VI* during the period from 1924 to 1998 in three sub-regions and the whole NSW wheat belt (*** $p < 0.001$, ** $p < 0.01$, * $p < 0.05$).

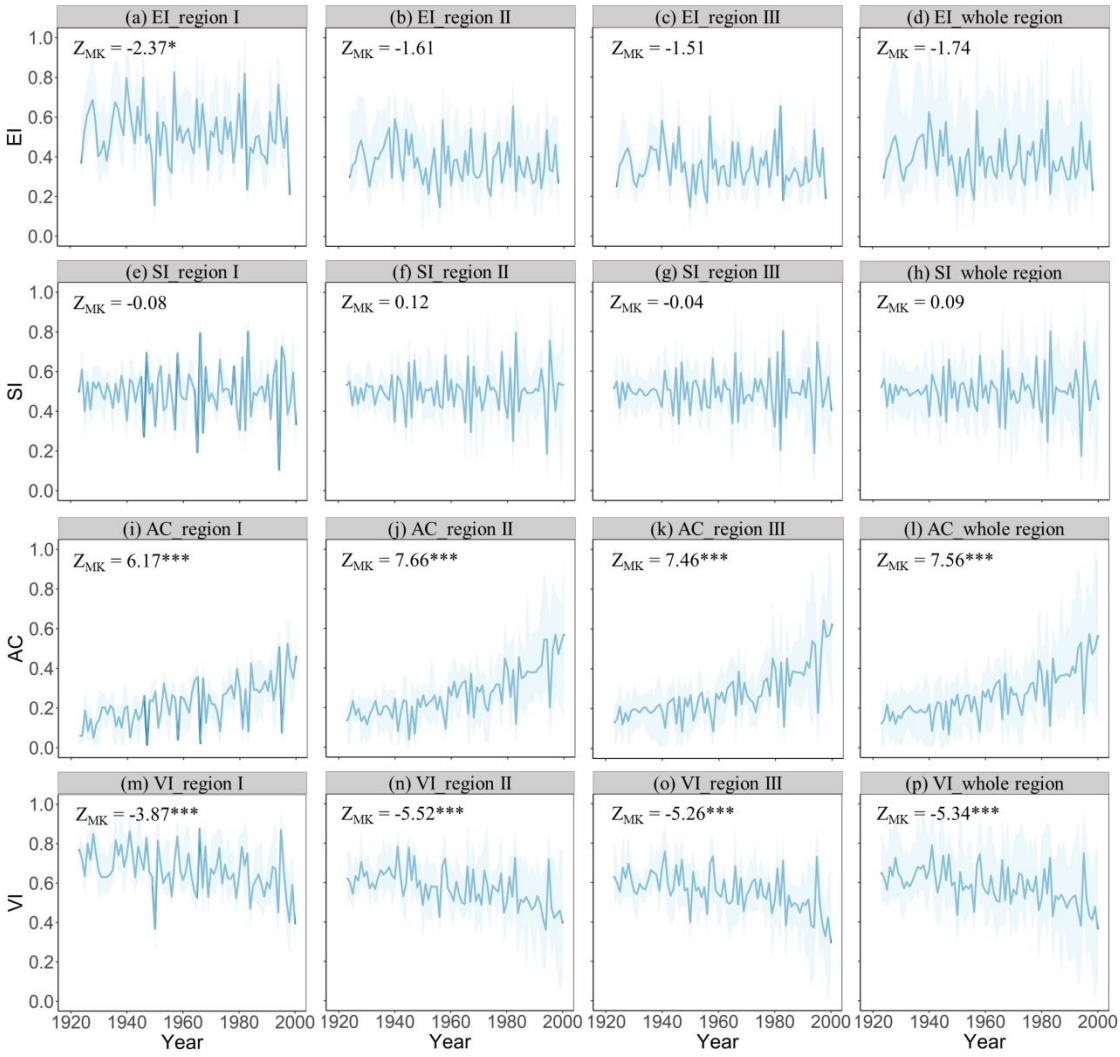

Figure 2-S6. The annual averaged value of *EI*, *SI*, *AC*, and *VI* based on FD method in three sub-regions and the whole NSW wheat belt in 1924-1998. The top and bottom boundaries of shaded areas represent the maximum and minimum value, respectively. Z_{MK} is the increasing (decreasing) rate of *EI*, *SI*, *AC*, and *VI* during the period from 1924 to 1998 in three sub-regions and the whole NSW wheat belt (*** $p < 0.001$, ** $p < 0.01$, * $p < 0.05$).

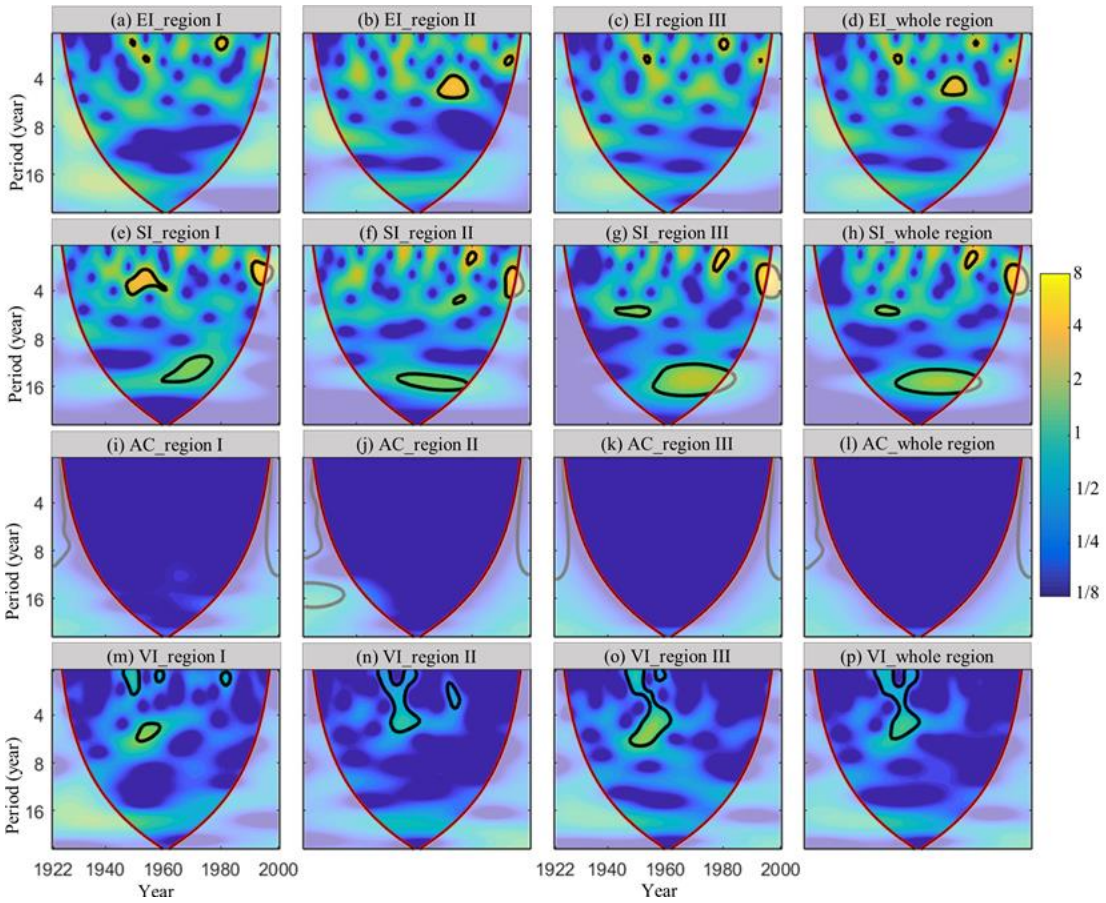

Figure 2-S7. The wavelet-spectra of annual *EI*, *SI*, *AC*, and *VI* based on HP method in three sub-regions and the whole NSW wheat belt in 1924-1998. The red line denotes the cones of influence, and the thick solid line shows the 95% confidence level. Yellow and blue area in the figure represent the peak and valley of wavelet energy density, respectively.

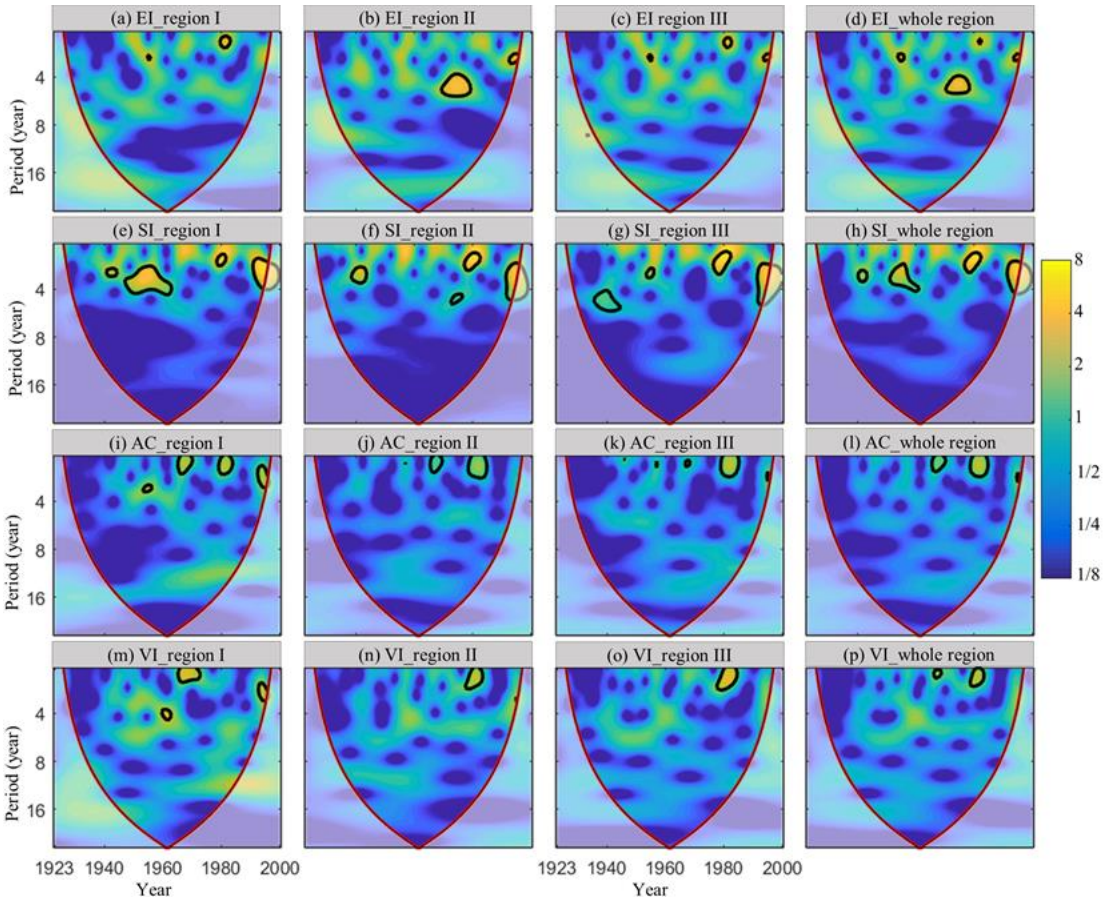

Figure 2-S8. The wavelet-spectra of annual *EI*, *SI*, *AC*, and *VI* based on FD method in three sub-regions and the whole NSW wheat belt in 1924-1998. The red line denotes the cones of influence, and the thick solid line shows the 95% confidence level. Yellow and blue area in the figure represent the peak and valley of wavelet energy density, respectively.

2.7 Reference

ABARES, 2021. https://www.agriculture.gov.au/abares/research-topics/agricultural-outlook/data#australian-crop-report-data. The last accessed date: 25 May 2021.

Abson, D.J., Dougill, A.J., Stringer, L.C., 2012. Using Principal Component Analysis for information-rich socio-ecological vulnerability mapping in Southern Africa. Applied Geography 35, 515-524.

Adger, W.N., 2006. Vulnerability. Global Environmental Change 16, 268-281.

Adimassu, Z., Kessler, A., 2016. Factors affecting farmers' coping and adaptation strategies to perceived trends of declining rainfall and crop productivity in the central Rift valley of Ethiopia. Environmental Systems Research 5, 13.

AEGIC, 2021. https://www.aegic.org.au/australian-grain-production-a-snapshot/. The last accessed date: 20 May 2021.

Ahmadalipour, A., Moradkhani, H., 2018. Multi-dimensional assessment of drought vulnerability in Africa: 1960-2100. Science of the Total Environment 644, 520-535.

Anderson, W.K., Hamza, M.A., Sharma, D.L., D'Antuono, M.F., Hoyle, F.C., Hill, N., Shackley, B.J., Amjad, M., Zaicou-Kunesch, C., 2005. The role of management in yield improvement of the wheat cropa review with special emphasis on Western Australia. Australian Journal of Agricultural Research 56, 1137-1149.

Bandyopadhyay, N., Bhuiyan, C., Saha, A., 2016. Heat waves, temperature extremes and their impacts on monsoon rainfall and meteorological drought in Gujarat, India. Natural Hazards 82, 367-388.

Bashan, A., Bartsch, R., Kantelhardt, J.W., Havlin, S., 2008. Comparison of detrending methods for fluctuation analysis. Physica A: Statistical Mechanics and its Applications 387, 5080-5090.

Beecham, S., Chowdhury, R.K., 2010. Temporal characteristics and variability of point rainfall: a statistical and wavelet analysis. International Journal of Climatology 30, 458-473.

Bogunovic, I., Pereira, P., Kisic, I., Sajko, K., Sraka, M., 2018. Tillage management impacts on soil compaction, erosion and crop yield in Stagnosols (Croatia). CATENA 160, 376-384.

Breiman, L., 2001. Random Forests. Machine Learning 45, 5-32.

Bryan, B.A., Huai, J., Connor, J., Gao, L., King, D., Kandulu, J., Zhao, G., 2015. What actually confers adaptive capacity? Insights from agro-climatic vulnerability of Australian wheat. PloS One 10.

Crimp, S., Mahani, M., Howden, M., 2019. Predicted climate change impacts on northern NSW farming systems. https://grdc.com.au/resources-and-publications/grdc-update-papers/tab-content/grdc-update-papers/2019/08/predicted-climate-change-impacts-on-northern-nsw-farming-systems. The last accessed date: 5 May 2021.

Dong, Z., Pan, Z., An, P., Wang, L., Zhang, J., He, D., Han, H., Pan, X., 2015. A novel method for quantitatively evaluating agricultural vulnerability to climate change. Ecological Indicators 48, 49-54.

Dong, Z., Pan, Z., He, Q., Wang, J., Huang, L., Pan, Y., Han, G., Xue, X., Chen, Y., 2018. Vulnerability assessment of spring wheat production to climate change in the Inner Mongolia region of China. Ecological Indicators 85, 67-78.

Ericksen P, Thornton P, Notenbaert A, Cramer L, Jones P, Herrero M., 2011. Mapping hotspots of climate change and food insecurity in the global tropics. CCAFS Report 5. Copenhagen, Denmark: CCAFS.

Feng, P., Liu, D.L., Wang, B., Waters, C., Zhang, M., Yu, Q., 2019a. Projected changes in drought across the wheat belt of southeastern Australia using a downscaled climate ensemble. International Journal of Climatology 39, 1041-1053.

Feng, P., Wang, B., Liu, D.L., Waters, C., Yu, Q., 2019b. Incorporating machine learning with biophysical model can improve the evaluation of climate extremes impacts on wheat yield in south-eastern Australia. Agricultural and Forest Meteorology 275, 100-113.

Feng, P., Wang, B., Liu, D.L., Xing, H., Ji, F., Macadam, I., Ruan, H., Yu, Q., 2018. Impacts of rainfall extremes on wheat yield in semi-arid cropping systems in eastern Australia. Climatic change 147, 555-569.

Fitzsimmons, R., 2001. Winter cereal production statistics, NSW 1922−1999: wheat, oats, barley: area production and yield: NSW by local government areas, individual years plus 5 and 10 year averages, 6th edn. Australian Institute of Agricultural Science and Technology,Wahroonga.

Franke, A., Baijukya, F., Kantengwa, S., Reckling, M., Vanlauwe, B., Giller, K.E., 2019. Poor farmers–poor yields: socio-economic, soil fertility and crop management indicators affecting climbing bean productivity in northern Rwanda. Experimental Agriculture 55, 14-34.

Gbetibouo, G.A., Ringler, C., Hassan, R., 2010. Vulnerability of the South African farming sector to climate change and variability: An indicator approach. Natural Resources Forum 34, 175-187.
Gomez-Macpherson, H., Richards, R., 1995. Effect of sowing time on yield and agronomic characteristics of wheat in south-eastern Australia. Australian Journal of Agricultural Research 46, 1381-1399.
GRDC, 2004. DAN459 - western farming systems project - NSW agriculture component. 2000-2004, https://grdc.com.au/research/reports/report?id=198. The last accessed date: 5 May 2021.
Grinsted, A., Moore, J.C., Jevrejeva, S., 2004. Application of the cross wavelet transform and wavelet coherence to geophysical time series. Nonlinear Processes in Geophysics 11, 561-566.
Han, J., Wang, J., Zhao, Y., Wang, Q., Zhang, B., Li, H., Zhai, J., 2018. Spatio-temporal variation of potential evapotranspiration and climatic drivers in the Jing-Jin-Ji region, North China. Agricultural and Forest Meteorology 256-257, 75-83.
Hinkel, J., 2011. "Indicators of vulnerability and adaptive capacity": Towards a clarification of the science–policy interface. Global Environmental Change 21, 198-208.
Hochman, Z., Gobbett, D.L., Horan, H., 2017. Climate trends account for stalled wheat yields in Australia since 1990. Global Change Biology 23, 2071-2081.
Howden, S.M., Soussana, J.F., Tubiello, F.N., Chhetri, N., Dunlop, M., Meinke, H., 2007. Adapting agriculture to climate change. Proceedings of the National Academy of Sciences of the United States of America 104, p.19691-19696.
Huai, J., 2016. Role of livelihood capital in reducing climatic vulnerability: insights of Australian Wheat from 1990–2010. PloS One 11, e0152277.
IPCC, 2007 Climate Change 2007: Impacts, Adaptation, and Vulnerability. Contribution of Working Group II to the Fourth Assessment Report of the Intergovernmental Panel on Climate Change. Cambridge University Press, Cambridge, U.K.
IPCC, 2012. Managing the risks of extreme events and disasters to advance climate change adaptation. Special report of the Intergovernmental Panel on Climate Change. Journal of Clinical Cambridge University Press, Cambridge, U.K.
Jeffrey, S.J., Carter, J.O., Moodie, K.B., Beswick, A.R., 2001. Using spatial interpolation to construct a comprehensive archive of Australian climate data. Environmental Modelling & Software 16, 309-330.
Jeong, J.H., Resop, J.P., Mueller, N.D., Fleisher, D.H., Yun, K., Butler, E.E., Timlin, D.J., Shim, K.-M., Gerber, J.S., Reddy, V.R., Kim, S.-H., 2016. Random Forests for Global and Regional Crop Yield Predictions. PloS One 11, e0156571.
Kamali, B., Abbaspour, K.C., Lehmann, A., Wehrli, B., Yang, H., 2018a. Spatial assessment of maize physical drought vulnerability in sub-Saharan Africa: Linking drought exposure with crop failure. Environmental Research Letters 13.
Kamali, B., Abbaspour, K.C., Wehrli, B., Yang, H., 2018b. Drought vulnerability assessment of maize in Sub-Saharan Africa: Insights from physical and social perspectives. Global and Planetary Change 162, 266-274.
Kendall, M. G., 1975. Rank Correlation Methods, Griffin, London
Kingwell, R., Pannell, D., 2005. Economic trends and drivers affecting the wheatbelt of Western Australia to 2030. Crop & Pasture Science 56, 553-561.
Kurukulasuriya, P., Mendelsohn, R., 2008. How Will Climate Change Shift Agro-Ecological Zones and Impact African Agriculture? The World Bank.
Lal, M., Singh, K., Rathore, L., Srinivasan, G., Saseendran, S., 1998. Vulnerability of rice and wheat yields in NW India to future changes in climate. Agricultural and Forest Meteorology 89, 101-114.
Li, L., Yao, N., Li, Y., Liu, D.L., Wang, B., Ayantobo, O.O., 2019. Future projections of extreme temperature events in different sub-regions of China. Atmospheric Research 217, 150-164.
Li, Y., Huang, H., Ju, H., Lin, E., Xiong, W., Han, X., Wang, H., Peng, Z., Wang, Y., Xu, J., Cao, Y., Hu, W., 2015. Assessing vulnerability and adaptive capacity to potential drought for winter-wheat under the RCP 8.5 scenario in the Huang-Huai-Hai Plain. Agriculture, Ecosystems & Environment 209, 125-131.
Li, Y., Xiong, W., Hu, W., Berry, P., Ju, H., Lin, E., Wang, W., Li, K., Pan, J., 2014. Integrated assessment of China's agricultural vulnerability to climate change: a multi-indicator approach. Climatic Change 128, 355-366.

Lobell, D.B., Schlenker, W., Costa-Roberts, J., 2011. Climate Trends and Global Crop Production Since 1980. Science 333, 616.
Lu, J., Carbone, G.J., Gao, P., 2017. Detrending crop yield data for spatial visualization of drought impacts in the United States, 1895–2014. Agricultural and Forest Meteorology 237-238, 196-208.
Mann, H.B., 1945. Nonparametric Tests Against Trend. Econometrica 13, 245-259.
McCarthy, J.J., Canziani, O.F., Leary, N.A., Dokken, D.J., White, K.S., 2001. Climate change 2001: Impacts, adaptation, and vulnerability. Contribution of Working Group II to the Third Assessment Report of the Intergovernmental Panel on Climate Change (IPCC). Global Ecology and Biogeography 12, 87-88.
Neset, T.-S., Wiréhn, L., Opach, T., Glaas, E., Linnér, B.-O., 2019. Evaluation of indicators for agricultural vulnerability to climate change: The case of Swedish agriculture. Ecological Indicators 105, 571-580.
Olesen, J.E., Trnka, M., Kersebaum, K.C., Skjelvåg, A.O., Seguin, B., Peltonen-Sainio, P., Rossi, F., Kozyra, J., Micale, F., 2011. Impacts and adaptation of European crop production systems to climate change. European Journal of Agronomy 34, 96-112.
Pandey, R., Jha, S.K., Alatalo, J.M., Archie, K.M., Gupta, A.K., 2017. Sustainable livelihood framework-based indicators for assessing climate change vulnerability and adaptation for Himalayan communities. Ecological Indicators 79, 338-346.
Ray, D.K., Gerber, J.S., MacDonald, G.K., West, P.C., 2015. Climate variation explains a third of global crop yield variability. Nature Communications 6, 1-9.
Ray, D.K., Mueller, N.D., West, P.C., Foley, J.A., Hart, J.P., 2013. Yield Trends Are Insufficient to Double Global Crop Production by 2050. PloS One 8, e66428.
Richards, R.A., Hunt, J.R., Kirkegaard, J.A., Passioura, J.B., 2014. Yield improvement and adaptation of wheat to water-limited environments in Australia—a case study. Crop and Pasture Science 65, 676-689.
Rossi, A., Massei, N., Laignel, B., 2011. A synthesis of the time-scale variability of commonly used climate indices using continuous wavelet transform. Global and Planetary Change 78, 1-13.
Roushangar, K., Alizadeh, F., Adamowski, J., 2018. Exploring the effects of climatic variables on monthly precipitation variation using a continuous wavelet-based multiscale entropy approach. Environmental Research 165, 176-192.
Sang, Y.F., Wang, Z., Liu, C., 2014. Comparison of the MK test and EMD method for trend identification in hydrological time series. Journal of Hydrology 510, 293-298.
Sayemuzzaman, M., Jha, M.K., 2014. Seasonal and annual precipitation time series trend analysis in North Carolina, United States. Atmospheric Research 137, 183-194.
Schirmer, J., Hanigan, I., 2015. Understanding the resilience of NSW farmers.
Semenov, M.A., Shewry, P.R., 2011. Modelling predicts that heat stress, not drought, will increase vulnerability of wheat in Europe. Scientific Reports 1, 66.
Senapati, N., Halford, N.G., Semenov, M.A., 2021. Vulnerability of European wheat to extreme heat and drought around flowering under future climate. Environmental Research Letters 16, 024052.
Sendhil, R., Jha, A., Kumar, A., Singh, S., 2018. Extent of vulnerability in wheat producing agro-ecologies of India: Tracking from indicators of cross-section and multi-dimension data. Ecological Indicators 89, 771-780.
Sonkar, G., Mall, R., Banerjee, T., Singh, N., Kumar, T.L., Chand, R., 2019. Vulnerability of Indian wheat against rising temperature and aerosols. Environmental Pollution 254, 112946.
Sun, C.X., Huang, G.H., Fan, Y., Zhou, X., Lu, C., Wang, X.Q., 2019. Drought Occurring with Hot Extremes: Changes Under Future Climate Change on Loess Plateau, China. Earth's Future 7, 587-604.
Torrence, C., Compo, G.P., 1998. A Practical Guide to Wavelet Analysis. Bulletin of the American Meteorological Society 79, 61-78.
Uddin, M.N., Saiful Islam, A.K.M., Bala, S.K., Islam, G.M.T., Adhikary, S., Saha, D., Haque, S., Fahad, M.G.R., Akter, R., 2019. Mapping of climate vulnerability of the coastal region of Bangladesh using principal component analysis. Applied Geography 102, 47-57.
Wang, B., Chen, C., Liu, D.L., Asseng, S., Yu, Q., Yang, X., 2015. Effects of climate trends and variability on wheat yield variability in eastern Australia. Climate Research 64, 173-186.
Wang, B., Feng, P., Liu, D.L., Waters, C., 2020. Modelling biophysical vulnerability of wheat to future climate change: A case study in the eastern Australian wheat belt. Ecological Indicators 114, 106290.

Wang, B., Liu, D.L., Asseng, S., Macadam, I., Yang, X., Yu, Q., 2017. Spatiotemporal changes in wheat phenology, yield and water use efficiency under the CMIP5 multimodel ensemble projections in eastern Australia. Climate Research 72, 83-99.

Wang, B., Liu, D.L., Macadam, I., Alexander, L.V., Abramowitz, G., Yu, Q., 2016. Multi-model ensemble projections of future extreme temperature change using a statistical downscaling method in south eastern Australia. Climatic Change 138, 85-98.

Wang, B., Liu, D.L., Waters, C., Yu, Q., 2018. Quantifying sources of uncertainty in projected wheat yield changes under climate change in eastern Australia. Climatic Change 151, 259-273.

Wang, H., Zhang, J., 2009. Analysis of Different Data Standardization Forms for Fuzzy Clustering Evaluation Results' Influence. 2009 3rd International Conference on Bioinformatics and Biomedical Engineering, pp. 1-4.

Watson, R.T., Zinyowera, M.C., Moss R.H., 1996. Climate Change 1995：Impacts, Adaptations and Mitigation of ClimateChange：Scientific—Technical Analyses. Cambridge University Press.

Watson, R.T., Zinyowera, M.C., Moss R.H., Dokken, D.J., 1997. IPCC Special Report on the Regional Impacts of Climate Change – An Assessment of Vulnerability. Cambridge University Press, Cambridge.

Yang, X., Chen, F., Lin, X., Liu, Z., Zhang, H., Zhao, J., Li, K., Ye, Q., Li, Y., Lv, S., Yang, P., Wu, W., Li, Z., Lal, R., Tang, H., 2015. Potential benefits of climate change for crop productivity in China. Agricultural and Forest Meteorology 208, 76-84.

Ye, T., Nie, J., Wang, J., Shi, P., Wang, Z., 2015. Performance of detrending models of crop yield risk assessment: evaluation on real and hypothetical yield data. Stochastic Environmental Research and Risk Assessment 29, 109-117.

Yue, Y., Li, J., Ye, X., Wang, Z., Zhu, A.X., Wang, J.A., 2015. An EPIC model-based vulnerability assessment of wheat subject to drought. Natural Hazards 78, 1629-1652.

Zaitchik, B.F., Macalady, A.K., Bonneau, L.R., Smith, R.B., 2006. Europe's 2003 heat wave: a satellite view of impacts and land–atmosphere feedbacks. International Journal of Climatology: A Journal of the Royal Meteorological Society 26, 743-769.

Zeri, M., Cunha-Zeri, G., Gois, G., Lyra, G.B., Oliveira-Júnior, J.F., 2019. Exposure assessment of rainfall to interannual variability using the wavelet transform. International Journal of Climatology 39, 568-578.

Zhao, J., Yang, X., Dai, S., Lv, S., Wang, J., 2015. Increased utilization of lengthening growing season and warming temperatures by adjusting sowing dates and cultivar selection for spring maize in Northeast China. European Journal of Agronomy 67, 12-19.

Chapter 3. Can agronomic options alleviate the risk of compound drought-heat events during the wheat flowering period in southeastern Australia?

This chapter is based on the following manuscript:

Li, S., Wang, B., Li Liu, D., Chen, C., Feng, P., Huang, M., Wang, X., Shi, L., Waters, C., Huete, A., 2024. Can agronomic options alleviate the risk of compound drought-heat events during the wheat flowering period in southeastern Australia? European Journal of Agronomy 153, 127030.

Abstract

The impacts of compound drought-heat (DH) events on crops are more devastating than a single extreme event of drought or heat. Previous studies mainly assessed the change of individual extreme climate events. However, studies quantifying the characteristics of DH events during crop growth periods are still lacking. To the best of our knowledge, there is no study that has quantified the potential of adjusting sowing time and changing cultivars to reduce the risk of DH events for wheat in Australia. We aimed to (1) develop a combined index to capture the DH events occurring during the wheat flowering period at six study sites in southeastern Australia's wheat belt; (2) quantify the changes in the frequency (*DHF*), duration (*DHD*), and intensity (*DHI*) of DH events under future climate; and (3) identify feasible agronomic options to reduce the risk of DH events. We used the APSIM model driven by climate projections from 27 GCMs for the period of 1981–2100 to simulate the wheat flowering time and daily plant available water (PAW) at 0-100 cm soil layer. The wheat sensitive period (WSP) was defined as the period from 2 weeks before flowering to 2 weeks after flowering time. A DH event occurs when the daily maximum temperature is higher than 28 ℃ and daily PAW is less than 40% of plant available water capacity for three consecutive days or more. Then, we assessed the *DHF*, *DHD*, and *DHI* under projected climate change. Finally, we investigated the potential of changing sowing time and cultivars to alleviate *DHF*, *DHD*, and *DHI* under different climate scenarios. According to the average values across six sites, the *DHF*, *DHD*, and *DHI* during the WSP increased by 15%, 12%, and 0.9% in 2040s, and 49%, 44%, and 5% in 2080s, respectively, compared to 2000s. Such increases in DH events were mainly due to enhanced heat events. Early sowing and planting better-performing wheat cultivars with early flowering had great potential to lower the risk of future DH events. They could reduce the *DHF*, *DHD*, and *DHI* by 15%-100%, 18%-100%, and 16%-100%, respectively, compared to without adaptation options. However, the strategy may introduce an increased frost risk across six sites, especially in regions with climates that are less dry and hot, such as Mudgee and Wagga Wagga. We expect our modelling work can provide useful information for developing effective

agronomic management practices to help Australian wheat growers better prepare for DH events under climate change. The newly proposed DH framework can be applied to other dryland wheat growing regions globally.

Keywords: Compound drought-heat events; Wheat flowering period; Agronomic options; Southeastern Australia; APSIM; Climate change

3.1. Introduction

Extreme climate and weather events are natural disasters that can plague agricultural production (Elahi et al., 2021). Instances of drought and heat disrupt the physiological processes of crops (Poudel et al., 2020; Prasad et al., 2008) and reduce crop cycle duration (García et al., 2018), thus decreasing yield. For example, drought events have resulted in an estimated average reduction of 10.1% of national cereal production during 1964–2007 across the globe, with heat events contributing a similar production loss of 9.1% (Lesk et al., 2016). It's worth noting that extreme events often occur simultaneously and interact with each other (Lesk et al., 2021; Prasad et al., 2008). Often, the impacts caused by compound drought-heat (DH) events are more devastating than a single extreme event (Cohen et al., 2021; Li et al., 2022). For instance, the probability of maize yield loss was increased by 4-31% over major maize-producing countries during 1961-2016 when single heat or drought events were transformed into DH events (Feng et al., 2019b). Additionally, the European 2018 summer DH, record-high summer temperature co-occurred with record-low rainfall, led to a widespread crop harvest failure across many European countries (Bastos et al., 2020).

Wheat is the most widely planted food crop around the world (FAO, 2021), and it is the staple food source for nearly 40% of the global population (Giraldo et al., 2019). Australia is one of the top five wheat exporters in the world: Australia has contributed annually 11.3% of the global wheat exports since 1961 (FAO, 2021) and is vital for global food security. Wheat in Australia is usually grown under rain-fed conditions and often suffers from drought during the growing season (Chenu et al., 2011; Chenu et al., 2013). In addition, untimely spring heat events often occurred during wheat flowering and grain filling periods (Alexander et al., 2010; Talukder et al., 2013), aggravating the negative effects of drought on wheat. However, most previous studies focused on assessing the impact of individual extreme events such as heat or drought and adaptation strategies for the individual events, rather than on the compound extreme events that co-occur simultaneously at a specific location. Additionally, the simple addition of the effect of two single events is not enough to characterize the impacts of the compound events (Cohen et al., 2021). For example, Ababaei and Chenu (2020) assessed the impact of heat stress on wheat growth based on the modified APSIM model (Holzworth et al., 2014). Madadgar et al. (2017) used a multivariate probabilistic model to investigate yield loss probability of the five largest crops in Australia (wheat, broad beans, canola, lupine, and barley) due to

drought. However, studies that quantify the characteristics and changes of DH events around wheat flowering time under climate change in Australia are still lacking.

Currently, DH events are normally investigated by combining temperature anomalies with meteorological drought indicators (monthly or seasonal precipitation, Standardized Precipitation Index, or Standardized Precipitation Evapotranspiration Index) (Geirinhas et al., 2021; Ribeiro et al., 2020; Wang et al., 2022), instead of using agricultural drought indicators. Meanwhile, due to the limitation of different temporal evolution between drought (weeks to months) and heat (days to weeks) (Mukherjee et al., 2020), most researchers defined DH events by detecting the heat events occurring within a long-term drought context (Geirinhas et al., 2021; Guo et al., 2022; Kong et al., 2020). The asymmetry of the time scale for drought (weekly, monthly, or seasonally scale) and heat (daily) in these DH frameworks leads to the inability to obtain the daily characteristics of DH events. Moreover, heat events mainly occur in the summer season, which is not the growth period of winter wheat, though several studies have investigated the DH events for summer crop maize (Feng et al., 2019b; Guo et al., 2022; Lesk et al., 2021; Li et al., 2022). Nevertheless, Australian wheat is likely to encounter simultaneous drought and heat stress around flowering time in spring, which can create nonnegligible losses in wheat grain number and grain weight (Lobell et al., 2015). To fill this knowledge gap, we developed a comprehensive combined index at a daily scale to investigate the characteristics of DH events that possibly occur during the wheat growing season.

Agronomic adaptative strategies have great potential to alleviate the impacts of extreme weather events on crops (Gouache et al., 2012; Korres et al., 2017; Vogel et al., 2019). Generally, the mechanism of these strategies includes escape and tolerance of extreme events. The escape is done through optimizing phenological development and sowing at a suitable time to avoid the susceptible growth stages of crops coinciding with the duration of abiotic stresses (e.g., frost, heat, and drought events) (Manavalan et al., 2009). For example, Stratonovitch and Semenov (2015) pointed out that a wheat cultivar with an early flowering date and longer grain filling duration had great potential to cope with heat stress compared with the existing cultivars. Additionally, Hunt et al. (2019) reported that early sowing has the potential to moderate the adverse effects of climate change on wheat in Australia. The tolerance to extreme events generally relies on the optimization of crop properties (e.g., better canopy and root architecture, stable turgor and volume of plant cells, and high strength of the antioxidant systems) (Hasanuzzaman & Fujita, 2011; Maqbool et al., 2017; Turner, 1980). For instance, Hasanuzzaman and Fujita (2011) and Mohi-Ud-Din et al. (2021) pointed out that drought and heat tolerance are dependent on the strength of the antioxidant systems of crops to endure oxidative stresses. Additionally, the traits of grain weight per tiller had a significant influence on wheat tolerance to heat and drought (Mondal et al., 2015). Compared with a single option, the combinations of early sowing and planting appropriate cultivars have a higher potential to help

crops cope with extreme climate and weather events (Pirttioja et al., 2019). Semenov and Stratonovitch (2015) found that if an optimal wheat cultivar was sown 2 to 4 weeks earlier, the yield could be further increased by 0.2-0.6 t ha^{-1} in Europe. However, to the best of our knowledge, no study has quantified the potential for mitigating the impact of DH events on wheat in Australia through of changes in cultivars and sowing time.

In this study, we used the APSIM-wheat model to simulate wheat phenology and soil water content. The DH events occurring in the wheat flowering period were firstly defined. Then, we evaluated characteristics of DH events under the historical and future climates based on 27 different global climate models (GCMs) from the Coupled Model Intercomparison Project Phase 6 (CMIP6) under two emission scenarios at six study sites in southeastern Australia. Also, we assessed the potential of sowing earlier and adopting different wheat cultivars to reduce the risk of DH events. The main objectives of this study were to (1) develop a combined index to capture the DH events occurring during the wheat flowering period at six study sites in southeastern Australia's wheat belt; (2) quantify the changes in the DH frequency (*DHF*), DH duration (*DHD*), and DH intensity (*DHI*) under future climate; and (3) identify feasible agronomic options to reduce the risk of future DH events.

3.2. Materials and methods

3.2.1 Study sites

The New South Wales (NSW) wheat belt is located in the southeast of Australia and spans a wide range of topographical and climatic conditions. The eastern parts consist of mountains up to 1100 m in elevation, while the western parts are mainly plains (Feng et al., 2020). During the wheat growing season (typically April-November), the rainfall gradient is increased from 172 mm in the west to 763 mm in the southeast. Conversely, the average temperature in the growth period gradually rises from southeast to northwest, ranging from 8.3 ℃ to 17.1 ℃ (Wang et al., 2017a). We selected six sites representing different agro-climatic zones across the NSW wheat belt in this study (Table 3-1). They are Walgett and Moree plains in the north of the wheat belt, Lachlan and Mudgee in the middle, and Balranald and Wagga Wagga located in the south (Figure 3-1). Wheat is grown under rain-fed conditions in the NSW wheat-belt, where it is sown in autumn (April-July), flowers in early to mid-spring, and matures in late spring (Liu, 2007; Wang et al., 2015a).

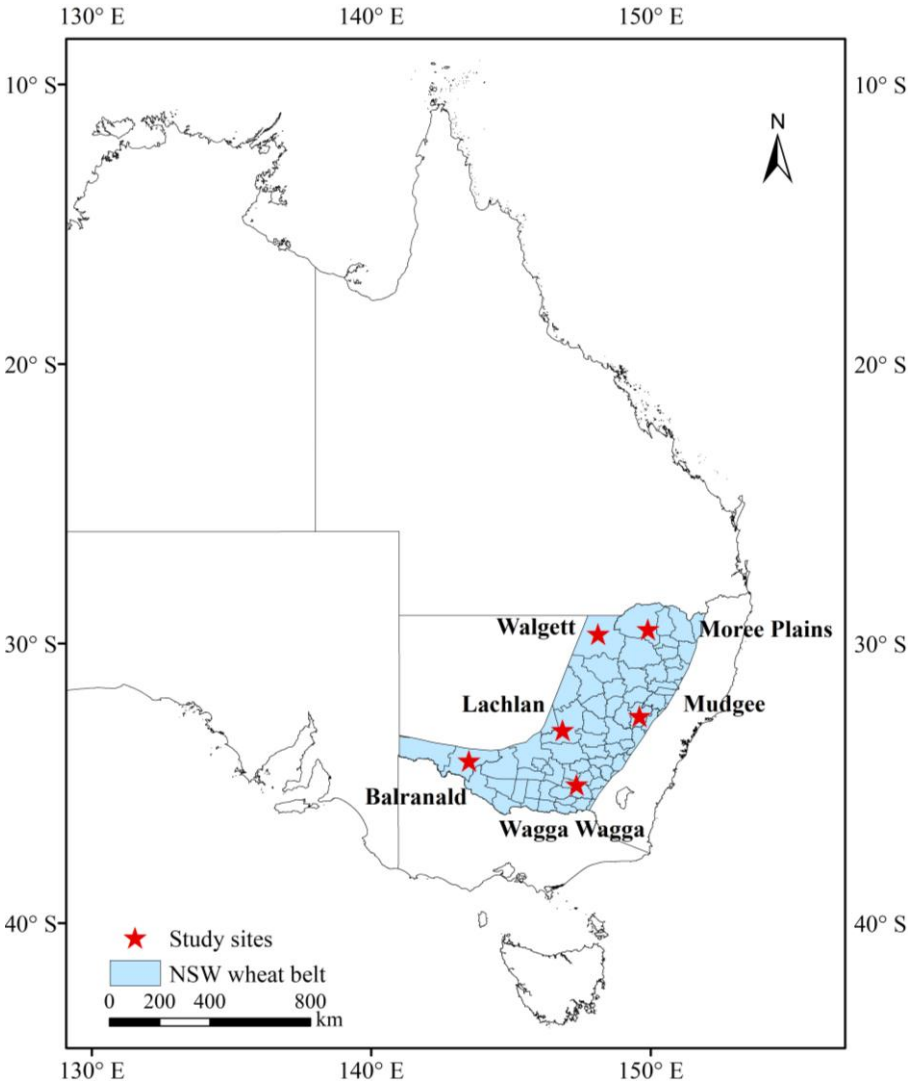

Figure 3-1. The location of six selected sites in New South Wales (NSW) wheat belt in southeastern Australia.

Table 3-1. Total rainfall, average value of daily maximum temperature (T_{max}), average value of daily minimum temperature (T_{min}), average value of daily mean temperature (T_{mean}), and plant available water holding capacity (PAWC) (0-100 cm) in the wheat growing season (April - November) from 1981 to 2020 at the six study sites (Walgett, Moree Plains, Lachlan, Mudgee, Balranald, and Wagga Wagga).

Sites	Latitude	Longitude	Rainfall (mm)	T_{max} (°C)	T_{min} (°C)	T_{mean} (°C)	PAWC (mm)
Walgett	-29.66	148.12	255.4	24.4	9.7	17.0	117.5
Moree Plains	-29.50	149.90	319.7	23.5	9.4	16.5	165.4
Lachlan	-33.10	146.85	277.3	21.1	7.7	14.4	129.1
Mudge	-32.60	149.60	438. 9	19.6	5.7	12.6	89.7
Balranald	-34.20	143.50	194. 5	21.2	7.7	14.4	92.0
Wagga Wagga	-35.05	147.35	365.1	18. 8	6.4	12.6	92.0

3.2.2 Data sources

3.2.2.1 Climate data

We downloaded the monthly gridded climate data for 27 GCMs of CMIP6 (Table 3-S1) from 1900 to 2100 from World Climate Research Program (WCRP) (https://esgf-node.llnl.gov/search/cmip6/). The simulation of CMIP6 was conducted under the combination of a representative concentration pathway (RCP) and a shared socio-economic pathway (SSP). We selected the data under SSP245 and SSP585 scenarios. SSP245 represents the scenario combining a middle socio-economic development road (SSP2) with the medium-low radiative forcing of 4.5 W/m^2 (RCP4.5). SSP585 represents the scenario combining a high energy-intensive, socio-economic developmental path (SSP5) with high radiative forcing 8.5 W/m^2 (RCP8.5) (Grose et al., 2020; Li et al., 2020; Yang et al., 2021; You et al., 2021).

Normally, the future climate projections from GCMs have coarse spatiotemporal resolution and cannot be directly used at study sites. We used a statistical downscaling method, NWAI-WG, proposed by Liu and Zuo (2012) to downscale the daily climate data for six selected sites. The specific procedures were as follows: firstly, the raw GCM data were downscaled to specific climate sites of interest by an inverse distance-weighted interpolation method. Then, we corrected the bias of monthly GCMs values for each site, making it consistent with the observed values. According to the correlation between historical climate data and future climate predictions, we calculated the parameters of the Stochastic Weather Generator (WGEN) (Richardson and Wright, 1984). Finally, the monthly scale value after bias correction was downscaled to the daily value through the modified WGEN.

3.2.2.2 Soil data

We obtained the soil hydraulic properties and other soil parameters from the Australian Soil Resource Information System (http://www.asris.csiro.au/). There were more than 800 soil profiles in agricultural areas of Australia, and most of them were parameterized for modeling (Dalgliesh et al., 2012). We used the soil profiles that are geographically closest to the six sites (Feng et al., 2020; Innes et al., 2015). Plant available water capacity (PAWC) represents the total amount of water a soil can store for crop to use. PAWC is calculated as the difference of volumetric water content between the upper drainage limit (DUL) and crop lower limit (Asseng et al., 2001; Wang et al., 2017b). The value of LL is specific to the crop, we used wheat LL in this study. The range of soil PAWC (0-100 cm) for six sites is from 89.7 to 165.4 mm (Table 3-1), due to different soil types in different regions.

3.2.3 APSIM model

We used APSIM (Agricultural Production Systems sIMulator) version 7.10 to simulate the phenology of wheat and soil water content on a daily basis for baseline period (2000s: 1981-2020) and two future periods (2040s: 2021-2060, 2080s: 2061-2100). APSIM is an agricultural production system simulation model developed by the Agricultural Production Systems Research Group (APSRU) in collaboration between CSIRO and Queensland Government (Holzworth et al., 2014; Keating et al., 2003). The model system has been widely validated and used all over the world and has played a powerful role in agricultural research (Amarasingha et al., 2015; Archontoulis et al., 2014; Flohr et al., 2018; Seyoum et al., 2017; Wang et al., 2017b). In particular, the APSIM wheat module has been applied in many studies throughout Australian agricultural areas (Asseng et al., 2011; Chenu et al., 2013). It can adequately simulate the growth process of wheat (Anwar et al., 2015) and the dynamics of soil water and nitrogen in agricultural systems (Archontoulis et al., 2014; Liu et al., 2014). Also, APSIM can assess the potential of different agronomic options (e.g., adjusting sowing date and changing different cultivars) to cope with climate change (Wang et al., 2019; Xiao et al., 2020).

Our simulations mainly involved wheat phenology and soil water dynamics. In the APSIM-Wheat model, wheat is divided into eight phases from sowing to maturity: 1) sowing to germination, 2) germination to emergence, 3) emergence to end of juvenile stage, 4) end of juvenile stage to floral initiation, 5) floral initiation to flowering, 6) flowering to start of grain filling, 7) start of grain filling to end of grain filling, and 8) end of grain filling to physiological maturity. The length of each phase is determined by the required accumulation of thermal time, which is modified by additional factors specific to each phase, such as vernalization and photoperiod (APSIM, 2015).

The SoilWat module is used to simulate the soil moisture status. It is a cascading water balance model that evolved from CERES (Jones et al., 1986) and PERFECT (Littleboy et al., 1992). SoilWat can simulate hydrological processes, including runoff, evaporation, saturated water flow, unsaturated water flow, leaching, and above saturation flow between layers on a daily basis, based on the lower limit (LL15), DUL, saturated (SAT), crop lower limit (CLL), and other hydraulic parameters. More detailed information about APSIM can be found in previous studies (Asseng et al., 2000; Hao et al., 2021; Keating et al., 2003).

3.2.4 APSIM simulations

We ran simulations for 6 sites with 27 GCMs over 1981 to 2100 under two emission scenarios using the APSIM-wheat model. The wheat cultivar *Janz* was used in this study. Due to its prevalence in NSW, this mid-maturity spring cultivar is widely cultivated and serves as a suitable representative for studying the impacts of climate change on wheat in the region (Kirkegaard and Lilley, 2007; Wang et al., 2009). In addition, *Janz* has also been well-parameterized in the APSIM model (Zheng et al., 2012). Based on the target sowing window between 27th April to 15th July (day 117 to day 196) for wheat *Janz* proposed by Zheng et al. (2012), we set a sowing rule to mimic real farm sowing practices. This approach considered the present soil water and the current rainfall to meet the certain moisture condition or when the sowing window is coming to an end. Sowing occurred when the following rule was met:

$$R_k \geq PAWC_{50} \times CR_k - SW_{k\text{-}1} \tag{3-1}$$

$$CR_k = \sqrt[3]{\frac{CA}{(1 + CB \times D_k)}} \tag{3-2}$$

$$CB = \frac{A_2^{\,3} - A_1^{\,3}}{S_s \times A_1^{\,3} - S_e \times A_2^{\,3}} \tag{3-3}$$

$$CA = A_1^{\,3} + S_s \times A_1^{\,3} \times CB \tag{3-4}$$

where R_k is rainfall of the kth day in the sowing window (27th April to 15th July); $PAWC_{50}$ is the plant available water capacity within 50 cm; $SW_{k\text{-}1}$ is the previous day's soil water content within the sowing window; CR_k is the inverse proportional function of the D_k (Eq. 3-2); D_k is day of year for the kth day in the sowing window. According to the sowing window we set, the value of CR_k was between 1.2-0.8, which gradually decreased with time. This setting balanced the limits of the sowing window and the need for soil moisture condition. We showed the CR_k value in 1981 of site Walgett as an example for better description (Figure 3-S1). A_1=1.2; A_2=0.8; S_s and S_e are the day of year for the start and the end of the sowing window, respectively. We set the sowing window from S_s=117 to S_e=196.

Due to the spatial heterogeneity of the soil profile and the spatiotemporal variations of precipitation, the soil water content is dynamic and varies in different sites. Our sowing rule aimed to make wheat in different regions across the wheat-belt sown under the most favorable water conditions in the sowing window, thus ensuring a higher germination rate. We considered that this is more reasonable and realistic than a sowing rule based on the amount of recent rainfall for sites across different rainfall zones with different soil moisture content during the sowing season. According to the sowing rules, soil properties, and climate projections of 27 GCMs, we performed the first set of APSIM simulations to identify the wheat phenology and plant available soil water (PAW). The output wheat phenological data and daily PAW data were used to determine and calculate the frequency, duration, and intensity of DH events in the sensitive flowering period of wheat. We analyzed their temporal and spatial variations, and they were used as the control scenarios without agronomic adaptative options to verify the potential of the agronomic options in avoiding DH events.

3.2.5 Drought, heat, and compound drought-heat events in the wheat flowering period

The wheat flowering period is critical to wheat growth and development (Cossani et al., 2009). It determines the wheat grain number and grain weight (Dias and Lidon, 2009; Frank and Bauer, 1982; Rawson and Bagga, 1979), and also is highly susceptible to heat and drought stress (Saini and Westgate, 1999; Shah and Paulsen, 2003; Stratonovitch and Semenov, 2015; Talukder et al., 2014; Vignjevic et al., 2015). Specifically, extreme events that occurred during the period from pre-flowering to 3 days after flowering can result in grain sterility and abortion (Tashiro & Wardlaw, 1990), which in turn reduces grain number. The extreme events that occurred 6-14 days after flowering led to a decline in the storage capacity of cereal grains (Saini & Westgate, 1999; Tashiro & Wardlaw, 1990), thereby diminishing the grain size and single-grain weight. We selected the period from 2 weeks before flowering to 2 weeks after flowering as the wheat sensitive period (WSP, 29 days) in this study. The WSP includes the heading stage, the flowering stage, part of the critical period for grain set, and the start of the linear phase of grain filling of wheat (APSIM, 2015; Pimstein et al., 2009; Zadoks et al., 1974). The annual WSPs at six sites were obtained based on the wheat flowering time simulated by APSIM.

We selected the general and well-accepted criteria to define drought and heat events in the WSP. That is, using the threshold of PAW to define whether wheat suffered water stress, and the threshold of daily maximum temperature (*TX*) was used to define whether heat stress occurred. Many experimental studies have found that 40% of PAWC can be the threshold for distinguishing water stress on wheat (Ciais et al., 2005; Granier et al., 1999). When the PAW falls below 40% of PAWC, the water uptake of wheat can be restricted, leading to adverse impacts on wheat growth and development, ultimately influencing the formation of yields (Kirkegaard and Lilley, 2007; Wenda-Piesik, 2011). Therefore, a drought event was

triggered when PAW in the 0-100 cm soil profile was lower than 40% of PAWC in this profile for consecutive three or more days. The reason why we only considered PAW in 0-100 cm soil layer is that the majority of wheat roots are distributed in 0-30 cm with a small fraction below 30 cm (Chen et al., 2014) and further with few roots below 100 cm (Fan et al., 2016; Gan et al., 2011). Considering a very small fraction of roots below 100 cm which has a small contribution to total water uptake, in this study we focused on the PAWC and soil water content within the 0-100 cm soil layer. In terms of heat definition, the optimal temperature range is normally 18 °C -28 °C around the wheat flowering stage (Mullarkey and Jones, 2000; Porter and Gawith, 1999). We used 28 °C as a threshold of temperature tolerance during the flowering period. When the daily maximum temperature is higher than 25-28 °C, the size and weight of wheat grain will be smaller (Lalic et al., 2013; Wheeler et al., 1996). Therefore, we defined heat events during WSP when the daily *TX* is higher than 28 °C for three consecutive days or more (Dodd et al., 2021; Mukherjee and Mishra, 2021; Mullarkey and Jones, 2000; Ristic et al., 2007). Based on the above-mentioned criteria for the definition of drought and heat events during WSP, we defined a compound DH event when heat and drought events occur simultaneously. Table 3-2 shows an example of one DH event occurring during the WSP.

We characterized the DH events from three dimensions: frequency, duration, and intensity. *DHF* refers to the ratio of the accumulative sum days of all DH events in WSP to the length of the window (29 days); *DHD* represents the maximum number of days within DH events in the WSP; *DHI* was defined as the mean weighted sum of PAW and *TX* excesses over the drought and heat thresholds, respectively, over the WSP.

$$DH_j = d_i \left| \left\{ \left(TX_{ij} \geq T_c \right) \bigcap \left(PAW_{ij} \leq \delta \times PAWC \right) \right\}, j = 1,2,...,N; i = l+1, l+2, ..., l+m_j, m_j \geq 3; w_s \leq d_i \leq w_e \right.$$

(3-5)

where DH_j is the *j*th DH event; N is the number of DH events in each WSP; d_i is the *i*th day in the WSP with the subscript l presenting the day before the start of the *j*th DH event; TX_{ij} is the maximum temperature of d_i in the *j*th DH event; T_c is the heat threshold temperature, which we took as 28 ℃; PAW_{ij} is plant available water at d_i in the *j*th DH event; δ is a constant to set starting point for drought effect as the amount of PAW ($\leq \delta \times PAWC$) in WSP, we set $\delta = 0.4$ (Ciais et al., 2005; Granier et al., 1999); w_s is the start day of WSP; w_e is the end day of WSP.

Table 3-2. Example of one compound drought-heat (DH) event occurring during the wheat sensitive period (WSP). d_i is the ith day in the WSP; w_s is the start day of WSP; w_e is the end day of WSP; TX_i is the maximum air temperature of ith day in WSP; PAW_i is the plant available water of ith day in WSP; $PAWC$ is plant available water capacity in 0-100 cm soil layer; DH_j is the jth DH event in the WSP.

d_i	$TX_i \geq 28$ ℃	$PAW_i \leq \delta \times PAWC$	
w_s	TRUE	FALSE	
…	FALSE	TRUE	
l+1	TRUE	TRUE	
l+2	TRUE	TRUE	
…	TRUE	TRUE	DH_j
$l+m_j$	TRUE	TRUE	
…	FALSE	FALSE	
w_e	TRUE	TRUE	

DHF was calculated as the cumulative sum of the consecutive days during each DH event (Eq. 3-6) in the WSP dividing by the length of the WSP (29 days).

$$DHF = \frac{\sum_{j=1}^{N} m_j}{w_e - w_s + 1}, j = 1, 2, ..., N, N \geq 1 \quad (3\text{-}6)$$

DHI was calculated based on the mean value of the daily intensity during the consecutive days of DH event over the WSP. We obtained the daily intensity by weighting the sum of the daily standardized values of drought intensity and the intensity of heat. The drought intensity is represented by the difference between the drought threshold ($\delta \times PAWC$) and the daily PAW divided by the difference between the drought threshold and the plant available water threshold of wheat permanent wilting point. It is a dimensionless value between 0 and 1, 1 is the highest drought intensity (Eq. 3-7).

$$DI_{ij} = \frac{\delta \times PAWC - PAW_{ij}}{\delta \times PAWC}, i = 1, 2, ..., m_j; j = 1, 2, ..., N \quad (3\text{-}7)$$

where DI_{ij} is the daily drought intensity for the ith day of the jth DH event in a given year; $\delta \times PAWC$ is the threshold to define drought according to extractable water, in which $PAWC$ is defined by soil properties; PAW_{ij} is the plant available water on the ith day of the jth DH event.

Heat intensity was defined by Eq. 3-8. The ratio of TX exceeding the heat threshold (T_c) to the wheat high killing temperature (T_s) exceeding of T_c was calculated as the heat intensity. Also, it is a dimensionless value between 0 and 1. 1 is the highest heat intensity.

$$HI_{ij} = \frac{TX_{ij} - T_c}{T_s - T_c}, i = 1, 2, ..., m_j; j = 1, 2, ..., N \tag{3-8}$$

where HI_{ij} is the daily heat intensity for the ith day of the jth DH event in a given year; TX_{ij} is the maximum temperature for the ith day of the jth DH event. We took T_s (the wheat high killing temperature) as 42 ℃, because Kumar and Charan (1998) pointed out that wheat was killed when exposed to 42 ℃ for more than 48 hours.

The daily DHI was calculated as the sum of the daily standardized values of heat intensity and drought intensity.

$$SDH_{ij} = \alpha DI_{ij} + (1 - \alpha) HI_{ij}, i = 1, 2, ..., m_j; j = 1, 2, ..., N \tag{3-9}$$

$$CDH_j = \frac{\sum_{i=1}^{m_j} SDH_{ij}}{m_j}, j = 1, 2, ..., N \tag{3-10}$$

$$DHI = \frac{\sum_{j=1}^{N} CDH_j}{N}, j = 1, 2, ..., N, N \geq 1 \tag{3-11}$$

where SDH_{ij} is the daily DH intensity for the ith day of the jth DH event in a given year; α is the weight for daily drought intensity, we used 0.5; CDH_j is the DH intensity for the jth DH event in the given year.

3.2.6 Agronomic adaptation options

Our study used two adaptation options: changing cultivars and sowing on an earlier date. *Janz* was used as a reference cultivar for designing virtual wheat genotypes. It is a mid-mature cultivar and does not require strong vernalization. When designing virtual wheat cultivars, we only modified three genetic parameters (tt_end_of_juvenile (TTEJ), tt_floral_initiation (TTFI), and tt_flowering (TTFW)) which affect phenology, to control the timing of wheat flowering and make the WSP escape from DH events, generating 4^3=64 virtual wheat varieties. Detailed definitions of these parameters can be found in Table 3-3. Early sowing is

widely considered to be helpful for Australian wheat to cope with climate change. Therefore, we advanced the original sowing window by one and two weeks, respectively, that is, day 110 to day 189 (20 April to 8 July) and 103-182 (13 April to 1 July). After advancing the sowing window, specific early sowing dates were still determined according to the sowing rules in 2.4. Based on the settings of these adaptive options, we ran a second set of APSIM simulations using 27 GCMs data to test the potential of individuals and combined the two adaptations in reducing DH risk in WSP, respectively. Then, we selected the agronomic options corresponding to minimum *DHF*, *DHD*, and *DHI* under the 2040s and 2080s at the six sites, respectively, as the better-performing agronomic options.

3.2.7 Data visualization

We conducted APSIM simulations based on 27 climate change models (GCMs) under two emission scenarios (SSP245 and SSP585), covering the period from 1989 to 2100. This resulted in 27 annual estimations of different DH indices for each year within each scenario. Initially, we calculated the multi-year average of each DH indices for the 2000s (1989-2020), 2040s (2021-2060), and 2080s (2061-2100) using the annual data, as we present our data according to these three periods in all figures. Then to synthesize these multiyear average estimations from the 27 GCMs into a single representation, we employed ensemble averaging. The single representations for the 2000s, 2040s, and 2080s under two scenarios at the six study sites were displayed in bar plots.

To create the box plot for projected changes in DH indices after adopting each adaptation, we initially computed the multiyear average of DH indices for the 2040s and 2080s using annual data from 27 GCMs, both before and after adaptation. Subsequently, we then compared the difference in DH indices between before and after adaptation, within each GCM and time period. The projected changes in DH indices in the 2040s and 2080s from the 27 GCMs were directly visualized in the boxplot. Box boundaries indicate the 25^{th} and 75^{th} percentiles across GCMs, and whiskers below and above the box indicate the 10^{th} and 90^{th} percentiles. The black lines and crosshairs within each box indicate the multi-model median and mean respectively.

Table 3-3. The reference cultivar (*Janz*) and range of three genetic parameters selected in the APSIM model. The $3*4^3= 192$ agronomic options were generated by all possible combinations of different parameters and sowing window (Wang et al., 2019).

Sowing window	Cultivar parameters	Definition	Unit	Step	*Janz*	Minimum value	Maximum value
27 April to 15 July	TTEJ	Thermal time from emergence to end of juvenile	°C·day	100	400	300	600
	TTFI	Thermal time from end juvenile to floral initiation	°C·day	100	458	358	658
	TTFW	Thermal time from floral initiation to flowering	°C·day	30	109	79	169
20 April to 8 July	TTEJ	Thermal time from emergence to end of juvenile	°C·day	100	400	300	600
	TTFI	Thermal time from end juvenile to floral initiation	°C·day	100	458	358	658
	TTFW	Thermal time from floral initiation to flowering	°C·day	30	109	79	169
13 April to 1 July	TTEJ	Thermal time from emergence to end of juvenile	°C·day	100	400	300	600
	TTFI	Thermal time from end juvenile to floral initiation	°C·day	100	458	358	658
	TTFW	Thermal time from floral initiation to flowering	°C·day	30	109	79	169

3.3. Results

3.3.1. Projected change in wheat flowering window

Figure 3-2 shows the projected changes in wheat flowering time between two future periods (2021-2060 and 2061-2100) and the baseline period (1981-2020) at six sites. The wheat flowering time was projected to be advanced in the future at all sites, with more advanced under SSP585 than under SSP245. Specifically, the wheat flowering time was 5-17 days earlier in the 2040s and 2080s under SSP245 compared to the 2000s. Under SSP585, wheat flowering time was 6-27 days earlier than that of the 2000s. Across the six sites, the flowering time of wheat in sites Mudgee and Wagga Wagga, which are located in the southeastern NSW wheat belt, was obviously earlier than that of the other four sites.

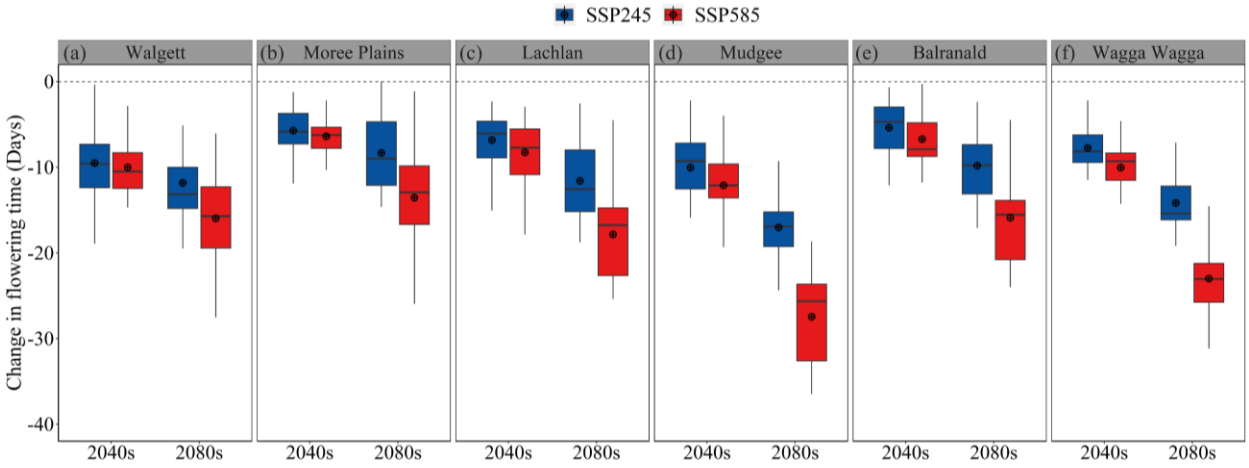

Figure 3-2. Projected changes in simulated flowering time at six sites. Changes were estimated between two future periods (2021-2060 and 2061-2100) and the baseline period (1981-2020) under SSP245 and SSP585 based on the 27 downscaled GCMs. Box boundaries indicate the 25th and 75th percentiles across GCMs, whiskers below and above the box indicate the 10th and 90th percentiles. The black lines and crosshairs within each box indicate the multi-model median and mean, respectively.

3.3.2 The characteristics and changes of DH

Figure 3-3 shows the *DHF*, *DHD*, and *DHI* in WSP at six sites under SSP245 and SSP585 using 27 GCMs in the 2000s, 2040s and 2080s. According to the six-site average values, the *DHF*, *DHD*, and *DHI* in WSP increased by 15%, 12%, and 0.9% in 2040s, and 49%, 44% and 5% in 2080s, respectively, compared with 2000s. The *DHF* in northern wheat belt, i.e., Walgett and Moree Plains were higher than that at other four sites (Figure 3-3 a-b). In 2000s, 2040s, and 2080s, the *DHF* at Walgett and Moree Plains were 0.01-0.14, 0.10-0.28, and 0.11-0.35 higher than that of the other four sites under SSP245, respectively. Also, similar changes appeared under SSP585. In the future, the *DHF* would increase at all sites except Balranald (Figure 3-3 e). Walgett had the largest *DHF* increases by 0.19 and 0.24 in 2040s and 2080s under SSP245, and 0.21 and 0.30 under SSP585, respectively (Figure 3-3 a). Moreover, when comparing sites with similar

latitude, the western sites had slightly higher *DHF* than that of the eastern sites. According to the average value of 2000s, 2040s, and 2080s under SSP245, the *DHF* at Walgett was 0.07 higher than that at Moree Plains, *DHF* at Lachlan was 0.05 higher than that at Mudgee, and the *DHF* at Balranald was 0.01 higher than that at Wagga Wagga. Similar to *DHF*, the *DHD*s at Walgett and Moree Plains were the highest among all six sites (Fig 3g-h), and their higher *DHD* was extended into the future. *DHD* would increase most in Walgett (Fig 3g), which was extended 3 days under both two SSPs in 2040s. *DHD* in 2080 increased more obviously, which were 4 and 8 days under SSP245 and SSP585, respectively. Also, the *DHD* at Lachlan was slightly increased in the future (Figure 3-3 i), while there was little difference between their historical and future *DHD* at Mudgee, Balranald, and Wagga Wagga (Figure 3-3 j-l). In addition, the changes in *DHI* at six sites were not significant in the future. There would be a slight increase in future *DHI* at Moree Plains, Lachlan, Mudgee, and Baranald (Figure 3-3 h-k), while the future *DHI* was almost the same as the historical *DHI* at Walgett and Wagga Wagga (Figure 3-3 g&l). Balranald, the lowest rainfall site presented a high drought intensity and thus had the highest *DHI* among all six sites (Figure 3-3 q). The characteristics and changes of individual drought and heat events can be found in the supplementary materials (section S1).

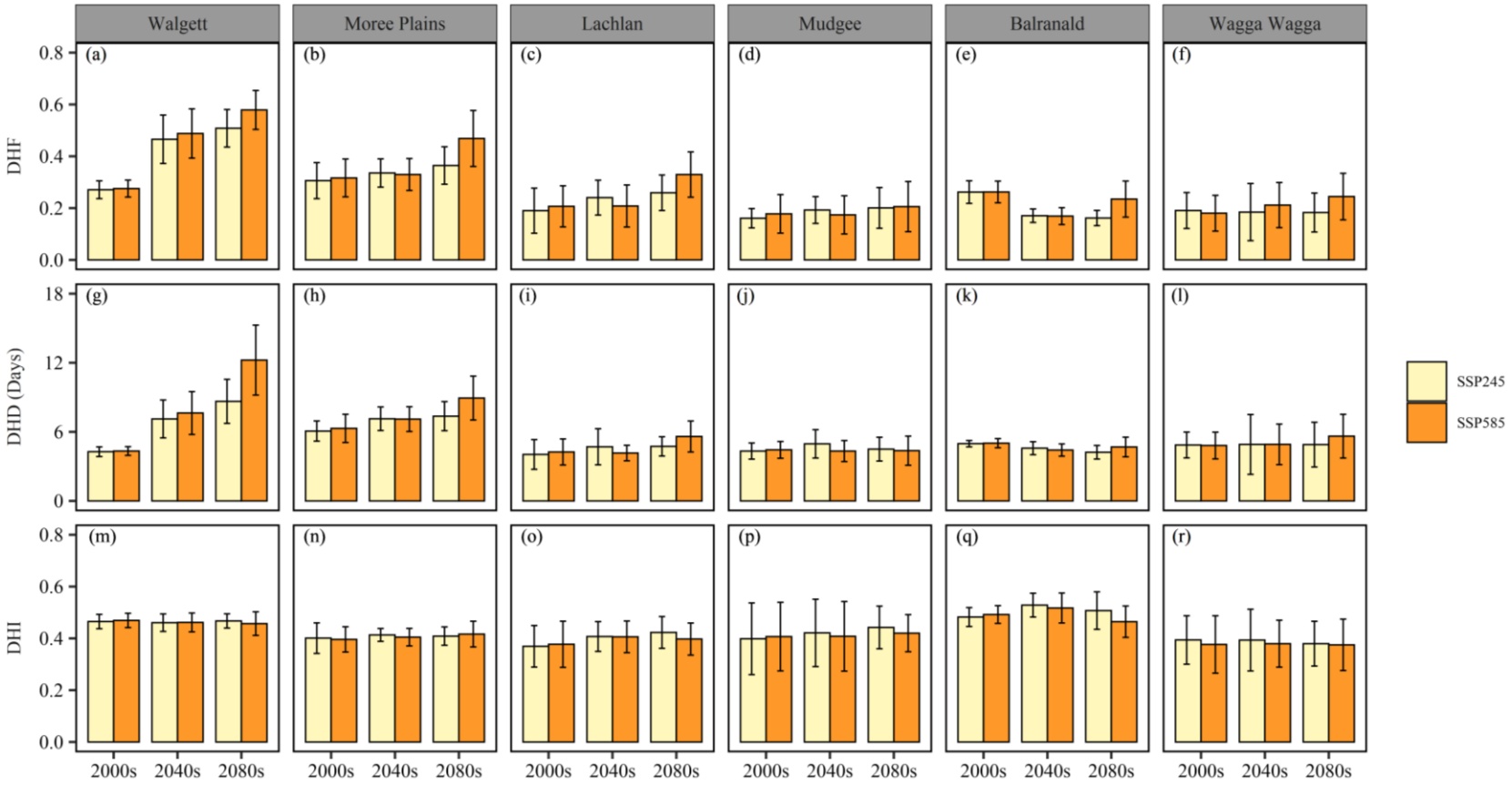

Figure 3-3 The averaged frequency (*DHF*), duration (*DHD*), and intensity (*DHI*) of compound drought-heat events during the wheat sensitive period (WSP) at six sites under SSP245 and SSP585 based on 27 GCMs in the 2000s (1989-2020), 2040s (2021-2060), and 2080s (2061-2100). The error bar represents the standard deviation of 27 GCMs.

3.3.3 Effects of changing wheat cultivars and sowing earlier

After comparing the DH indices of 64 virtual wheat cultivars at six sites in 2040s and 2080s, we selected the cultivars corresponding to the minimum *DHF*, *DHD*, and *DHI* as the better-performing wheat cultivars for each period at each site. Figure 3-4 represents the reduction rates of *DHF*, *DHD*, and *DHI* after planting better-performing wheat cultivars compared with those when planting *Janz*. The six-site average *DHF*, *DHD*, and *DHI* decreased by 44%, 41%, and 42%, respectively, after sowing the better-performing wheat cultivars at all sites, throughout 2040s to 2080s under SSP245. For the two future periods, there were better effects on alleviating DH risk in 2040s compared to that in 2080s. *DHF* values averaged across 6 sites would be decreased by 51% and 48% under SSP245 and SSP585 in 2040s, but in 2080s only by 37% and 21%, respectively. Similar changes were observed in the other two indices. That is, according to average values of six sites under SSP245, the *DHD* and *DHI* were decreased by 47% for both indices in 2040s and by 36% and 38% in 2080s, respectively. Under SSP585, *DHD* and *DHI* decreased by 45% and 48% in 2040s, and by 22% and 27% in 2080s, respectively. Comparing the results among six sites, we found that the reduction rates of DH indices in the three eastern sites (Moree Plains, Mudgee, and Wagga Wagga) of the wheat belt were higher than those in the western sites (Walgett, Lachlan, and Balranald) at similar latitudes. For instance, the reduction percentage of *DHI* under SSP245 was 10%, 25%-53%, and 23%-45% higher at Moree Plains, Mudgee, and Wagga Wagga (Figure 3-3 n, p, and r) than Walgett, Lachlan, and Balranald (Figure 3-3 m, o, and q), respectively, across 2040s and 2080s. Also, similar changes were presented in *DHF* and *DHD* under two SSPs, except for the reduction rates of *DHF* at Moree Plains (Figure 3-4 b) were lower than that in Walgett (Figure 3-4 a).

We compared the changes in *DHF*, *DHD*, and *DHI* of different sowing window at six sites in 2040s and 2080s under SSP245 and SSP585, then selected the sowing window corresponding to the minimum *DHF*, *DHD*, and *DHI* as the ideal sowing time. The *DHF*, *DHD*, and *DHI* in the WSP at six sites were decreased under SSP245 and SSP585 after applying ideal sowing time (Figure 3-5). The six-site average reduction rates in *DHF*, *DHD*, and *DHI* were 28%, 28%, and 16%, respectively, throughout 2040s to 2080s under SSP245. However, the alleviation effects of ideal sowing time on DH in 2040s were better than that in 2080s. According to the average values of six sites, the *DHF* were reduced by 34% in 2040s, but only by 22% in 2080s after applying ideal sowing time under SSP245. In addition, the ideal sowing time had better effects on alleviating DH in three southeastern sites (Mudgee, Balranald, and Wagga Wagga) (Figure 3-5 d-f, j-l, and p-r) than three northwestern sites (Walgett, Moree Plains, and Lachlan) (Figure 3-5 a-c, g-i, and m-o). For example, under SSP245, *DHD* reducing rates in three southeastern sites were from 21% to 65% throughout 2040s and 2080s, higher than 12%-24% in three northwestern sites. Also, these trends appeared under SSP585. Furthermore, advancing sowing window could not reduce the *DHI* in the northernmost sites

of Walgett and Moree Plains (Figure 3-5 m and Figure 3-5 n). The contribution of adaptation options to reduce the individual drought and heat events can be found in supplementary materials (section S2).

3.3.4 The better-performing agronomic options for mitigating DH in WSP

We selected the better-performing agronomic options corresponding to each DH indices in the 2040s and 2080s (Table 3-4&3-5). Under SSP245 and SSP585, most of the better-performing agronomic options were combined planting better-performing wheat cultivars with sowing 2 weeks earlier, and the combined options were more important in the distant future (2080s). As for the genetic parameters of better-performing wheat cultivars in better-performing agronomic options, the TTFJ and TTFI were smaller than that of *Janz*, under two SSPs at all sites. The TTFW varied at different sites, and in most cases, it was 30°Cd smaller than that of *Janz*.

Under the better-performing agronomic options, *DHF*, *DHD*, and *DHI* in the WSP at six sites were all obviously decreased under SSP245 and SSP585 (Figure 3-6). The better-performing agronomic options performed better than adjusting sowing window or planting better-performing cultivars alone (Figure 3-7). They resulted in the averaged *DHF*, *DHD*, and *DHI* of six sites in 2040s and 2080s under SSP245 a further reduction of 10%-16%, 14%-17%, and 14%-15% from adaptive measure of just planting better-performing cultivars. There was a further reduction of 25%-40%, 25%-41%, and 36%-47%, respectively, from just advancing sowing window. Also, similar trends appeared under SSP585 (Figure 3-S5). Nevertheless, same as better-performing cultivars and ideal sowing time, better-performing agronomic options had better effects on mitigating the risk of DH in 2040s than that in 2080s. Taking the data under SSP245 as an example, the average *DHF* of six sites was decreased by 67% in 2040s, but in 2080s only by 57%. Similarly, the average *DHD* in 2040s and 2080s decreased by 57% and 52%, respectively, and the average *DHI* decreased by 53% and 44%, respectively. Comparing the reduction rate of DH indices among six sites, the better-performing agronomic options had the best effects at Mudgee (Figure 3-6 d, j, and p) and Wagga Wagga (Figure 3-6 f, l, and r), located in the southeast of NSW wheat belt. Specifically, under SSP245, the *DHF* of these two sites decreased by 89%-100% (Figure 3-6 d&f), while that of Walgett, Moree Plains, Lachlan, and Balranald decreased by 13%-66% (Figure 3-6 a, b, c, and e). Similarly, the *DHD* and *DHI* decreased by 87%-100% (Figure 3-6 j&l) and 79%-100% (Figure 3-6 p&r) in Mudgee and Wagga Wagga, respectively, and those in the other four sites decreased by 27%-49% (Figure 3-6 g, h, i, and k) and 8%-62% respectively (Figure 3-6 m, n, o, and q). Similarly, the above-mentioned trends appeared under SSP585.

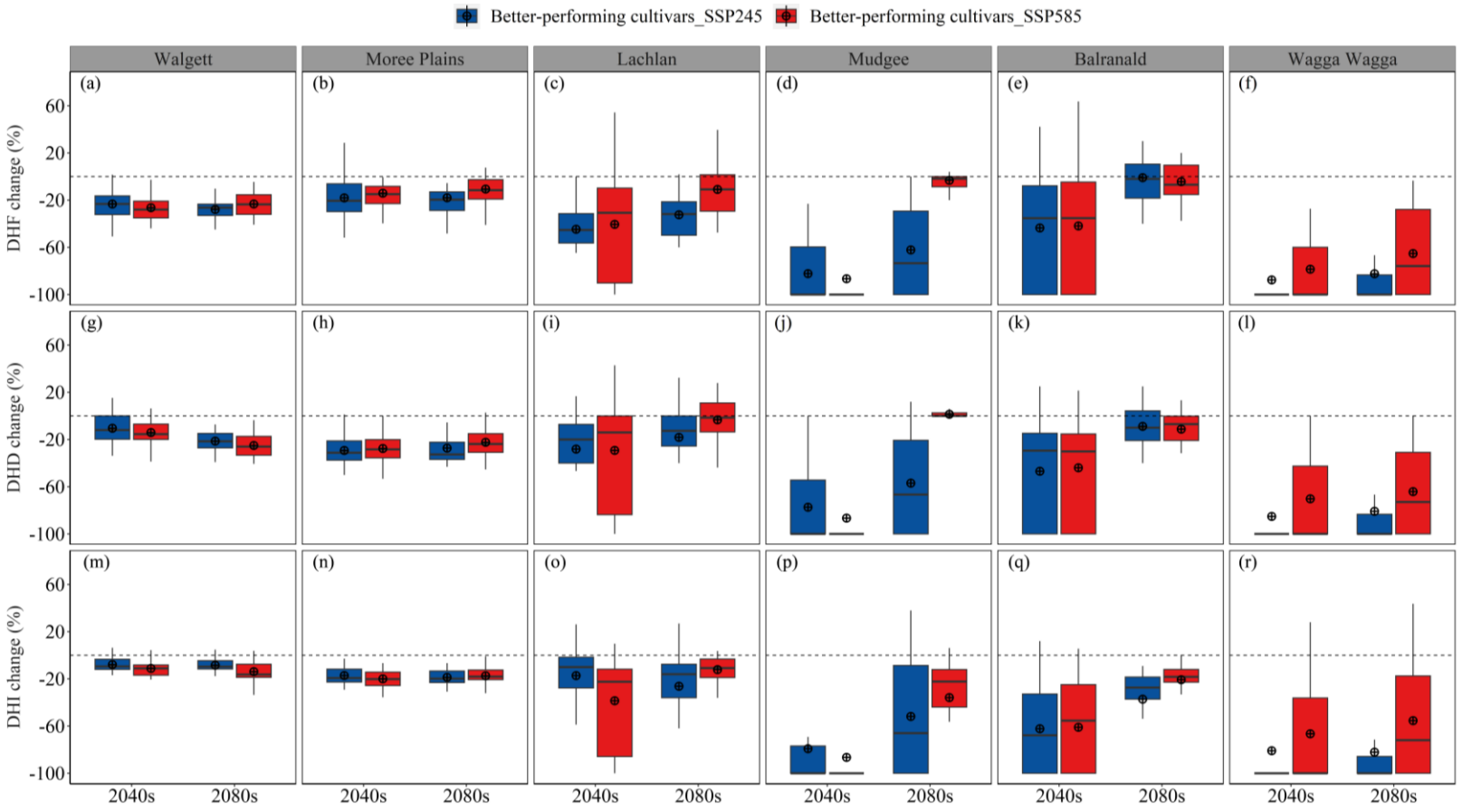

Figure 3-4. Projected changes in compound drought-heat frequency (*DHF*), duration (*DHD*), and intensity (*DHI*) during the wheat sensitive period (WSP) at six sites. Changes were estimated between before and after adopting better-performing wheat cultivars for 2040s (2021–2060) and 2080s (2061–2100) under SSP245 and SSP585 based on the 27 GCMs. Box boundaries indicate the 25th and 75th percentiles across GCMs, whiskers below and above the box indicate the 10th and 90th percentiles. The black lines and crosshairs within each box indicate the multi-model median and mean, respectively.

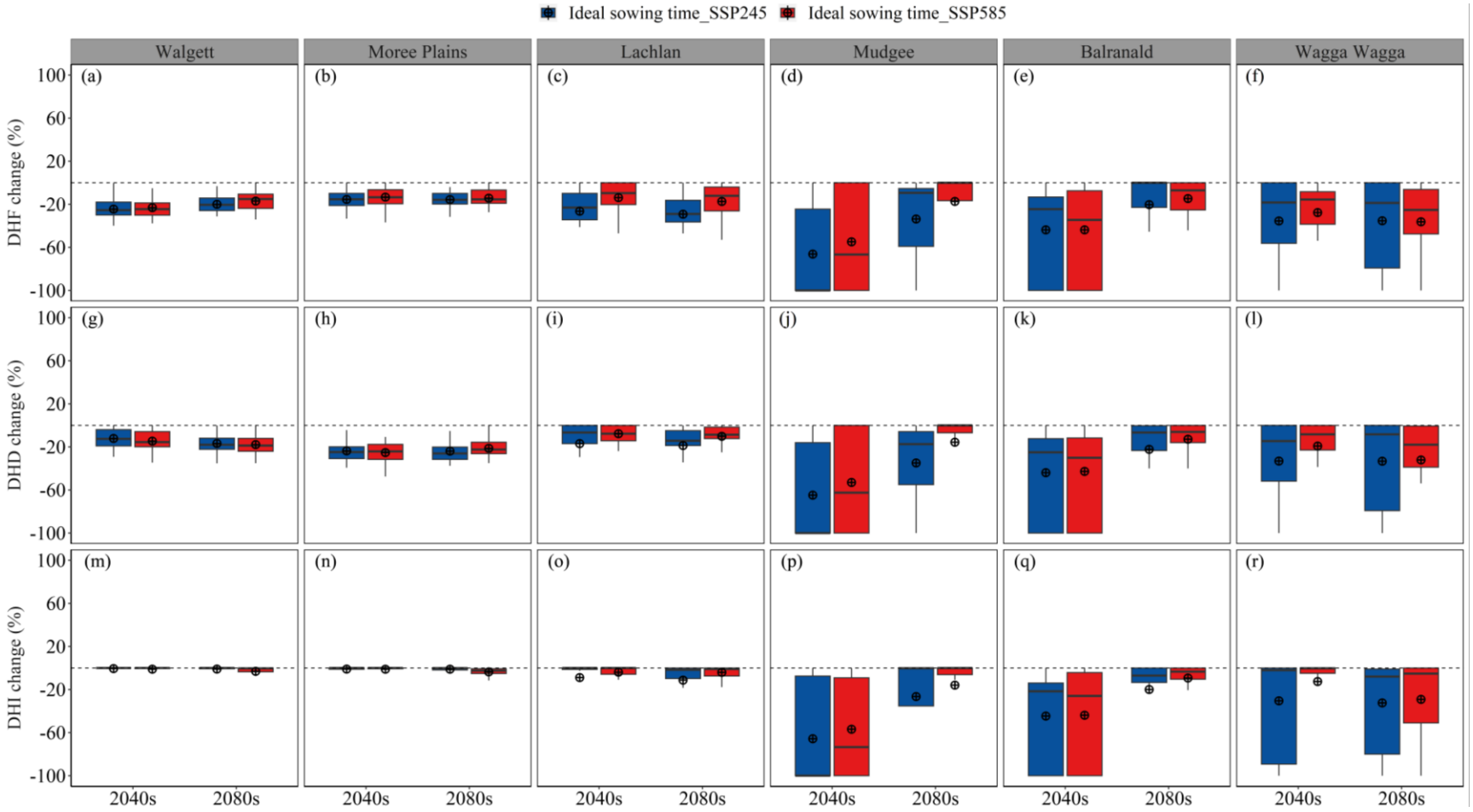

Figure 3-5. Projected changes in compound drought-heat frequency (*DHF*), duration (*DHD*), and intensity (*DHI*) during the wheat sensitive period (WSP) at six sites. Changes were estimated between before and after using ideal sowing time for 2040s (2021–2060) and 2080s (2061–2100) under SSP245 and SSP585 based on the 27 GCMs. Box boundaries indicate the 25th and 75th percentiles across GCMs, whiskers below and above the box indicate the 10th and 90th percentiles. The black lines and crosshairs within each box indicate the multi-model median and mean, respectively.

Table 3-4. The details of the better-performing agronomic options in the 2040s (2021-2060) and 2080s (2061-2100) under SSP245 at six sites and the information of original management. The units for tt_end_of_juvenile (TTEJ), tt_floral_initiation (TTFI), and tt_flowering (TTFW) are all °Cd.

SSP245	Indices	Station	2040s				2080s			
			TTEJ	TTFI	TTFW	Sowing window	TTEJ	TTFI	TTFW	Sowing window
Better-performing agronomic options	*DHF*	Walgett	300	358	79	13 April to 1 July	300	358	79	13 April to 1 July
		Moree Plains	300	358	79	13 April to 1 July	300	358	79	13 April to 1 July
		Lachlan	300	358	79	13 April to 1 July	300	358	79	13 April to 1 July
		Mudge	300	358	79	27 April to 15 July	300	358	79	13 April to 1 July
		Balranald	300	358	169	27 April to 15 July	300	358	169	13 April to 1 July
		Wagga Wagga	300	358	79	13 April to 1 July	300	358	79	13 April to 1 July
	DHD	Walgett	300	358	79	13 April to 1 July	300	358	79	13 April to 1 July
		Moree Plains	300	358	79	20 April to 8 July	300	358	79	13 April to 1 July
		Lachlan	300	358	109	13 April to 1 July	300	358	139	13 April to 1 July
		Mudge	300	358	109	13 April to 1 July	300	358	79	13 April to 1 July
		Balranald	300	358	79	13 April to 1 July	300	358	169	13 April to 1 July
		Wagga Wagga	300	358	79	13 April to 1 July	300	358	79	13 April to 1 July
	DHI	Walgett	300	358	79	27 April to 15 July	300	358	79	13 April to 1 July
		Moree Plains	300	358	79	27 April to 15 July	300	358	79	27 April to 15 July
		Lachlan	300	358	79	13 April to 1 July	300	358	169	27 April to 15 July
		Mudge	300	358	139	27 April to 15 July	300	358	139	27 April to 15 July
		Balranald	300	358	139	27 April to 15 July	300	358	169	27 April to 15 July
		Wagga Wagga	300	358	79	13 April to 1 July	300	358	79	27 April to 15 July
Original management			400	458	109	27 April to 15 July	400	458	109	27 April to 15 July

Table 3-5. The details of the better-performing agronomic options in the 2040s (2021-2060) and 2080s (2061-2100) under SSP585 at six sites and the information of original management. The units for tt_end_of_juvenile (TTEJ), tt_floral_initiation (TTFI), and tt_flowering (TTFW) are all °Cd.

SSP585	Indices	Station	2040s				2080s			
			TTEJ	TTFI	TTFW	Sowing window	TTEJ	TTFI	TTFW	Sowing window
Better-performing agronomic options	*DHF*	Walgett	300	358	79	13 April to 1 July	300	358	79	13 April to 1 July
		Moree Plains	300	358	79	13 April to 1 July	300	358	79	13 April to 1 July
		Lachlan	300	358	79	13 April to 1 July	300	358	79	13 April to 1 July
		Mudge	300	358	79	27 April to 15 July	300	358	79	13 April to 1 July
		Balranald	300	358	79	27 April to 15 July	300	358	79	13 April to 1 July
		Wagga Wagga	300	358	79	13 April to 1 July	300	358	79	13 April to 1 July
	DHD	Walgett	300	358	79	13 April to 1 July	300	358	79	13 April to 1 July
		Moree Plains	300	358	79	27 April to 15 July	300	358	79	13 April to 1 July
		Lachlan	300	358	79	27 April to 15 July	300	358	79	13 April to 1 July
		Mudge	300	358	79	27 April to 15 July	300	358	109	13 April to 1 July
		Balranald	300	358	79	13 April to 1 July	300	358	109	13 April to 1 July
		Wagga Wagga	300	358	79	13 April to 1 July	300	358	109	13 April to 1 July
	DHI	Walgett	300	358	79	27 April to 15 July	300	358	79	13 April to 1 July
		Moree Plains	300	358	169	13 April to 1 July	300	358	79	27 April to 15 July
		Lachlan	300	358	79	13 April to 1 July	300	358	79	13 April to 1 July
		Mudge	300	358	79	27 April to 15 July	300	358	79	13 April to 1 July
		Balranald	300	358	79	27 April to 15 July	300	358	79	13 April to 1 July
		Wagga Wagga	300	358	79	13 April to 1 July	300	358	79	13 April to 1 July
Original management			400	458	109	27 April to 15 July	400	458	109	27 April to 15 July

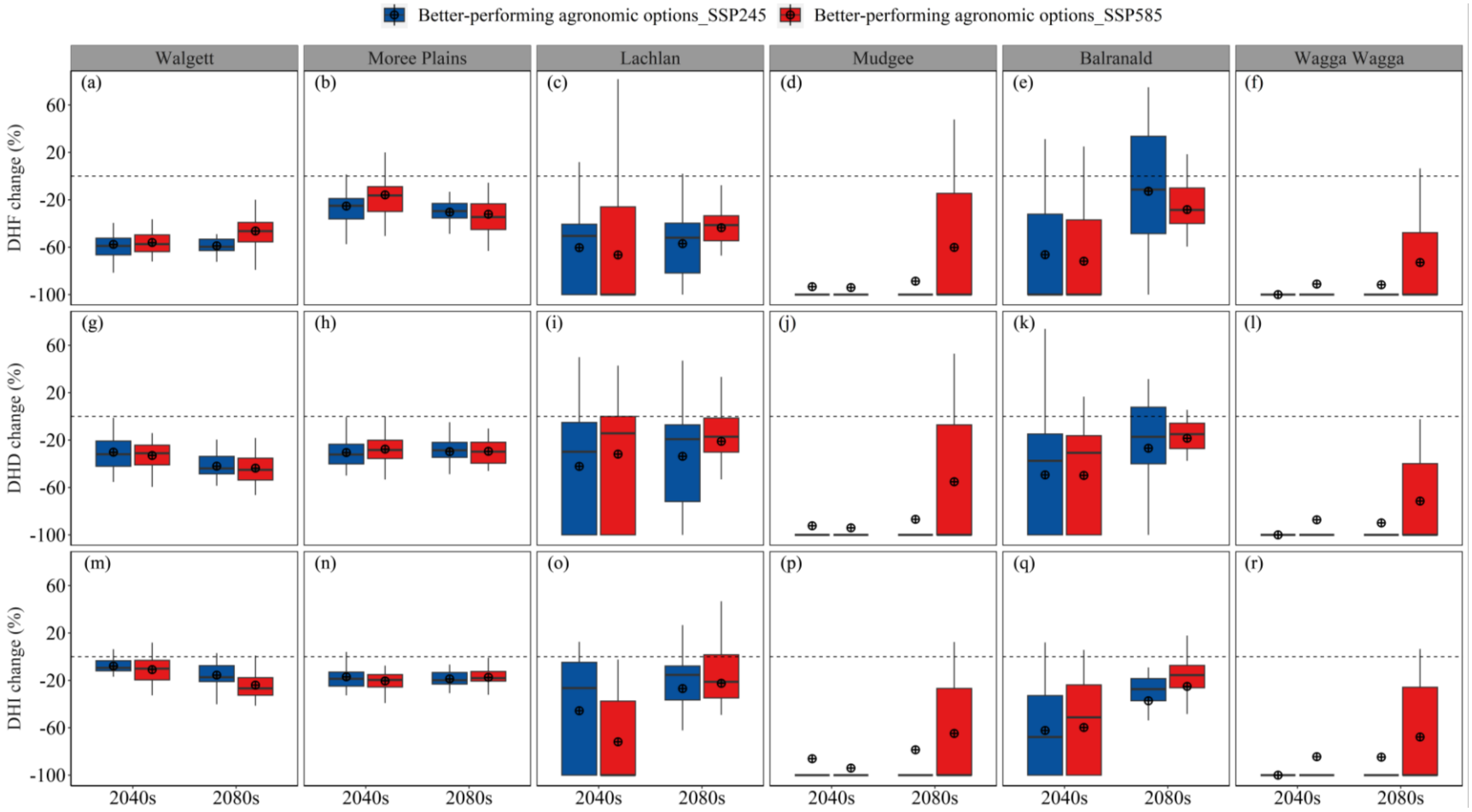

Figure 3-6. Projected changes in compound drought-heat frequency (*DHF*), duration (*DHD*), and intensity (*DHI*) during the wheat sensitive period (WSP) at six sites. Changes were estimated between before and after using better-performing agronomic options for 2040s (2021–2060) and 2080s (2061–2100) under SSP245 and SSP585 based on the 27 downscaled GCMs. Box boundaries indicate the 25th and 75th percentiles across GCMs, whiskers below and above the box indicate the 10th and 90th percentiles. The black lines and crosshairs within each box indicate the multi-model median and mean respectively.

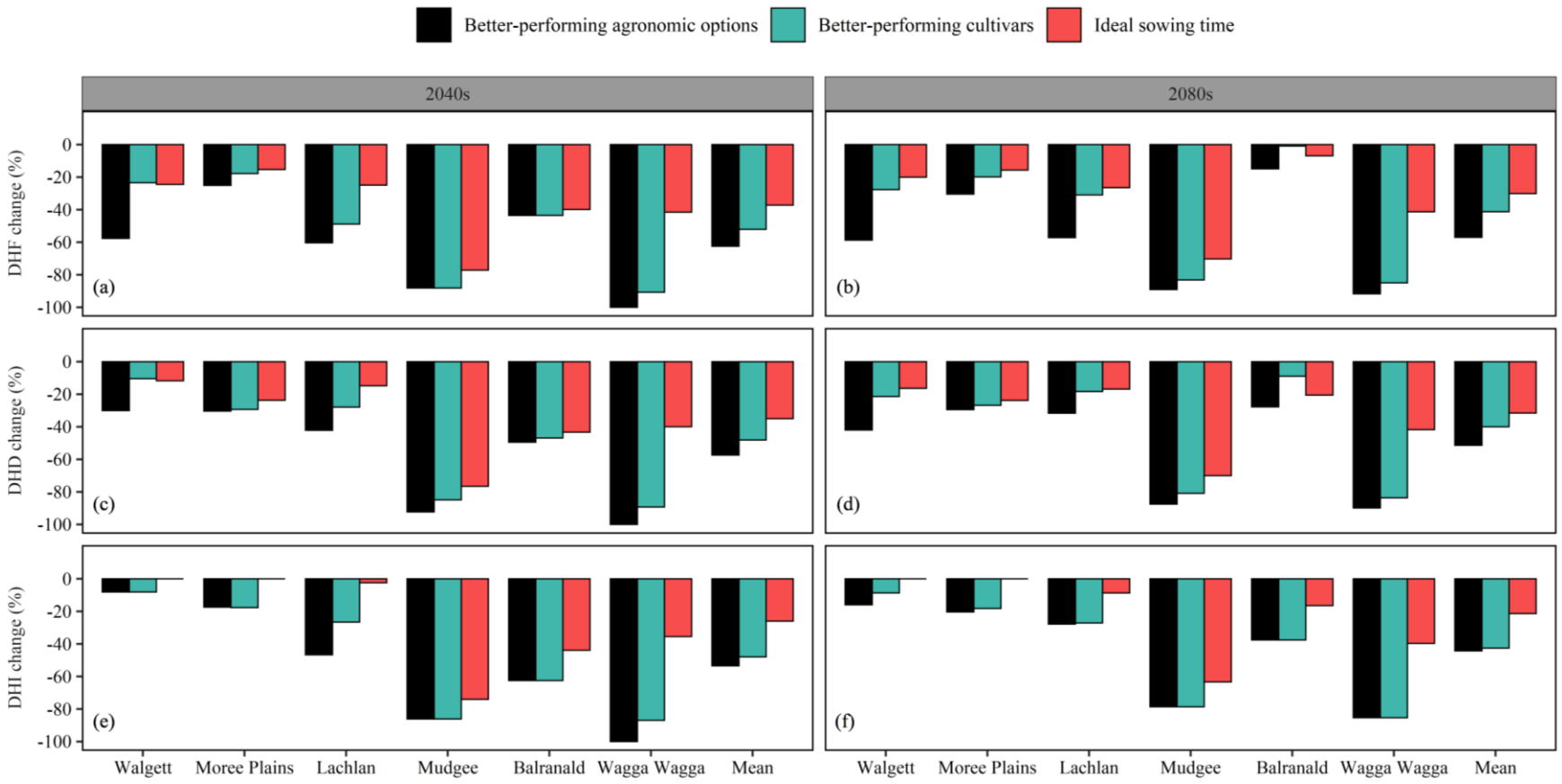

Figure 3-7. Projected changes in compound drought-heat frequency (*DHF*), duration (*DHD*), and intensity (*DHI*) during the wheat sensitive period (WSP). Changes were estimated between before and after using better-performing agronomic options for 2040s (2021–2060) and 2080s (2061–2100) under SSP245.

3.4. Discussion

Our study examined the effects of projected climate change on wheat flowering time using APSIM driven by multiple climate models. Under future projected climate change, the wheat flowering time was expected to be advanced at all six sites (Figure 3-2). Specifically, the wheat flowering time was 5-17 days earlier in the 2040s and 2080s under SSP245 compared to historical period. Under SSP585, wheat flowering time was 6-27 days earlier than baseline. This was consistent with previous studies which showed that simulated days to flowering were shortened under future climate due to global warming (Wang et al., 2017a; Zheng et al., 2012). Wheat flowering time advanced from the middle or late September in the 2000s to the middle or late August in the 2040s and 2080s under projected climate change. Additionally, we found that *DHF*, *DHD*, and *DHI* almost all increased in the future (Figure 3-3), which is consistent with the results of previous studies. For example, Sedlmeier et al. (2018) and Zhou et al. (2019) reported that the frequency, intensity, and influenced area of DH events are all increased in the warm season. Besides, we found that drought events in WSP would not change too much in the future (Figure 3-S3) while heat events would clearly increase (Figure 3-S4). Therefore, the increase in DH events was mainly due to the increase in heat stress, which is consistent with the findings of Zhang et al (2022), who reported the increased temperature dominated the increase in DH events. The reason may be that drought is a recurring climate feature in Australia (Ummenhofer et al., 2009), and the drought frequency, duration, and intensity are at a high level (Figure 3-S3). In this case, when heat becomes more frequent, more DH events will occur.

Spatially, we found that in Walgett and Moree Plains, located in the northern NSW wheat belt, the increases of *DHF* and *DHD* in the future were larger than that at the other four sites in the central and southern part of the wheat belt, Lachlan, Mudgee, Balranald, and Wagga Wagga (Figure 3-3). The reason is that these two northern sites have a higher temperature. Specifically, the average daily maximum temperature in the wheat growing season in Walgett and Moree Plains is 2.3-4.8 ℃ higher than that in Lachlan, Mudgee, Balranald, and Wagga Wagga (Table 3-1). Coupled with the gradual warming climate in the future, the frequency and duration of heat in Walgett and Moree Plains would be higher than those in the other four sites (Figure 3-S4). Meanwhile, the drought frequency and duration were also high in Walgett and Moree Plains (Figure 3-S3). Therefore, in the case of a significant increase in heat events and frequent drought events, DH events naturally occur more frequently in the two sites. By contrast, for Lachlan, Mudgee, Balranald, and Wagga Wagga, which are located in the middle to the south of the wheat belt, the *DHF* and *DHD* did not increase much in the future. The reason is that the wheat flowering time in these sites was more advanced in the future (Figure 3-2), helping wheat escape the DH events under projected climate change during the flowering period. In addition, the *DHI* in Balranald was the highest among all sites. This

is because Balranald is the driest site with the largest drought intensity (Figure 3-S3) located in the westernmost area. In summary, DH events are prone to occur in the north and west of the wheat belt, and the frequency, duration, and intensity of DH events would increase in the future.

Additionally, we tested the potential of single and combined agronomic options in alleviating DH events. We adopted two adaptation practices, changing sowing time and wheat cultivars. Such agronomic options are cost-friendly and easily adopted by farmers. We discovered that either single or combined agronomic options would be effective in reducing *DHF*, *DHD*, and *DHI* in WSP (Figs. 3-5). We found that better-performing wheat cultivars under future climate had a shorter vegetative period compared to reference cultivar, *Janz*. Also, this is consistent with Devasirvatham et al. (2016) and Wang et al. (2019), who proposed that early flowering wheat has a higher resilience to extreme weather events. We found that both better-performing cultivars and ideal sowing time promote wheat to flower earlier than the original mid-spring, keeping the sensitive flowering period in a cooler season. With the decrease of heat stress in the cooler season, the risk of DH also decreases, even though the NSW wheat belt is prone to drought in spring and winter (Feng et al., 2019a). On the basis of planting early flowering wheat, advancing the sowing time can further promote wheat flowering earlier and ensure the sensitive flowering period is completed prior to frequent DH events, thus escaping DH events to a greater extent.

Although adopting early time of sowing and early flowering cultivar under future climate can significantly reduce the DH risks during WSP, there might also be yield penalties or other climatic risks. Adopting early flowering wheat cultivar would shorten the length of the vegetative season, leading to the reduction of the growth period to intercept the radiation, nutrition, and CO_2 for the accumulation of photosynthate, which affects biomass accumulation and yield formation (Zheng et al., 2012; García et al., 2018). In contrast, it is generally believed that early sowing the wheat with suitable maturity time can boost wheat yield (Hunt et al., 2019; Kerr et al., 1992), but it should be no earlier than mid-April. The main reason is the greater competition for assimilates between the growing spike and the elongating stem (Gomez-Macpherson and Richards, 1995). The combination of the two adaptations may make the adverse effects stronger. However, these adverse impacts can be overcome by genetically prolonging the grain filling stage and shortening the stems of winter wheat (Gomez-Macpherson and Richards, 1995; Kerr et al., 1992).

In addition to agronomic options aimed at escaping DH events, other options focused on enhancing the tolerance of wheat to drought and heat stress may also have the potential to alleviate the adverse impacts resulting from DH events. For instance, the options of genetic improvement of wheat to drought and heat stress, straw or residue mulching, soil management techniques, appropriate amount and methods of fertilization, and the application of exogenous protectants, etc. These options can improve both crop water

and nutrient use efficiency and increase soil moisture retention (Akter & Rafiqul Islam, 2017; Dodd et al., 2011). Therefore, it is imperative to explore and validate the effectiveness of these agronomic options to escape DH events in future work.

Furthermore, we found that the frost risks were increased in the 2040s and 2080s across six sites under SSP245 and SSP585 under the optimal agronomic options. This increase was particularly notable in regions with climates that are less dry and hot, such as Mudgee and Wagga Wagga (Figure 3-S10). Specifically, frost frequency (FF) at Mudgee was increased by 2%-77% in the 2040s and 2080s under two scenarios. Frost intensity (FI) increased by 62%-88% at Wagga Wagga. By combining frost-tolerant traits in wheat cultivars or implementing protective measures such as delving of surfaced soils, the negative impacts of increased frosts may be further reduced (Farre et al., 2003; Rebbeck et al., 2007; Zheng et al., 2015). Although our optimal agronomic options demonstrate a significant reduction in DH risks by 89%-100% at two southeastern sites of Mudgee and Wagga Wagga, these options also resulted in a notable increase in the risk of frost during WSP. Therefore, farmers and decision-makers should carefully consider local climate conditions and frost patterns when determining suitable agronomic options, especially for regions that are characterized by less dry-hot climates. Additionally, it's worth noting that our suggested agronomic options did not greatly increase the exposure of wheat to spring frosts at four other sites, making them viable choices for regions with dry-hot climates.

For the first time, we defined compound DH events in WSP and assessed the characteristics of DH events under projected climate change in southeastern Australia's wheat growing regions. Our results can provide important information for better management of climate risk within the grain industry, but there are still limitations to our approach. First, similar with previous studies on adaptation of wheat to projected climate change (Semenov et al., 2014; Wang et al., 2019), we only changed sowing time and cultivar, but did not consider other strategies to increase soil moisture. For example, residue retention and straw mulching are demonstrated to reduce soil surface evaporation, which is beneficial to the wheat growth in Australia (Dang et al., 2006; Hunt et al., 2013). However, they are not included in our study due to the heavy calculation load caused by the many agronomic option combinations. Second, we only used one crop model. Recently, multiple crop model ensembles provided more robust results than single models in simulating crop growth and development (Rötter et al., 2015). Tao et al. (2017) designed ideal crop genotypes based on multi-model ensembles. We acknowledge that our results relied on the simulations of APSIM model. Further works with multiple crop model comparisons are needed to reduce the uncertainty in research results. Third, we only considered the simultaneous drought and heat stresses during wheat flowing period. However, the risk of frost in late spring is also non-negligible for Australian wheat (Wang et al., 2015b; Zheng et al., 2012).

Therefore, it is necessary to consider more extreme climate events to study the compound and interaction of multiple hazards as comprehensively as possible.

3.5. Conclusion

We developed the compound drought-heat index to assess the occurrences of simultaneous water and heat stresses during WSP under the expected effects of climate change in Australia. We found that the *DHF*, *DHD*, and *DHI* in WSP were projected to increase by 15%, 12%, and 0.9% in 2040s, and 49%, 44%, and 5% in 2080s, respectively, averaged across six sites compared with baseline climate. The increased DH events were mainly due to the increase in heat stress, especially at sites located in the northern NSW wheat belt with dry-hot climate. In addition, we demonstrated the adaptative effects of early sowing and wheat cultivars with shorter vegetative phase on reducing the risk of DH events. These agronomic options facilitated wheat to escape the jeopardizing effects of compound drought-heat events under projected climate change at study sites. However, they may introduce an increased frost risk across six study sites, especially in regions with climates that are less dry and hot, such as Mudgee and Wagga Wagga. We believe that our study will provide helpful information for farmers in Australia to mitigate the adverse effects of extreme climate events on wheat. The framework we developed here can be extended to other dryland wheat growing regions globally.

3.6 Supporting information

3.6.1. Supplementary methods

We defined that frost occurs when the daily minimum temperature is lower than 2 °C for three or more consecutive days. Frost frequency (FF) refers to the ratio of the accumulative sum days of all frost events in WSP to the length of the window (29 days); frost duration (FD) represents the maximum number of days within frost events in the WSP; frost intensity (FI) was defined by Eq. 3-S1-3-S3). The ratio of the difference between the daily minimum temperature and the frost threshold to the difference between wheat low killing temperature and frost threshold was calculated as the frost intensity.

$$FI_{ij} = \frac{TI_{ij} - T_t}{T_r - T_t}, \qquad i = 1, 2, ..., m_j, j = 1, 2, ..., N \tag{3-S1}$$

$$CFI_j = \frac{\sum_{i=1}^{m_j} FI_{ij}}{m_j}, j = 1, 2, ..., N \tag{3-S2}$$

$$FI = \frac{\sum_{j=1}^{N} CFI_j}{N}, j = 1, 2, ..., N, N \geq 1 \quad (3\text{-S3})$$

where FI_{ij} is the daily frost intensity for the *i*th day of the *j*th frost event during WSP in a given year; TI_{ij} is the minimum temperature for the *i*th day of the *j*th frost event; Tt is the frost threshold temperature, which we took as 2 ℃. We took T_r (the wheat low killing temperature) as -5 ℃ (Single, 1985); CFI_j is the frost intensity for the *j*th frost event in the given year.

3.6.2. Supplementary results

3.6.2.1 The characteristics and changes of individual drought and heat events

The frequency, duration, and intensity of drought events (DF, DD, and DI) that occurred during the wheat sensitive period (WSP) at the six sites under SSP245 and SSP585 using 27 GCMs in the 2000s, 2040s, and 2080s were shown in figure 3-S7. We found that the DF, DD, and DI did not exhibit significant differences among the three time periods. Through a comparison of drought risks across six sites, they can be grouped into two categories. Walgett, Moree Plains, and Balranald exhibited similar values for DF, DD, and DI, which were all higher than the values in the other three sites during three periods under two scenarios. Specifically, the higher values were 0.80-0.85 for DF (Figure 3-S7 a, b, &e), 23-24 days for DD (Figure 3-7 g, h, &kk), and 0.45-0.55 for DI (Figure 3-S7 m, n, &q), whereas the corresponding lower values for the other three sites were 0.62-0.71 for DF (Figure 3-S 7 c, d, &f), 18-19 days for DD (Figure 3-S 7 i, j, &l), and 0.32-0.46 for DI (Figure 3-S 7 o, p, &r).

Figure 3-S8 shows the frequency, duration, and intensity of heat events (HF, HD, and HI) in WSP at six sites under SSP245 and SSP585 using 27 GCMs in the 2000s, 2040s, and 2080s. According to the six-site average values, the HF, HD, and HI in WSP increased by 14%, 13%, and 23% in 2040s, and 34%, 31%, and 24% in 2080s, respectively, compared with the 2000s. The HF in the northern sites, Walgett and Moree Plains, were higher than that at the other four sites (Figure 3-S 8 a-b&g-h). Under SSP245, the HF and HD at Walgett and Moree Plains were 0.11-0.30 and 2-3 days higher than that of the other four sites in 2040s, 0.10-0.36 and 2-4 days higher in 2080s, respectively. Also, similar changes appeared under SSP585. There was little difference in HI among the six stations (Figure 3-S 8 m-r).

3.6.2.2 The changes in individual drought and heat events after applying optimal adaptation options

Under the optimal agronomic options, DF, DD, and DI in the WSP at six sites were all obviously decreased under SSP245 and SSP585 (Figure 3-S9). The six-site average reduction rates in DF, DD, and DI were 20%, 20%, and 29%, respectively, throughout 2040s to 2080s under SSP245. However, the alleviation effects of

optimal agronomic options on drought in 2080s were better than that in 2040s. According to the average values of six sites, the DF, DD, and DI were reduced by 19%, 18%, and 29% in 2040s, but by 24%, 25%, and 31% in 2080s under SSP245.

We compared the changes in HF, HD, and HI before and after applying the optimal adaptation options at six sites in 2040s and 2080s under SSP245 and SSP585. We found that the HF, HD, and HI in the WSP at six sites were decreased under optimal agronomic options (Figure 3-S10). The six-site average reduction rates in HF, HD, and HI were 60%, 51%, and 47%, respectively, throughout 2040s to 2080s under SSP245. However, the alleviation effects of optimal agronomic options on heat events in 2040s were better than that in 2080s. According to the average values of six sites, the HF, HD, and HI were reduced by 66%, 55%, and 53% in 2040s, but by 53%, 48%, and 41% in 2080s under SSP245. In addition, the optimal sowing time had better effects on reducing heat events in two southeastern sites (Mudgee and Wagga Wagga) (Figure 3-S10 d, j, p, f, l, &r). For example, under SSP245, HD reducing rates in two southeastern sites were from 74% to 95% throughout 2040s and 2080s, higher than 27%-50% in the other four sites. Also, these trends were observed in the reducing rates of HF and HI.

3.6.3. Supplementary figures

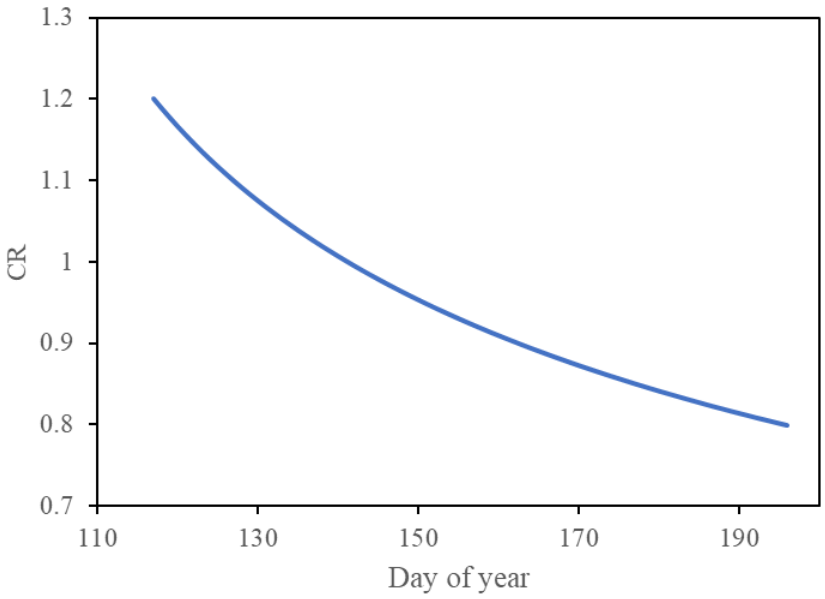

Figure 3-S1. The value of CR in site Walgett during the sowing window (day 117 to 196).

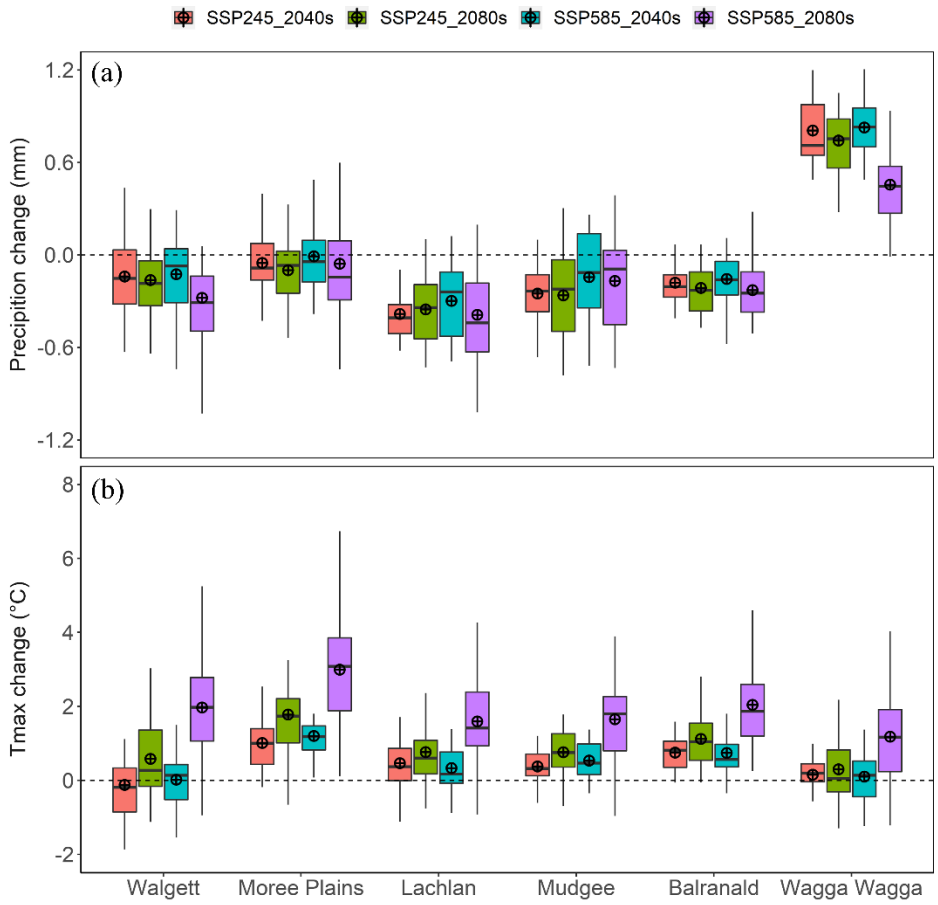

Figure 3-S2. Projected changes in rainfall, maximum temperature (T_{max}) during wheat sensitive period (WSP) at six sites based on the 27 GCMs in the 2040s and the 2080s under SSP245 and SSP585 compared to the baseline. Box boundaries indicate the 25th and 75th percentiles across 27 GCMs, whiskers below and above the box indicate the 10th and 90th percentiles. The black lines and crosshairs within each box indicate the multi-model median and mean, respectively.

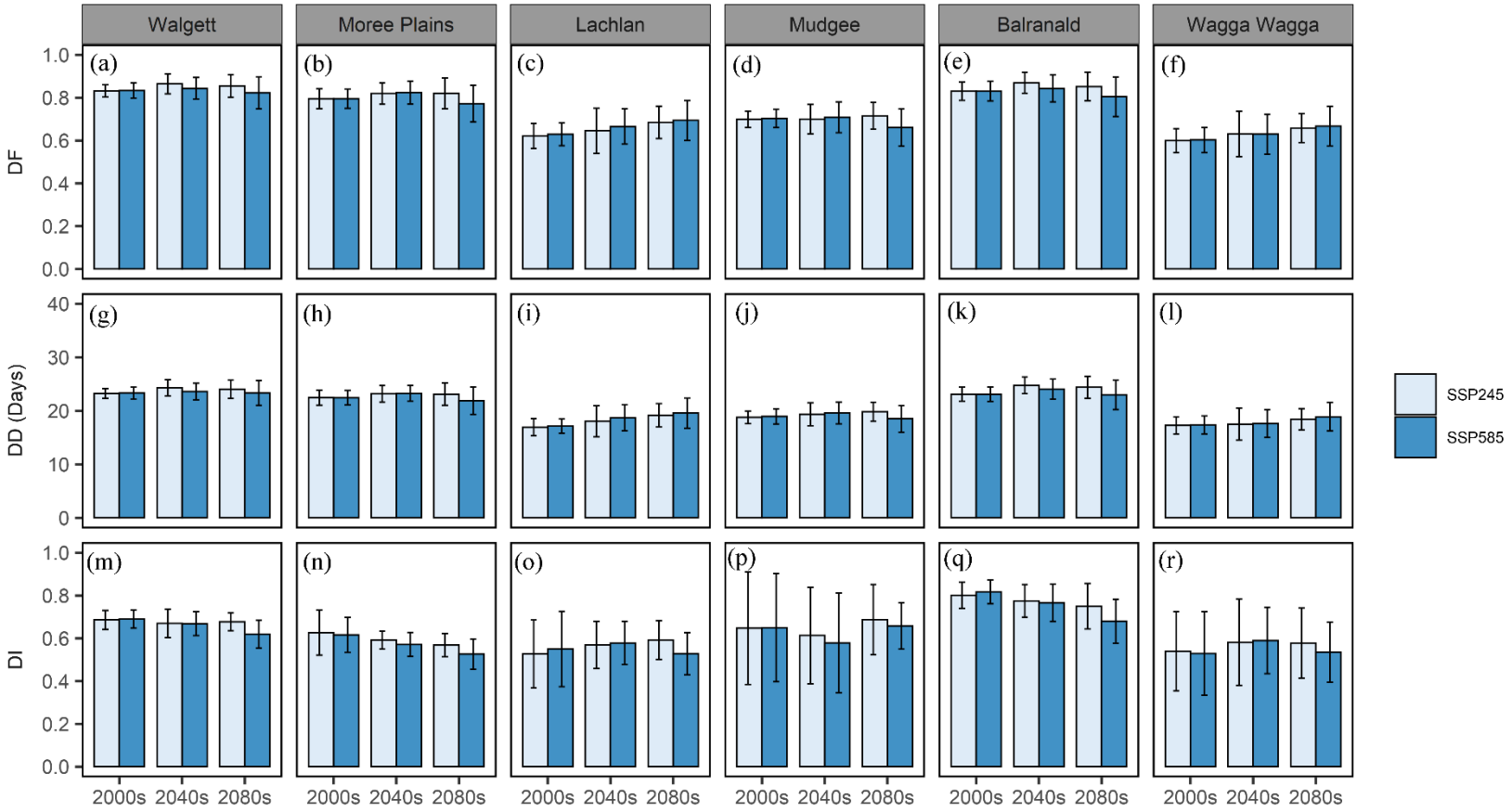

Figure 3-S3. The individual drought frequency (DF), duration (DD), and intensity (DI) in the periods of compound drought-heat at six sites under SSP245 and SSP585 using 27 GCMs in the 2000s (1989-2020), 2040s (2021-2060), and 2080s (2061-2100).

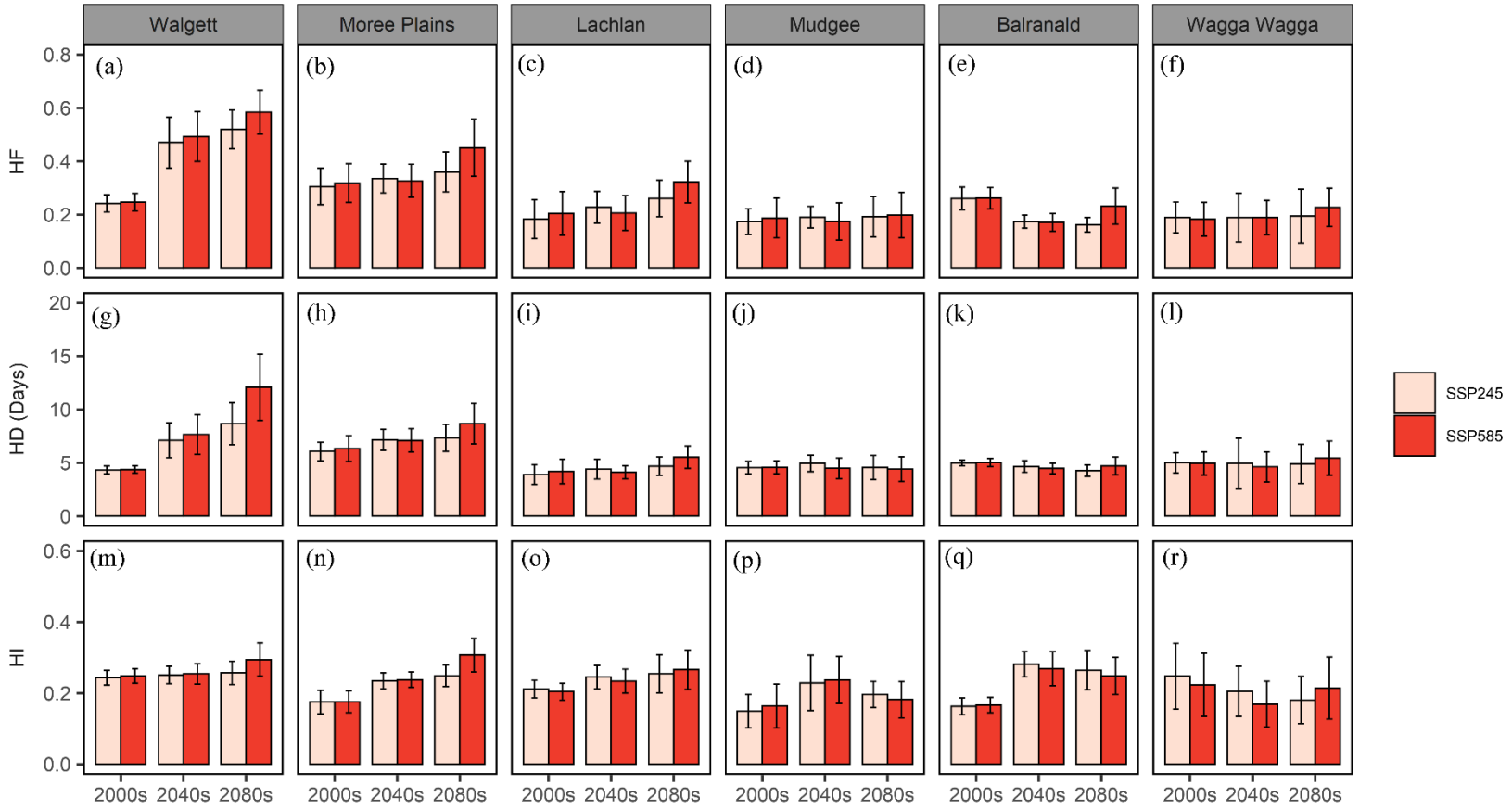

Figure 3-S4. The individual heat frequency (HF), duration (HD), and intensity (HI) in the periods of compound drought-heat at six sites under SSP245 and SSP585 using 27 GCMs in the 2000s (1989-2020), 2040s (2021-2060), and 2080s (2061-2100).

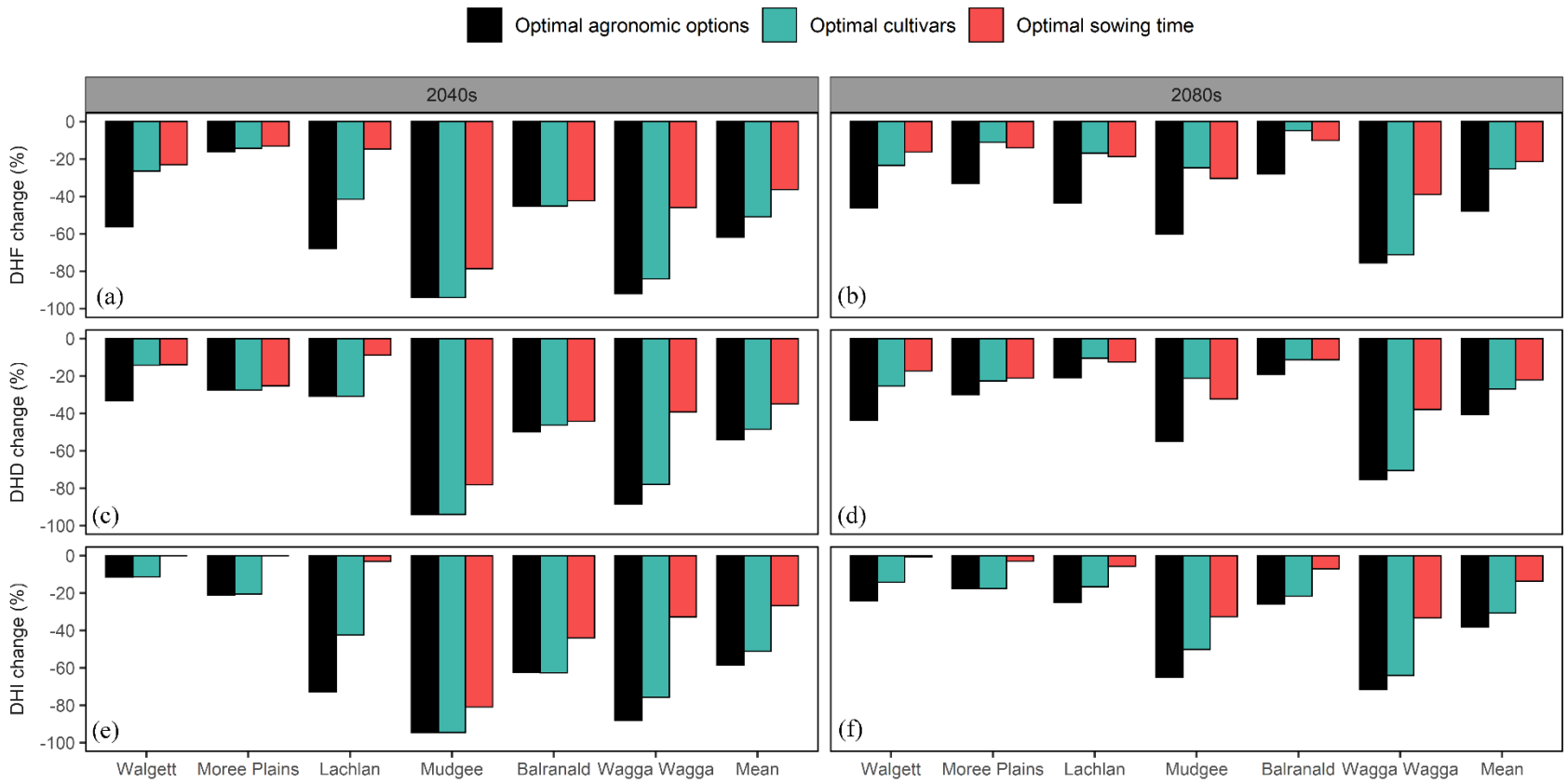

Figure 3-S5. Projected changes in compound drought-heat frequency (DHF), duration (DHD), and intensity (DHI) during the wheat sensitive period (WSP, 14 days before and after flowering time) under four agronomic options at six sites. Changes were estimated between before and after using agronomic options for each corresponding future periods (2040s: 2021–2060 and 2080s: 2061–2100) under SSP585 based on the 27 downscaled GCMs.

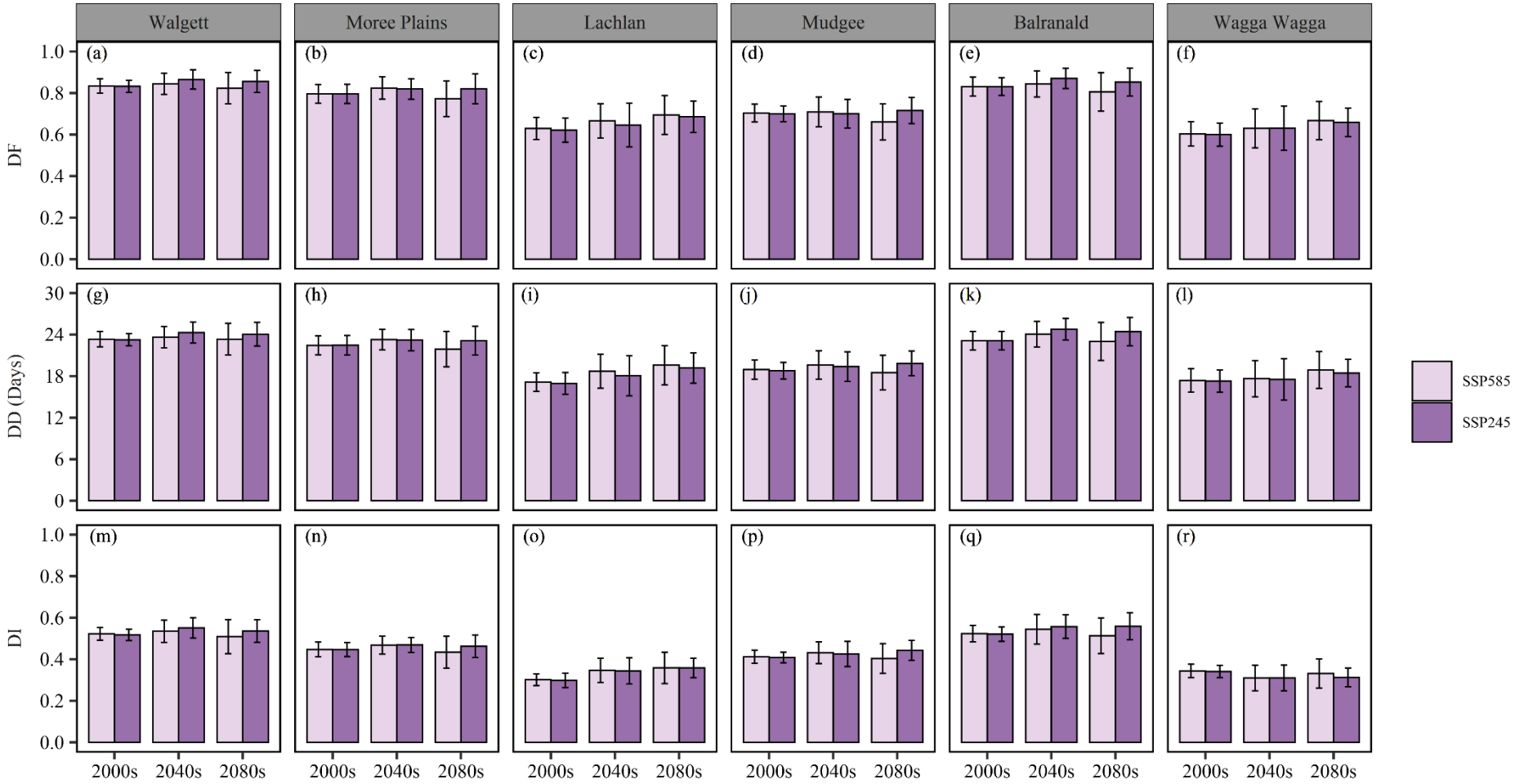

Figure 3-S6. The drought frequency (DF), duration (DD), and intensity (DI) in the wheat sensitive period (WSP, 14 days before and after flowering time) at six sites under SSP245 and SSP585 using 27 GCMs in the 2000s (1989-2020), 2040s (2021-2060), and 2080s (2061-2100).

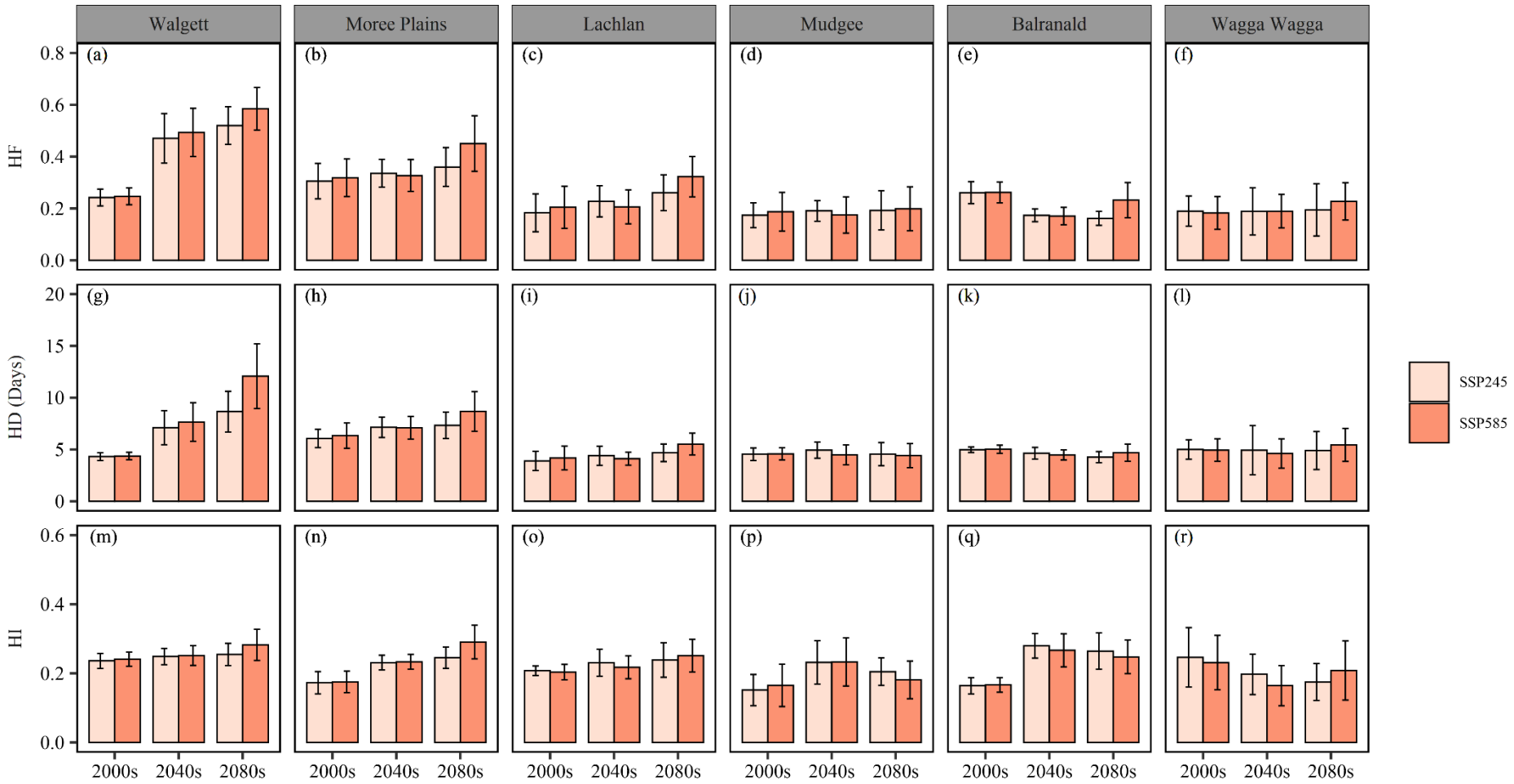

Figure 3-S7. The heat frequency (HF), duration (HD), and intensity (HI) in the wheat sensitive period (WSP, 14 days before and after flowering time) at six sites under SSP245 and SSP585 using 27 GCMs in the 2000s (1989-2020), 2040s (2021-2060), and 2080s (2061-2100).

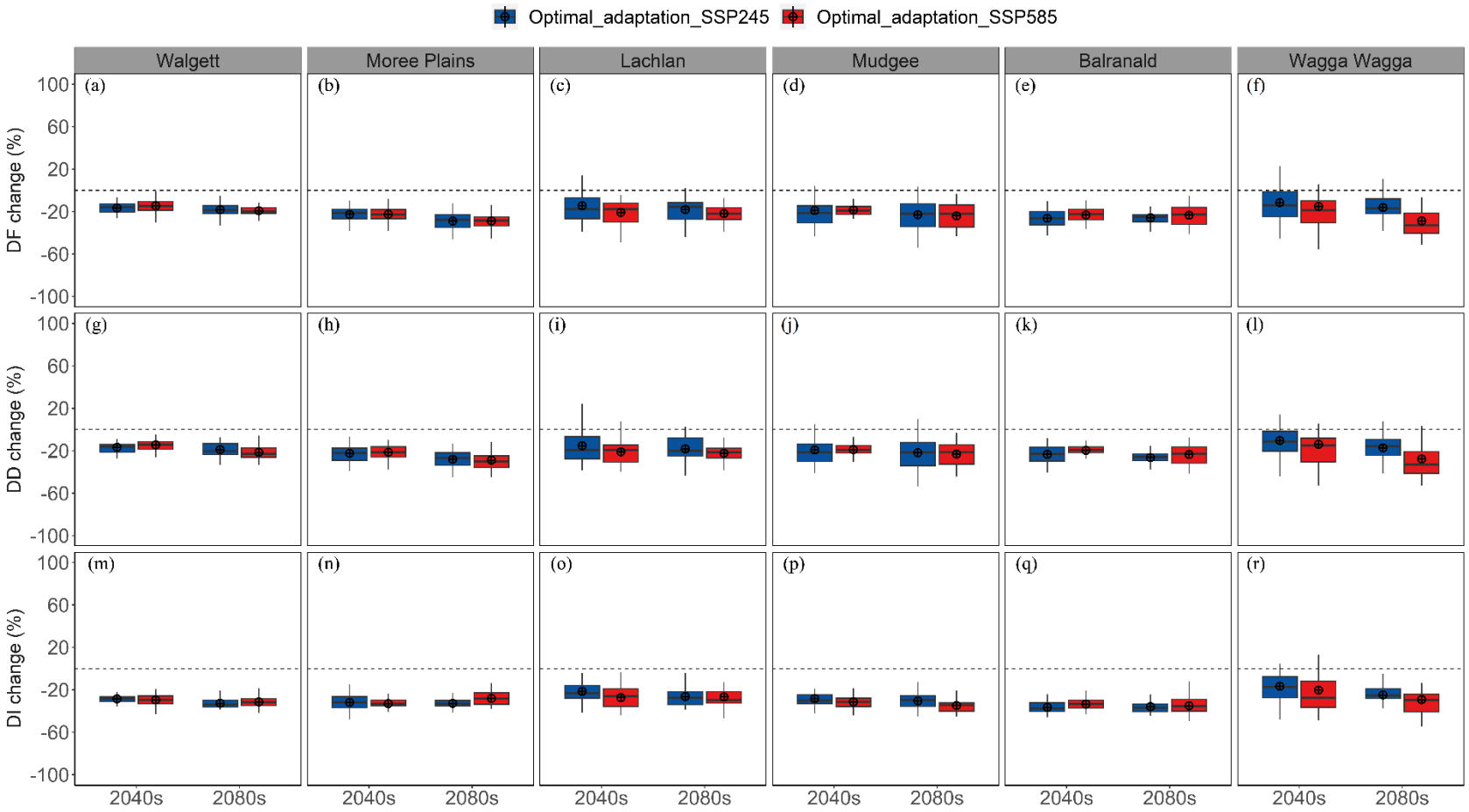

Figure 3-S8. Projected changes in drought frequency (DF), duration (DD), and intensity (DI) during the wheat sensitive period (WSP, 14 days before and after flowering time) at six sites. Changes were estimated between before and after using optimal agronomic options for 2040s (2021–2060) and 2080s (2061–2100) under SSP245 and SSP585 based on the 27 downscaled GCMs. Box boundaries indicate the 25th and 75th percentiles across GCMs, whiskers below and above the box indicate the 10th and 90th percentiles. The black lines and crosshairs within each box indicate the multi-model median and mean respectively.

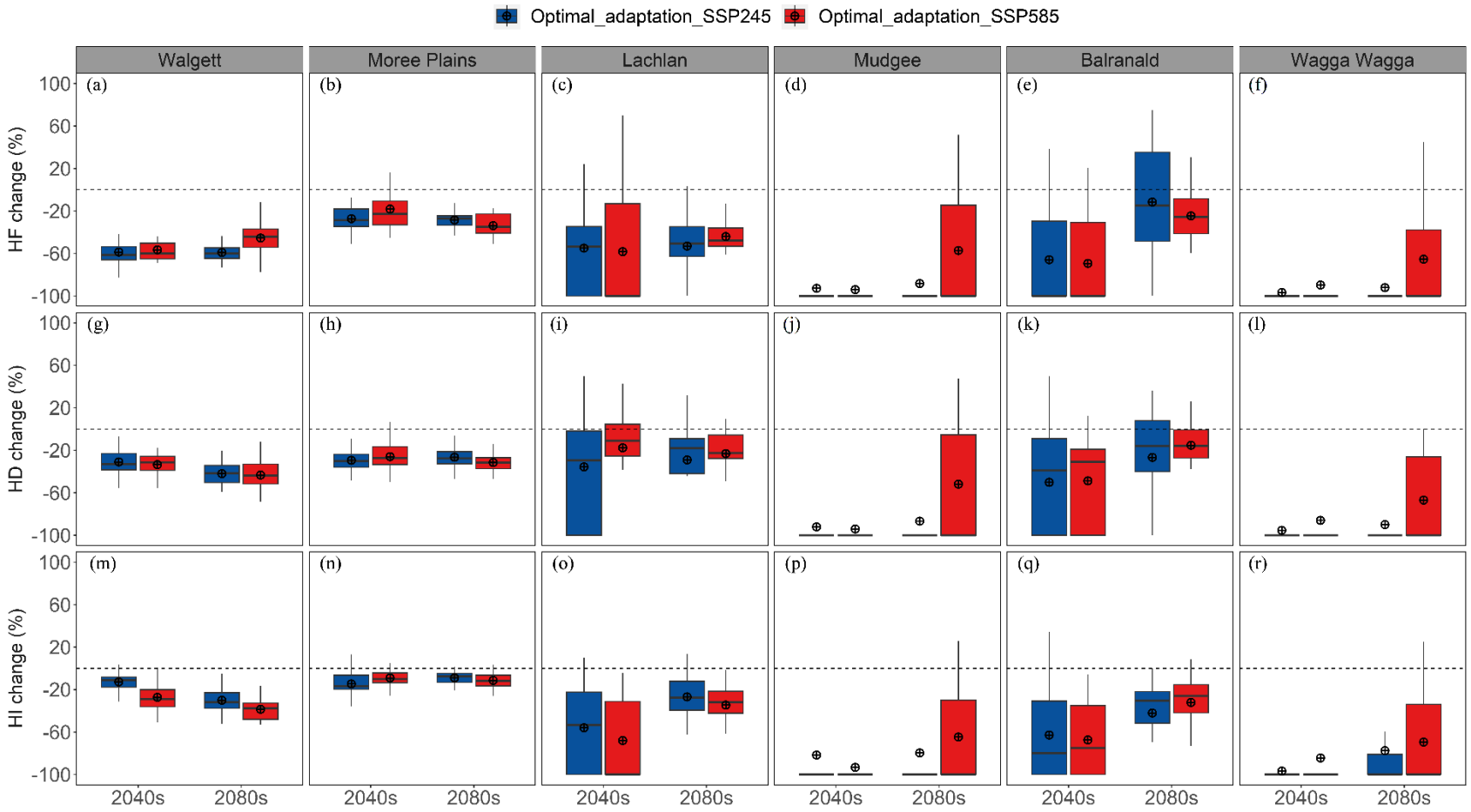

Figure 3-S9. Projected changes in heat frequency (HF), duration (HD), and intensity (HI) during the wheat sensitive period (WSP, 14 days before and after flowering time) at six sites. Changes were estimated between before and after using optimal agronomic options for 2040s (2021–2060) and 2080s (2061–2100) under SSP245 and SSP585 based on the 27 downscaled GCMs. Box boundaries indicate the 25th and 75th percentiles across GCMs, whiskers below and above the box indicate the 10th and 90th percentiles. The black lines and crosshairs within each box indicate the multi-model median and mean respectively.

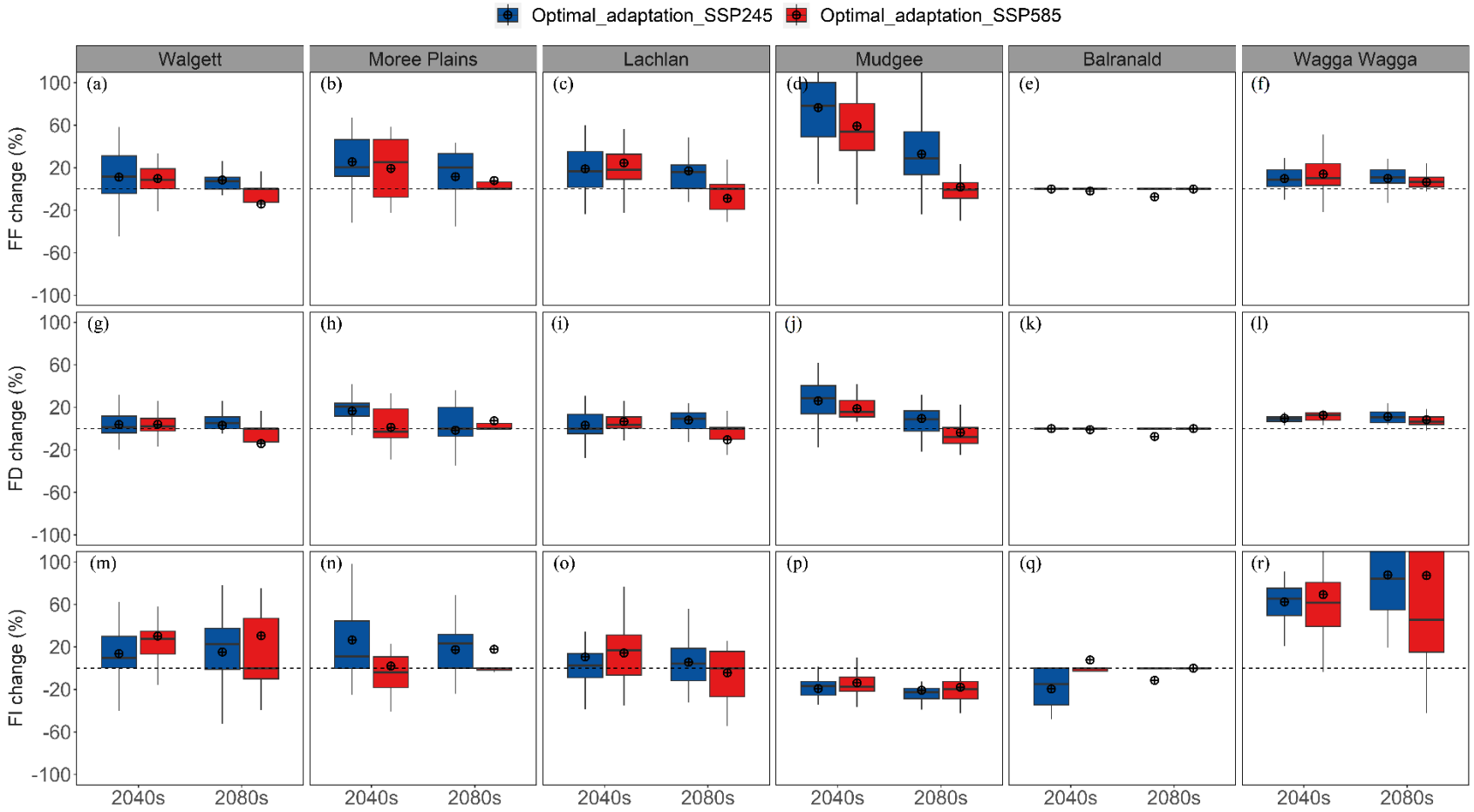

Figure 3-S10. Projected changes in frost frequency (FF), duration (FD), and intensity (FI) during the wheat sensitive period (WSP, 14 days before and after flowering time) at six sites. Changes were estimated between before and after using optimal agronomic options for 2040s (2021–2060) and 2080s (2061–2100) under SSP245 and SSP585 based on the 27 downscaled GCMs. Box boundaries indicate the 25th and 75th percentiles across GCMs, whiskers below and above the box indicate the 10th and 90th percentiles. The black lines and crosshairs within each box indicate the multi-model median and mean respectively.

3.6.4. Supplementary tables

Table 3-S1. List of 27 GCMs from CMIP6 under SSP245 and SSP585 used in this study.

Model ID	Name of GCM	Abbreviation	Country	Institute ID
1	ACCESS-CM2	ACC1	Australia	CSIRO-ACCES
2	ACCESS-ESM1-5	ACC2	Australia	CSIRO-ACCES
3	BCC-CSM2-MR	BCCC	China	BCC
4	CanESM5	Can1	Canada	CCCma
5	CanESM5-CanOE	Can2	Canada	CCCma
6	CIESM	CIES	China	THU
7	CMCC-CM2-SR5	CMCS	Italy	CMCC
8	CNRM-CM6-1	CNR2	France	CNRM-CERFACS
9	CNRM-CM6-1-HR	CNR3	France	CNRM-CERFACS
10	CNRM-ESM2-1	CNR1	France	CNRM-CERFACS
11	EC-Earth3	ECE1	Europe	EC-EARTH-Consortium
12	EC-Earth3-Veg	ECE2	Europe	EC-EARTH-Consortium
13	FGOALS-g3	FGOA	China	CAS
14	GFDL-CM4	GFD1	USA	NOAA-GFDL
15	GFDL-ESM4	GFD2	USA	NOAA-GFDL
16	GISS-E2-1-G	GISS	USA	NASA-GISS
17	HadGEM3-GC31-LL	HadG	England	MOHC
18	INM-CM4-8	INM1	Russia	INM
19	INM-CM5-0	INM2	Russia	INM
20	IPSL-CM6A-LR	IPSL	France	IPSL
21	MIROC6	MIR1	Japan	MIROC
22	MIROC-ES2L	MIR2	Japan	MIROC
23	MPI-ESM1-2-HR	MPI1	German	MPI-M
24	MPI-ESM1-2-LR	MPI2	German	MPI-M
25	MRI-ESM2-0	MTIE	Japan	MRI
26	NESM3	NESM	China	NUIST
27	UKESM1-0-LL	UKES	England	MOHC

3.7 Reference

Ababaei, B., Chenu, K., 2020. Heat shocks increasingly impede grain filling but have little effect on grain setting across the Australian wheatbelt. Agricultural and Forest Meteorology 284, 107889.

Akter, N., & Rafiqul Islam, M., 2017. Heat stress effects and management in wheat. A review. Agronomy for Sustainable Development, 37(5), 37.

Alexander, B., Hayman, P., McDonald, G., Talukder, H., Gill, G., 2010. Characterising the risk of heat stress on wheat in South Australia: meteorology, climatology and the design of a field heating chamber, Proceedings of the 15th Australian agronomy conference, Lincoln, New Zealand.

Amarasingha, R.P.R.K., Suriyagoda, L.D.B., Marambe, B., Gaydon, D.S., Galagedara, L.W., Punyawardena, R., Silva, G.L.L.P., Nidumolu, U., Howden, M., 2015. Simulation of crop and water productivity for rice (Oryza sativa L.) using APSIM under diverse agro-climatic conditions and water management techniques in Sri Lanka. Agricultural Water Management 160, 132-143.

Anwar, M.R., Liu, D.L., Farquharson, R., Macadam, I., Abadi, A., Finlayson, J., Wang, B., Ramilan, T., 2015. Climate change impacts on phenology and yields of five broadacre crops at four climatologically distinct locations in Australia. Agricultural Systems 132, 133-144.

APSIM, 2015. The APSIM-Wheat Module (7.5 R3008).

Archontoulis, S.V., Miguez, F.E., Moore, K.J., 2014. Evaluating APSIM Maize, Soil Water, Soil Nitrogen, Manure, and Soil Temperature Modules in the Midwestern United States. Agronomy Journal 106, 1025-1040.

Asseng, S., Foster, I. A. N., Turner, N. C., 2011. The impact of temperature variability on wheat yields. Global Change Biology 17, 997-1012.

Asseng, S., Turner, N.C., Keating, B.A., 2001. Analysis of water-and nitrogen-use efficiency of wheat in a Mediterranean climate. Plant and Soil 233, 127-143.

Asseng, S., van Keulen, H., Stol, W., 2000. Performance and application of the APSIM Nwheat model in the Netherlands. European Journal of Agronomy 12, 37-54.

Bastos, A., Ciais, P., Friedlingstein, P., Sitch, S., Pongratz, J., Fan, L., Wigneron, J.P., Weber, U., Reichstein, M., Fu, Z., Anthoni, P., Arneth, A., Haverd, V., Jain, A.K., Joetzjer, E., Knauer, J., Lienert, S., Loughran, T., McGuire, P.C., Tian, H., Viovy, N., Zaehle, S., 2020. Direct and seasonal legacy effects of the 2018 heat wave and drought on European ecosystem productivity. Science advances 6, eaba2724.

Chen, Y.L., Palta, J., Clements, J., Buirchell, B., Siddique, K.H.M., Rengel, Z., 2014. Root architecture alteration of narrow-leafed lupin and wheat in response to soil compaction. Field Crops Research 165, 61-70.

Chenu, K., Cooper, M., Hammer, G.L., Mathews, K.L., Dreccer, M.F., Chapman, S.C., 2011. Environment characterization as an aid to wheat improvement: interpreting genotype–environment interactions by modelling water-deficit patterns in North-Eastern Australia. Journal of Experimental Botany 62, 1743-1755.

Chenu, K., Deihimfard, R., Chapman, S.C., 2013. Large-scale characterization of drought pattern: a continent-wide modelling approach applied to the Australian wheatbelt – spatial and temporal trends. New Phytologist 198, 801-820.

Ciais, P., Reichstein, M., Viovy, N., Granier, A., Ogée, J., Allard, V., Aubinet, M., Buchmann, N., Bernhofer, C., Carrara, A., Chevallier, F., De Noblet, N., Friend, A.D., Friedlingstein, P., Grünwald, T., Heinesch, B., Keronen, P., Knohl, A., Krinner, G., Loustau, D., Manca, G., Matteucci, G., Miglietta, F., Ourcival, J.M., Papale, D., Pilegaard, K., Rambal, S., Seufert, G., Soussana, J.F., Sanz, M.J., Schulze, E.D., Vesala, T., Valentini, R., 2005. Europe-wide reduction in primary productivity caused by the heat and drought in 2003. Nature 437, 529-533.

Cohen, I., Zandalinas, S.I., Huck, C., Fritschi, F.B., Mittler, R.J.P.P., 2021. Meta-analysis of drought and heat stress combination impact on crop yield and yield components. Physiologia Plantarum 171, 66-76.

Cossani, C.M., Slafer, G.A., Savin, R., 2009. Yield and biomass in wheat and barley under a range of conditions in a Mediterranean site. Field Crops Research 112, 205-213.
Dalgliesh, N., Cocks, B., Horan, H., 2012. APSoil-providing soils information to consultants, farmers and researchers, 16th Australian Agronomy Conference, Armidale, NSW.
Dang, Y.P., Dalal, R.C., Routley, R., Schwenke, G.D., Daniells, I., 2006. Subsoil constraints to grain production in the cropping soils of the north-eastern region of Australia: an overview. Australian Journal of Experimental Agriculture 46, 19-35.
Devasirvatham, V., Tan, D.K., Trethowan, R.M., 2016. Breeding strategies for enhanced plant tolerance to heat stress, Advances in plant breeding strategies: Agronomic, abiotic and biotic stress traits. Springer, pp. 447-469.
Dias, A.S., Lidon, F.C., 2009. Evaluation of Grain Filling Rate and Duration in Bread and Durum Wheat, under Heat Stress after Anthesis. Journal of Agronomy and Crop Science 195, 137-147.
Dodd, R.J., Chadwick, D.R., Harris, I.M., Hines, A., Hollis, D., Economou, T., Gwynn-Jones, D., Scullion, J., Robinson, D.A., Jones, D.L., 2021. Spatial co-localisation of extreme weather events: a clear and present danger. Ecology Letters 24, 60-72.
Dodd, I. C., Whalley, W. R., Ober, E. S., & Parry, M. a. J., 2011. Genetic and management approaches to boost UK wheat yields by ameliorating water deficits. Journal of Experimental Botany, 62(15), 5241-5248.
Elahi, E., Khalid, Z., Tauni, M.Z., Zhang, H., Lirong, X.J.T., 2021. Extreme weather events risk to crop-production and the adaptation of innovative management strategies to mitigate the risk: A retrospective survey of rural Punjab, Pakistan. Technovation, 102255.
Fan, J., McConkey, B., Wang, H., Janzen, H., 2016. Root distribution by depth for temperate agricultural crops. Field Crops Research 189, 68-74.
Farre, I., Foster, I., Biddulph, B., Asseng, S., 2003. Is there a value in having a frost forecast for wheat in the South-West of Western Australia.
FAO, 2021. The Food and Agriculture Organization of the United Nations. Statistic data base. https://www.fao.org/faostat/en/#data/QCL.
Feng, P., Liu, D.L., Wang, B., Waters, C., Zhang, M., Yu, Q., 2019a. Projected changes in drought across the wheat belt of southeastern Australia using a downscaled climate ensemble. International Journal of Climatology 39, 1041-1053.
Feng, P., Wang, B., Liu, D.L., Waters, C., Xiao, D., Shi, L., Yu, Q., 2020. Dynamic wheat yield forecasts are improved by a hybrid approach using a biophysical model and machine learning technique. Agricultural and Forest Meteorology 285-286, 107922.
Feng, S., Hao, Z., Zhang, X., Hao, F., 2019b. Probabilistic evaluation of the impact of compound dry-hot events on global maize yields. Science of The Total Environment 689, 1228-1234.
Flohr, B.M., Hunt, J.R., Kirkegaard, J.A., Evans, J.R., Lilley, J.M., 2018. Genotype × management strategies to stabilise the flowering time of wheat in the south-eastern Australian wheatbelt. Crop and Pasture Science 69, 547-560.
Frank, A.B., Bauer, A., 1982. Effect of Temperature and Fertilizer N on Apex Development in Spring Wheat1. Agronomy journal 74, 504-509.
Gan, Y., Liu, L., Cutforth, H., Wang, X., Ford, G., 2011. Vertical distribution profiles and temporal growth patterns of roots in selected oilseeds, pulses and spring wheat. Crop and Pasture Science 62, 457-466.
García, G. A., Miralles, D. J., Serrago, R. A., Alzueta, I., Huth, N., & Dreccer, M. F. (2018). Warm nights in the Argentine Pampas: Modelling its impact on wheat and barley shows yield reductions. Agricultural Systems, 162, 259-268.
Geirinhas, J.L., Russo, A., Libonati, R., Sousa, P.M., Miralles, D.G., Trigo, R.M., 2021. Recent increasing frequency of compound summer drought and heatwaves in Southeast Brazil. Environmental Research Letters 16, 034036.
Giraldo, P., Benavente, E., Manzano-Agugliaro, F., Gimenez, E., 2019. Worldwide Research Trends on Wheat and Barley: A Bibliometric Comparative Analysis. Agronomy 9, 352.

Gomez-Macpherson, H., Richards, R.A., 1995. Effect of sowing time on yield and agronomic characteristics of wheat in south-eastern Australia. Australian Journal of Agricultural Research 46, 1381-1399.

Gouache, D., Le Bris, X., Bogard, M., Deudon, O., Pagé, C., Gate, P., 2012. Evaluating agronomic adaptation options to increasing heat stress under climate change during wheat grain filling in France. European Journal of Agronomy 39, 62-70.

Granier, A., Bréda, N., Biron, P., Villette, S., 1999. A lumped water balance model to evaluate duration and intensity of drought constraints in forest stands. Ecological Modelling 116, 269-283.

Grose, M.R., Narsey, S., Delage, F.P., Dowdy, A.J., Bador, M., Boschat, G., Chung, C., Kajtar, J.B., Rauniyar, S., Freund, M.B., Lyu, K., Rashid, H., Zhang, X., Wales, S., Trenham, C., Holbrook, N.J., Cowan, T., Alexander, L., Arblaster, J.M., Power, S., 2020. Insights From CMIP6 for Australia's Future Climate. Earth's Future 8, e2019EF001469.

Guo, Y., Lu, X., Zhang, J., Li, K., Wang, R., Rong, G., Liu, X., Tong, Z., 2022. Joint analysis of drought and heat events during maize (Zea mays L.) growth periods using copula and cloud models: A case study of Songliao Plain. Agricultural Water Management 259, 107238.

Hao, S., Ryu, D., Western, A., Perry, E., Bogena, H., Franssen, H.J.H., 2021. Performance of a wheat yield prediction model and factors influencing the performance: A review and meta-analysis. Agricultural Systems 194, 103278.

Hasanuzzaman, M., & Fujita, M., 2011. Selenium Pretreatment Upregulates the Antioxidant Defense and Methylglyoxal Detoxification System and Confers Enhanced Tolerance to Drought Stress in Rapeseed Seedlings. Biological Trace Element Research, 143(3), 1758-1776.

Holzworth, D.P., Huth, N.I., deVoil, P.G., Zurcher, E.J., Herrmann, N.I., McLean, G., Chenu, K., van Oosterom, E.J., Snow, V., Murphy, C.J.E.M., Software, 2014. APSIM–evolution towards a new generation of agricultural systems simulation. Environmental Modelling & Software 62, 327-350.

Hunt, J.R., Browne, C., McBeath, T.M., Verburg, K., Craig, S., Whitbread, A.M., 2013. Summer fallow weed control and residue management impacts on winter crop yield though soil water and N accumulation in a winter-dominant, low rainfall region of southern Australia. Crop and Pasture Science 64, 922-934.

Hunt, J.R., Lilley, J.M., Trevaskis, B., Flohr, B.M., Peake, A., Fletcher, A., Zwart, A.B., Gobbett, D., Kirkegaard, J.A., 2019. Early sowing systems can boost Australian wheat yields despite recent climate change. Nature Climate Change 9, 244-247.

Innes, P.J., Tan, D.K.Y., Van Ogtrop, F., Amthor, J.S., 2015. Effects of high-temperature episodes on wheat yields in New South Wales, Australia. Agricultural and Forest Meteorology 208, 95-107.

Jones, C. A., & Kiniry, J. R., 1986. A simulation model of maize growth and development. Texas A & M University Press, College Station.

Keating, B.A., Carberry, P.S., Hammer, G.L., Probert, M.E., Robertson, M.J., Holzworth, D., Huth, N.I., Hargreaves, J.N.G., Meinke, H., Hochman, Z., McLean, G., Verburg, K., Snow, V., Dimes, J.P., Silburn, M., Wang, E., Brown, S., Bristow, K.L., Asseng, S., Chapman, S., McCown, R.L., Freebairn, D.M., Smith, C.J., 2003. An overview of APSIM, a model designed for farming systems simulation. European Journal of Agronomy 18, 267-288.

Kerr, N.J., Siddique, K.H.M., Delane, R.J., 1992. Early sowing with wheat cultivars of suitable maturity increases grain yield of spring wheat in a short season environment. Australian Journal of Experimental Agriculture 32, 717-723.

Kirkegaard, J.A., Lilley, J.M., 2007. Root penetration rate a benchmark to identify soil and plant limitations to rooting depth in wheat. Australian Journal of Experimental Agriculture. Australian Journal of Experimental Agriculture 47, 590-602.

Kong, Q., Guerreiro, S.B., Blenkinsop, S., Li, X.-F., Fowler, H.J., 2020. Increases in summertime concurrent drought and heatwave in Eastern China. Weather and Climate Extremes 28, 100242.

Korres, N.E., Norsworthy, J.K., Burgos, N.R., Oosterhuis, D.M., 2017. Temperature and drought impacts on rice production: An agronomic perspective regarding short- and long-term adaptation measures. Water Resources and Rural Development 9, 12-27.

Kumar Tewari, A., Charan Tripathy, B., 1998. Temperature-Stress-Induced Impairment of Chlorophyll Biosynthetic Reactions in Cucumber and Wheat1. Plant Physiology 117, 851-858.
Lalic, B., Eitzinger, J., Mihailovic, D. T., Thaler, S., & Jancic, M., 2013. Climate change impacts on winter wheat yield change–which climatic parameters are crucial in Pannonian lowland? Journal of Agricultural Science 151, 757-774.
Lesk, C., Coffel, E., Winter, J., Ray, D., Zscheischler, J., Seneviratne, S.I., Horton, R., 2021. Stronger temperature–moisture couplings exacerbate the impact of climate warming on global crop yields. Nature Food 2, 683-691.
Lesk, C., Rowhani, P., Ramankutty, N., 2016. Influence of extreme weather disasters on global crop production. Nature 529, 84-87.
Li, E., Zhao, J., Pullens, J.W.M., Yang, X., 2022. The compound effects of drought and high temperature stresses will be the main constraints on maize yield in Northeast China. Science of The Total Environment 812, 152461.
Li, S.Y., Miao, L.J., Jiang, Z.H., Wang, G.J., Gnyawali, K.R., Zhang, J., Zhang, H., Fang, K., He, Y., Li, C.J.A.i.C.C.R., 2020. Projected drought conditions in Northwest China with CMIP6 models under combined SSPs and RCPs for 2015–2099. Advances in Climate Change Research 11, 210-217.
Littleboy, M., Silburn, D., Freebairn, D., Woodruff, D., Hammer, G., Leslie, J., 1992. Impact of soil erosion on production in cropping systems. I. Development and validation of a simulation model. Australian Journal of Soil Research 30, 757-774.
Liu, D.L., 2007. Incorporating vernalization response functions into an additive phenological model for reanalysis of the flowering data of annual pasture legumes. Field Crops Research 101, 331-342.
Liu, D.L., Anwar, M.R., O'Leary, G., Conyers, M.K., 2014. Managing wheat stubble as an effective approach to sequester soil carbon in a semi-arid environment: Spatial modelling. Geoderma 214-215, 50-61.
Liu, D.L., Zuo, H., 2012. Statistical downscaling of daily climate variables for climate change impact assessment over New South Wales, Australia. Climatic Change 115, 629-666.
Lobell, D.B., Hammer, G.L., Chenu, K., Zheng, B., McLean, G., Chapman, S.C., 2015. The shifting influence of drought and heat stress for crops in northeast Australia. Global Change Biology 21, 4115-4127.
Madadgar, S., AghaKouchak, A., Farahmand, A., Davis, S.J., 2017. Probabilistic estimates of drought impacts on agricultural production. Geophysical Research Letters 44, 7799-7807.
Manavalan, L. P., Guttikonda, S. K., Phan Tran, L.-S., & Nguyen, H. T., 2009. Physiological and Molecular Approaches to Improve Drought Resistance in Soybean. Plant and Cell Physiology, 50(7), 1260-1276.
Maqbool, M. A., Aslam, M., & Ali, H., 2017. Breeding for improved drought tolerance in Chickpea (Cicer arietinum L.). Plant Breeding, 136(3), 300-318.
Mohi-Ud-Din, M., Siddiqui, N., Rohman, M., Jagadish, S. V. K., Ahmed, J. U., Hassan, M. M., Hossain, A., & Islam, T., 2021. Physiological and biochemical dissection reveals a trade-off between antioxidant capacity and heat tolerance in bread wheat (Triticum aestivum L.). Antioxidants, 10(3), 351.
Mondal, S., Singh, R. P., Huerta-Espino, J., Kehel, Z., & Autrique, E., 2015. Characterization of Heat- and Drought-Stress Tolerance in High-Yielding Spring Wheat. Crop Science, 55(4), 1552-1562.
Mukherjee, S., Ashfaq, M., Mishra, A.K., 2020. Compound Drought and Heatwaves at a Global Scale: The Role of Natural Climate Variability-Associated Synoptic Patterns and Land-Surface Energy Budget Anomalies. Journal of Geophysical Research: Atmospheres 125, e2019JD031943.
Mukherjee, S., Mishra, A.K., 2021. Increase in Compound Drought and Heatwaves in a Warming World. Geophysical Research Letters 48, e2020GL090617.
Mullarkey, M., Jones, P., 2000. Isolation and analysis of thermotolerant mutants of wheat. Journal of Experimental Botany 51, 139-146.

Pimstein, A., Eitel, J. U. H., Long, D. S., Mufradi, I., Karnieli, A., & Bonfil, D. J., 2009. A spectral index to monitor the head-emergence of wheat in semi-arid conditions. Field Crops Research, 111(3), 218-225.
Pirttioja, N., Palosuo, T., Fronzek, S., Räisänen, J., Rötter, R.P., Carter, T.R., 2019. Using impact response surfaces to analyse the likelihood of impacts on crop yield under probabilistic climate change. Agricultural and Forest Meteorology 264, 213-224.
Porter, J.R., Gawith, M., 1999. Temperatures and the growth and development of wheat: a review. European Journal of Agronomy 10, 23-36.
Poudel, P.B., Poudel, M.R., 2020. Heat stress effects and tolerance in wheat: A review. Journal of Biology and Today's World 9, 1-6.
Prasad, P.V.V.; Staggenborg, S.A.; Ristic, Z, 2008. Impacts of drought and/or heat stress on physiological, developmental, growth, and yield processes of crop plants. In Response of Crops to Limited Water: Ahuja, L.H., Saseendran, S.A., Eds.; Advances in Agricultural Systems Modeling Series 1. ASA-CSSA: Madison, WI, USA, 2008; pp. 301–355.
Rawson, H., Bagga, A., 1979. Influence of Temperature Between Floral Initiation and Flag Leaf Emergence on Grain Number in Wheat. Australian Journal of Plant Physiology 6, 391-400.
Rebbeck, M., Lynch, C., Hayman, P.T., Sadras, V.O., 2007. Delving of sandy surfaced soils reduces frost damage in wheat crops. Australian Journal of Agricultural Research 58, 105-112.
Ribeiro, A.F.S., Russo, A., Gouveia, C.M., Páscoa, P., Zscheischler, J.J.B., 2020. Risk of crop failure due to compound dry and hot extremes estimated with nested copulas. Biogeosciences 17, 4815-4830.
Richardson, C. W., & Wright, D. A., 1984. A model for generating daily weather variables.United States Department of Agriculture, Agriculture Research Service, Washington, DC, USA, 1-86.
Ristic, Z., Bukovnik, U., Prasad, P.V.V., 2007. Correlation between Heat Stability of Thylakoid Membranes and Loss of Chlorophyll in Winter Wheat under Heat Stress. Crop Science 47, 2067-2073.
Rötter, R.P., Tao, F., Höhn, J.G., Palosuo, T., 2015. Use of crop simulation modelling to aid ideotype design of future cereal cultivars. Journal of Experimental Botany 66, 3463-3476.
Saini, H.S., Westgate, M.E., 1999. Reproductive development in grain crops during drought. Advances in agronomy 68, 59-96.
Sedlmeier, K., Feldmann, H., Schädler, G., 2018. Compound summer temperature and precipitation extremes over central Europe. Theoretical and Applied Climatology 131, 1493-1501.
Semenov, M.A., Stratonovitch, P., Alghabari, F., Gooding, M.J., 2014. Adapting wheat in Europe for climate change. Journal of Cereal Science 59, 245-256.
Semenov, M.A., Stratonovitch, P., 2015. Adapting wheat ideotypes for climate change: accounting for uncertainties in CMIP5 climate projections. Climate Research 65, 123-139.
Seyoum, S., Chauhan, Y., Rachaputi, R., Fekybelu, S., Prasanna, B., 2017. Characterising production environments for maize in eastern and southern Africa using the APSIM Model. Agricultural and Forest Meteorology 247, 445-453.
Shah, N.H., Paulsen, G.M., 2003. Interaction of drought and high temperature on photosynthesis and grain-filling of wheat. Plant and Soil 257, 219-226.
Single, W., 1985. Frost injury and the physiology of the wheat plant. Journal of the Australian Institute of Agricultural Science.
Stratonovitch, P., Semenov, M.A., 2015. Heat tolerance around flowering in wheat identified as a key trait for increased yield potential in Europe under climate change. Journal of Experimental Botany 66, 3599-3609.
Talukder, A.S.M.H.M., McDonald, G.K., Gill, G.S., 2013. Effect of short-term heat stress prior to flowering and at early grain set on the utilization of water-soluble carbohydrate by wheat genotypes. Field Crops Research 147, 1-11.
Talukder, A.S.M.H.M., McDonald, G.K., Gill, G.S., 2014. Effect of short-term heat stress prior to flowering and early grain set on the grain yield of wheat. Field Crops Research 160, 54-63.
Tao, F., Rötter, R.P., Palosuo, T., Díaz-Ambrona, C.G.H., Mínguez, M.I., Semenov, M.A., Kersebaum, K.C., Nendel, C., Cammarano, D., Hoffmann, H., Ewert, F., Dambreville, A., Martre, P., Rodríguez, L.,

Ruiz-Ramos, M., Gaiser, T., Höhn, J.G., Salo, T., Ferrise, R., Bindi, M., Schulman, A.H., 2017. Designing future barley ideotypes using a crop model ensemble. European Journal of Agronomy 82, 144-162.

Tashiro, T., Wardlaw, I., 1990. The Response to High Temperature Shock and Humidity Changes Prior to and During the Early Stages of Grain Development in Wheat. Australian Journal of Plant Physiology 17, 551-561.

Turner, N. C., 1980. Turgor maintenance by osmotic adjustment: a review and evaluation. Adaptation of plants to water and high temperature stress, 87-103.

Ummenhofer, C.C., England, M.H., McIntosh, P.C., Meyers, G.A., Pook, M.J., Risbey, J.S., Gupta, A.S., Taschetto, A.S.J.G.R.L., 2009. What causes southeast Australia's worst droughts? Geophysical Research Letters 36.

Vignjevic, M., Wang, X., Olesen, J.E., Wollenweber, B., 2015. Traits in Spring Wheat Cultivars Associated with Yield Loss Caused by a Heat Stress Episode after Anthesis. Journal of Agronomy and Crop Science 201, 32-48.

Vogel, E., Donat, M.G., Alexander, L.V., Meinshausen, M., Ray, D.K., Karoly, D., Meinshausen, N., Frieler, K., 2019. The effects of climate extremes on global agricultural yields. Environmental Research Letters 14, 054010.

Wang, B., Chen, C., Li Liu, D., Asseng, S., Yu, Q., Yang, X., 2015a. Effects of climate trends and variability on wheat yield variability in eastern Australia. Climate Research 64, 173-186.

Wang, B., Feng, P., Chen, C., Li Liu, D., Waters, C., Yu, Q., 2019. Designing wheat ideotypes to cope with future changing climate in South-Eastern Australia. Agricultural Systems 170, 9-18.

Wang, B., Li Liu, D., Asseng, S., Macadam, I., Yang, X., Yu, Q., 2017a. Spatiotemporal changes in wheat phenology, yield and water use efficiency under the CMIP5 multimodel ensemble projections in eastern Australia. Climate Research 72, 83-99.

Wang, B., Liu, D.L., Asseng, S., Macadam, I., Yu, Q., 2015b. Impact of climate change on wheat flowering time in eastern Australia. Agricultural and Forest Meteorology 209-210, 11-21.

Wang, B., Liu, D.L., Asseng, S., Macadam, I., Yu, Q., 2017b. Modelling wheat yield change under CO2 increase, heat and water stress in relation to plant available water capacity in eastern Australia. European Journal of Agronomy 90, 152-161.

Wang, C., Li, Z., Chen, Y., Li, Y., Liu, X., Hou, Y., Wang, X., Kulaixi, Z., Sun, F., 2022. Increased Compound Droughts and Heatwaves in a Double Pack in Central Asia. Remote Sensing 14, 2959.

Wang, J., Wang, E., Luo, Q., Kirby, M., 2009. Modelling the sensitivity of wheat growth and water balance to climate change in Southeast Australia. Climatic Change 96, 79-96.

Wenda-Piesik, A., 2011. Volatile Organic Compound Emissions by Winter Wheat Plants (Triticum aestivum L.) under Fusarium spp. Infestation and Various Abiotic Conditions. Polish Journal of Environmental Studies 20.

Wheeler, T.R., Batts, G.R., Ellis, R.H., Hadley, P., Morison, J.I.L., 1996. Growth and yield of winter wheat (Triticum aestivum) crops in response to CO2 and temperature. The Journal of Agricultural Science 127, 37-48.

Xiao, D., Liu, D.L., Wang, B., Feng, P., Waters, C., 2020. Designing high-yielding maize ideotypes to adapt changing climate in the North China Plain. Agricultural Systems 181, 102805.

Yang, X., Zhou, B., Xu, Y., Han, Z., 2021. CMIP6 evaluation and projection of temperature and precipitation over China. Advances in Atmospheric Sciences 38, 817-830.

You, Q., Cai, Z., Wu, F., Jiang, Z., Pepin, N., Shen, S.S.P., 2021. Temperature dataset of CMIP6 models over China: evaluation, trend and uncertainty. Climate Dynamics 57, 17-35.

Zadoks, J. C., Chang, T. T., & Konzak, C. F. J. W. R., 1974. A decimal code for the growth stages of cereals. 14(6), 415-421.

Zhang, Y., Hao, Z., Feng, S., Zhang, X., Hao, F., 2022. Changes and driving factors of compound agricultural droughts and hot events in eastern China. Agricultural Water Management 263, 107485.

Zheng, B., Chapman, S.C., Christopher, J.T., Frederiks, T.M., Chenu, K., 2015. Frost trends and their estimated impact on yield in the Australian wheatbelt. Journal of Experimental Botany 66, 3611-3623.

Zheng, B., Chenu, K., Fernanda Dreccer, M., Chapman, S.C., 2012. Breeding for the future: what are the potential impacts of future frost and heat events on sowing and flowering time requirements for Australian bread wheat (Triticum aestivium) varieties? Global Change Biology 18, 2899-2914.

Zhou, S., Zhang, Y., Park Williams, A., Gentine, P.J.Sa, 2019. Projected increases in intensity, frequency, and terrestrial carbon costs of compound drought and aridity events. Sci. Adv. 5, eaau5740.

Chapter 4. Compound drought and temperature events intensify wheat yield loss in Australia

This manuscript is under review for publication in the journal Earth's Future.

Abstract

The escalation in extreme weather events has raised concerns for agriculture. The quantification of the impacts of extreme events on crop yield has predominantly concentrated on individual events like drought or heat. Understanding compound extreme events can aid climate impact assessment, offering more comprehensive insights and clear directions for better risk assessment and management within the agricultural sector. Numerous instances have showcased the destructive effects of compound extreme events on crop yields, surpassing those of individual events. However, their influence extent is region-specific and not fully understood in Australia's crop belt. Using a biophysical-statistical modeling approach, we quantified the impacts of drought, heat, frost, and compound drought and extreme temperature (DET) events on wheat yield variations in Australia. We firstly developed indices for these different extreme events during the wheat reproductive period using the APSIM model and then applied these indices in multiple linear regression model to quantify their impacts on the variation of wheat yield. We found that, during 1990-2021, individual drought, heat, and frost events collectively contributed 45% of yield variation, while the percentage increased to 55% after including DET events, with some regions even up to 86%. In extreme low-yield years, the relative importance of DET events surpassed the sum importance of individual drought, heat, and frost events, reaching 68% and 52% in years with yields below the 5^{th} and 10^{th} percentiles, respectively. Our findings highlight the need to factor compound extreme weather events into climate risk management to inform the mitigation of yield losses or crop failure.

Keywords: compound drought and extreme temperature events; wheat yield; APSIM; relative importance

4.1 Introduction

Extreme weather events are key drivers of grain production variability (Iizumi & Ramankutty, 2016). For instance, they contributed 18%–43% of the inter-annual yield variation for the top four crops in the world (maize, wheat, rice, and soybeans) during 1961-2008 (Vogel et al., 2019). Over the past decades, there has been a notable rise in the frequency and intensity of extreme events (Manning et al., 2019; Myhre et al., 2019; Zwiers et al., 2013), with more co-occurrence of multiple extremes in both space and time (Hao et al., 2022; Lesk & Anderson, 2021; Sarhadi et al., 2018). Such increases in compound extreme events are projected to continue or even escalate under future climate change (Wang et al., 2023). The compound

extreme events can present severe challenges to agricultural cropping systems. They give rise to more extreme situations than individual extreme events (drought, heat, or frost) (AghaKouchak et al., 2020) and generally cause more damaging impacts (Cohen et al., 2021; Li, et al., 2022). For example, during the summer of 2018 in Europe, compound drought-heat events resulted in widespread crop harvest failure across many European countries (Bastos et al., 2020). In 2016, France experienced the most severe crop yield loss in the past half-century due to the combination of abnormally wet and hot climate conditions (Ben-Ari et al., 2018). Additionally, the simultaneous occurrence of frost and drought led to a wheat harvest failure in about 12% of the cropping area across Brazil in the late spring of 2006 (Júnior et al., 2021).

Compared to other compound events, the simultaneous co-occurrence of drought and extreme temperature events have more serious adverse impacts on crops (Li, et al., 2022; Potopová et al., 2021) and there was much more specific case evidence to link them with especially poor crop harvests (Christian, Jordan I. et al., 2020; Ciais et al., 2005; Júnior et al., 2021; Lesk et al., 2022; Yuan et al., 2018). Thus, it is critically important to understand the characteristics of compound drought and extreme temperature (DET) events and their impacts on crops, which is of great significance for assisting crops to adapt to climate change and realize a stable increase in crop yields.

Different methods have been used to assess the impacts of DET events on crop yields over the past two decades (Lesk et al., 2022; Li, et al., 2022; Potopová et al., 2021). One approach is to compare the yield for specific years when compound extreme events occur with normal-year yield, proving that compound extreme events are the major drivers of severe yield losses (Beillouin et al., 2020; Ben-Ari et al., 2018). For example, in 2003, the European compound drought and heatwave resulted in 11% and 21% of yield drops than usual in wheat and maize, respectively (García-Herrera et al., 2010). The studies employing the aforementioned method often focus on specific instances or short timeframes, they may not fully capture the long-term magnitude and implications of compound extreme events impacts. By contrast, the assessment method based on the joint distributions using copula and cloud models can demonstrate the long-term impacts of compound extremes on crop yields (Feng & Hao, 2020; Feng et al., 2019). Ribeiro et al. (2020) found that, compared to individual drought or heat, the likelihood of wheat and barley yield losses increased by 8%-29% under compound dry and hot conditions from 1989 to 2016 in Spain. However, these studies only obtain the probabilities or likelihood of the yield loss led by compound extremes, the magnitude of the long-term impacts on crop yields is still unclear. The third approach combined self-developed indices of compound extremes with models to quantify their long-term impacts on crops (Potopová et al., 2021; Simanjuntak et al., 2023; Zampieri et al., 2017). For example, according to the yield response function estimated with individual and compound metrics from 1981 to 2015 in the United States, the impact of heat stress on maize yields has been amplified up to fourfold when coupled with water stress (Haqiqi et al.,

2021). However, these studies employed compound metrics with broad timescales (seasonal or monthly) and primarily focused on maize or soybean, with limited studies addressing the precise long-term implications for wheat. (Hamed et al., 2021; Haqiqi et al., 2021; Lesk et al., 2021; Luan et al., 2021).

Australia is one of the top wheat exporters, consistently contributing about 11% of global wheat exports since 1961 (FAO, 2021). Nevertheless, Australian wheat generally relies on seasonal rainfall, making it highly susceptible to climate variability (Feng et al., 2022). During the past decades, recurring drought in Australia has resulted in large wheat yield losses (Chenu et al., 2013; Feng et al., 2020). The untimely radiation frost in spring (Marcellos & Single, 1975) and the increasing heat events around wheat flowering and grain-filling stages (Ababaei & Chenu, 2020) both can simultaneously co-occur with drought, therefore aggravating the adverse impacts on wheat. However, the previous studies on the impacts of extreme events on Australian wheat were based on single extreme events (Ababaei & Chenu, 2020; Feng et al., 2018; Madadgar et al., 2017; Telfer et al., 2018). To our knowledge, no study has quantified the impacts of DET events on wheat yield in Australia's crop belt. Therefore, a precise assessment of the impacts of DET events on wheat yield is urgently needed for a more comprehensive understanding of climate risks facing grain production in Australia.

Here, we quantified the long-term impacts of both individual and compound drought and extreme temperature events on wheat yield in Australia's crop belt from 1990 to 2021, using a biophysical-statistical modeling approach. This approach allows accurate quantification of extreme weather events (drought, heat, frost, and DET events) that occur during the wheat reproductive period (WRP), providing a basis for precisely quantifying their impacts. We aim to (1) study the characteristics of individual and DET events during 1990-2021; (2) quantify the impacts of individual and DET events on wheat yield variation in 12 subregions in the Australian crop belt; (3) identify the relative importance of individual and DET events to wheat yield variation during low-yield years. We expect the findings from this study will aid the climate impacts assessment, to offer more comprehensive insights and clear directions for better risk assessment and management within the agricultural industry.

4.2 Materials and Methods

4.2.1 Study area

Our study area was the Australian crop belt, which is across the eastern, southeastern, and western parts of Australia. It contains 12 Australian Bureau of Agricultural and Resource Economics and Sciences (ABARES) classification regions (Figure 4-1 and Table 4-1). Since the crop belt spans a wide range of latitude and longitude, it has a large precipitation and temperature gradient. The annual cumulative rainfall (1990-2021) increased from 253 mm in the inland area to 911 mm closer to the coastal region, and the

average temperature rose from 13.5°C in the south to 23.9°C in the north. Wheat, the most important crop in Australia's crop belt, normally is grown under rainfed conditions during April-November (Wang et al., 2018).

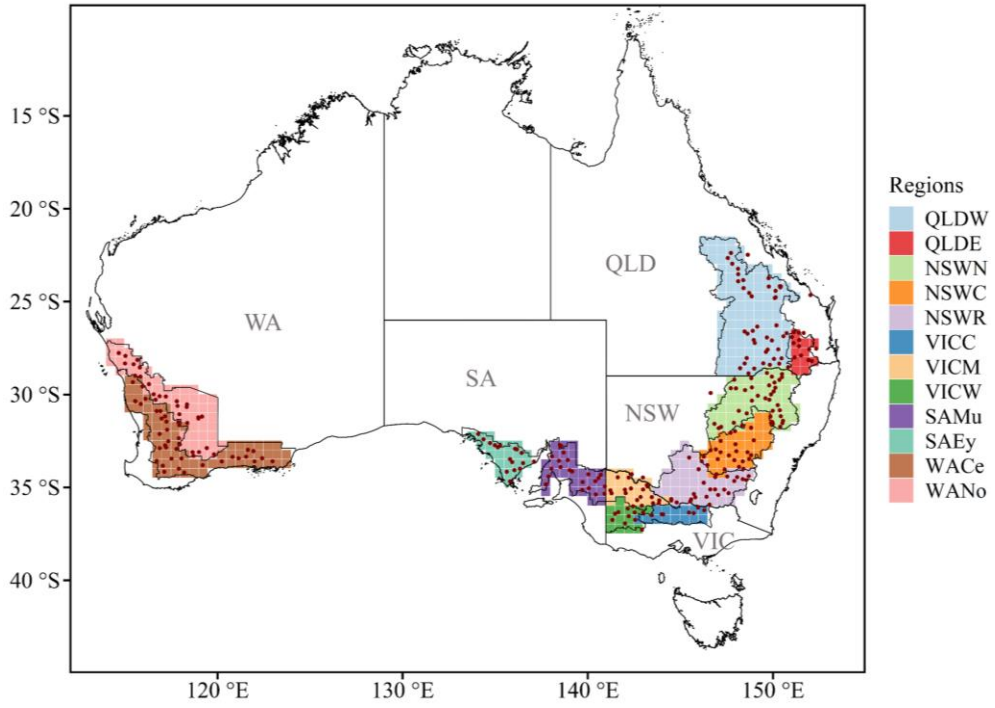

Figure 4-1. The map of Australia's crop belt including 12 subregions and 453 grids (0.5°×0.5°). The red dots represent 296 soil locations used for the APSIM model.

Table 4-1. Mean wheat yield, annual cumulative rainfall, and mean temperature in 12 subregions of Australia's crop belt during 1990-2021. Values in the bracket are the standard deviation.

Subregions	Yield (t/ha)	Rainfall (mm)	Tmean (°C)
QLD Western Downs and Central Highlands (QLDW)	1.41 (0.49)	550.16 (191.40)	21.17 (0.60)
QLD Eastern Darling Downs (QLDE)	2.00 (0.79)	641.06 (173.40)	18.32 (0.51)
NSW North West Slopes and Plains (NSWN)	1.83 (0.81)	547.53 (169.29)	18.88 (0.61)
NSW Central West (NSWC)	1.83 (0.83)	563.26 (172.98)	16.89 (0.58)
NSW Riverina (NSWR)	2.37 (0.92)	445.79 (139.96)	16.67 (0.55)
VIC Central North (VICC)	2.35 (0.93)	510.57 (147.29)	15.05 (0.52)
VIC Mallee (VICM)	1.63 (0.64)	302.60 (98.57)	16.81 (0.46)
VIC Wimmera (VICW)	2.42 (0.91)	452.48 (105.11)	14.81 (0.47)
SA Murray Lands and Yorke Peninsula (SAMu)	2.14 (0.58)	352.88 (91.92)	16.35 (0.40)
SA Eyre Peninsula (SAEy)	1.46 (0.46)	341.21 (83.33)	17.33 (0.40)
WA Central and Southern Wheat Belt (WACe)	1.91 (0.34)	422.34 (90.52)	17.26 (0.41)
WA Northern and Eastern Wheat Belt (WANo)	1.37 (0.36)	311.36 (82.73)	19.00 (0.52)

4.2.2 Data sources

We downloaded the historical (1990-2021) gridded climate data from Scientific Information for Land Owners (SILO, 2023). It provides gridded daily climate data with a resolution of 0.05 degrees throughout Australia. We first focused on the grid cells that were located inside our study area and 41,534 grid cells were acquired. We then upscaled these grid cells from 0.05 to 0.5 degrees, to reduce the excessive calculation load (Feng et al., 2022). Finally, we obtained 453 grids of 0.5-degree for the whole Australia's crop belt (Figure 4-1).

Soil hydraulic properties and parameters were derived from the APSoil database (Apsoil, 2022). 296 soil sites were selected to ensure that each climate-data grid has a corresponding soil profile that is geographically closest to its center point. They were all parameterized for modeling (Dalgliesh et al., 2012).

Actual wheat yield data in 12 ABARES regions were obtained from the commodities survey statistics from 1990 to 2021 (ABARES, 2023). We used MK test to analyze the trends of wheat yields for each region and found that there was no significant trend for the period of 1990-2021 (Table 4-S2). Therefore, we employed yield anomaly (Eq. 4-1) to quantify the contribution of weather extremes on yield variation, aiming represent the magnitude of deviation from the mean yield in annual absolute yields in each sub-region (Schauberger et al., 2017).

$$\Delta Y_t = Y_t - \overline{Y_t} \tag{4-1}$$

where Y_t is the wheat yield for tth year and $\overline{Y_t}$ is the mean wheat yield across Australia's crop belt over the period 1990-2021.

4.2.3 APSIM simulation

APSIM (Agricultural Production System sIMulator) version 7.10 (Holzworth et al., 2014) was used in this study. APSIM is a modeling framework that describes the biophysical process of the agricultural system (Keating et al., 2003). It has been applied and well-validated in numerous studies of the Australia's wheat production system (Asseng et al., 2011; Feng et al., 2022). We used climate data and soil information to drive APSIM to simulate the phenology of wheat and daily soil water content from 1990 to 2021 at 0.5° grid cell. The choice of wheat cultivars and the setting of the sowing window were based on previous studies in the same study area (Feng et al., 2022; Wang, et al., 2018).

4.2.4 Drought, heat, frost, and compound drought and extreme temperature events

Firstly, we defined the three types of individual extreme events: drought, heat, and frost. Drought occurs when the water content in the 0-100cm soil layer is lower than 40% of plant available water capacity (PAWC)

for three or more consecutive days. PAWC quantifies the maximum volume of water that soil can retain for crop utilization. It is determined by the difference in volumetric water content between the drained upper limit (DUL) and the lower limit of crop (LL) represents the total amount of water a soil can store for crops to use (Asseng et al., 2001; Wang et al., 2017). Previous studies have shown that when the amount of extractable soil water for wheat is below 40% of PWAC, the stomatal conductance, root growth, tiller number, and yield of wheat can decrease (Ciais et al., 2005; Granier et al., 1999; Kirkegaard & Lilley, 2007). Generally, heat occurs when the daily maximum temperature is higher than a threshold of 28 °C for three or more consecutive days, causing both grain size and grain weight of wheat to decrease (Lalic et al., 2013; Wheeler et al., 1996). As for frost, we used 2 °C as the threshold to define frost events (Liu et al., 2011). This is consistent with Farre et al. (2010), who reported that when a daily minimum temperature was below 2 °C during wheat flowering, it would cause yield loss. Normally, heat and frost do not occur at the same time during the wheat growth period, while droughts do co-occur with heat or frost. When the timing aligns and drought, heat, or frost events overlap, it is indicative of a DET event.

According to the above definition, we identified the occurrence of each drought, heat, frost, and DET event during the WRP from the initial floral stage to the end of grain filling stage. The reason why we choose WRP instead of the whole wheat growth season is that these extreme events are far more harmful when they occur in WRP than in other growth stages (Cohen et al., 2021). To separate the effects of individual extremes from those of compound extreme events, individual drought, heat, or frost events were picked when DET did not occur (Table 4-2). We used the cumulative sum of the daily intensity during WRP for of each extreme event to characterize its severity.

Table 4-2. Example of one compound drought and extreme temperature (DET) event occurring in the wheat reproductive period (WRP). d_i is the ith day in the WRP; w_s and w_e are the start day and the end day of WRP, respectively.

d_i	Drought	Heat	Frost	DET
w_s	NO	NO	YES	NO
…	NO	NO	YES	NO
…	NO	NO	YES	NO
…	YES	NO	YES	YES
…	YES	NO	YES	YES
l	YES	NO	YES	YES
l+1	YES	NO	NO	NO
l+2	YES	NO	NO	NO
...	YES	NO	NO	NO
…	YES	YES	NO	YES
$l+m_j$	YES	YES	NO	YES
…	YES	YES	NO	YES
…	NO	YES	NO	NO
…	NO	YES	NO	NO
w_e	NO	YES	NO	NO

4.2.4.1 Daily intensity of drought, heat, and frost.

Firstly, we calculated the daily drought, heat, and frost intensity in WRP respectively. Daily drought intensity is calculated as the ratio of the difference between the drought threshold (δ×PAWC) and the daily PAW to the drought threshold. This yields a dimensionless value ranging from 0 to 1, where 1 represents the highest possible intensity of drought (Eq. 4-2).

$$DI_i = \begin{cases} 0, & PAW \geq \delta PAWC \\ \dfrac{\delta PAWC - PAW_i}{\delta PAWC}, & PAW < \delta PAWC \end{cases} \qquad i = 1, 2, ..., w_e - w_s + 1 \tag{4-2}$$

where DI_i is the daily intensity of drought events for the ith day during WRP in a given year; the drought threshold is defined as $\delta \times PAWC$, where $PAWC$ is decided by soil properties and δ is set at 0.4 in this study (Ciais et al., 2005; Granier et al., 1999); PAW_i is the plant available water on the ith day during WRP; w_s marking the start and w_e the end of WRP.

The daily intensity of heat event is calculated based on Eq. 4-3. It calculates the heat intensity as ratio of the excess of TX over the heat threshold (T_c) to the excess of wheat high killing temperature (T_s) over the T_c. This metric also ranges from 0 to 1, with 1 indicating the maximum heat intensity.

$$HI_i = \begin{cases} 0, & T_c \geq TX_i \\ \dfrac{TX_i - T_c}{T_s - T_c}, & T_c < TX_i < T_s \\ 1, & T_s \leq TX_i \end{cases} \qquad i = 1, 2, ..., w_e - w_s + 1 \tag{4-3}$$

where HI_i is the daily intensity of heat events for the ith day during WRP; TX_i refers to the highest temperature recorded on the ith day during WRP; T_c serves as the threshold for heat event, which was taken as 28 ℃. The lethal temperature for wheat (T_s), is identified as 42 ℃, drawing on the research by Kumar Tewari and Charan Tripathy (1998), who documented that wheat was killed when subjected to temperatures of 42 ℃ periods extending beyond 48 hours.

The daily frost intensity was defined by Eq. 4-4. The ratio of the difference between TI and the frost threshold (T_t) to the difference between wheat low killing temperature (T_r) and T_t was calculated as the frost intensity.

$$FI_i = \begin{cases} 0, & T_t \leq TI_i \\ \dfrac{TI_i - T_t}{T_r - T_t}, & T_r < TI_i < T_t \\ 1, & T_r \geq TI_i \end{cases} \qquad i = 1, 2, ..., w_e - w_s + 1 \tag{4-4}$$

where FI_i represents the daily intensity for frost event for the ith day during WRP; TI_i indicates the minimum temperature on the ith day during WRP; The frost threshold temperature, T_t, is set 2 ℃. We took T_r (the wheat low killing temperature) as -5 ℃ (Single, 1985).

4.2.4.2 Annual intensity of DET.

The definition of DET events can be expressed below:

$$DET_j = d_i \left| \left\{ \left(TX_{ij} \geq 28 \right) \bigcap \left(PAW_{ij} \leq \delta \times PAWC \right) \right\} \bigcup \left\{ \left(TI_{ij} \leq 2 \right) \bigcap \left(PAW_{ij} \leq \delta \times PAWC \right) \right\}, \\ j = 1, 2, ..., N; i = l+1, l+2, ..., l+m_j, m_j \geq 3; w_s \leq d_i \leq w_e \tag{4-5}$$

where DET_j is the jth DET event; N represents the total number of DET events occurring within each WRP; d_i refers to the ith day during the WRP, with the subscript l indicating the day immediately preceding the commencement of the jth DET event; TX_{ij} and TI_{ij} stand for the maximum and minimum temperatures, respectively, on d_i during the jth DET event; PAW_{ij} is plant available water on d_i within the jth DH event.

The annual DET intensity (DETI) was derived by adding the cumulative sum of the intensity of all DET events within WRP (Eq. 4-6). The intensity of each DET event was calculated based on the daily intensity (Eq. 4-7). The daily DET intensity is determined by weighted aggregating the daily standardized values for drought, heat, and frost intensities (Eq. 4-8).

$$DETI = \sum_{j=1}^{N} CDETI_j, j = 1, 2, ..., N, N \geq 1 \tag{4-6}$$

$$CDETI_j = \sum_{i=1}^{m_j} SDETI_{ij}, j = 1, 2, ..., N \tag{4-7}$$

$$SDETI_{ij} = \alpha DI_{ij} + \left(1-\alpha\right) HI_{ij} + \left(1-\alpha\right) FI_{ij}, i = 1, 2, ..., m_j; j = 1, 2, ..., N \tag{4-8}$$

where $SDETI_{ij}$ represents the daily DET intensity for the ith day of the jth DET event of a given year; DI_{ij} , HI_{ij}, and FI_{ij} correspond to the daily drought, heat, and frost intensities, respectively, for the ith day of the jth DET event; the coefficient α, assigned a value of 0.5, serves as the weighting factor for the daily drought intensity; $CDETI_j$ quantifies the intensity of the jth DET in the given year.

4.2.4.3 Annual intensity of drought, heat, and frost.

Following the exclusion of DET episodes, the daily intensities for the remaining occurrences of drought, heat, and frost were cumulatively tallied to determine the annual intensity of each of these three extreme events, as outlined in Equations 4-9 to 4-14.

$$DI = \sum_{k=1}^{M} CDI_{ik}, k = 1, 2, ..., M \tag{4-9}$$

$$CDI_k = \sum_{i=1}^{u} DI_{ik}, k = 1, 2, ..., M; i = l+1, l+2, ..., u \quad (4\text{-}10)$$

where CDI_k is the intensity of kth drought event in each WRP removing the DET episodes; DI_{ik} is the daily intensity of drought event on the ith day of the kth drought event during the WRP; DI is the annual intensity of drought events.

$$HI = \sum_{s=1}^{O} CHI_{is}, s = 1, 2, ..., O \quad (4\text{-}11)$$

$$CHI_s = \sum_{i=1}^{u} HI_{is}, s = 1, 2, ..., O; i = l+1, l+2, ..., u \quad (4\text{-}12)$$

where CHI_s is the intensity of sth heat event in each WRP removing the DET episodes; HI_{is} is the daily intensity of heat event on the ith day of the sth heat event during the WRP; HI is the annual intensity of heat events.

$$FI = \sum_{i=1}^{P} CFI_{iv}, v = 1, 2, ..., P \quad (4\text{-}13)$$

$$CFI_v = \sum_{i=1}^{u} FI_{iv}, v = 1, 2, ..., P; i = l+1, l+2, ..., u \quad (4\text{-}14)$$

where CFI_v is the intensity of vth frost eventin each WRP removing the DET episodes; FI_{is} is the daily frost intensity for the ith day of the vth frost event during the WRP; FI is the annual intensity of frost events.

The Mann-Kendall trend test was utilized to assess the statistical significance of the time series trends for DI, HI, FI, and DETI. The test's standardized statistic, Z, was used to determine the direction of these trends, with a positive Z value indicating an upward trend and a negative Z value denoting a downward trend. Time series trends were deemed statistically significant at both the 5% and 1% significance levels (corresponding to 95% and 99% confidence intervals) if $|Z| > 1.96$ and $|Z| > 2.58$. (Han et al., 2018; Li et al., 2022)

4.2.5 Impacts of DET events on wheat yield variation

The annual intensities of drought, heat, frost, and DET at the grid level were aggregated to the region level to establish the relationship with wheat yield anomaly. We developed two multiple linear regression (MLR) models to explain the impacts of DET events on wheat yields. One of the MLR models covered only individual extreme indices as the independent variables (Eq. 4-14), and the other model included DETI and considered both the individual and compound extreme indices (Eq. 4-15). The determination coefficients (R^2) measure the covariance of the actual and predicted wheat yield anomaly. By comparing the difference

of the R^2 for two MLR models, we can quantify the contribution of DET events to wheat yield variability. The two MLR models were both performed in 12 ABARES regions and the whole Australian crop belt. The R package "relaimpo" was employed to determine the relative significance of each independent variable. (Groemping, 2006). This package generates the metric “lmg”, which represents the contribution to R^2 of each variable.

$$\Delta Y = \alpha_0 + \alpha_D{}' DI + \alpha_H{}' HI + \alpha_F{}' FI + \varepsilon_s \quad (4\text{-}15)$$

$$\Delta Y = \alpha_1 + \alpha_D DI + \alpha_H HI + \alpha_F FI + \alpha_{DET} DETI + \varepsilon_{DET} \quad (4\text{-}16)$$

where ΔY denotes estimated yield anomaly; α_D', α_H', and α_F' are regression coefficients in the first MLR model which used DI, HI, and FI as independents, reflecting the response of yield sensitivity to drought, heat, and frost; α_D, α_H, α_F, and α_{DET} are regression coefficients in the second MLR model which used DI, HI, FI, and DETI as independents, reflecting the response of yield sensitivity to drought, heat, frost, and DET; α_0 and α_1 are the intercepts for each MLR model, respectively, and ε_s and ε_{DET} are the residual errors.

Prior to fitting the model, the Variance Inflation Factor (VIF) was computed to identify potential multicollinearity among the independent variables across the 12 regions. VIF quantifies the extent to which the variance of an estimated regression coefficient increases due to multicollinearity, with values spanning from 1 to infinity. A VIF of 1 indicates that there is no multicollinearity among variables, and the larger the VIF, the stronger the multicollinearity among variables (Liu et al., 2019).

4.2.6 Relative importance of DET events on wheat yield variation in different levels of low-yield years

We combined the 32-year wheat yield anomaly from the 12 ABARES regions as a single dataset. Then we used the 5th, 10th, 15th, 20th, 25th, 30th, 35th, 40th, 45th, and 50th percentiles of this dataset as the thresholds to select different levels of low-yield years. The wheat yield anomaly at each level and corresponding DI, HI, FI, and DETI were fitted in the MLR model to generate the relative importance of each variable for each low-yield level.

4.3. Results

4.3.1 Spatial and temporal characteristics of drought, heat, frost, and DET events

Figure 2 shows the temporal variations of annual DI, HI, and FI during WRP from 1990 to 2021. For all 12 regions, the inter-annual variation of DI was higher than that of HI or FI. Moreover, the most pronounced fluctuations of DI were observed in three regions within Victoria, with DI values ranging from 0.01 to 0.53 in VICC, 0.07 to 0.60 in VICM, and 0 to 0.56 in VICW (Figure 4-2 f-h). In contrast, the variations in DI were the smallest in Western Australia, ranging from 0.10 to 0.41 in WACe and 0.13 to 0.55 in WANo

(Figure 4-2 k-l). The long-term (1990-2021) annual mean of DI was highest in VICM and WANo, with a value of 0.34 (Figure 4-2 g&l). While the lowest annual mean DI was 0.19 in VICW (Figure 4-2 h). From 1990 to 2021, the HI was generally maintained at a low level in all regions, close to 0, with only a few years having a value of 0.2. The highest year-to-year variation occurred in NSWR (Figure 4-2 e), with a range of 0-0.24, followed by that of VICC and VICW (Figure 4-2 f&h), with a range of 0-0.18. While QLDE had a rare occurrence of heat events throughout this period (Figure 4-2 b). On average, the HI in the 12 subregions remained low, with VICW and NSWR having the highest annual mean HI at 0.03 (Figure 4-2 h&e), while QLDE had the lowest mean HI at 0.002 (Figure 4-2 b). The temporal variations of FI showed noticeable fluctuations in most regions. Among these regions, QLDE exhibited the most significant variations in FI, ranging from 0-0.45 (Figure 4-2 b). While in regions of SAMu, SAEy, WACe, and WANo, the FIs were consistently low to nearly 0 (Figure 4-2 i-l). The multi-year average FI was highest at 0.11 in QLDE (Figure 4-2 b) and was lowest at around 0.002 in three western subregions (SAEy, WACe, and WANo) (Figure 4-2 j-l).

The temporal variations of DETI are displayed in Figure 4-3 alongside the wheat yield variations. DETI also exhibited fluctuations throughout the period from 1990 to 2021 in all 12 regions. The most pronounced fluctuations of DETI were exhibited in QLDW, with values ranging from 0.01 to 0.61 (Figure 4-3 a), while the region of SAEy showed the slightest fluctuations, with values ranging from 0 to 0.15 (Figure 4-3 j). There were slight increases in DETI after 2000 in all subregions, and on average, the DETI after 2000 was higher by 0.01 to 0.13 compared to those before 2000. Based on the multi-year average DETI, the region QLDW experienced the highest DETI, with a value of 0.33 (Figure 4-3 a), while the region VICW and SAEy had the lowest DETI, both at 0.06 (Figure 4-3 g&j). Additionally, wheat yield anomaly varied greatly from year to year, which was negatively impacted by DETI. Except for the two regions of QLDW and SAMu (Figure 4-3 a&i), the wheat yield anomaly showed significantly negative correlations with DETI. The highest correlation coefficients were in the three regions that belong to New South Wales (NSW), with values of -0.66 and -0.72, respectively (Figure 4-3 c-e).

Figure 4-2. Temporal variations of drought intensity, heat intensity, and frost intensity during WRP from 1990 to 2021 in 12 regions across Australian crop belt. Z_D, Z_H, and Z_F are the increasing (decreasing) rates of drought intensity (DI), heat intensity (HI), and frost intensity (FI) from 1990 to 2021, respectively (*** $p < 0.001$, ** $p < 0.01$, * $p < 0.05$).

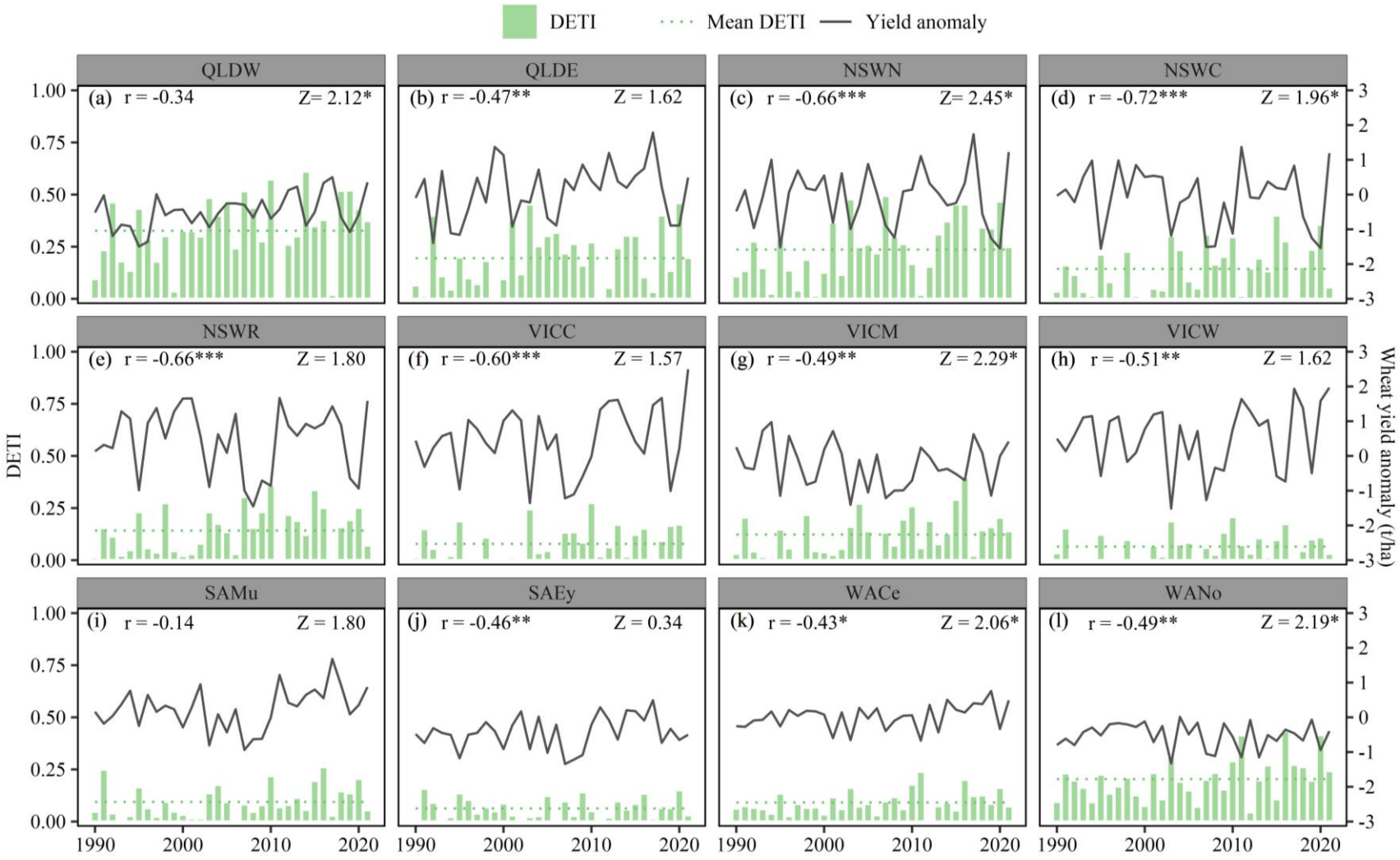

Figure 4-3. Wheat yield anomaly and intensity of compound drought and extreme temperature events (DETI) over the 12 regions in Australia from 1990 to 2021. *r* is the correlation coefficient between wheat yield anomaly and DETI. Z is the increasing (decreasing) rates of DETI from 1990 to 2021 (*** $p < 0.001$, ** $p < 0.01$, * $p < 0.05$).

The spatial distribution of mean DI, HI, FI, and DETI during 1990-2021in the Australian crop belt is presented in Figure 4-4. The values of DI ranged from 0-0.62, which were slightly higher in inland areas. The western part of NSW and Western Australia (WA) had the highest mean DI (Figure 4-4 a). The HI within WRP ranged widely from 0.0006 to 0.28, a few grid cells located east and south of the crop belt experienced high HI values, while most of the crop belt had relatively low HI values (Figure 4-4 b). There was also a wide range in FI, 0.0003 - 0.22, which gradually increased from west to east of the Australian crop belt (Figure 4-4 c). The DETI values ranged from 0 to 0.50 across Australia's crop belt, representing a north-south gradient that gradually decreased (Figure 4-4 d).

4.3.2 The impacts of extreme weather events on wheat yield variation during 1990-2021

The VIFs of the independent variables in MLR models were from 1.01 to 2.79 across 12 subregions (Table 4-S1), suggesting that there was no significant multicollinearity among the variables and the coefficient values estimated in our models remained stable and reliable. Figure 4-5 (a&b) shows the comparison between actual and estimated wheat yield anomaly. The individual drought, heat, and frost could explain 45% of wheat yield variation across Australia (Figure 4-5 a). After including the index of DET, the accuracy in reproducing the actual wheat yield anomaly of the MLR model was increased to 55% (Figure 4-5 b), which means that DET can account for 10% wheat yield variation across Australia.

The R^2 values for MLR models with and without DET as an independent variable are shown in Figure 4-5 ©. The impacts of individual and compound drought and extreme temperature events varied across different regions. Without DET, three single extreme indices could explain 12%-85% yield variation of 12 subregions with the highest R^2 in region NSWC and the smallest one in region QLDW. When including DET as an additional variable in the MLR model, the values of R^2 increased for all 12 regions, ranging from 0.17 to 0.86. This implies that the inclusion of DET improved the ability of the model to explain the anomaly in wheat yield caused by extreme weather events in each region. Notably, this improvement was the greatest in WANo region and the least in SAMu region.

To compare the contribution of different extreme indices to wheat yield variation, we obtained the relative importance of DI, HI, FI, and DETI in each region from the MLR model (Figure 4-5 d). The values of relative importance varied across different regions, with the range of 0.33-0.82 in DI, 0.01-0.15 in HI, 0.003-0.10 in FI, and 0.03-0.44 in DETI. Except for the regions of QLDW and SAMu, DI was consistently regarded as the most important index for all regions. The DETI was the second most important index. The relative importance of HI and FI were similar and demonstrated the lowest values in all regions, except for the SAMu region.

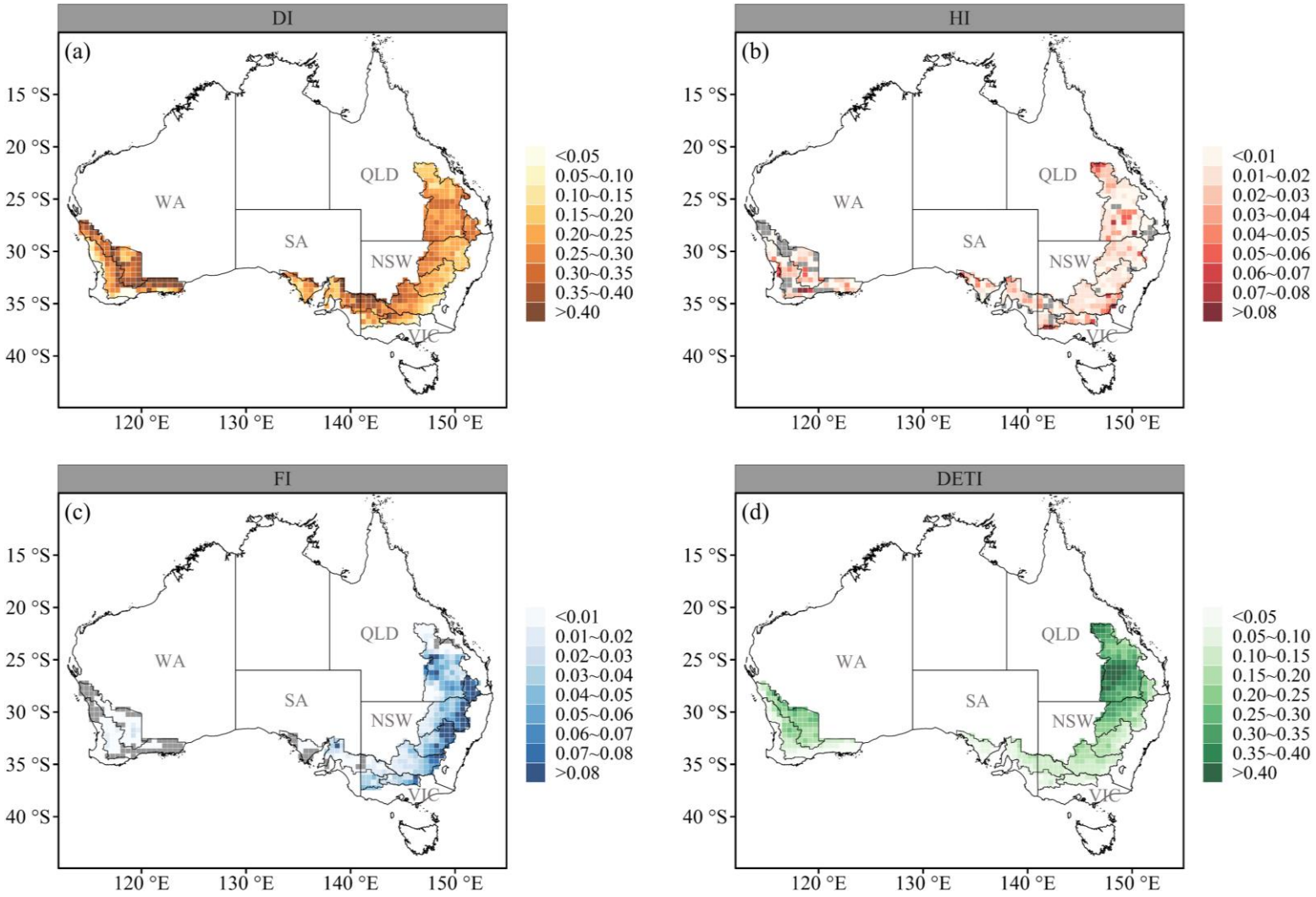

Figure 4-4. Spatial distributions of average intensity of DET (compound drought and extreme temperature events) (DETI), drought (DI), heat (HI), and frost (FI) during wheat reproductive growth period in 1990-2021 across Australia's crop belt. The grey grids indicate where there are no extreme weather events.

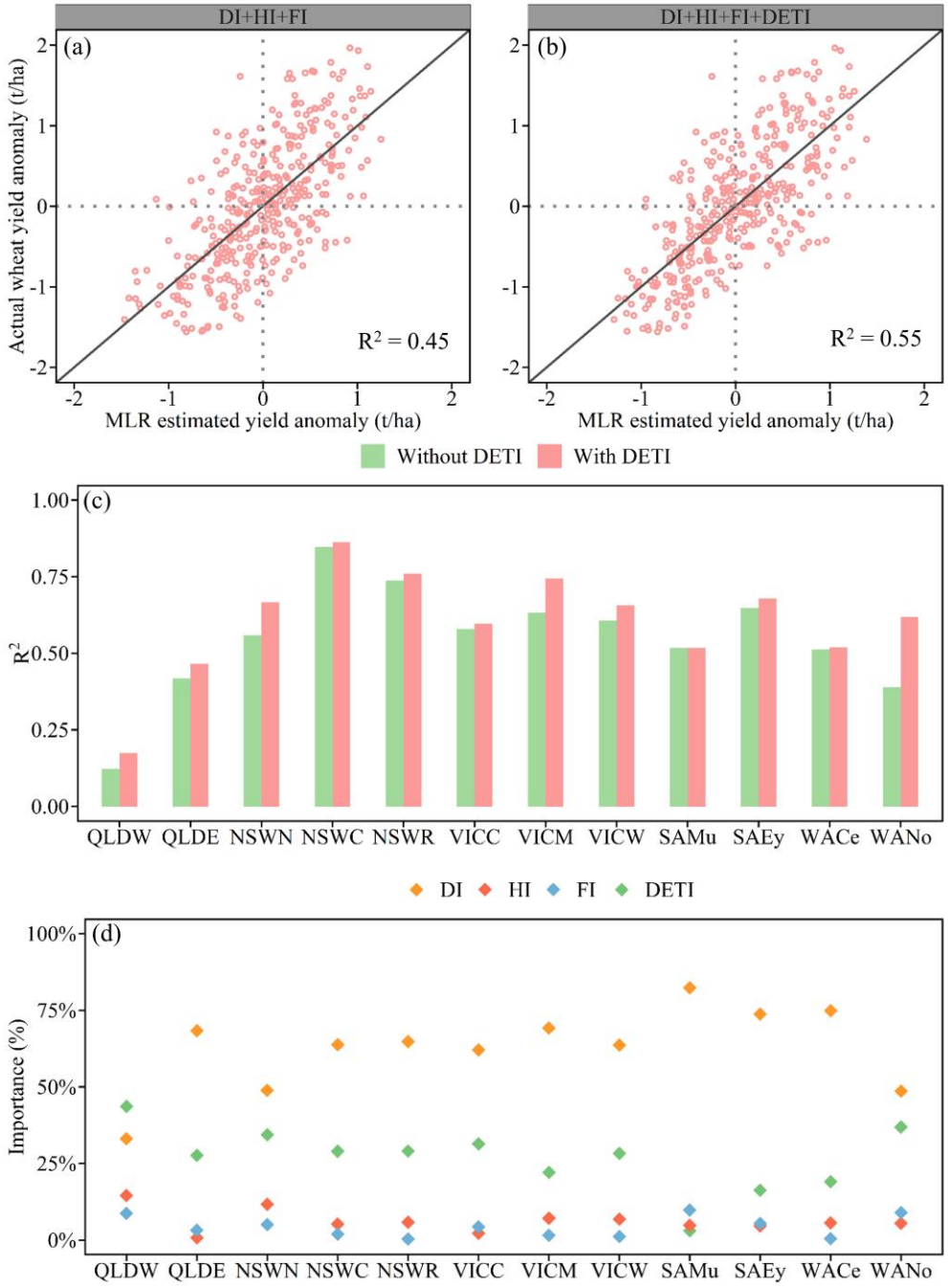

Figure 4-5. The comparison of observed and MLR estimated wheat yield anomaly using two sets of extreme weather events from 1990 to 2021 in Australia's crop belt: **(a)** observed vs. estimated yield variation based on the indices of drought intensity (DI) +heat intensity (HI) +frost intensity (FI), **(b)** observed vs. estimated yields based on the indices of DI+HI+FI+DET intensity (DETI). The determination coefficients (R^2) of multiple linear regression models in estimating wheat yield variation with and without the index of compound drought and extreme temperature events in 12 subregions **(c)**, and the relative importance of extreme climate indices to wheat yield variation in 12 subregions based on multiple linear regression models **(d)**.

4.3.3 The contribution of extreme weather events in low-yield years

The relative importance of DI, HI, FI, and DETI for each low-yield level is shown in Figure 4-6. We found that DETI dominated the wheat yield variation in extreme low-yield years (5th and 10th percentile), the relative importance exceeded 50%, surpassing the combined contribution of DI, HI, and FI. However, in the other levels of low-yield years, DI became the dominant factor influencing yield variation, with importance ranging from 54% to 74%, while DETI showed less importance than DI at 18%-29%. Additionally, the relative importance of HI and FI were 5%-14% and 1%-5%, respectively, which were much lower than that of DI or DETI in all levels of low-yield years. But both HI and FI exhibited their highest relative importance in extremely low-yield years (5th, 10th, and 15th percentile) compared to moderate low-yield years.

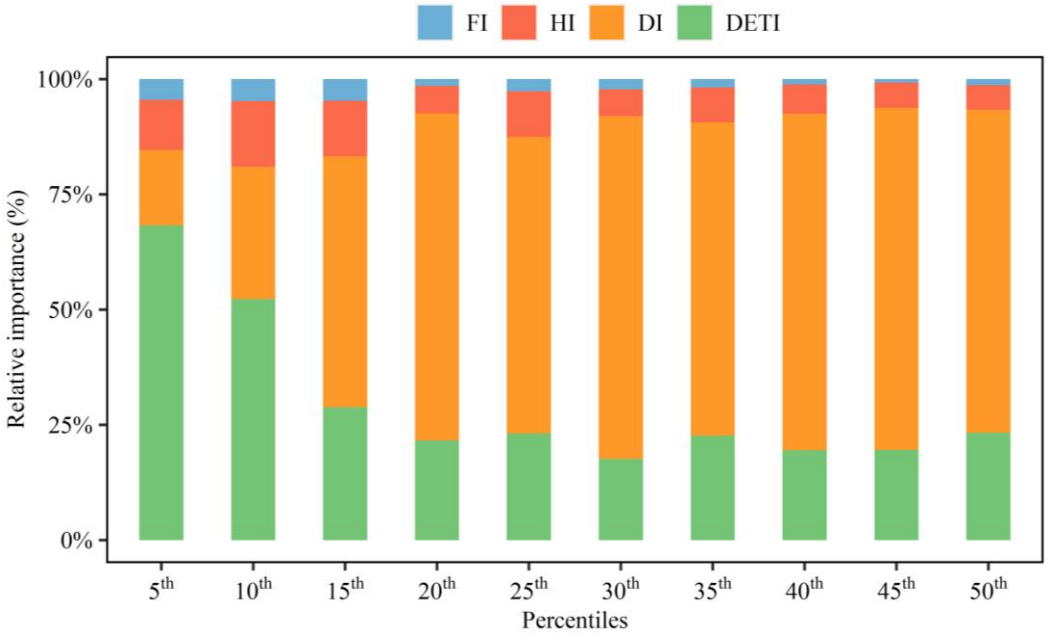

Figure 4-6. Relative importance of extreme weather events to wheat yield variation in low-yield years determined by different percentiles of wheat yields in Australia's crop belt. FI: frost intensity, HI: heat intensity, DI: drought intensity, DETI: intensity of compound drought and extreme temperature events.

4.4. Discussion

We quantified the intensity of individual drought, heat, and frost events as well as DET events to assess their impacts on wheat in Australia from 1990 to 2021. The DI had great inter-annual variations across entire Australia's crop belt in the past 30 years, and it exhibited higher values in subregions located near inland areas. The spatial-temporal distribution of DI aligned with findings from previous studies (Chenu et al., 2013; Feng et al., 2020; Hu et al., 2020). In terms of the HI and FI, as the season shifts from spring to summer during the stage of wheat floral initial to the end of grain-filling, frost events gradually decrease

while heat events increase (Zheng et al., 2012). In addition, in the mid-late period of the WRP (flowering and grain filling), drought events are more frequent. Therefore, there is a higher frequency of heat events coinciding with drought events compared to frost events (Figure 4-S2) (Chenu et al., 2013). This is the reason why, after removing the period of DET, the HI was low across the entire crop belt (Figure 4-4 b), while the FI was similar to the frost intensity containing the period of DET (Chenu et al., 2013; Zheng et al., 2012), which was higher in the eastern part and lower in the western rregions of the crop belt (Figure 4-4 c).

Between 1990 and 2021, there was an increased DETI in all 12 subregions (Figure 4-3). Notably, regions of QLDW, NSWN, NSWC, VICM, WACe, and WANo exhibited particularly pronounced increases during this period. This upward trend could be attributed to a combination of increasing drought and heat occurrences (Figure 4-S2). Spatially, the DETI exhibited a decreasing gradient from north to south of Australia's crop belt, aligning with the distribution of the maximum temperature during WRP (Figure 4-S1 a), which was consistent with the distribution of heat events in the previous study in the same study area (Collins & Chenu, 2021). Therefore, it is evident that the spatial distribution of DETI in Australia's crop belt was dominated by the extreme high temperature.

There were negative correlations between DETI and wheat yield anomaly, and the yield decreased obviously in the years when DETI increased, such as 1995, 2003, 2008, and 2020 (Figure 4-3). After including the DETI as an additional variable in the regression model, the estimated wheat yield anomaly in Australia's crop belt was closer to the actual yield anomaly during the years with a negative yield anomaly (Figure 4-5 a&b). In essence, the improvement of R^2 resulting from DETI mainly comes from low-yield years.

Regarding the 12 subregions, the explanations of individual and compound drought and extreme temperature events were region-specific (Figure 4-5 c). The R^2 was both low before and after including DET events in QLDE and QLDW, indicating that the impacts of extreme events on wheat yield variation in Queensland were not as great as in other states. This divergence could be attributed to the fact that, unlike the winter-dominant rainfall in other states, Queensland has a summer-dominant rainfall pattern (Backhouse & Burgess, 2002; Wang et al., 2020). Combined with the region's clay soils, which have a large water-holding capacity, this allows for sufficient rainfall storage before autumn, the typical sowing time for wheat in Australia, thus buffering the adverse impacts of climate (Nix & Fitzpatrick, 1969; Wang, Li Liu, et al., 2018). In the other 10 subregions, the most notable increments in R^2 were observed in NSWN, VICM, and WANo, with values of 0.11, 0.11, and 0.23 respectively. This phenomenon could be attributed to these regions having the highest DETI values within their respective states. Particularly noteworthy, WANo exhibited the most substantial increase in R^2 upon the inclusion of DET events. This is likely because

Western Australia is predominantly characterized by sandy soil, which is prone to structural degradation (Hamza & Anderson, 2002) and has a lower water capacity compared to other states in Australia (Padarian et al., 2014). Consequently, the soil buffer in Western Australia is limited, making it more susceptible to DET events compared to other regions.

The relative importance of drought, heat, frost, and DET to wheat yield variation during 1990-2021 was similar across the 12 subregions (Figure 4-5 d). Except for QLDE, drought contributed the most in the other 11 subregions, all exceeding 50%. It is not surprising that drought is the primary impact event for the long-term wheat yield variation in Australia, as Australia's crop belt is located in arid and semi-arid areas, and wheat mainly relies on seasonal rainfall (Wang et al., 2020). Lobell et al. (2015) predicted that the yield losses attributed to drought would consistently be higher than that of other extreme events in the coming half-century. Note that DET is the second most important event impacting the wheat yield variation in Australia. Generally, compound extreme events can have more severe impacts on crops than individual extreme events (Cohen et al., 2021; Ribeiro et al., 2020), while the relative importance of DET was lower than that of drought in our study. This difference might be attributed to the division of individual and compound extreme events. Compound extreme events have a higher level of extremity compared to individual extreme events, their duration and frequency could be lower than individual extreme events in the same growth period. Meanwhile, in a continuous long-time series, high-intensity compound events do not occur every year. As shown in Figure 4-3, there are more years with below-average DETI than years with above-average DETI.

Generally, years with high DETI values can cause sharp drops in wheat yields, as demonstrated by the years 1995, 2003, 2008, and 2020 in Figure 4-3. Therefore, we selected different levels of low-yield years based on the percentiles of the dataset encompassing all years across the 12 subregions to evaluate the corresponding relative importance of each extreme event to wheat yield anomaly. Notably, in the extreme low-yield years (years of wheat yield lower than 5^{th} and 10^{th}), the relative importance of DETI was the highest, which not only exceeded that of DI but even surpassed the sum of the importance of DI, HI, and FI (Figure 4-6). This agrees well with the previous studies that linked severe yield loss with compound temperature and moisture stress (Christian, Jordan I et al., 2020; García-Herrera et al., 2010; Glotter & Elliott, 2016; Wegren, 2011). In this study, we identified the average DETI value of extreme low-yield years as 0.23, which can be used as the threshold for assessing whether DET events are likely to result in severe yield loss. By integrating this threshold with robust forecasting methods for extreme weather events, the early warning of severe yield loss is expected to be realized. This will serve as a reminder to policymakers and farmers to prioritize adapting to DET events, with the aim of mitigating or preventing significant yield losses or crop failures in Australia.

We assessed the impacts of DET events from 1990 to 2021 and identified the contribution of DET events to wheat yield variation in long-term series and low-yield years in Australia's crop belt. Nonetheless, there are some limitations that need to be considered. The analysis employed regional average wheat yield data, lacking information specific to local or individual farm levels. Additionally, due to the broad scope of wheat yield data, the wheat varieties and agricultural practices integrated into the APSIM model were also at a regional level. This approach might disregard variations in local cultivars and management techniques. However, this constraint underscores the significance of gathering and integrating more location-specific data to enhance the precision and applicability of future investigations. Furthermore, this study is limited by its reliance on a single crop simulation model. Different crop models diverge in their foundational assumptions, algorithms, and parameter configurations. As a result, even when given identical inputs, they can produce disparate results (Asseng et al., 2013). It might be more robust to employ ensembles of multiple crop models to simulate crop growth and soil water dynamics, as this can yield more reliable outcomes (Rötter et al., 2015). This also emphasizes the need for localized data to facilitate the development of multiple models.

4.5. Conclusion

Our study assessed the impacts of drought, heat, frost, and DET events on wheat yield variation in Australia's crop belt from 1990 to 2021, using the 12-subregion wheat yield data obtained from ABARES. We found that DET intensity had a large inter-annual variation with a small increasing trend and showed a north-south decreasing gradient across Australia's crop belt. This spatial distribution was mainly dominated by high temperatures. Additionally, extreme weather events contributed 55% of wheat yield change in the entire crop belt. Regarding the relative importance of four types of extreme events to wheat yield variation in the long-term series, drought had the greatest impact, followed by DET, then heat, and finally frost. However, in extreme low-yield years, DET ranked the highest, followed by drought, then heat, and finally frost. Specifically, the relative importance of DET events surpassed the sum importance of individual drought, heat, and frost events, reaching 68% and 52% in years with yields below the 5^{th} and 10^{th} percentiles, respectively. Our findings highlight the significant impact of DET on the long-term fluctuations in wheat yield, indicating its potential to cause significant yield losses in Australia. We expect these results will raise awareness about the significance of DET events for both farmers and policymakers. Consequently, efforts should be directed toward driving specific adaptive strategies, refining policy frameworks, and fostering technological innovations to strengthen agricultural resilience in the face of climate extremes.

4.6 Supporting information

Table 4-S1. The variance inflation factor (VIF) for independent variables in multiple linear regression models in 12 subregions.

	DET	Drought	Heat	Frost
QLD Western Downs and Central Highlands (QLDW)	1.68	2.03	2.79	1.44
QLD Eastern Darling Downs (QLDE)	1.24	1.22	1.05	1.08
NSW North West Slopes and Plains (NSWN)	1.65	1.98	2.09	1.16
NSW Central West (NSWC)	1.91	2.21	1.31	1.10
NSW Riverina (NSWR)	1.70	2.19	1.39	1.07
VIC Central North (VICC)	1.95	2.18	1.24	1.02
VIC Mallee (VICM)	1.07	1.38	1.38	1.01
VIC Wimmera (VICW)	2.12	1.87	2.07	1.09
SA Murray Lands and Yorke Peninsula (SAMu)	1.24	1.39	1.32	1.12
SA Eyre Peninsula (SAEy)	1.23	1.37	1.29	1.02
WA Central and Southern Wheat Belt (WACe)	1.33	1.67	1.34	1.04
WA Northern and Eastern Wheat Belt (WANo)	1.53	1.26	1.66	1.27

Table 4-S2 Results of the Mann-Kendall test for wheat yields in 12 subregions. Z is the increasing (decreasing) rates of wheat yield from 1990 to 2021 (* $p < 0.05$).

Subregions	Z
QLD Western Downs and Central Highlands (QLDW)	2.12*
QLD Eastern Darling Downs (QLDE)	1.48
NSW North West Slopes and Plains (NSWN)	0.05
NSW Central West (NSWC)	-0.73
NSW Riverina (NSWR)	0.18
VIC Central North (VICC)	1.41
VIC Mallee (VICM)	-0.50
VIC Wimmera (VICW)	1.12
SA Murray Lands and Yorke Peninsula (SAMu)	1.70
SA Eyre Peninsula (SAEy)	1.22
WA Central and Southern Wheat Belt (WACe)	2.22*
WA Northern and Eastern Wheat Belt (WANo)	-0.08

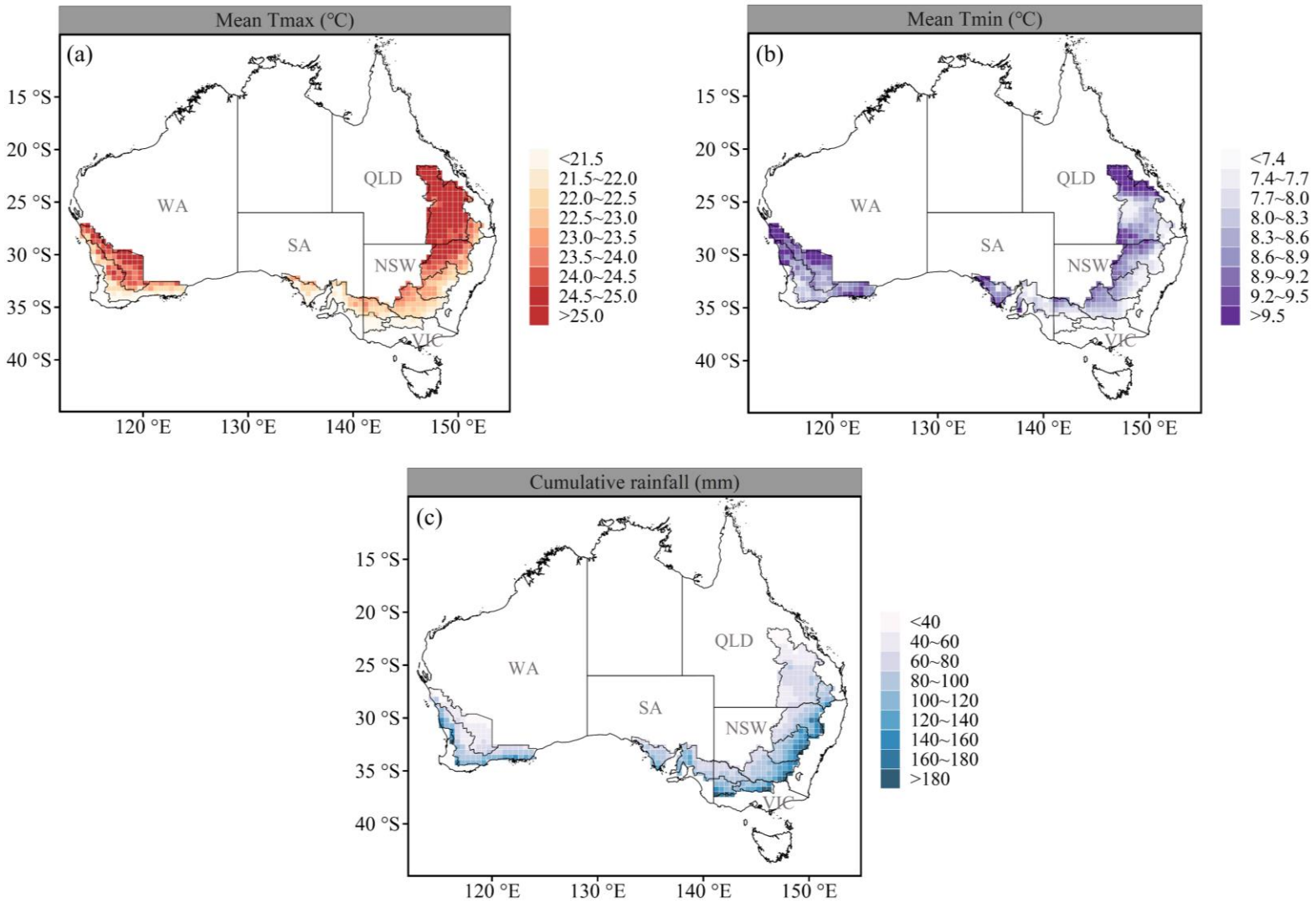

Figure 4-S1 Spatial distribution of mean Tmax, Tmin, and cumulative rainfall during wheat reproductive growth period from 1990 to 2021 across Australia's wheat belt.

Figure 4-S2 Temporal variations of the individual drought intensity (DI), heat intensity (HI), and frost intensity (FI) during the periods of compound drought and extreme temperature events in 12 subregions from 1990 to 2021.

4.7 Reference

Ababaei, B., & Chenu, K., 2020. Heat shocks increasingly impede grain filling but have little effect on grain setting across the Australian wheatbelt. Agricultural and Forest Meteorology, 284, 107889.

ABARES, 2023. Farm Data Portal - Beta - DAFF (agriculture.gov.au). The last accessed date: 05 Jan 2023.

Aghakouchak, A., Chiang, F., Huning, L. S., Love, C. A., Mallakpour, I., Mazdiyasni, O., Moftakhari, H., Papalexiou, S. M., Ragno, E., & Sadegh, M., 2020. Climate Extremes and Compound Hazards in a Warming World. Annual Review of Earth and Planetary Sciences, 48(1), 519-548.

Apsoil, 2022. https://www.longpaddock.qld.gov.au/silo/gridded-data/. The last accessed date: 20 May 2022.

Asseng, S., Foster, I., & Turner, N. C. J. G. C. B., 2011. The impact of temperature variability on wheat yields. Global Change Biology, 17(2), 997-1012.

Asseng, S., Turner, N., & Keating, B. a. J. P., 2001. Analysis of water-and nitrogen-use efficiency of wheat in a Mediterranean climate. Plant and Soil, 233(1), 127-143.

Backhouse, D., & Burgess, L. W., 2002. Climatic analysis of the distribution of Fusarium graminearum, F. pseudograminearum and F. culmorum on cereals in Australia. Australasian Plant Pathology, 31, 321-32.

Bastos, A., Ciais, P., Friedlingstein, P., Sitch, S., Pongratz, J., Fan, L., Wigneron, J. P., Weber, U., Reichstein, M., Fu, Z., Anthoni, P., Arneth, A., Haverd, V., Jain, A. K., Joetzjer, E., Knauer, J., Lienert, S., Loughran, T., Mcguire, P. C., Tian, H., Viovy, N., & Zaehle, S., 2020. Direct and seasonal legacy effects of the 2018 heat wave and drought on European ecosystem productivity. SCIENCE ADVANCES, 6(24), eaba2724.

Beillouin, D., Schauberger, B., Bastos, A., Ciais, P., & Makowski, D. J. P. T. O. T. R. S. B., 2020. Impact of extreme weather conditions on European crop production in 2018. Philosophical Transactions of the Royal Society B, 375(1810), 20190510.

Ben-Ari, T., Boé, J., Ciais, P., Lecerf, R., Van Der Velde, M., & Makowski, D., 2018. Causes and implications of the unforeseen 2016 extreme yield loss in the breadbasket of France. Nature communications, 9(1), 1627.

Chenu, K., Deihimfard, R., & Chapman, S. C., 2013. Large-scale characterization of drought pattern: a continent-wide modelling approach applied to the Australian wheatbelt – spatial and temporal trends. New Phytologist, 198(3), 801-820.

Christian, J. I., Basara, J. B., Hunt, E. D., Otkin, J. A., & Xiao, X., 2020. Flash drought development and cascading impacts associated with the 2010 Russian heatwave. Environmental Research Letters, 15(9), 094078.

Ciais, P., Reichstein, M., Viovy, N., Granier, A., Ogée, J., Allard, V., Aubinet, M., Buchmann, N., Bernhofer, C., Carrara, A., Chevallier, F., De Noblet, N., Friend, A. D., Friedlingstein, P., Grünwald, T., Heinesch, B., Keronen, P., Knohl, A., Krinner, G., Loustau, D., Manca, G., Matteucci, G., Miglietta, F., Ourcival, J. M., Papale, D., Pilegaard, K., Rambal, S., Seufert, G., Soussana, J. F., Sanz, M. J., Schulze, E. D., Vesala, T., & Valentini, R., 2005. Europe-wide reduction in primary productivity caused by the heat and drought in 2003. Nature, 437(7058), 529-533.

Cohen, I., Zandalinas, S. I., Huck, C., Fritschi, F. B., & Mittler, R., 2021a. Meta-analysis of drought and heat stress combination impact on crop yield and yield components. Physiologia Plantarum, 171(1), 66-76.

Collins, B., & Chenu, K., 2021. Improving productivity of Australian wheat by adapting sowing date and genotype phenology to future climate. Climate Risk Management, 32, 100300.

Dalgliesh, N., Cocks, B., & Horan, H., 2012. APSoil-providing soils information to consultants, farmers and researchers. Paper presented at the 16th Australian Agronomy Conference, Armidale, NSW.

FAO, 2020. The Food and Agriculture Organization of the United Nations. Statistic data base. https://www.fao.org/faostat/en/#data/QCL. The last accessed date: 25 May 2021.

Farre, I., Foster, I., Biddulph, B., & Asseng, S., 2010. Is there a value in having a frost forecast for wheat in the South-West of Western Australia. Paper presented at the Food Security from Sustainable Agriculture: 15th Australian Agronomy Conference. Lincoln, New Zealand.

Feng, P., Wang, B., Liu, D. L., Xing, H., Ji, F., Macadam, I., Ruan, H., & Yu, Q., 2018. Impacts of rainfall extremes on wheat yield in semi-arid cropping systems in eastern Australia. Climatic Change, 147(3), 555-569.

Feng, P., Wang, B., Luo, J.-J., Liu, D. L., Waters, C., Ji, F., Ruan, H., Xiao, D., Shi, L., & Yu, Q., 2020. Using large-scale climate drivers to forecast meteorological drought condition in growing season across the Australian wheatbelt. Science of the Total Environment, 724, 138162.

Feng, P., Wang, B., Macadam, I., Taschetto, A. S., Abram, N. J., Luo, J.-J., King, A. D., Chen, Y., Li, Y., Liu, D. L., Yu, Q., & Hu, K., 2022. Increasing dominance of Indian Ocean variability impacts Australian wheat yields. Nature Food, 3(10), 862-870.

Feng, S., & Hao, Z., 2020. Quantifying likelihoods of extreme occurrences causing maize yield reduction at the global scale. Science of the Total Environment, 704, 135250.

Feng, S., Hao, Z., Zhang, X., & Hao, F., 2019. Probabilistic evaluation of the impact of compound dry-hot events on global maize yields. Science of the Total Environment, 689, 1228-1234.

García-Herrera, R., Díaz, J., Trigo, R. M., Luterbacher, J., & Fischer, E. M., 2010. A Review of the European Summer Heat Wave of 2003. Critical Reviews in Environmental Science and Technology, 40(4), 267-306.

Glotter, M., & Elliott, J., 2016. Simulating US agriculture in a modern Dust Bowl drought. Nature plants, 3(1), 16193.

Granier, A., Bréda, N., Biron, P., & Villette, S., 1999. A lumped water balance model to evaluate duration and intensity of drought constraints in forest stands. Ecological Modelling, 116(2), 269-283.

Groemping, U., 2006. Relative Importance for Linear Regression in R: The Package relaimpo. Journal of Statistical Software, 17(1), 1 - 27.

Hamed, R., Van Loon, A. F., Aerts, J., & Coumou, D., 2021. Impacts of compound hot–dry extremes on US soybean yields. Earth Syst. Dynam., 12(4), 1371-1391.

Hamza, M., & Anderson, W., 2002. Improving soil physical fertility and crop yield on a clay soil in Western Australia. Australian Journal of Agricultural Research, 53(5), 615-620.

Han, J., Wang, J., Zhao, Y., Wang, Q., Zhang, B., Li, H., & Zhai, J., 2018. Spatio-temporal variation of potential evapotranspiration and climatic drivers in the Jing-Jin-Ji region, North China. Agricultural and Forest Meteorology, 256-257, 75-83.

Hao, Z., Hao, F., Xia, Y., Feng, S., Sun, C., Zhang, X., Fu, Y., Hao, Y., Zhang, Y., & Meng, Y., 2022. Compound droughts and hot extremes: Characteristics, drivers, changes, and impacts. Earth-Science Reviews, 104241.

Haqiqi, I., Grogan, D. S., Hertel, T. W., & Schlenker, W., 2021. Quantifying the impacts of compound extremes on agriculture. Hydrol. Earth Syst. Sci., 25(2), 551-564.

Hu, T., Van Dijk, A. I. J. M., Renzullo, L. J., Xu, Z., He, J., Tian, S., Zhou, J., & Li, H., 2020. On agricultural drought monitoring in Australia using Himawari-8 geostationary thermal infrared observations. International Journal of Applied Earth Observation and Geoinformation, 91, 102153.

Iizumi, T., & Ramankutty, N. J. E. R. L., 2016. Changes in yield variability of major crops for 1981–2010 explained by climate change. 11(3), 034003.

Júnior, R. D. S. N., Martre, P., Finger, R., Van Der Velde, M., Ben-Ari, T., Ewert, F., Webber, H., Ruane, A. C., & Asseng, S., 2021. Extreme lows of wheat production in Brazil. Environmental Research Letters, 16(10), 104025.

Keating, B. A., Carberry, P. S., Hammer, G. L., Probert, M. E., Robertson, M. J., Holzworth, D., Huth, N. I., Hargreaves, J. N. G., Meinke, H., Hochman, Z., Mclean, G., Verburg, K., Snow, V., Dimes, J. P., Silburn, M., Wang, E., Brown, S., Bristow, K. L., Asseng, S., Chapman, S., Mccown, R. L., Freebairn, D. M., & Smith, C. J., 2003. An overview of APSIM, a model designed for farming systems simulation. European Journal of Agronomy, 18(3), 267-288.

Kirkegaard, J. A., & Lilley, J. M., 2007. Root penetration rate a benchmark to identify soil and plant limitations to rooting depth in wheat %J Australian Journal of Experimental Agriculture. Australian Journal of Experimental Agriculture, 47(5), 590-602.

Kumar Tewari, A., & Charan Tripathy, B., 1998. Temperature-Stress-Induced Impairment of Chlorophyll Biosynthetic Reactions in Cucumber and Wheat. Plant Physiology, 117(3), 851-858.

Lalic, B., Eitzinger, J., Mihailovic, D., Thaler, S., & Jancic, M. J. T. J. O. a. S., 2013. Climate change impacts on winter wheat yield change–which climatic parameters are crucial in Pannonian lowland? Journal of Agricultural Science, 151(6), 757-774.

Lesk, C., & Anderson, W., 2021. Decadal variability modulates trends in concurrent heat and drought over global croplands. Environmental Research Letters, 16(5), 055024.

Lesk, C., Anderson, W., Rigden, A., Coast, O., Jägermeyr, J., Mcdermid, S., Davis, K., & Konar, M., 2022. Compound heat and moisture extreme impacts on global crop yields under climate change. Nature Reviews Earth & Environment, 3, 872–889.

Lesk, C., Coffel, E., Winter, J., Ray, D., Zscheischler, J., Seneviratne, S. I., & Horton, R., 2021. Stronger temperature–moisture couplings exacerbate the impact of climate warming on global crop yields. Nature Food, 2(9), 683-691.

Li, E., Zhao, J., Pullens, J. W. M., & Yang, X., 2022. The compound effects of drought and high temperature stresses will be the main constraints on maize yield in Northeast China. Science of the Total Environment, 812, 152461.

Li, S., Wang, B., Feng, P., Liu, D. L., Li, L., Shi, L., & Yu, Q., 2022. Assessing climate vulnerability of historical wheat yield in south-eastern Australia's wheat belt. Agricultural Systems, 196, 103340.

Liu, D. L., Timbal, B., Mo, J., Fairweather, H. J. I. J. O. C. C. S., & Management., 2011. A GIS-based climate change adaptation strategy tool. International Journal of Climate Change Strategies and Management.

Lobell, D. B., Hammer, G. L., Chenu, K., Zheng, B., Mclean, G., & Chapman, S. C., 2015. The shifting influence of drought and heat stress for crops in northeast Australia. Global Change Biology, 21(11), 4115-4127.

Luan, X., Bommarco, R., Scaini, A., & Vico, G., 2021. Combined heat and drought suppress rainfed maize and soybean yields and modify irrigation benefits in the USA. Environmental Research Letters, 16(6), 064023.

Madadgar, S., Aghakouchak, A., Farahmand, A., & Davis, S. J., 2017. Probabilistic estimates of drought impacts on agricultural production. Geophysical Research Letters, 44(15), 7799-7807.

Manning, C., Widmann, M., Bevacqua, E., Van Loon, A. F., Maraun, D., & Vrac, M. J. E. R. L., 2019. Increased probability of compound long-duration dry and hot events in Europe during summer (1950–2013). Environmental Research Letters, 14(9), 094006.

Marcellos, H., & Single, W., 1975. Temperatures in wheat during radiation frost. Australian Journal of Experimental Agriculture, 15(77), 818-822.

Myhre, G., Alterskjær, K., Stjern, C. W., Hodnebrog, Ø., Marelle, L., Samset, B. H., Sillmann, J., Schaller, N., Fischer, E., Schulz, M., & Stohl, A., 2019. Frequency of extreme precipitation increases extensively with event rareness under global warming. Scientific Reports, 9(1), 16063.

Nix, H. A., & Fitzpatrick, E. A., 1969. An index of crop water stress related to wheat and grain sorghum yields. Agricultural Meteorology, 6(5), 321-337.

Padarian, J., Minasny, B., Mcbratney, A. B., & Dalgliesh, N., 2014. Predicting and mapping the soil available water capacity of Australian wheatbelt. Geoderma Regional, 2-3, 110-118.

Potopová, V., Lhotka, O., Možný, M., & Musiolková, M., 2021. Vulnerability of hop-yields due to compound drought and heat events over European key-hop regions. International Journal of Climatology, 41(S1), E2136-E2158.

Qaseem, M. F., Qureshi, R., & Shaheen, H., 2019. Effects of Pre-Anthesis Drought, Heat and Their Combination on the Growth, Yield and Physiology of diverse Wheat (Triticum aestivum L.) Genotypes Varying in Sensitivity to Heat and drought stress. Scientific Reports, 9(1), 6955.

Ribeiro, A. F. S., Russo, A., Gouveia, C. M., Páscoa, P., & Zscheischler, J. J. B., 2020. Risk of crop failure due to compound dry and hot extremes estimated with nested copulas. Biogeosciences, 17(19), 4815-4830.

Sarhadi, A., Ausín, M. C., Wiper, M. P., Touma, D., & Diffenbaugh, N. S., 2018. Multidimensional risk in a nonstationary climate: Joint probability of increasingly severe warm and dry conditions. SCIENCE ADVANCES, 4(11), eaau3487.

Schauberger, B., Gornott, C., & Wechsung, F., 2017. Global evaluation of a semiempirical model for yield anomalies and application to within-season yield forecasting. Global Change Biology, 23(11), 4750-4764.

SILO, 2023. Long Paddock, 2023, Home LongPaddock | Queensland Government. The last accessed date: 24 Jan 2023.

Simanjuntak, C., Gaiser, T., Ahrends, H. E., Ceglar, A., Singh, M., Ewert, F., & Srivastava, A. K., 2023. Impact of climate extreme events and their causality on maize yield in South Africa. Scientific Reports, 13(1), 12462.

Single, W., 1985. Frost injury and the physiology of the wheat plant. Journal of the Australian Institute of Agricultural Science.

Telfer, P., Edwards, J., Bennett, D., Ganesalingam, D., Able, J., & Kuchel, H., 2018. A field and controlled environment evaluation of wheat (Triticum aestivum) adaptation to heat stress. Field Crops Research, 229, 55-65.

Vogel, E., Donat, M. G., Alexander, L. V., Meinshausen, M., Ray, D. K., Karoly, D., Meinshausen, N., & Frieler, K. J. E. R. L., 2019. The effects of climate extremes on global agricultural yields. Environmental Research Letters, 14(5), 054010.

Wang, A., Tao, H., Ding, G., Zhang, B., Huang, J., & Wu, Q., 2023. Global cropland exposure to extreme compound drought heatwave events under future climate change. Weather and Climate Extremes, 40, 100559.

Wang, B., Feng, P., Waters, C., Cleverly, J., Liu, D. L., & Yu, Q., 2020. Quantifying the impacts of pre-occurred ENSO signals on wheat yield variation using machine learning in Australia. Agricultural and Forest Meteorology, 291, 108043.

Wang, B., Li Liu, D., Waters, C., & Yu, Q., 2018. Quantifying sources of uncertainty in projected wheat yield changes under climate change in eastern Australia. Climatic Change, 151(2), 259-273.

Wang, B., Liu, D. L., Asseng, S., Macadam, I., & Yu, Q., 2017. Modelling wheat yield change under CO2 increase, heat and water stress in relation to plant available water capacity in eastern Australia. European Journal of Agronomy, 90, 152-161.

Wang, B., Liu, D. L., O'leary, G. J., Asseng, S., Macadam, I., Lines-Kelly, R., Yang, X., Clark, A., Crean, J., & Sides, T., 2018. Australian wheat production expected to decrease by the late 21st century. Global Change Biology, 24(6), 2403-2415.

Wegren, S. K., 2011. Food Security and Russia's 2010 Drought. Eurasian Geography and Economics, 52(1), 140-156.

Wheeler, T. R., Batts, G. R., Ellis, R. H., Hadley, P., & Morison, J. I. L., 1996. Growth and yield of winter wheat (Triticum aestivum) crops in response to CO2 and temperature. The Journal of Agricultural Science, 127(1), 37-48.

Yuan, X., Wang, L., & Wood, E. F., 2018. Anthropogenic intensification of southern African flash droughts as exemplified by the 2015/16 season. Bulletin of the American Meteorological Society, 99(1), S86-S90.

Zampieri, M., Ceglar, A., Dentener, F., & Toreti, A. J. E. R. L., 2017. Wheat yield loss attributable to heat waves, drought and water excess at the global, national and subnational scales. Environmental Research Letters, 12(6), 064008.

Zheng, B., Chenu, K., Fernanda Dreccer, M., & Chapman, S. C., 2012. Breeding for the future: what are the potential impacts of future frost and heat events on sowing and flowering time requirements for Australian bread wheat (Triticum aestivium) varieties? Global Change Biology, 18(9), 2899-2914.

Zwiers, F. W., Alexander, L. V., Hegerl, G. C., Knutson, T. R., Kossin, J. P., Naveau, P., Nicholls, N., Schär, C., Seneviratne, S. I., & Zhang, X., 2013. Climate Extremes: Challenges in Estimating and Understanding Recent Changes in the Frequency and Intensity of Extreme Climate and Weather Events. In Climate Science for Serving Society: Research, Modeling and Prediction Priorities (pp. 339-389). Dordrecht: Springer Netherlands.

Chapter 5. The contribution of climate drivers to compound drought and temperature events increased in recent decades in Australia's wheat belt

This manuscript is under internal review before submitting to Journal for publication.

Abstract

The destructive impacts of compound climate extreme events on crops exceed those of any individual events. Improving the understanding of the historical changes in compound extreme events and their drivers can help enhance our capability to identify and manage the risks of compound events, which is crucial for protecting crop survival and maintaining production. Here, we used a hybrid biophysical-statistical modeling approach to assess the connections between large-scale climate drivers of ENSO/IOD and compound drought and extreme temperature (DET) events across Australia's wheat belt from 1900 to 2020. We also investigated the probability of extreme high-intensity DET events during various ENSO or IOD phases. We found that the impacts of ENSO and IOD on DET events varied across different phases and distinct temporal periods. The eastern part of Australia's wheat belt was more responsive to ENSO and IOD than the western parts. Specifically, El Niño and positive IOD phases were associated with greater DET intensity and greater probability of occurring high-intensity DET events, whereas La Niña and negative IOD phases tend to result in lower DET intensity and lower probability of occurring high-intensity DET events, compared to the neutral conditions. The mean probability of experiencing high-intensity DET events ranges from 10% to 26% during La Niña and IOD negative phases, but from 34% to 54% during El Niño and IOD positive phases. The area with a greater than 50% probability of experiencing high-intensity DET events was expanded across Australia's wheat belt, with grid cells increased by 38 from the 1920s to 1960s and 56 from the 1960s to 2000s during strong El Niño, and 30 and 32 during strong IOD positive phases. In general, the role of ENSO in triggering severe DET events during wheat reproductive period surpassed that of the IOD during the three historical periods. Our findings highlight the need to assess the spatial-temporal response of compound events to climate drivers to inform the early warning and management of compound weather and climate extremes.

Keywords: climate drivers; compound drought and extreme temperature events; ENSO; IOD; probability

5.1. Introduction

Compound events, characterized by the spatiotemporal coexistence of multiple independent weather and climate extremes (Leonard et al., 2014; Seneviratne et al., 2012; Zscheischler et al., 2018), pose significant challenges to agricultural cropping systems. For example, following the 2006 dry-cold coupling, 12% of the wheat cropping area in Brazil failed to harvest (Júnior et al., 2021). In 2016, the co-occurrence of heavy rain and heatwave led to the most severe wheat yield reduction over the past half-century in France (Ben-Ari et al., 2018). Additionally, many European countries experienced widespread crop failure after the 2018 compound drought and heat events (Bastos et al., 2020). Unfortunately, the occurrence of compound events has notably increased in recent decades (Hao et al., 2022; Sarhadi et al., 2018), and projections indicate that this pattern is likely to continue and potentially intensify under future climate change (Wang, A. et al., 2023). Considering the devastating impacts and growing risks, it is vital to improve understanding of compound events to effectively safeguard crop survival and sustain production.

Among various types of compound events, compound drought and extreme temperature events have been observed to have the most frequent associations with severe yield loss cases since 2000 (García-Herrera et al., 2010; Glotter & Elliott, 2016; Herring et al., 2018; Júnior et al., 2021; Li et al., 2022; Wegren, 2011). Such compound drought and extreme temperature events are triggered by the interaction of various processes across the atmosphere, land, and ocean, mainly dividing into land-atmospheric interactions and sustained anomalies in large-scale circulation (Hao et al., 2022; Seneviratne et al., 2012). Notably, large-scale circulation patterns have been witnessed favoring the development and amplification of compound drought and extreme temperature events across many global regions (Mishra et al., 2020; Mukherjee et al., 2020). In 1983 summer, a strong El Niño Southern Oscillation (ENSO) intensified the compound drought-heat events in the cropping area of southeast South Africa and North America (Anderson et al., 2019). The strong ENSO and positive Indian Ocean Dipole (IOD) phase brought the high risk of compound dry and hot events in Australia during 1958-2020 (Reddy et al., 2022). It is not surprising to link the compound drought and extreme temperature events with large-scale circulation patterns, considering the commonly proven influence of oceanic circulations on weather conditions in many regions (Cai et al., 2011; Dittus et al., 2018; Mason & Goddard, 2001; Sun et al., 2017). However, previous studies identified the responses of compound drought and extreme temperature events to large-scale climate drivers in a long time series period, ignoring the evolving nature of these responses over time (Hao, Y. et al., 2020; Ionita et al., 2021; Mukherjee et al., 2020; Reddy et al., 2022). Recent studies proved climate drivers are non-stationary phenomena, with observed changes over time in the characteristics of ENSO and IOD (Abram et al., 2020; Freund et al., 2019). Therefore, their influence on DET events is likely to be dynamic rather than static. The definition of DET events also varied in different studies. According to Hao et al. (2018), the definition

utilized a binary response variable, which ignored DET intensity information. This information is vital for understanding the responses to climate drivers. For definitions of DET events on a monthly or seasonal scale, without considering the asymmetry in the duration of drought (several months) and heat events (several days), which reduced the accuracy of quantifying DET events.

Probabilistic assessment is an effective tool for risk evaluation and management (Ganguli & Reddy, 2013), allowing the quantification of the interdependence between multivariate random variables (e.g. DET events and climate drivers) (Kwon et al., 2019; Ribeiro et al., 2019). Coupla, as a widely adopted method in probabilistic assessment, has been used for analyzing the joint and conditional probabilities of multivariate variables across diverse fields, including agriculture and environmental studies (Hu, 2006; Schölzel & Friederichs, 2008). For instance, Vikas Poonia (Poonia et al., 2021) used the copula to construct joint dependence structures between drought duration and severity during the period 1982-2013 in India. The output conditional probability and return periods highlighted the hotspot regions that were prone to prolonged and intense droughts. Xiang et al. (2023) utilized a copula-based probabilistic approach to examine the dependence between wheat yield loss and different drought conditions in New South Wales, Australia. They identified the region-specific drought thresholds corresponding to a given yield loss probability. Hao, Z. et al. (2020) employed a copula approach to establish the conditional distribution of heat events under drought conditions across the United States. They found an increase in the probability of heat events coinciding with droughts in the western, southern, and northeastern U.S., while this probability decreased in the Midwest and southeastern U.S.

Australia is a significant contributor to the global food supply, accounting for 11% of the global wheat exports annually since 1961 (FAO, 2021). However, the rain-fed planting pattern determines that Australia's wheat production is highly dependent on climate conditions (Feng et al., 2022). Given that Australia is prone to DET events and the expected increase in their frequency due to future climate change (Li et al., 2024; Ridder et al., 2020; Wang, C. et al., 2023), the wheat industry in Australia undoubtedly faces significant challenges. Additionally, it is widely recognized that climate variability in Australia is significantly impacted by climate drivers originating from the surrounding oceans (Ashok et al., 2003; King et al., 2014; Risbey et al., 2009), and the DET event has also been proven to be affected (Feng & Hao, 2021; Mukherjee et al., 2020; Zhang et al., 2023). For, example, Papari (2022) indicated that in Australia's east, a high frequency and severity DET season occurred once in every two seasons of strong El Niño events or strong El Niño with strong IOD positive. Nevertheless, previous studies primarily focused on the impact of large-scale climate drivers on DET events that appeared in summer (Feng & Hao, 2021; Reddy et al., 2022), without considering winter crops like wheat (which typically grows in April to November, from austral

Autumn to Spring) (Wang, Liu, et al., 2018). In addition, there is no study assessing the impacts of ENSO and IOD on the probability of DET events in Australia's wheat belt in the past ten decades.

In this study, we employed a hybrid biophysical-statistical modeling approach to evaluate the evolving influences of large-scale climate drivers on DET events during three historical periods: 1900-1940, 1941-1980, and 1981-2020, across Australia's wheat belt. This approach enables the specific quantification of DET events appearing in the wheat reproductive period (WRP), providing a basis for precise analysis of the conditional probability associated with DET risks for wheat to climate drivers. Our main objectives are to: (1) quantify the changes in DET events and climate drivers over the three historical periods; (2) assess the influence of large-scale climate drivers on DET events in Australia's wheat belt; (3) identify the conditional probability of high-intensity DET events under different phases of climate drivers. We expect this study can improve the understanding of the patterns and drivers of DET events in Australia, thereby providing a foundation for developing early warnings for DET risks. This will, in turn, assist stakeholders in optimizing resource allocation and planning response adaptations in the agriculture sector.

5.2. Methods and materials

5.2.1 Study area

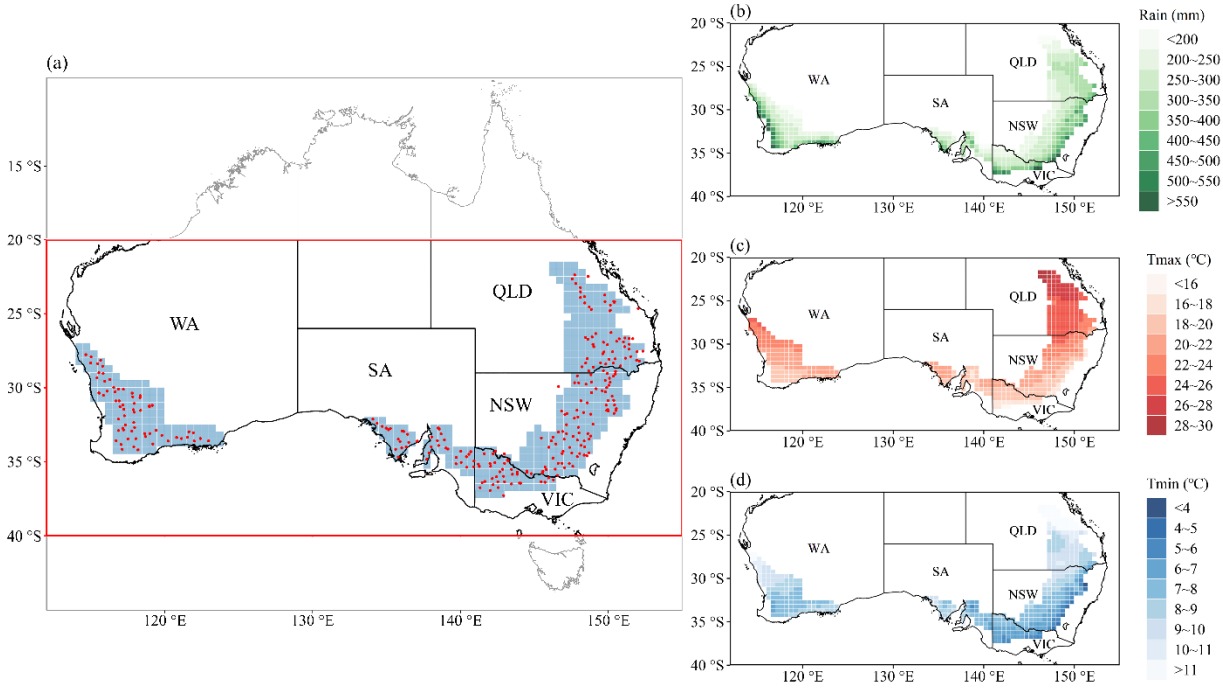

Figure 5-1. (a) The spatial extent of Australia's wheat belt with 296 soil sites; (b) annual mean cumulative rainfall during wheat growing season of April to November; (c) annual mean maximum temperature from April to November; (d) annual mean minimum temperature from April to November.

This study focused on Australia's wheat belt, which spans across several states, including Western Australia, South Australia, Victoria, New South Wales, and Queensland. Owing to the vast geographical spread, the climate varies across the belt, with the western parts experiencing a Mediterranean climate, characterized by wet winters and dry summers (Turner & Asseng, 2005), while the eastern areas have a more temperate climate (Burbidge, 1960; Hallett et al., 2018). The rainfall and temperature both display a significant gradient across the crop belt. The annual cumulative rainfall increased from 253 mm in the drier inland region to 911 mm in the coastal areas. Simultaneously, the average temperature rose from 13.5°C in the south to 23.9°C in the north. Wheat, the predominant crop in this belt, is primarily cultivated in rain-fed environments. The wheat growing season extends from April through November (Wang, Li Liu, et al., 2018).

5.2.2 Data

The historical climate data for the period 1900-2020 was sourced from the Scientific Information for Land Owners (SILO, 2023). This dataset offers detailed daily climate data across Australia, with a fine resolution of 0.05 degrees. Our initial step involved selecting grid cells within Australia's crop belt, resulting in the acquisition of 41,534 grids. To manage the computational burden, we upscaled these cells from a resolution of 0.05 degrees to 0.5 degrees (Feng et al., 2022). This upscaling was adopted following evidence that such an upscaling does not significantly alter the magnitude or spatial distribution of extreme weather events (Perkins & Alexander, 2013). As a consequence, it yielded 453 grids of 0.5-degree resolution covering the entire Australia's crop belt, as illustrated in Figure 5-1.

In addition, we incorporated soil hydraulic properties and parameters from the APSoil database (Apsoil, 2022). A total of 296 soil sites were chosen, to align each climate data grid to a geographically proximate soil profile. These profiles are systematically parameterized for modeling and are ready for direct use in simulations (Dalgliesh et al., 2012).

The climate variability in Australia is mainly influenced by three large-scale climate drivers, namely the Indian Ocean Dipole (IOD), the El Niño–Southern Oscillation (ENSO), and the Southern Annular Mode (SAM). IOD can be characterized by the Dipole Mode Index (DMI), which describes the difference in sea surface temperature (SST) between the tropical western (50ºE-70ºE, 10ºS-10ºN) and southeastern Indian Ocean (90ºE-110ºE, 10ºS-Equator) (Saji et al., 1999). The ENSO cycle, describing the fluctuation between warm El Niño and cold La Niña events in the tropical Pacific (McPhaden et al., 2006), is monitored through various indicators. Such as the Southern Oscillation Index (SOI), which tracks the anomalies in sea level pressure between Darwin and Tahiti, and the Niño 3 and Niño 4 indices, which measure SST in the tropical Pacific Ocean (Hanley et al., 2003). We selected SOI as ENSO indices in this study because it is based on

sea level pressure, complementing the IOD, which is based on SST. Additionally, the SOI is widely recognized in Australia for estimating the impacts of ENSO (Feng et al., 2022). The SAM characterizesthe non-seasonal oscillation of strong westerly winds between the northern and southern extents, consistently present in the mid to high latitudes of the southern hemisphere (Marshall, 2003). We downloaded the three indices from the National Oceanic and Atmospheric Administration Earth System Research Laboratories Physical Sciences Laboratory (https://psl.noaa.gov/). However, the correlation analysis between three climate drivers and DET intensity reveals that the relationship between the SAM and DET intensity is not significant in over half the area of the wheat belt (Figure 5-S1). Therefore, only IOD and ENSO were considered in this study.

5.2.3 APSIM simulations

APSIM (Agricultural Production System sIMulator) is a sophisticated modeling framework that simulates the biophysical process in agricultural systems (Archontoulis et al., 2014; Asseng et al., 1998; Holzworth et al., 2014; Keating et al., 2003; Yang et al., 2018), it has been well-calibrated in various studies on Australian wheat production (ASSENG et al., 2011; Wang, Liu, et al., 2018). In this study, APSIM model version 7.10 was used to simulate the dynamic of soil water and wheat phenology at 0.5° grid cell from 1900 to 2020. The wheat cultivars and sowing time were state-specific, set up based on the previous study of Wang, Liu, et al. (2018) (Table 5-S1). The select wheat cultivars were sowing either when the accumulated rainfall surpassed 25mm in 7 consecutive days, or at the end date of the sowing window if the rainfall criteria were not met. The dynamic output data of phenology information and daily plant available water were used to calculate DET intensity.

5.2.4 DET events

DET events refer to occurrences where drought intersects with either heat or frost, both temporally and spatially (Eq. 5-1) (Li et al., 2024). Drought events occur when the plant's available water within 0-100 cm soil depth is lower than 40% of the plant available water capacity (PAWC) for three or more consecutive days. PAWC quantifies the maximum volume of water that soil can retain for crop utilization. It is determined by the difference in volumetric water content between the drained upper limit (DUL) and the lower limit of crop (LL) represents the total amount of water a soil can store for crops to use (Asseng et al., 2001; Wang et al., 2017). When the amount of extractable soil water for wheat falls below 40% of the PAWC, the stomatal conductance, root growth, tiller number, and yield of wheat were proven to decrease (Ciais et al., 2005; Kirkegaard & Lilley, 2007). Therefore, we used 40% of the PAWC as the drought threshold in this study. Heat events are characterized by daily maximum temperatures exceeding a threshold of 28 °C for three or more consecutive days. Such conditions have been observed to adversely affect wheat production, leading to a reduction in both the size and weight of the wheat grains (Lalic et al., 2013; Wheeler

et al., 1996). Frost events are defined using a daily minimum temperature threshold of 2 °C (Liu et al., 2011). This definition aligns with the findings of Farre et al. (2010), who reported that yield losses in wheat occur when daily minimum temperatures drop below 2 °C during the flowering stage of the wheat.

$$DET_j = d_i \left| \left\{ \left(TX_{ij} \geq 28 \right) \cap \left(PAW_{ij} \leq \delta \times PAWC \right) \right\} \cup \left\{ \left(TI_{ij} \leq 2 \right) \cap \left(PAW_{ij} \leq \delta \times PAWC \right) \right\}, \quad j = 1, 2, ..., N; i = l+1, l+2, ..., l+m_j, m_j \geq 3; w_s \leq d_i \leq w_e \tag{5-1}$$

where DET_j is the jth DET event; N represents the total number of DET events occurring within each WRP; d_i refers to the ith day during the WRP, with the subscript l indicating the day immediately preceding the commencement of the jth DET event; TX_{ij} and TI_{ij} stand for the maximum and minimum temperatures, respectively, on d_i during the jth DET event; PAW_{ij} is plant available water on d_i within the jth DH event.

According to the above definition, we focused on the identification of DET events occurring within the WRP from the initial floral stage to the end of the grain-filling stage. This period is more susceptible to weather and climate events than other growth stages (Cohen et al., 2021). The daily DET intensity was calculated by the weighted sum of daily drought intensity, heat intensity, and frost intensity (Eq. 5-2). The DET intensity for each occurrence was calculated by the cumulative sum of daily DET intensity during this DET event (Eq. 5-3), then the annual DET intensity was represented by the sum of intensity for all DET events occurring within the WRP (Eq. 5-4).

$$SDETI_{ij} = \alpha DI_{ij} + \left(1-\alpha\right) HI_{ij} + \left(1-\alpha\right) FI_{ij}, i = 1, 2, ..., m_j; j = 1, 2, ..., N \tag{5-2}$$

$$CDETI_j = \sum_{i=1}^{m_j} SDETI_{ij}, j = 1, 2, ..., N \tag{5-3}$$

$$DETI = \sum_{j=1}^{N} CDETI_j, j = 1, 2, ..., N, N \geq 1 \tag{5-4}$$

where $SDETI_{ij}$ represents the daily DET intensity for the ith day of the jth DET event of a given year; DI_{ij} , HI_{ij}, and FI_{ij} correspond to the daily drought, heat, and frost intensities, respectively, for the ith day of the jth DET event; the coefficient α, assigned a value of 0.5, serves as the weighting factor for the daily drought intensity; $CDETI_j$ quantifies the intensity of the jth DET in the given year.

5.2.5 ENSO and IOD

We employed the SOI to characterize the variability of the ENSO, and the DMI to describe the variability of the IOD (Feng et al., 2022). During El Niño (negative SOI values) or the positive phase of the IOD (positive DMI values) in the colder seasons, northeastern Australia and the southern coast experience

unusually drier and hotter conditions. Conversely, La Niña (positive SOI values) and the negative phase of the IOD (negative DMI values) bring cooler and more humid conditions to these regions (Min et al., 2013). We adopted the classification criteria for varied ENSO's strength set by Casselman et al, which distinguishes the moderate and strong ENSO events. Specifically, moderate ENSO (IOD) events are those where the SOI (DMI) index lies within a range of ±0.5 to ±1 standard deviation (σ) from its mean value during the WRP. In contrast, strong events are identified when the index surpasses ±1σ of its mean value during the WRP (Table 5-1) (Casselman et al., 2021; Reddy et al., 2021).

Table 5-1. Classification standard for various strengths of ENSO and IOD.

Climate Drivers	Phases	Indices
ENSO	Strong El Niño	SOI <-1σ
	Moderate El Niño	-1σ≤ SOI <-0.5σ
	Neutral	-0.5σ≤ SOI <0.5σ
	Moderate La Niña	0.5σ≤ SOI <1σ
	Strong La Niña	SOI >1σ
IOD	Strong IOD positive	DMI >1σ
	Moderate IOD positive	0.5σ≤ DMI <0.5σ
	Neutral	-0.5σ≤ DMI <0.5σ
	Moderate IOD negative	-1σ≤ DMI <-0.5σ
	Strong IOD negative	DMI <-1σ

To examine the impact of the ENSO and the IOD on DET events, we analyzed the composite mean differences in DET intensity. This was done by comparing DET intensities during strong and moderate phases of ENSO and IOD against those observed during their respective neutral phases.

5.2.6 Probabilistic estimation of ENSO and IOD impacts on DET events

5.2.6.1 Copula

Copula, a statistical tool first proposed by Sklar (1973), is designed to describe the dependency structure between two or more random variables. It constructs the multivariate distribution by connecting the marginal distributions of the individual random variables (Frees & Valdez, 1998). Since being introduced in the early 1950s, copulas have been widely applied across several disciplines of applied mathematics, including finance, insurance, and reliability theory (Jaworski et al., 2010). In recent years, their application has extended to the fields of agriculture and climate research, where they are used to analyze the complex dependencies among different climate extremes or between climate conditions and crop production (Guo et al., 2022; Nguyen-Huy et al., 2017; Ribeiro et al., 2019) In this study, we employed a 2-dimensional copula function to explore the dependency relationship between ENSO/IOD (x) and DET intensity (y). Their joint distribution can be described as Eq. 5-5:

$$F_{x,y}(x,y) = C\left[F_x(x), F_y(y)\right] \tag{5-5}$$

where $F_{x,y}(x,y)$ is the joint distribution function; C is the copula function; $F_x(x)$ and $F_y(y)$ are the marginal distributions of random variables x and y, respectively.

We constructed the copula function in each grid cell. The first step for the construction is to determine the marginal distributions of random variables. We employed the Normal, Uniform, and Logistic distributions to fit the variables, selecting the optimal marginal distribution based on the lowest AIC (Akaike information criterion) values (Sakamoto et al., 1986). The next step is to fit the copula function. We compared six commonly used functions, Frank, Clayton, Gumbel, t, Gaussian, and Joe, choosing the function with the lowest AIC value for the fitting processes (Table 5-2).

5.2.6.2 Estimating the conditional probability of high-intensity DET events occurring under various ENSO/IOD phases

According to the copula joint distribution of ENSO/IOD and DET intensity, we calculated the conditional probability of high-intensity DET events (y) under various phases of climate drivers (x) (Eq. 5-6 ~ 5-10). The high-intensity DET events are defined as occurrences where the DET intensity exceeds the 90th percentile threshold from 1900 to 2020 in each grid, i.e., Y=90th. We used 4 thresholds to define five different phases of ENSO/IOD in this study, i.e., X_1=-1σ, X_2=-0.5σ, X_3=0.5σ, and X_4=1σ.

$$F_{Y|X}(y) = P(y \geq Y | x \leq X_1) = \frac{F_x(X_1) - C[F_x(X_1) - F_y(Y)]}{F_x(X_1)} \quad (5\text{-}6)$$

$$F_{Y|X}(y) = P(y \geq Y | X_1 < x \leq X_2) = \frac{(F_x(X_2) - C[F_x(X_2) - F_y(Y)]) - (F_x(X_1) - C[F_x(X_1) - F_y(Y)])}{F_x(X_2) - F_x(X_1)} \quad (5\text{-}7)$$

$$F_{Y|X}(y) = P(y \geq Y | X_2 < x \leq X_3) = \frac{(F_x(X_3) - C[F_x(X_3) - F_y(Y)]) - (F_x(X_2) - C[F_x(X_2) - F_y(Y)])}{F_x(X_3) - F_x(X_2)} \quad (5\text{-}8)$$

$$F_{Y|X}(y) = P(y \geq Y | X_3 < x \leq X_4) = \frac{(F_x(X_4) - C[F_x(X_4) - F_y(Y)]) - (F_x(X_3) - C[F_x(X_3) - F_y(Y)])}{F_x(X_4) - F_x(X_3)} \quad (5\text{-}9)$$

$$F_{Y|X}(y) = P(y > Y | x > X_4) = \frac{(1 - F_y(Y)) - (F_x(X4) - C[F_x(X_4) - F_y(Y)])}{1 - F_x(X_4)} \quad (5\text{-}10)$$

where $F_{Y|X}$ is the conditional probability distribution function; P represents the probability under various scenarios; C is the copula function; F is the marginal distribution; x and y correspond to the value of SOI/DMI and DET intensity, respectively, X_1, X_2, X_3, and X4 are specific conditional values of x, and Y is the conditional value of y.

Table 5-2. Copula functions used in this study.

Name	Mathematical Description	Parameter range
Frank	$-\frac{1}{\theta}\ln\left[1+\frac{\left(\exp\left(-\theta_u\right)-1\right)-\left(\exp\left(-\theta_v\right)-1\right)}{\left(\exp\left(-\theta\right)-1\right)}\right]$	$(-\infty,0)\cup(0,+\infty)$
Clayton	$\max\left(u^{-\theta}+v^{-\theta}-1,0\right)^{-1/\theta}$	[-1,+ ∞)\0
Gumbel	$\exp\left\{-\left[\left(-\ln\left(u\right)\right)^{\theta}+\left(-\ln\left(v\right)\right)^{\theta}\right]^{1/\theta}\right\}$	[1,+ ∞)
t	$\int_{-\infty}^{t_k^{-1}(u)}\int_{-\infty}^{t_k^{-1}(v)}\frac{1}{2\pi\sqrt{1-\theta^2}}\left[1+\frac{x^2-2\theta xy+y^2}{k\left(1-\theta^2\right)}\right]^{-(k+2)/2}dxdy$	(-∞,+∞)
Gaussian	$\Phi_{\theta}\left(\Phi^{-1}\left(u\right),\Phi^{-1}\left(v\right)\right)$	[-1,1]
Joe	$1-\left[\left(1-u\right)^{\theta}+\left(1-v\right)^{\theta}+\left(1-u\right)^{\theta}\left(1-v\right)^{\theta}\right]^{1/\theta}$	[1,+ ∞)

5.3. Results

5.3.1 Spatial characteristics of DET events

Figure 5-2 (a)-(c) shows the spatial distributions of DETI across 0.5º grid cells within Australia's wheat belt in three historical periods. There was notable spatial heterogeneity observed in DETI throughout the wheat belt regions, ranging from 0.4 to 14.3 in the 1920s, 0.4 to 12.1 in the 1960s, and 0.4 to 14.0 in the 2000s. The DETI was much higher in the eastern area compared to that in the western part of Australia's wheat belt. However, there was a consistent upward trend in the DETI for the western region from the 1920s through to the 2000s. In contrast, the eastern region exhibited a decline in DETI from the 1920s to the 1960s, followed by an increase from the 1960s to the 2000s.

The mean DETI across five different states, as depicted in Figure 5-2 (d)-(f), showed the ranking from highest to lowest as QLD > NSW > WA > VIC > SA for all three periods. There was a steady increase in the mean DETI for SA and WA from the 1920s to the 2000s, with values rising from 2.7 to 3.0 to 3.3 in SA, and from 3.7 to 4.4 to 4.8 in WA. The other three states, QLD, NSW, and VIC, experienced a decrease in

DETI from the 1920s to the 1960s, followed by an increase from the 1960s to the 2000s, with QLD going from 8.7 to 7.6 to 9.3, NSW from 6.5 to 5.1 to 6.1, and VIC from 3.5 to 3.1 to 4.0.

5.3.2 Temporal Variations of DETI and Climate Drivers

Figures 2 (g) and (h) present temporal fluctuations of DETI and the mean climate driver indices during the WRP from 1900 to 2020. The DETI varied greatly over the study period, with the lowest recorded at 0.8 in 1955 and peaking at 9.5 in 1957. The responses of DETI to ENSO and IOD were found to be inverse, positive-phase ENSO events (positive SOI) had a negative impact on DETI, whereas negative-phase IOD events negatively affected DETI. For example, low DETI was recorded in 1906, 1917, 1973-1975, 1998, and 2010, years that experienced an El Niño and negative IOD phase. The SOI showed substantial fluctuations from 1900 to 2020 but did not exhibit a clear long-term signal. In contrast, the DMI presented a discernible long-term pattern, with fewer years recording a negative DMI and an increased occurrence of positive DMI during the 2000s compared to the 1920s.

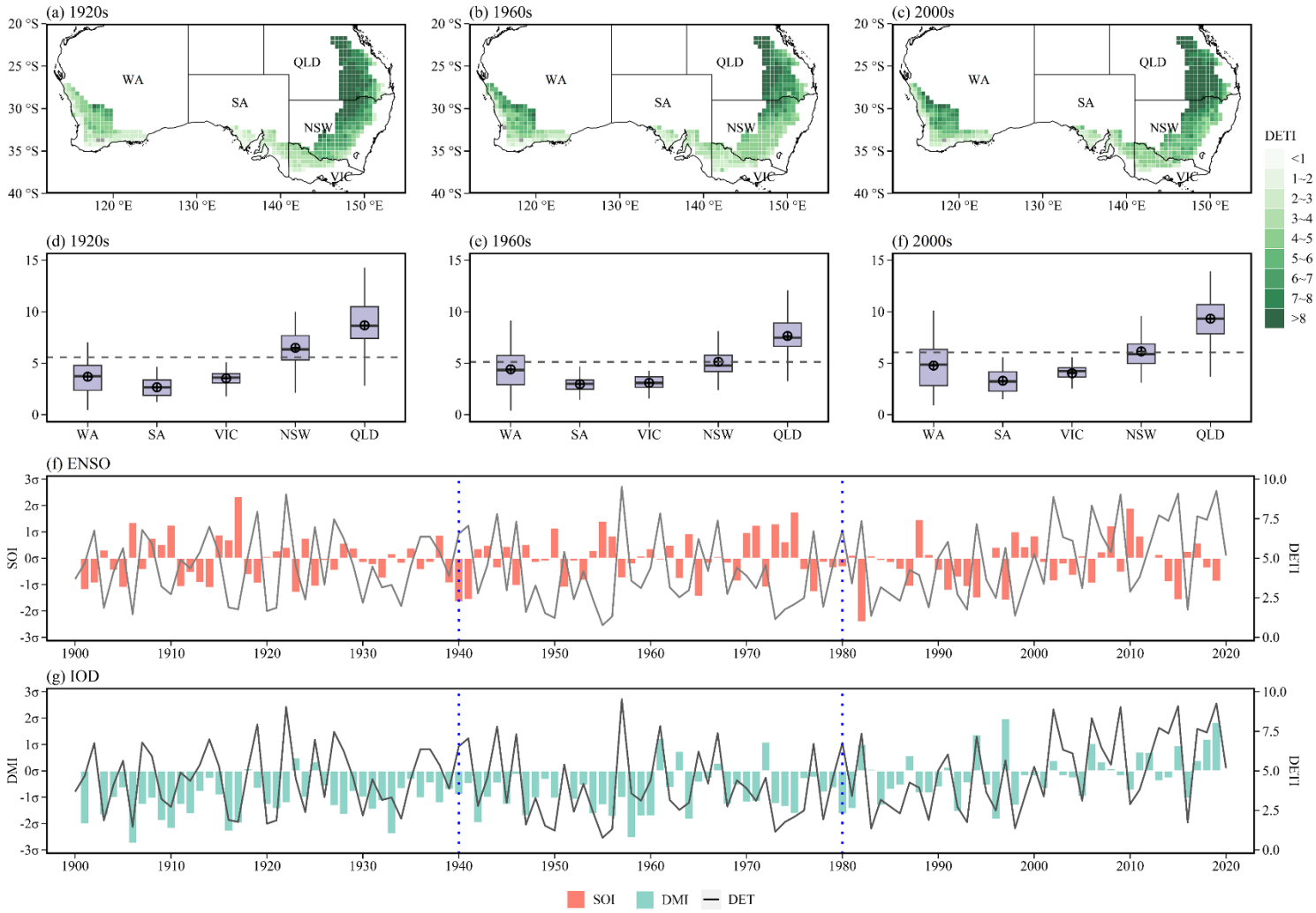

Figure 5-2. (a)-(c) The spatial distribution of average intensity of DET (compound drought and extreme temperature) in three historical periods 1920s (1900-1940), 1960s (1941-1980), and 2000s (1981-2020); (d)-(f) The DET intensity (DETI) for each state in 1920s, 1960s, and 2000s, box boundaries indicate the 25th and 75th percentiles across grids, whiskers below and above the box indicate the 10th and 90th percentiles. The black lines and crosshairs within each box indicate the multi-grid median and mean, respectively; (g)&(h) Annual mean DET intensity (black lines) and wheat reproductive period mean climate driver indices (bars) during 1900-2020.

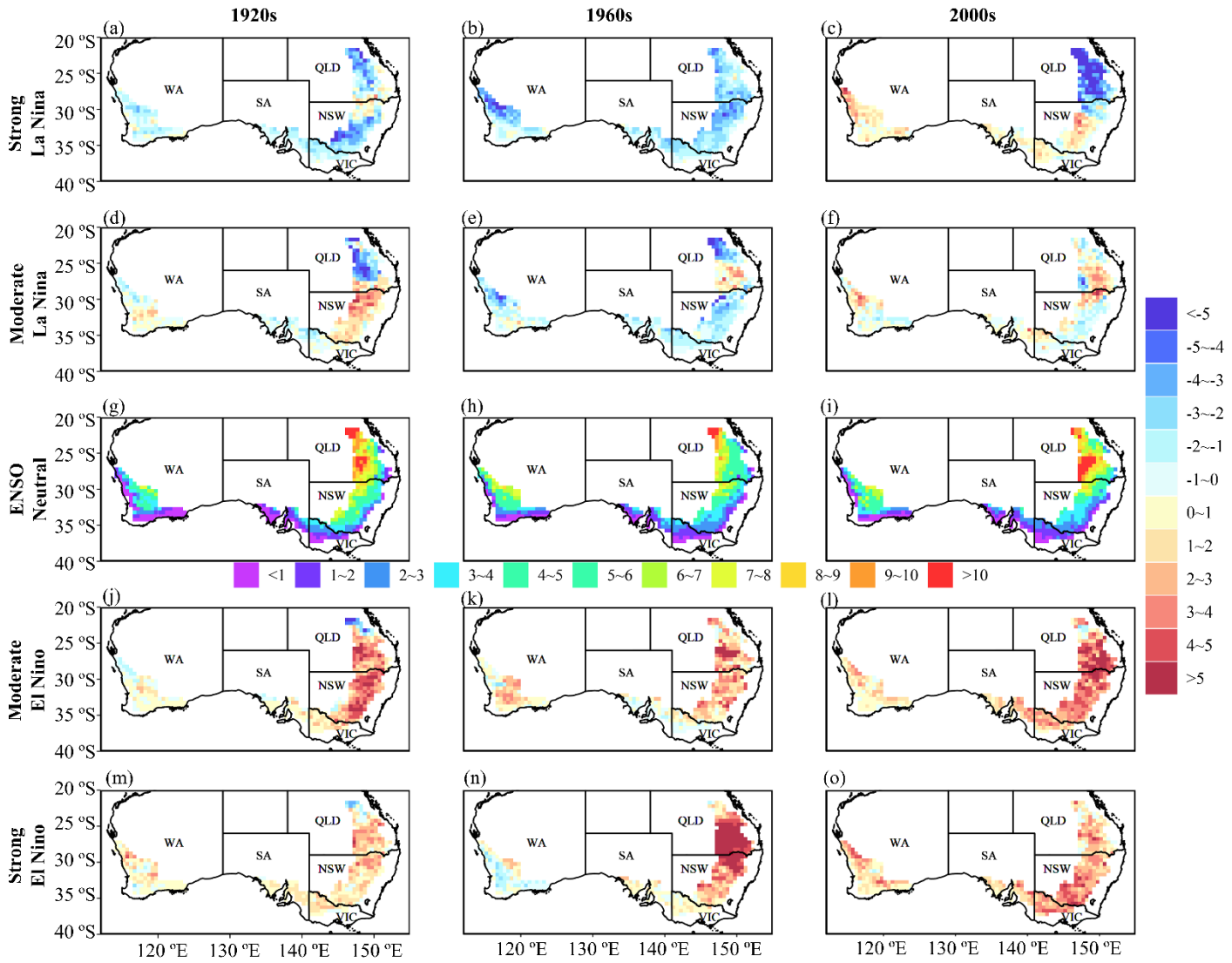

Figure 5-3. Composite differences of DETI (intensity of compound drought and extreme temperature events) during the various phases of ENSO against the ENSO neutral conditions. The spatial distribution of DETI during the neutral conditions is shown in the center (g), (h), and (i).

5.3.3 The influence of ENSO and IOD on DETI

5.3.3.1 ENSO

Figure 5-3 presents the composite differences between DETI during different phases of El Niño/La Niña and ENSO neutral over three historical periods across Australia's wheat belt. The central maps (g)-(i) show the spatial distribution of DETI during ENSO neutral in the 1920s, 1960s, and 2000s, which serve as a baseline for comparison. The DETI across Australia's wheat belt was largely influenced by ENSO, with lower DETI value during La Niña phases (Figure 5-3 a-f) and higher DETI during El Niño phases (Figure 5-3 j-o). However, the extent of ENSO's influence varied across different regions and periods. During the strong La Niña phase, most grids in the 1920s and 1960s experienced lower DETI values than during neutral conditions (Figure 5-3 a&b). Contrastingly, in the 2000s, DETI values were higher than neutral conditions across the wheat belt, especially in the western and southern parts (Figure 5-3 c). Moderate La Niña phases saw higher DETI values in more grids compared to neutral conditions, mainly in the southeast in the 1920s, northeast in the 1960s, and east in the 2000s (Figure 5-3 d-f). Throughout moderate El Niño phases, the entire wheat belt recorded higher DETI values than during neutral conditions, with notable increases in the east during the 1920s and 2000s (Figure 5-3 j&l). The 1960s experienced a more uniform DETI increase across the entire belt (Figure 5-3 k). Furthermore, during strong El Niño events, the northeastern part of the wheat belt displayed the highest positive differences in the DETI from neutral conditions, while in the western region, there were slight negative differences in the 1960s (Figure 5-3n). Spatial variability in the positive differences of DETI across Australia's wheat belt was minimal in the 1920s (Figure 5-3 m). However, in the 2000s, strong El Niño conditions contributed to an increase in DETI values throughout the entire wheat belt, with the increases being particularly pronounced in the southeastern region (Figure 5-3 n).

When examining DETI composite differences in the five states during strong La Niña, there was a general trend for lower DETI values compared to neutral conditions in the 1920s and 1960s, with averages ranging from -0.9 to -2.4. Conversely, the 2000s saw a slight increase in average DETI by 0.1 to 1.2 in WA, SA, VIC, and NSW, except for QLD, which experienced a decrease of 4.73 (Figure 5-4 a). During moderate La Niña events, DETI values were slightly lower than neutral in the 1920s and 1960s, with mean reductions ranging from -0.1 to -1.8, but the 2000s saw increases of 0.1 to 0.3 (Figure 5-4 c). El Niño phases consistently resulted in higher DETI values than neutral across all states, with moderate El Niño phases showing increases of 0.2 to 3.3 in the 1920s, 0.3 to 2.5 in the 1960s, and 1.0 to 3.7 in the 2000s (Figure 5-4 g). During strong El Niño, the increases ranged from 0.7 to 1.5 in the 1920s, 0.6 to 6.1 in the 1960s, and 1.5 to 3.2 in the 2000s (Figure 5-4 i).

5.3.3.2 IOD

Figure 5-5 showcases the composite differences in DETI during positive and negative phases of the IOD compared to the IOD neutral phases in Australia's wheat belt across three distinct periods: the 1920s, 1960s, and 2000s. Maps (g), (h), and (i) in the center serve as a reference, displaying the spatial distribution of DETI during the IOD neutral states for each period. During the strong IOD negative phase, the DETI values were basically lower than those observed during IOD neutral across the whole wheat belt (Figure 5-5 a-c). Initially, in the 1920s, this reduction was uniformly spread throughout the wheat belt. However, over time, by the 1960s and further into the 2000s, the decrease became more pronounced and focused on the eastern regions of the wheat belt. During the moderate negative phase of IOD, most areas within the wheat belt exhibited decreased DETI values relative to the neutral IOD conditions (Figure 5-5 d-f). However, in the 1920s, the northeastern region of the wheat belt recorded increased DETI values. This zone of elevated DETI values diminished by the 1960s and transitioned to lower DETI values compared to the neutral condition by the 2000s. For moderate IOD positive phases, the 1920s and 1960s saw generally lower DETI values across Australia's wheat belt when compared to neutral IOD conditions (Figure 5-5 j&k). Contrastingly, in the 2000s, this phase was associated with higher DETI values throughout the majority of the wheat belt, except the northeastern region (Figure 5-5 l). Additionally, during the strong IOD positive phase, the 1960s displayed predominantly higher DETI values compared to the neutral IOD conditions across the wheat belt, with the exception of a very small area located in the east coastal area where decreased DETI was observed (Figure 5-5 n). In the 2000s, there was a notable increase in the number of grids indicating significant high-intensity DET events compared to the 1960s, with the highest values in the southeastern wheat belt (Figure 5-5 o).

From the perspective of the five states, strong IOD negative phases historically led to lower DETI values than IOD neutral periods, with the average DETI reductions ranging from -1.1 to -1.9 in the 1920s, widened to -0.7 to -3.5 in the 1960s, and further expanded to -1.1 to -5.8 in the 2000s, as shown in Figure 5-4 (b). Notably, the decreases in DETI values in WA, SA, and VIC were smaller than those observed in NSW and QLD. Similarly, during the moderate IOD negative phases, DETI values were generally lower than those in neutral conditions, (Figure 5-4 d). Specifically, the average reductions in DETI values were between -0.8 and -2.0 in the 1920s, -0.2 to -2.4 in the 1960s, and -0.6 to -4.4 in the 2000s. During moderate IOD positive phases, DETI values remained lower than those in neutral conditions for the 1920s and 1960s, with average reductions ranging from -1.0 to -4.4 and -0.6 to -3.5, respectively. However, in the 2000s, DETI values increased beyond neutral conditions across all states except QLD, showing an increase of 0.5 to 1.6. The strong IOD positive phases consistently resulted in higher DETI values than neutral conditions across all states, with increases ranging from 0.3 to 2.3 in the 1960s and 0.5 to 3.2 in the 2000s.

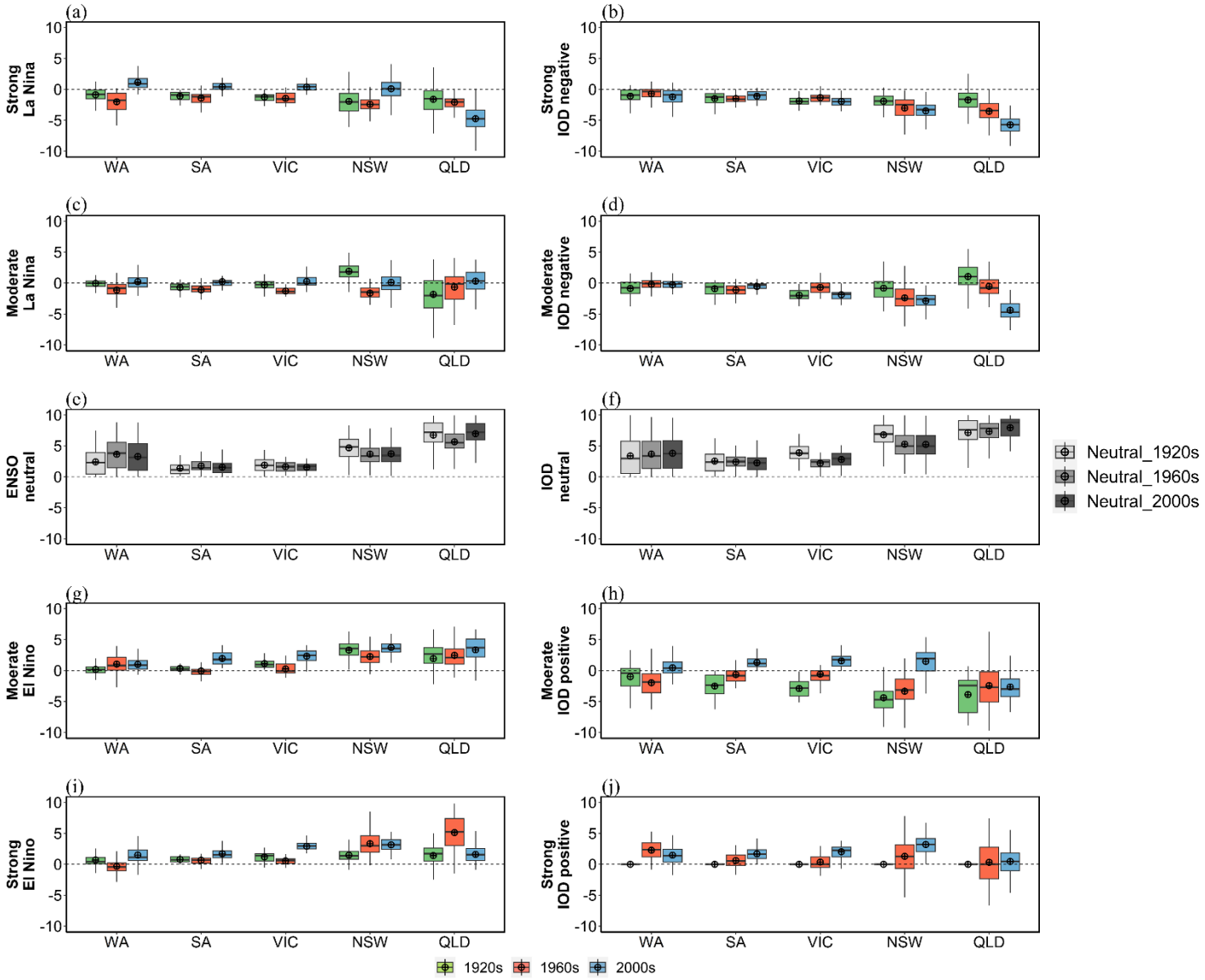

Figure 5-4. Composite differences of DETI (intensity of compound drought and extreme temperature events) during the various phases of ENSO/IOD against the neutral conditions for five states. The DETI during the neutral conditions is shown in the center (c) and (f).

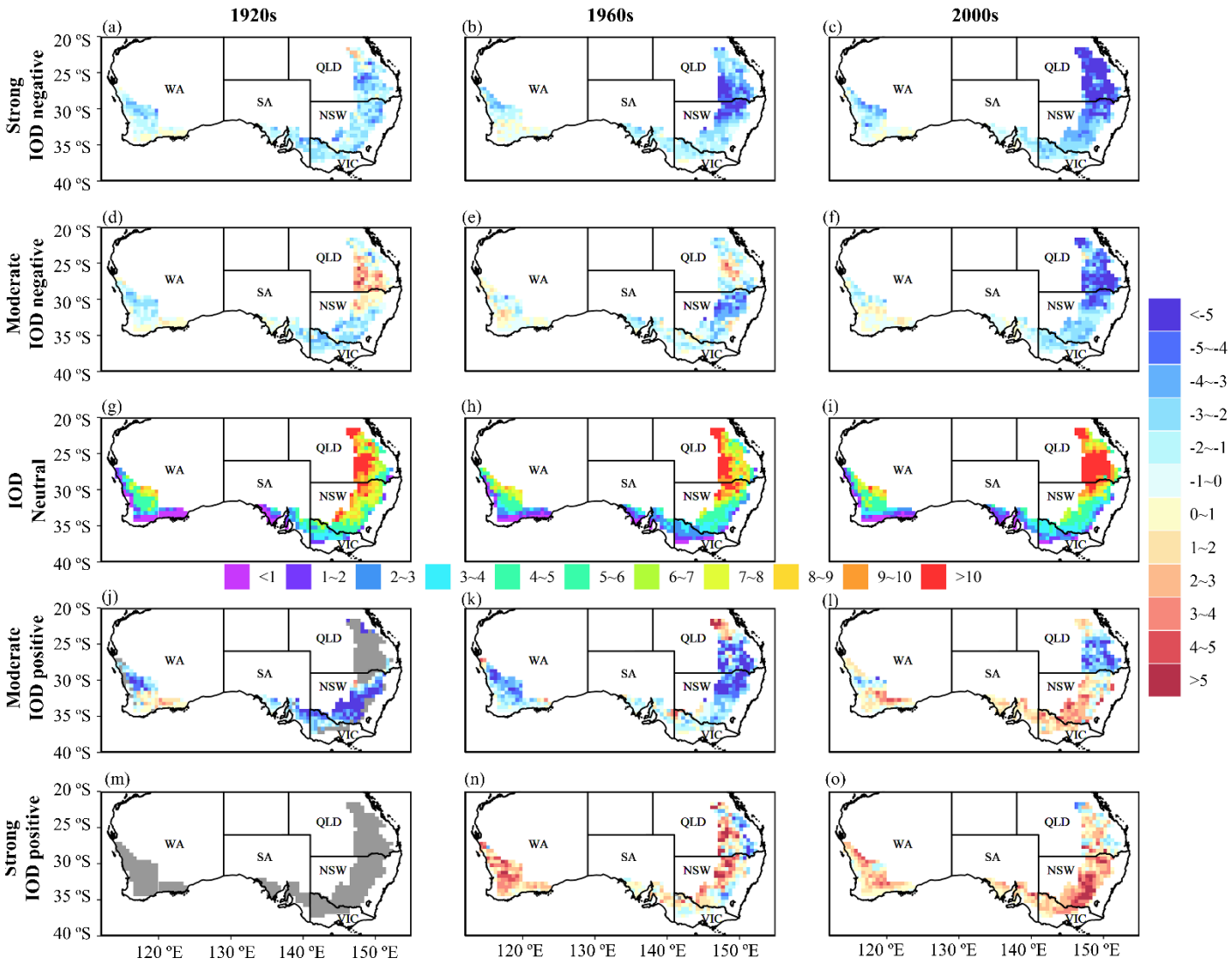

Figure 5-5. The spatial distribution of composite differences of DETI (intensity of compound drought and extreme temperature events) during the various phases of IOD against the IOD neutral conditions. The spatial distribution of DETI during the neutral conditions is shown in the center (g), (j), and (i). The grey grids indicated where no moderate/strong IOD positive phases occurred.

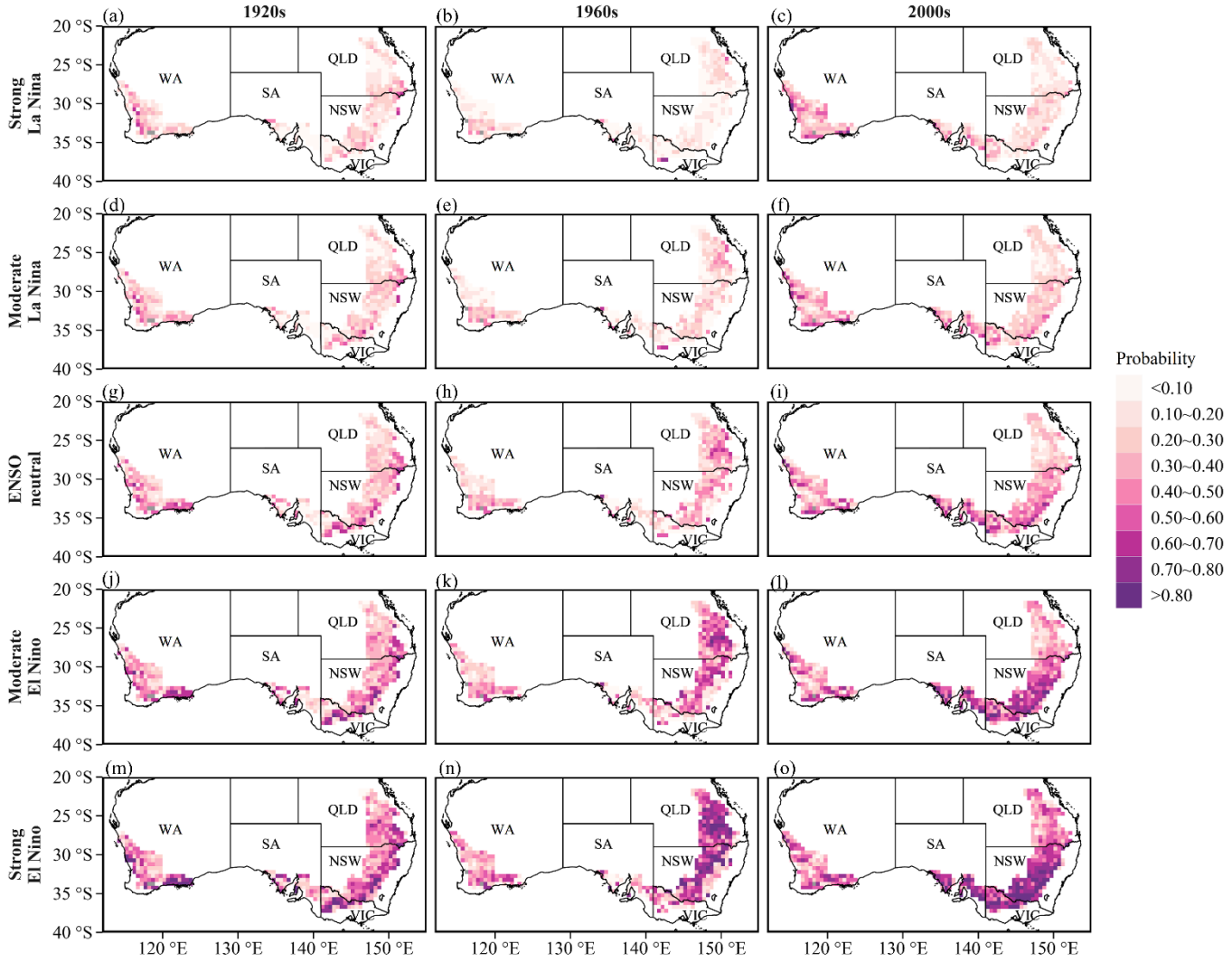

Figure 5-6. The probability of high-intensity DET (compound drought and extreme temperature) events during the various phases of ENSO across Australia's wheat belt. The high-intensity DET events occur when DET intensity is higher than the 90th percentile value during ENSO neutral phase.

5.3.4 The probability of high-intensity DETI events during different ENSO and IOD phases

Figure 5-6 presents the spatial distributions of the probability of high-intensity DETI events during different ENSO phases across Australia's wheat belt. High-intensity DET events were defined as seasons in which the DETI exceeds the 90th percentile value during the ENSO neutral phase. The spatial distribution of this conditional probability across the Australian wheat belt varied greatly with the phase of ENSO and over time. In general, the probability of high-intensity DET events increased as ENSO transitions from La Niña to El Niño, with the mean probability ranging from 18% during strong La Niña to 46% during strong El Niño in the 1920s (Figure 5-6 a, d, g, j, and m), 10% to 46% in the 1960s, and 22% to 54% in the 2000s. Additionally, this rise in probability was notably more pronounced in the southern and eastern regions of Australia's wheat belt compared to the western region across all three periods (e.g. Figure 5-6 a, d, g, j, and m). Across three distinct periods, the probabilities of experiencing high-intensity DET events in relation to various ENSO phases exhibited a temporal fluctuation. Specifically, the mean probability declined from a range of 18%-46% in the 1920s to 10%-46% in the 1960s, before rising to 22%-54% in the 2000s. Concurrently, the distribution of grids with high probability was also dynamic across the wheat belt. Initially concentrated in coastal regions during the 1920s (Figure 5-6 m), the focal areas of high probability transitioned through northern and central regions in the 1960s Figure 5-6 n), eventually concentrating in southeastern regions of Australia's wheat belt in the 2000s Figure 5-6 o).

Figure 5-7 shows the spatial distribution of the probability of high-intensity DETI events during different IOD phases across Australia's wheat belt, revealing dynamic changes across different IOD phases and over time. The probability of high-intensity DET events became larger due to the transition of IOD phases from negative to positive. For instance, the mean probability increased from 16% during the strong IOD negative phase to 42% during the strong IOD positive phase in the 1920s (Figure 5-7 a, d, g, j, and m), 13% to 45% in the 1960s, and 10% to 51% in the 2000s. Throughout the three study periods, the distribution of probabilities for high-intensity DET events exhibited variability across different IOD phases. Notably, during IOD negative and neutral phases, probabilities for high-intensity DET events were constantly reduced from the 1920s to 2000s across Australia's wheat belt. Specifically, decreasing from 16% to 10% during strong IOD negative phases, 22% to 15% during moderate IOD negative phases, and 28% to 25% during IOD neutral. However, during IOD positive phases, the probabilities increased over time, increasing from 36% to 37% during moderate IOD positive phase and 42% to 51% during strong IOD positive phase. Furthermore, the spatial distribution of grids with a high probability of experiencing high-intensity DET events was dynamic across the wheat belt throughout the three study periods. Initially, during the 1920s, grids with a high probability were predominantly located in the western and northern regions (Figure 5-7

m). By the 1960s, these areas of high probability shifted towards the eastern regions (Figure 5-7 n), and by the 2000s, the focus had moved to the southeastern regions of Australia's wheat belt Figure 5-7 o).

We counted the number of grids exhibiting a greater than 50% probability of experiencing high-intensity DET events during different ENSO and IOD phases across three distinct periods: the 1920s, 1960s, and 2000s, as detailed in Table 5-3. We found that the number of girds with a greater than 50% probability occurring high-intensity DET events increased as ENSO phases transitioned from La Niña to El Niño, from 10 to 177 in the 1920s, 4 to 215 in the 1960s, and 23 to 271 in the 2000s. Meanwhile, this number during strong and moderate El Niño phases witnessed a notable increase from the 1920s to the 2000s, advancing from 110 to 188 for moderate El Niño phases and from 177 to 271 for strong El Niño phases, respectively. Particularly, during the strong El Niño phase of the 2000s, more than half of the grids across the wheat belt (the number of grids is 452 in Australia's wheat belt) were found to have a greater than 50% probability of experiencing high-intensity DET events. Similar to ENSO, the number of girds exhibiting a greater than 50% probability of high-intensity DET events escalated with the shift in IOD phases from negative to positive. Specifically, this number rose from 13 to 169 grids during the 1920s, from 6 to 199 grids in the 1960s, and from 9 to 231 grids in the 2000s. Furthermore, during the strong IOD positive phase, there was a notable increase in this number over time, rising from 169 to 231. Additionally, the extent of the area with a greater than 50% probability of experiencing high-intensity DET events was larger during strong El Niño phases in comparison to strong IOD positive phases. Specifically, the number of grids was greater by 8, 16, and 40 in the 1920s, 1960s, and 2000s, respectively, during strong El Niño phases compared to those during strong IOD positive phases.

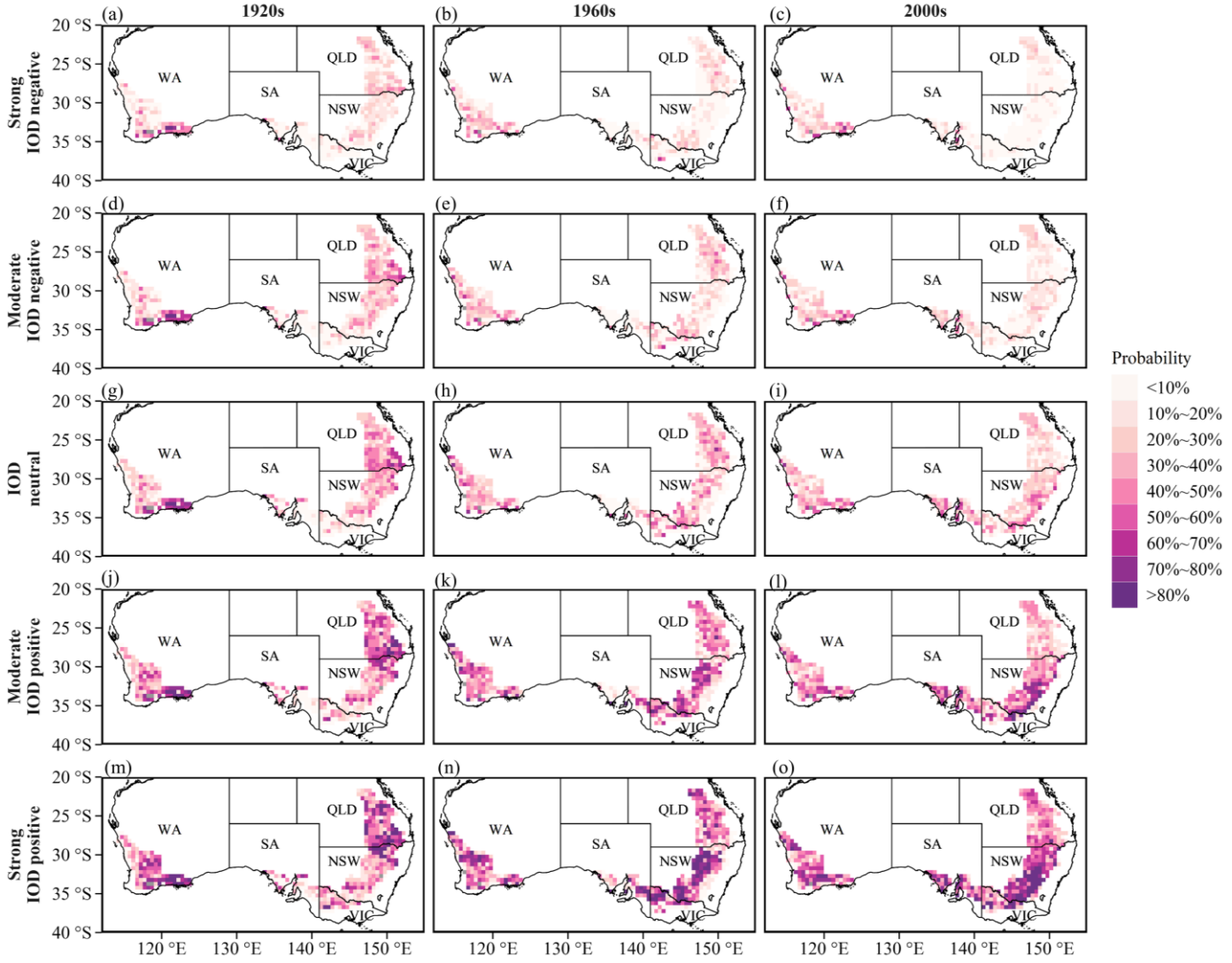

Figure 5-7. The probability of high-intensity DET (compound drought and extreme temperature) events during the various phases of IOD across Australia's wheat belt. Here the high-intensity DET events refer to a season where DET intensity is higher than the 90th percentile value during IOD neutral phase.

Table 5-3. The number of grids exhibiting a greater than 50% probability of experiencing high-intensity DET events during different ENSO and IOD phases across three distinct periods: the 1900-1940 (1920s), 1941-1980 (1960s), and 1981-2020 (2000s).

ENSO	1900-1940	1941-1980	1981-2020	IOD	1900-1940	1941-1980	1981-2020
Strong La Niña	10	4	23	Strong IOD negative	13	6	9
Moderate La Niña	14	8	34	Moderate IOD negative	40	12	11
Neutral	61	32	88	IOD Neutral	66	40	39
Moderate El Niño	110	125	188	Moderate IOD positive	127	143	116
Strong El Niño	177	215	271	Strong IOD positive	169	199	231

5.4. Discussion

Large-scale climate drivers have been widely proven to play a driving role in the occurrence and development of extreme weather and climate events such as droughts or heat in Australia (Reddy et al., 2021; Ummenhofer et al., 2011; White et al., 2014; Zhang et al., 2021). This study assessed the connection between large-scale climate drivers of ENSO/IOD and compound drought and extreme temperature events during the wheat reproductive period across Australia's wheat belt, then investigated the probability of extreme high-intensity DET events during various ENSO or IOD phases. We firstly focused on the wheat reproductive period rather than the austral summer, as this critical phase is susceptible to extreme weather events and typically occurs from August to November for Australia's wheat (Innes et al., 2015). This period overlaps the concurrence of El Niño with the positive phase of IOD during June–October (Ummenhofer et al., 2011), a powerful driver identified for its potential to induce frequent and severe compound extreme weather events (Reddy et al., 2022).

Our results demonstrated that the influences of climate drivers on DET events varied in different ENSO/IOD phases and over distinct historical periods. Generally, the eastern part of Australia's wheat belt was more susceptible to ENSO and IOD than the western parts (Figure 5-3 & Figure 5-5). Specifically, El Niño and positive IOD phases are associated with heightened DETI, whereas La Niña and negative IOD phases tend to result in reduced DETI. This is consistent with a previous study, which highlighted a notable rise in the risk of compound drought and heatwaves in summer across eastern Australia during the simultaneous occurrence of El Niño events and positive IOD phases (Reddy et al., 2022). The probability of high-intensity DET events under various ENSO and IOD phases also demonstrated a tendency where the probability increased with transitioning from La Niña to El Niño or from negative IOD to positive IOD

phases. Furthermore, the grid cells with high probabilities were predominantly concentrated in eastern Australia's wheat belt. These results align well with the well-known climatic pattern, in eastern Australia, where dry and hot years typically coincide with El Niño and/or a positive IOD phase, whereas cold and wet years are associated with La Niña and/or a negative IOD phase (Meyers et al., 2007; Min et al., 2013).

The role of ENSO in triggering severe DET events surpassed that of IOD. This is evidenced by the results that both mean and median composite differences were consistently positive and more pronounced during moderate to strong El Niño phases compared to similar phases of positive IOD. Moreover, the count of grid cells exhibiting a greater than 50% probability of high-intensity DET events was higher during strong El Niño periods compared to strong positive IOD phases. This is similar to the findings of a study quantifying the association between co-occurring phases of ENSO and IOD and compound drought and heatwave characteristics during Australia's extended summer season (Reddy et al., 2022). However, our results differ in that we found that a strong IOD positive phase can also induce severe DET events (Figure 5-5 n&o). This discrepancy may be due to the previous study's focus on the summer season, whereas the wheat reproductive periods in Australia typically occur during the winter and spring (Cann et al., 2020; Innes et al., 2015). It is the season that coincides with the peaking period for IOD positive phases, which is from September to November (Cai et al., 2009).

During the three distinct periods of the 1920s, 1960s, and 2000s, the regional influences varied during each ENSO and IOD phase. Under ENSO's influence, there were no consistent patterns in the evolution of DETI over three periods. Whether this is related to the frequent interannual fluctuations of SOI needs further investigation (Figure 5-2 f). Notably, IOD exhibited more predictable behavior, from the 1920s to the 2000s, its positive phases consistently led to increases in the positive composite differences of DETI (Figure 5-5 j-k and m-o), while its negative phases raised the negative composite differences (Figure 5-5 a-c and d-f). It indicated that the influences of positive and negative IOD phases went in two extreme directions. This trend could be attributed to the increasing frequency of positive DMI values over time and a decrease in occurrences of negative DMI values (Figure 5-2 g), Moreover, the magnitude of IOD negative phases has diminished, with the minimum DMI value decreasing progressively from -2.7σ in the 1920s to -2.5σ in the 1960s, and further to -1.8σ in the 2000s. Additionally, the reduction years with negative DMI values is a worthy worrying phenomenon (Feng et al., 2022). In the context of global warming, if the DMI consistently rises to the point where negative values completely disappear, all years with positive DMI could result in prolonged and continuous DET events. Whether the influences of IOD will exceed those of ENSO under climate change may need further investigation.

High-intensity DET events were most likely to occur during strong El Niño and strong positive phases of the IOD. Over the period from the 1920s to the 2000s, there was an increase in the number of grid cells

with more than a 50% probability of experiencing high-intensity DET events during these phases (Table 5-3). A contributing factor may be the dominant influence of the ENSO on Australia's wheat belt rainfall from the 1920s to the 1960s (Feng et al., 2022), with the occurrence of strong El Niño phases doubling from three to six instances. In the 2000s, Liu et al. (2023) further demonstrated that the ENSO's role in elevating temperatures and reducing rainfall was augmented by the shift of the Atlantic Multidecadal Oscillation from its negative to positive phase, enhancing these effects through atmospheric teleconnection mechanisms over the last two decades. Regarding the IOD, there was a consistent increase in the DMI from the 1920s to the 2000s, with the maximum DMI value escalating from 0.5 in the 1920s to 1.2 in the 1960s and reaching 2.0 in the 2000s. Furthermore, several studies have reported an intensification of the IOD's impact on Australia's wheat yields in recent decades, primarily through its influence on the rainfall patterns (Feng et al., 2022; Yuan & Yamagata, 2015).

This study presents several limitations that warrant attention. Primarily, the APSIM simulations used to model wheat phenology and plant-available water were executed based on management practices at a state scale, lacking the information of local or individual farm-level practices. Such an approach potentially overlooks the variability inherent in local or farm-specific management strategies. This limitation highlights the critical need for incorporating more detailed, location-specific data to refine the accuracy and relevance of future research efforts. Furthermore, we only assessed the influences of ENSO and IOD on DET events. However, other climate drivers like Madden-Julian oscillation (MJO), thermocline and the Interdecadal Pacific Oscillation (IPO) also impact the Australia's temperature and rainfall (Kirono et al., 2010; Marshall et al., 2014). Expanding future research to consider these additional climate drivers could enrich our understanding of the complex interplay between climate forces and compound extreme weather events.

5.5. Conclusion

Our study assessed the influences of large-scale climate drivers ENSO and IOD on DET events occurring during the WRP across Australia's wheat belt in three historical periods (1920s, 1960s, and 2000s). We found that the impacts of ENSO and IOD varied across different phases and distinct temporal periods. The eastern part of Australia's wheat belt was more responsive to ENSO and IOD than the western parts. Specifically, El Niño and positive IOD phases were associated with greater DETI and greater probability of occurring high-intensity DET events, whereas La Niña and negative IOD phases tend to result in lower DETI and lower probability of occurring high-intensity DET events, compared to the neutral conditions. The mean probability of experiencing high-intensity DET events ranges from 10% to 26% during La Niña and IOD negative phases, but from 34% to 54% during El Niño and IOD positive phases. From the 1920s to the 2000s, the area with a greater than 50% probability of experiencing high-intensity DET events during strong El Niño and strong positive IOD phases was expanded across Australia's wheat belt, with grid cells

increased by 38 and 56 during strong El Niño, and 30 and 32 during strong IOD positive phases. In general, the role of ENSO in triggering severe DET events during WRP surpassed that of the IOD during the three historical periods. Our findings highlighted the dynamic impacts of large-scale climate drivers on DET events during WRP in Australia over time, enhancing the comprehension of the relationships between climate drivers and compound weather and climate extremes. This insight bolsters our capacity to recognize and manage the risks posed by these extremes, ultimately improving adaptative potential for grain production under climate change.

5.6 Supporting information

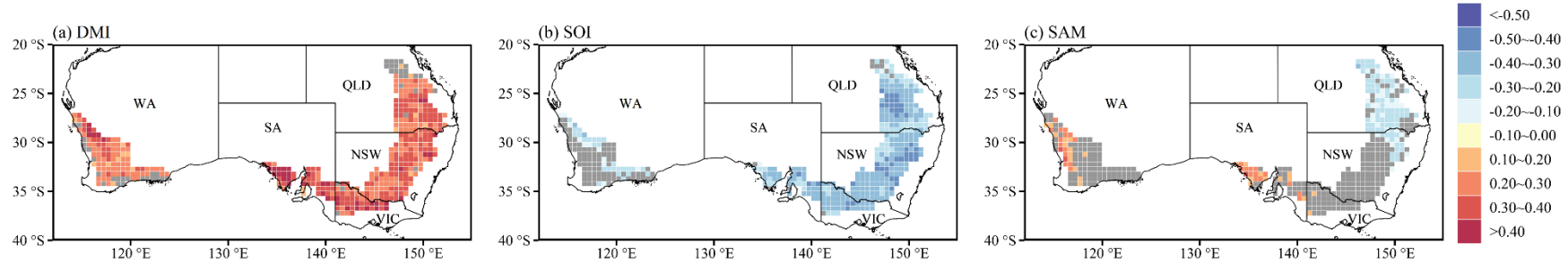

Figure 5-S1 Pearson correlation between the intensity of compound drought and extreme temperature events and Dipole Mode Index (DMI), Southern Oscillation Index (SOI), and Southern Annular Mode (SAM) during the wheat reproductive period from 1900 to 2020.

Table 5-S1 Sowing windows and cultivars for current climate conditions for the five different states.

State	Sowing window	Reference cultivar
WA	10 May-20 June	Spear
SA	1 May-10 June	Janz
VIC	1 May-10 June	Yitpi
NSW	10 May-20 June	Ventura
QLD	1 May-10 June	Hartog

5.7 Reference

Abram, N. J., Hargreaves, J. A., Wright, N. M., Thirumalai, K., Ummenhofer, C. C., & England, M. H., 2020. Palaeoclimate perspectives on the Indian Ocean dipole. Quaternary Science Reviews, 237, 106302.

Anderson, W. B., Seager, R., Baethgen, W., Cane, M., & You, L., 2019. Synchronous crop failures and climate-forced production variability. SCIENCE ADVANCES, 5(7), eaaw1976.

Apsoil, 2022. https://www.longpaddock.qld.gov.au/silo/gridded-data/. The last accessed date: 20 May 2022.

Archontoulis, S. V., Miguez, F. E., & Moore, K. J., 2014. Evaluating APSIM Maize, Soil Water, Soil Nitrogen, Manure, and Soil Temperature Modules in the Midwestern United States. Agronomy Journal, 106(3), 1025-1040.

Ashok, K., Guan, Z., & Yamagata, T., 2003. Influence of the Indian Ocean Dipole on the Australian winter rainfall. Geophysical Research Letters, 30(15).

Asseng, S., Foster, I., & Turner, N. C., 2011. The impact of temperature variability on wheat yields. Global Change Biology, 17(2), 997-1012.

Asseng, S., Keating, B. A., Fillery, I. R. P., Gregory, P. J., Bowden, J. W., Turner, N. C., Palta, J. A., & Abrecht, D. G., 1998. Performance of the APSIM-wheat model in Western Australia. Field Crops Research, 57(2), 163-179.

Bastos, A., Ciais, P., Friedlingstein, P., Sitch, S., Pongratz, J., Fan, L., Wigneron, J. P., Weber, U., Reichstein, M., Fu, Z., Anthoni, P., Arneth, A., Haverd, V., Jain, A. K., Joetzjer, E., Knauer, J., Lienert, S., Loughran, T., Mcguire, P. C., Tian, H., Viovy, N., & Zaehle, S., 2020. Direct and seasonal legacy effects of the 2018 heat wave and drought on European ecosystem productivity. SCIENCE ADVANCES, 6(24), eaba2724.

Ben-Ari, T., Boé, J., Ciais, P., Lecerf, R., Van Der Velde, M., & Makowski, D., 2018. Causes and implications of the unforeseen 2016 extreme yield loss in the breadbasket of France. Nature communications, 9(1), 1627.

Burbidge, N. T., 1960. The phytogeography of the Australian region. Australian Journal of Botany, 8(2), 75-211.

Cai, W., Sullivan, A., & Cowan, T., 2009. Rainfall teleconnections with Indo-Pacific variability in the WCRP CMIP3 models. Journal of Climate, 22(19), 5046-5071.

Cai, W., Van Rensch, P., Cowan, T., & Hendon, H. H., 2011. Teleconnection pathways of ENSO and the IOD and the mechanisms for impacts on Australian rainfall. Journal of Climate, 24(15), 3910-3923.

Cann, D. J., Schillinger, W. F., Hunt, J. R., Porker, K. D., & Harris, F. a. J., 2020. Agroecological advantages of early-sown winter wheat in semi-arid environments: A comparative case study from southern Australia and Pacific Northwest United States. Frontiers in Plant Science, 11, 502382.

Casselman, J. W., Taschetto, A. S., & Domeisen, D. I. V., 2021. Nonlinearity in the pathway of El Niño–Southern Oscillation to the tropical North Atlantic. Journal of Climate, 34(17), 7277-7296.

Ciais, P., Reichstein, M., Viovy, N., Granier, A., Ogée, J., Allard, V., Aubinet, M., Buchmann, N., Bernhofer, C., Carrara, A., Chevallier, F., De Noblet, N., Friend, A. D., Friedlingstein, P., Grünwald, T., Heinesch, B., Keronen, P., Knohl, A., Krinner, G., Loustau, D., Manca, G., Matteucci, G., Miglietta, F., Ourcival, J. M., Papale, D., Pilegaard, K., Rambal, S., Seufert, G., Soussana, J. F., Sanz, M. J., Schulze, E. D., Vesala, T., & Valentini, R., 2005. Europe-wide reduction in primary productivity caused by the heat and drought in 2003. Nature, 437(7058), 529-533.

Cohen, I., Zandalinas, S. I., Huck, C., Fritschi, F. B., & Mittler, R., 2021. Meta-analysis of drought and heat stress combination impact on crop yield and yield components. Physiologia Plantarum, 171(1), 66-76.

Dalgliesh, N., Cocks, B., & Horan, H., 2012. APSoil-providing soils information to consultants, farmers and researchers. Paper presented at the 16th Australian Agronomy Conference, Armidale, NSW.

Dittus, A. J., Karoly, D. J., Donat, M. G., Lewis, S. C., & Alexander, L. V., 2018. Understanding the role of sea surface temperature-forcing for variability in global temperature and precipitation extremes. Weather and Climate Extremes, 21, 1-9.
FAO, 2021. The Food and Agriculture Organization of the United Nations. Statistic data base. https://www.fao.org/faostat/en/#data/QCL. The last accessed date: 25 May 2021.
Farre, I., Foster, I., Biddulph, B., & Asseng, S., 2010. Is there a value in having a frost forecast for wheat in the South-West of Western Australia. Paper presented at the Food Security from Sustainable Agriculture: 15th Australian Agronomy Conference. Lincoln, New Zealand.
Feng, P., Wang, B., Macadam, I., Taschetto, A. S., Abram, N. J., Luo, J.-J., King, A. D., Chen, Y., Li, Y., Liu, D. L., Yu, Q., & Hu, K., 2022. Increasing dominance of Indian Ocean variability impacts Australian wheat yields. Nature Food, 3(10), 862-870.
Feng, S., & Hao, Z., 2021. Quantitative contribution of ENSO to precipitation-temperature dependence and associated compound dry and hot events. Atmospheric Research, 260, 105695.
Frees, E. W., & Valdez, E. A., 1998. Understanding relationships using copulas. North American actuarial journal, 2(1), 1-25.
Freund, M. B., Henley, B. J., Karoly, D. J., Mcgregor, H. V., Abram, N. J., & Dommenget, D., 2019. Higher frequency of Central Pacific El Niño events in recent decades relative to past centuries. Nature Geoscience, 12(6), 450-455.
Ganguli, P., & Reddy, M. J., 2013. Probabilistic assessment of flood risks using trivariate copulas. Theoretical and Applied Climatology, 111(1), 341-360.
García-Herrera, R., Díaz, J., Trigo, R. M., Luterbacher, J., & Fischer, E. M., 2010. A Review of the European Summer Heat Wave of 2003. Critical Reviews in Environmental Science and Technology, 40(4), 267-306.
Glotter, M., & Elliott, J. J. N. P., 2016. Simulating US agriculture in a modern Dust Bowl drought. Nature plants, 3(1), 1-6.
Guo, Y., Lu, X., Zhang, J., Li, K., Wang, R., Rong, G., Liu, X., & Tong, Z., 2022. Joint analysis of drought and heat events during maize (Zea mays L.) growth periods using copula and cloud models: A case study of Songliao Plain. Agricultural Water Management, 259, 107238.
Hallett, C. S., Hobday, A. J., Tweedley, J. R., Thompson, P. A., Mcmahon, K., & Valesini, F. J., 2018. Observed and predicted impacts of climate change on the estuaries of south-western Australia, a Mediterranean climate region. Regional Environmental Change, 18(5), 1357-1373.
Hanley, D. E., Bourassa, M. A., O'brien, J. J., Smith, S. R., & Spade, E. R., 2003. A quantitative evaluation of ENSO indices. Journal of Climate, 16(8), 1249-1258.
Hao, Y., Hao, Z., Feng, S., Zhang, X., & Hao, F., 2020. Response of vegetation to El Niño-Southern Oscillation (ENSO) via compound dry and hot events in southern Africa. Global and Planetary Change, 195, 103358.
Hao, Z., Hao, F., Singh, V. P., & Zhang, X., 2018. Quantifying the relationship between compound dry and hot events and El Niño–southern Oscillation (ENSO) at the global scale. Journal of Hydrology, 567, 332-338.
Hao, Z., Hao, F., Xia, Y., Feng, S., Sun, C., Zhang, X., Fu, Y., Hao, Y., Zhang, Y., & Meng, Y., 2022. Compound droughts and hot extremes: Characteristics, drivers, changes, and impacts. Earth-Science Reviews, 104241.
Hao, Z., Li, W., Singh, V. P., Xia, Y., Zhang, X., & Hao, F., 2020. Impact of dependence changes on the likelihood of hot extremes under drought conditions in the United States. Journal of Hydrology, 581, 124410.
Herring, S. C., Christidis, N., Hoell, A., Kossin, J. P., Schreck Iii, C. J., & Stott, P. A., 2018. Explaining extreme events of 2016 from a climate perspective. Bulletin of the American Meteorological Society, 99(1), S1-S157.
Holzworth, D. P., Huth, N. I., Devoil, P. G., Zurcher, E. J., Herrmann, N. I., Mclean, G., Chenu, K., Van Oosterom, E. J., Snow, V., Murphy, C., Moore, A. D., Brown, H., Whish, J. P. M., Verrall, S., Fainges, J., Bell, L. W., Peake, A. S., Poulton, P. L., Hochman, Z., Thorburn, P. J., Gaydon, D. S.,

Dalgliesh, N. P., Rodriguez, D., Cox, H., Chapman, S., Doherty, A., Teixeira, E., Sharp, J., Cichota, R., Vogeler, I., Li, F. Y., Wang, E., Hammer, G. L., Robertson, M. J., Dimes, J. P., Whitbread, A. M., Hunt, J., Van Rees, H., Mcclelland, T., Carberry, P. S., Hargreaves, J. N. G., Macleod, N., Mcdonald, C., Harsdorf, J., Wedgwood, S., & Keating, B. A., 2014. APSIM – Evolution towards a new generation of agricultural systems simulation. Environmental Modelling & Software, 62, 327-350.

Hu, L., 2006. Dependence patterns across financial markets: a mixed copula approach. Applied financial economics, 16(10), 717-729.

Innes, P. J., Tan, D. K. Y., Van Ogtrop, F., & Amthor, J. S., 2015. Effects of high-temperature episodes on wheat yields in New South Wales, Australia. Agricultural and Forest Meteorology, 208, 95-107.

Ionita, M., Caldarescu, D. E., & Nagavciuc, V., 2021. Compound hot and dry events in Europe: variability and large-scale drivers. Frontiers in Climate, 3, 688991.

Jaworski, P., Durante, F., Hardle, W. K., & Rychlik, T., 2010. Copula theory and its applications (Vol. 198): Springer.

Júnior, R. D. S. N., Martre, P., Finger, R., Van Der Velde, M., Ben-Ari, T., Ewert, F., Webber, H., Ruane, A. C., & Asseng, S., 2021. Extreme lows of wheat production in Brazil. Environmental Research Letters, 16(10), 104025.

Keating, B. A., Carberry, P. S., Hammer, G. L., Probert, M. E., Robertson, M. J., Holzworth, D., Huth, N. I., Hargreaves, J. N. G., Meinke, H., Hochman, Z., Mclean, G., Verburg, K., Snow, V., Dimes, J. P., Silburn, M., Wang, E., Brown, S., Bristow, K. L., Asseng, S., Chapman, S., Mccown, R. L., Freebairn, D. M., & Smith, C. J., 2003. An overview of APSIM, a model designed for farming systems simulation. European Journal of Agronomy, 18(3), 267-288.

King, A. D., Klingaman, N. P., Alexander, L. V., Donat, M. G., Jourdain, N. C., & Maher, P., 2014. Extreme rainfall variability in Australia: Patterns, drivers, and predictability. Journal of Climate, 27(15), 6035-6050.

Kirkegaard, J. A., & Lilley, J. M., 2007. Root penetration rate a benchmark to identify soil and plant limitations to rooting depth in wheat %J Australian Journal of Experimental Agriculture. Australian Journal of Experimental Agriculture, 47(5), 590-602.

Kirono, D. G. C., Chiew, F. H. S., & Kent, D. M., 2010. Identification of best predictors for forecasting seasonal rainfall and runoff in Australia. Hydrological Processes, 24(10), 1237-1247.

Kwon, M., Kwon, H.-H., & Han, D., 2019. Spatio-temporal drought patterns of multiple drought indices based on precipitation and soil moisture: A case study in South Korea. International Journal of Climatology, 39(12), 4669-4687.

Lalic, B., Eitzinger, J., Mihailovic, D., Thaler, S., & Jancic, M. J. T. J. O. a. S., 2013. Climate change impacts on winter wheat yield change–which climatic parameters are crucial in Pannonian lowland? Journal of Agricultural Science, 151(6), 757-774.

Leonard, M., Westra, S., Phatak, A., Lambert, M., Van Den Hurk, B., Mcinnes, K., Risbey, J., Schuster, S., Jakob, D., & Stafford-Smith, M., 2014. A compound event framework for understanding extreme impacts. WIREs Climate Change, 5(1), 113-128.

Li, E., Zhao, J., Pullens, J. W. M., & Yang, X., 2022. The compound effects of drought and high temperature stresses will be the main constraints on maize yield in Northeast China. Science of the Total Environment, 812, 152461.

Li, S., Wang, B., Liu, D. L., Chao, C., Feng, P., Mingxia, H., Xiaofang, W., Shi, L., Cathy, W., Alfredo, H., & Yu, Q., 2024. Can agronomic options alleviate the risk of compound drought-heat events during wheat flowering period in southeastern Australia? European Journal of Agronomy.

Liu, D. L., Timbal, B., Mo, J., Fairweather, H. J. I. J. O. C. C. S., & Management., 2011. A GIS-based climate change adaptation strategy tool. International Journal of Climate Change Strategies and Management.

Liu, G., Li, J., & Ying, T., 2023. Atlantic Multidecadal Oscillation modulates the relationship between El Niño–Southern Oscillation and fire weather in Australia. Atmos. Chem. Phys., 23(16), 9217-9228.

Marshall, A. G., Hudson, D., Wheeler, M. C., Alves, O., Hendon, H. H., Pook, M. J., & Risbey, J. S., 2014. Intra-seasonal drivers of extreme heat over Australia in observations and POAMA-2. Climate Dynamics, 43(7), 1915-1937.

Marshall, G. J., 2003. Trends in the Southern Annular Mode from observations and reanalyses. Journal of Climate, 16(24), 4134-4143.

Mason, S. J., & Goddard, L., 2001. Probabilistic precipitation anomalies associated with EN SO. Bulletin of the American Meteorological Society, 82(4), 619-638.

Mcphaden, M. J., Zebiak, S. E., & Glantz, M. H., 2006. ENSO as an integrating concept in earth science. Science, 314(5806), 1740-1745.

Meyers, G., Mcintosh, P., Pigot, L., & Pook, M., 2007. The years of El Niño, La Niña, and interactions with the tropical Indian Ocean. Journal of Climate, 20(13), 2872-2880.

Min, S. K., Cai, W., & Whetton, P., 2013. Influence of climate variability on seasonal extremes over Australia. Journal of Geophysical Research: Atmospheres, 118(2), 643-654.

Mishra, V., Thirumalai, K., Singh, D., & Aadhar, S., 2020. Future exacerbation of hot and dry summer monsoon extremes in India. npj Climate and Atmospheric Science, 3(1), 10.

Mukherjee, S., Ashfaq, M., & Mishra, A. K., 2020. Compound Drought and Heatwaves at a Global Scale: The Role of Natural Climate Variability-Associated Synoptic Patterns and Land-Surface Energy Budget Anomalies. JGR Atmospheres, 125(11), e2019JD031943.

Nguyen-Huy, T., Deo, R. C., An-Vo, D.-A., Mushtaq, S., & Khan, S., 2017. Copula-statistical precipitation forecasting model in Australia's agro-ecological zones. Agricultural Water Management, 191, 153-172.

Papari, J. R., 2022. Heatwaves and compounding drought-heatwaves in Australia: historical changes, association with ENSO and IOD, and influence on bushfire fuels.

Perkins, S. E., & Alexander, L. V., 2013. On the measurement of heat waves. Journal of Climate, 26(13), 4500-4517.

Poonia, V., Jha, S., & Goyal, M. K., 2021. Copula based analysis of meteorological, hydrological and agricultural drought characteristics across Indian river basins. International Journal of Climatology, 41(9), 4637-4652.

Reddy, P. J., Perkins-Kirkpatrick, S. E., Ridder, N. N., & Sharples, J. J., 2022. Combined role of ENSO and IOD on compound drought and heatwaves in Australia using two CMIP6 large ensembles. Weather and Climate Extremes, 37, 100469.

Reddy, P. J., Perkins-Kirkpatrick, S. E., & Sharples, J. J., 2021. Interactive influence of ENSO and IOD on contiguous heatwaves in Australia. Environmental Research Letters, 17(1), 014004.

Ribeiro, A. F. S., Russo, A., Gouveia, C. M., & Páscoa, P., 2019. Copula-based agricultural drought risk of rainfed cropping systems. Agricultural Water Management, 223, 105689.

Ridder, N. N., Pitman, A. J., Westra, S., Ukkola, A., Do, H. X., Bador, M., Hirsch, A. L., Evans, J. P., Di Luca, A., & Zscheischler, J., 2020. Global hotspots for the occurrence of compound events. Nature communications, 11(1), 5956.

Risbey, J. S., Pook, M. J., Mcintosh, P. C., Wheeler, M. C., & Hendon, H. H., 2009. On the remote drivers of rainfall variability in Australia. Monthly Weather Review, 137(10), 3233-3253.

Saji, N. H., Goswami, B. N., Vinayachandran, P. N., & Yamagata, T., 1999. A dipole mode in the tropical Indian Ocean. Nature, 401(6751), 360-363.

Sakamoto, Y., Ishiguro, M., & Kitagawa, G., 1986. Akaike information criterion statistics. Dordrecht, The Netherlands: D. Reidel, 81(10.5555), 26853.

Sarhadi, A., Ausín, M. C., Wiper, M. P., Touma, D., & Diffenbaugh, N. S., 2018. Multidimensional risk in a nonstationary climate: Joint probability of increasingly severe warm and dry conditions. SCIENCE ADVANCES, 4(11), eaau3487.

Schölzel, C., & Friederichs, P., 2008. Multivariate non-normally distributed random variables in climate research – introduction to the copula approach. Nonlin. Processes Geophys., 15(5), 761-772.

Seneviratne, S., Nicholls, N., Easterling, D., Goodess, C., Kanae, S., Kossin, J., Luo, Y., Marengo, J., Mcinnes, K., & Rahimi, M., 2012. Changes in climate extremes and their impacts on the natural physical environment.

SILO, 2023. Long Paddock, 2023, Home LongPaddock | Queensland Government. The last accessed date: 24 Jan 2023.

Sklar, A., 1973. Random variables, joint distribution functions, and copulas. Kybernetika, 9(6), 449-460.

Sun, Q., Miao, C., Qiao, Y., & Duan, Q., 2017. The nonstationary impact of local temperature changes and ENSO on extreme precipitation at the global scale. Climate Dynamics, 49, 4281-4292.

Turner, N. C., & Asseng, S., 2005. Productivity, sustainability, and rainfall-use efficiency in Australian rainfed Mediterranean agricultural systems. Australian Journal of Agricultural Research, 56(11), 1123-1136.

Ummenhofer, C. C., Sen Gupta, A., Briggs, P. R., England, M. H., Mcintosh, P. C., Meyers, G. A., Pook, M. J., Raupach, M. R., & Risbey, J. S., 2011. Indian and Pacific Ocean influences on southeast Australian drought and soil moisture. Journal of Climate, 24(5), 1313-1336.

Wang, A., Tao, H., Ding, G., Zhang, B., Huang, J., & Wu, Q., 2023. Global cropland exposure to extreme compound drought heatwave events under future climate change. Weather and Climate Extremes, 40, 100559.

Wang, B., Li Liu, D., Waters, C., & Yu, Q., 2018. Quantifying sources of uncertainty in projected wheat yield changes under climate change in eastern Australia. Climatic Change, 151(2), 259-273.

Wang, B., Liu, D. L., O'leary, G. J., Asseng, S., Macadam, I., Lines-Kelly, R., Yang, X., Clark, A., Crean, J., & Sides, T., 2018. Australian wheat production expected to decrease by the late 21st century. Global Change Biology, 24(6), 2403-2415.

Wang, C., Li, Z., Chen, Y., Ouyang, L., Li, Y., Sun, F., Liu, Y., & Zhu, J., 2023. Drought-heatwave compound events are stronger in drylands. Weather and Climate Extremes, 42, 100632.

Wegren, S. K., 2011. Food Security and Russia's 2010 Drought. Eurasian Geography and Economics, 52(1), 140-156.

Wheeler, T. R., Batts, G. R., Ellis, R. H., Hadley, P., & Morison, J. I. L., 1996. Growth and yield of winter wheat (Triticum aestivum) crops in response to CO2 and temperature. The Journal of Agricultural Science, 127(1), 37-48.

White, C. J., Hudson, D., & Alves, O., 2014. ENSO, the IOD and the intraseasonal prediction of heat extremes across Australia using POAMA-2. Climate Dynamics, 43(7), 1791-1810.

Xiang, K., Wang, B., Liu, D. L., Chen, C., Waters, C., Huete, A., & Yu, Q., 2023. Probabilistic assessment of drought impacts on wheat yield in south-eastern Australia. Agricultural Water Management, 284, 108359.

Yang, X., Zheng, L., Yang, Q., Wang, Z., Cui, S., & Shen, Y., 2018. Modelling the effects of conservation tillage on crop water productivity, soil water dynamics and evapotranspiration of a maize-winter wheat-soybean rotation system on the Loess Plateau of China using APSIM. Agricultural Systems, 166, 111-123.

Yuan, C., & Yamagata, T., 2015. Impacts of IOD, ENSO and ENSO Modoki on the Australian Winter Wheat Yields in Recent Decades. Scientific Reports, 5(1), 17252.

Zhang, W., Mao, W., Jiang, F., Stuecker, M. F., Jin, F.-F., & Qi, L., 2021. Tropical Indo-Pacific Compounding Thermal Conditions Drive the 2019 Australian Extreme Drought. Geophysical Research Letters, 48(2), e2020GL090323.

Zhang, Y., Hao, Z., Feng, S., Zhang, X., & Hao, F., 2023. Changed relationship between compound dry-hot events and ENSO at the global scale. Journal of Hydrology, 621, 129559.

Zscheischler, J., Westra, S., Van Den Hurk, B. J. J. M., Seneviratne, S. I., Ward, P. J., Pitman, A., Aghakouchak, A., Bresch, D. N., Leonard, M., Wahl, T., & Zhang, X., 2018. Future climate risk from compound events. Nature Climate Change, 8(6), 469-477.

Chapter 6. Final conclusions future research

6.1 Final conclusions

This study assessed the vulnerability of Australia's wheat to climate change, gaining a foundational understanding of the connections between wheat yields and climate conditions. It then focused on the compound dry and hot events, systematically analyzing their historical evolution, impacts on wheat yield, and driving factors. The indices and analytical frameworks established in this study provided new insights into the climatic risks confronting wheat yield. Main outcomes of this thesis can be summarized as follows:

The hotspots of wheat yield vulnerability to climate change were located in the northwestern parts of the New South Wales wheat belt. Priority adaptations and investments to mitigate the adverse impacts of climate change should be implemented in these areas. The mean vulnerability of the wheat belt consistently decreasing from 1924 to 1998. This is mainly due to increased adaptive capacity with the improvement of agronomic management practices, and technological and socio-economic progress.

The compound drought-heat index to assess the occurrences of simultaneous water and heat stresses during WSP under the expected effects of climate change in Australia was developed in this project. The frequency, duration, and intensity of compound dry and hot events were projected to increase in the future, compared with baseline climate. The increased compound dry and hot events were mainly due to the increase in heat stress, especially at sites located in the northern NSW wheat belt with a dry-hot climate. In addition, the early sowing and wheat cultivars with shorter vegetative phases had adaptative effects on reducing the risk of compound dry and hot events. These agronomic options facilitated wheat to escape the jeopardizing effects of compound drought-heat events under projected climate change at study sites. However, they may introduce an increased frost risk across six study sites, especially in regions with climates that are less dry and hot, such as Mudgee and Wagga Wagga. This study will provide helpful information for farmers in Australia to mitigate the adverse effects of extreme climate events on wheat. The framework developed here can be extended to other dryland wheat growing regions globally.

The impacts of drought, heat, frost, and compound drought and extreme temperature (DET) events on wheat yield variation in Australia's wheat belt for the past three decades were assessed in this project, using the 12-subregion wheat yield data obtained from ABARES. The DET events intensity had a large inter-annual variation with a small increasing trend and showed a north-south decreasing gradient across Australia's crop belt. This spatial distribution was mainly dominated by high temperatures. Additionally, extreme weather events contributed 55% of wheat yield change in the entire crop belt. Regarding the relative importance of DET events to wheat yield variation, it was second to that of drought in the long-term series.

However, in extreme low-yield years, the relative importance of DET events surpassed the sum importance of individual drought, heat, and frost events, reaching 68% and 52% in years with yields below the 5th and 10th percentiles, respectively. Our findings highlight the significant impact of DET on the long-term fluctuations in wheat yield, indicating its potential to cause significant yield losses in Australia. I expect these results will raise awareness about the significance of DET events for both farmers and policymakers. Consequently, efforts should be directed toward driving specific adaptive strategies, refining policy frameworks, and fostering technological innovations to strengthen agricultural resilience in the face of climate extremes.

This project assessed the influences of large-scale climate drivers ENSO and IOD on DET events occurring during the wheat reproductive period across Australia's wheat belt from the beginning of the last century to the present. The impacts of ENSO and IOD varied across different phases and distinct temporal periods. The eastern part of Australia's wheat belt was more responsive to ENSO and IOD than the western parts. Specifically, El Niño and positive IOD phases were associated with greater DET intensity and greater probability of occurring high-intensity DET events, whereas La Niña and negative IOD phases tend to result in lower DET intensity and lower probability of occurring high-intensity DET events, compared to the neutral conditions. In general, the role of ENSO in triggering severe DET events during WRP surpassed that of the IOD. Our findings highlighted the evolving influence of large-scale climate drivers on DET events during WRP in Australia over time, enhancing the comprehension of the relationships between climate drivers and compound weather and climate extremes. This insight strengthens our ability to identify and mitigate the risks associated with these extremes, ultimately improving adaptative potential for grain production under climate change.

6.2 Limitations and future research

This study presents limitations that warrant attention.

(1). In this research, the APSIM simulations that modeled wheat phenology and plant-available water were conducted using management practices on a state-wide scale, without incorporating data from local or individual farm-level practices. This limitation highlights the importance of collecting and integrating more detailed, location-specific data to improve the accuracy and relevance of future studies.

(2). This study is constrained by using only one crop simulation model. Various crop models differ in their underlying assumptions, algorithms, and parameter configurations, leading to different

outputs even with the same inputs. Employing a combination of several crop models for simulating crop growth and soil water dynamics could lead to more dependable results. This limitation underlines the importance of obtaining localized data to support the creation of hybrid models in future studies.